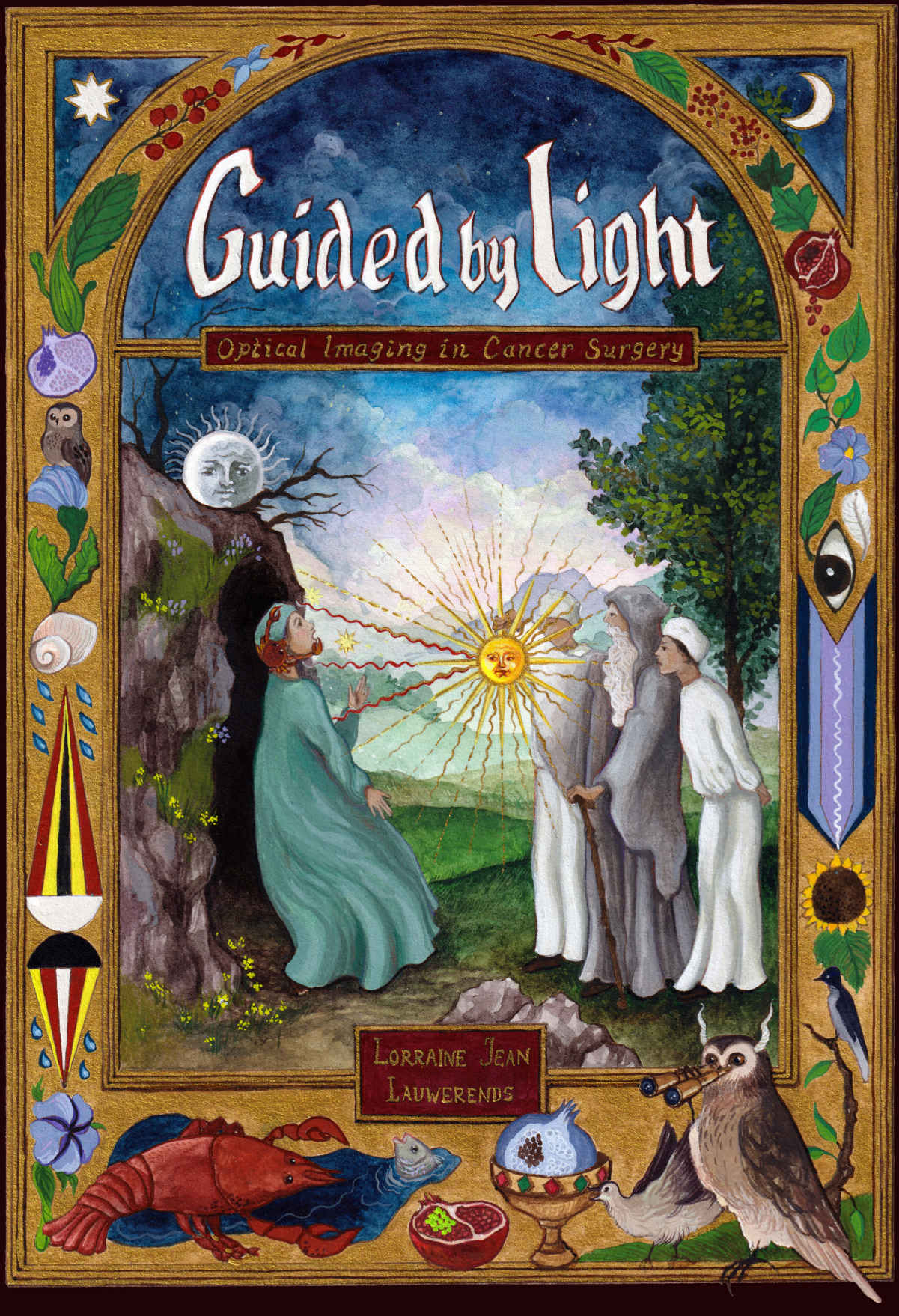
Guided by Light
Optical Imaging in Cancer Surgery
Lorraine Jean Lauwerends

Stellingen behorende bij het Proefschrift:

Guided by Light - Optical Imaging in Cancer Surgery

1. The ultimate measure of fluorescence imaging's clinical value is its impact on intraoperative decision-making. *(this thesis)*

2. Real-time fluorescence-guided surgery can improve tumor resections by enabling timely intraoperative identification and correction of inadequate margins. *(this thesis)*

3. *Ex vivo* fluorescence imaging under controlled conditions ("black-box imaging") enables identification of inadequate surgical margins without disrupting workflow in the operating room. *(this thesis)*

4. The integration of Raman spectroscopy's depth profiling capability with fluorescence imaging could reduce the need for frozen section analysis in margin assessment. *(this thesis)*

5. The absence of standardized fluorescence imaging and margin assessment protocols risks inconsistency, emphasizing the need for clear, indication-specific guidelines. *(this thesis)*

6. The successful integration of clinical artificial intelligence depends as much on understanding its technological capabilities as on anticipating its effects on how care is organized, experienced, and entrusted.

7. What is perceived as dysfunction often arises from a mismatch between the individual and their environment.

8. The capacity to keep going is too often mistaken for the capacity to keep well.

9. Technology should strengthen, not erode, interhuman connection in our increasingly digital world.

10. The kitchen is one of the few spaces where science, art, and tradition converge to create something that is both essential and deeply personal.

11. If you don't learn to slow down on purpose, your body will do it for you.

Guided by Light

Optical Imaging in Cancer Surgery

Lorraine Jean Lauwerends

Financial support for the publication of this thesis was generously provided by: The Erasmus University Rotterdam and the Department of Otorhinolaryngology, Head and Neck Surgery, and:

ChipSoft

Cover design:	L.J. Lauwerends (lorrainejean.com)
Lay-out:	ProefschriftMaken | proefschriftmaken.nl
Print by:	ProefschriftMaken | proefschriftmaken.nl
ISBN:	978-94-6534-752-3

© L.J. Lauwerends, 2026, Rotterdam, the Netherlands
All rights reserved. No parts of this publication may be reproduced in any form or by any means without permission of the author.

Guided by Light

Optical Imaging in Cancer Surgery

Geleid door licht

Optische beeldvorming in kanker chirurgie

Thesis

to obtain the degree of Doctor from
Erasmus University Rotterdam
by command of the
rector magnificus

Prof.dr.ir. A.J. Schuit

and in accordance with the decision of the Doctorate Board.
The public defence shall be held on

Wednesday 2 December 2026 at 10.30 hrs

by

Lorraine Jean Lauwerends

born in Rotterdam, the Netherlands.

Erasmus University Rotterdam

DOCTORAL COMMITTEE

Promoter:	Prof. dr. R.J. Baatenburg de Jong
	Prof. Dr. A.L. Vahrmeijer
Co-promoter:	Dr. S. Keereweer
	Dr. D.E. Hilling
Assessment committee:	Prof. dr. R.P. Takes
	Dr. S.E.M. Veldhuijzen van Zanten
	Prof. dr. M.J.H. Witjes

VOOR

Robert Eugène Lauwerends

1978 - 2023

'Doctorandus' E.R. (Euclides Ramos) Pachito

1964 - 2026

'Those granted the gift of seeing more deeply
can see beyond form, and concentrate on
the wondrous aspect hiding behind every form,
which is called life.'

HILMA AF KLINT

TABLE OF CONTENTS

Chapter 1.	General introduction and outline of thesis	9
Part I:	**Reviewing Intraoperative Imaging Technologies**	19
Chapter 2.	Current intraoperative imaging techniques to improve surgical resection of laryngeal cancer: a systematic review	21
Chapter 3.	Fluorescence-guided surgery in colorectal cancer; a review on clinical results and future perspectives	55
Part II:	**Conceptual Foundations of Fluorescence Imaging in Cancer Surgery**	87
Chapter 4.	Real-time fluorescence imaging in intraoperative decision making for cancer surgery	89
Chapter 5.	Real-time fluorescence imaging for cancer surgery: a pathologist's perspective - authors' reply	111
Part III:	**Advances in Fluorescence Imaging for Head and Neck Cancer**	117
Chapter 6.	Tumor marker expression in head and neck malignancies to identify potential targets for intraoperative molecular near-infrared imaging	119
Chapter 7.	Near-infrared fluorescence imaging-guided surgery using cRGD-ZW800 to improve surgical resection margins in oral cancer: a phase I/II feasibility trial	141
Part IV:	**Integrating Fluorescence Imaging with Raman Spectroscopy**	177
Chapter 8.	The complementary value of intraoperative fluorescence imaging and Raman spectroscopy for cancer surgery: combining the incompatibles	179
Chapter 9.	Development of a near-infrared Raman spectroscopy setup compatible with fluorescence-guided surgery	203
Chapter 10.	Optimizing tumor resection: the added value of Raman spectroscopy in fluorescence-guided cancer surgery	219
PART V:	**Summary and General Discussion**	249
Chapter 11.	Summary	251
Chapter 12.	General discussion and future perspectives	257

Appendix 273
I. Nederlandse samenvatting 275
II. List of abbreviations 278
III. List of publications 280
IV. Contributing authors 283
V. PhD Portfolio 284
VI. Acknowledgments | Dankwoord 286
VII. About the author 289


1

Chapter 1

General introduction and outline of this thesis

GENERAL INTRODUCTION

The history of scientific discovery is one of observation - a quest to perceive, understand, and manipulate that which is hidden. This pursuit has seen a profound expression in the field of medical science. The birth of medical imaging, a fundamental milestone in this evolution, has shaped the landscape of diagnosis and treatment.

In the early phases of medical history, our understanding was confined to what could be directly observed with the naked eye. Anatomical studies were limited to superficial examinations and speculations, often leading to misconceptions and inaccuracies. The advent of the microscope in the 17th century marked a turning point, offering a window into the previously invisible world of microorganisms and cellular structures. This development in observational capability laid the groundwork for modern pathology and microbiology.

As the centuries progressed, the refinement and expansion of imaging technologies continued at an unprecedented pace. The discovery of X-rays in 1895 ushered in an era of radiological imaging, allowing for the non-invasive visualization of internal body structures. This was followed by the development of computed tomography (CT) and magnetic resonance imaging (MRI), further expanding our diagnostic arsenal. These technologies, along with advancements in ultrasound and nuclear medicine, have provided clinicians with powerful tools to detect and monitor countless medical conditions with remarkable accuracy and detail.

Imaging in the Realm of Cancer Surgery

The evolution of imaging technologies has been particularly impactful in the realm of oncologic surgery. The delineation of tumor margins, vital in achieving successful surgical outcomes, has historically been challenging, particularly in complex anatomical regions such as the head and neck. Traditional methods rely heavily on the surgeon's experience, visual and tactile feedback, often leading to inadequate resection margins.

The introduction of advanced imaging modalities, such as intraoperative ultrasound, optical coherence tomography, photoacoustic imaging and narrow-band imaging, began to bridge this gap, yet each had limitations in terms of resolution or specificity for tumor tissues. Within this context, intraoperative fluorescence imaging represents a paradigm shift. By enabling surgeons to visualize malignant tissues with a level of detail previously unattainable in the operating room, fluorescence imaging has the potential to significantly enhance the precision of tumor resection, minimize damage to healthy tissues, and improve overall patient outcomes.

Fluorescence Imaging

Fluorescence imaging stands out in the field of surgical oncology due to its ability to visualize malignancy in real-time with exceptional sensitivity and contrast. This method utilizes the phenomenon of fluorescence - the emission of light by a substance that has absorbed light or other electromagnetic radiation - to highlight malignant tissues.

Fluorescence imaging employs fluorescent agents that can be broadly categorized into non-specific and targeted agents. Non-specific fluorescent agents accumulate in tumors due to the enhanced permeability and retention effect, while targeted agents (consisting of a fluorophore that has been conjugated to a specific targeting ligand) are designed to bind to specific molecular markers expressed by tumor cells, enhancing the specificity of tumor detection. Although autofluorescence imaging, which relies on the endogenous fluorescence of biological tissues, is another technique in this field, this thesis focuses on fluorescence imaging using exogenously administered agents due to their higher specificity and versatility in targeting tumor cells.

An important factor in the advancement of fluorescence imaging towards clinical practice is its application within the near-infrared (NIR) spectrum (700-900 nm). NIR fluorescence stands out due to its deep tissue penetration and reduced autofluorescence from adjacent tissues, offering enhanced visualization of tumor margins. Yet, implementing NIR fluorescence imaging faces obstacles, including the necessity for (the development of) NIR tracers that are patient-safe and tumor-specific, along with specialized equipment to detect NIR fluorescence. Despite these challenges, the potential of NIR fluorescence imaging to improve surgical outcomes is significant. By enabling more precise excision of tumors while sparing healthy tissue, fluorescence-guided surgery (FGS) promises to enhance the accuracy of surgeries, decrease recurrence rates, sparing healthy tissues and ultimately improve patient prognoses.

Specific Challenges in Head and Neck Cancer Surgery

Head and neck cancers (HNC) present significant surgical challenges due to the critical functions and complex anatomy of the affected region. Inadequate margins (i.e., ≤ 5 mm) occur in 67-85% of cases [1-3], frequently necessitating additional treatment and lowering the chance of survival [2, 4-7]. The precise removal of cancer without compromising speech, swallowing, and other vital functions is thus paramount.

Selective frozen section analysis, the current gold standard for assessing tumor margins during surgery, is limited by its time-consuming nature, restricted examination scope, and proneness to sampling errors, leading to a high false-negative rate [8, 9]. Achieving clear tumor margins while preserving vital structures remains a delicate and demanding task.

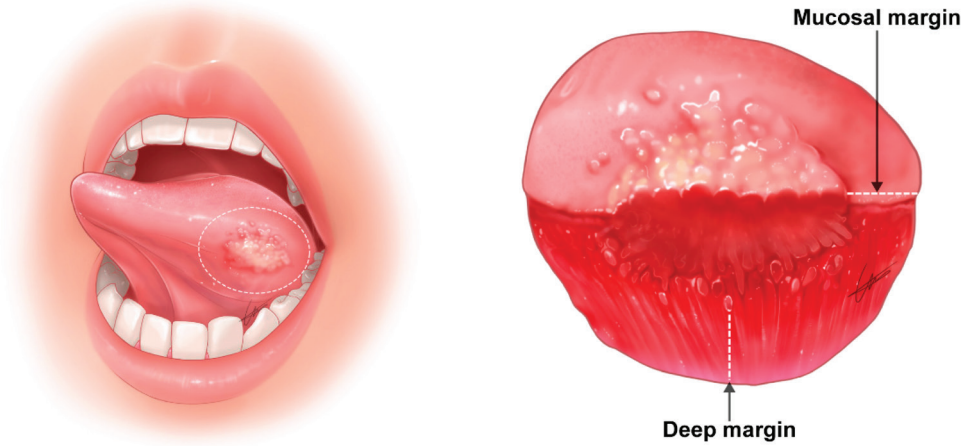

Figure 1. Resection of oral cancer (a) Dotted line indicates mucosal safety margin around lateral tongue tumor; (b) surgical specimen that includes primary tumor and normal surrounding tissues. The resection margin includes mucosal and deep margins. *Reproduced with permission from Jang et al.[10]*

At the Erasmus MC, the implementation and establishment of specimen-driven intraoperative assessment of resection margins as the standard of care, exemplifies an advanced method for ensuring adequate resections [7, 11]. This approach, supported by a relocation *(parallel tagging)* procedure, has significantly increased adequate resection margins (from 15% to 58%) and improved disease-specific survival by enabling accurate additional resections during the initial surgery [12]. Still, an inadequate margin rate of 42% presents ample room for improvement. Therefore, there is a clear need for more accurate, objective, intraoperative techniques for tumor margin identification.

Here, fluorescence imaging emerges as a promising tool by offering real-time, targeted visualization of malignant tissues, enhancing the precision of tumor removal in the head and neck region. This targeted approach is pivotal for improving patient outcomes after HNC surgery, where the margin of error is exceptionally narrow.

Specific Challenges in Colorectal Cancer Surgery

Colorectal cancer (CRC) surgery also encounters significant challenges, primarily due to the intricate anatomy and essential functions of the gastrointestinal tract. Tumor-positive resection margins are associated with a marked decrease in overall survival [13-15]. Additionally, complications such as anastomotic leaks and injuries to structures like the ureters pose serious risks [16-18]. These complications lead to high morbidity, reoperations, extended hospital stays, and increased healthcare costs.

Traditional intraoperative margin assessment methods face similar limitations to those in HNC surgery, highlighting the need for improved techniques. NIR fluorescence imaging offers a promising solution by providing (real-time) targeted visualization of malignant tissues, potentially enhancing the precision of CRC resection and reducing complications. Its ability to penetrate deep tissue and produce high-contrast images without interfering with the surgical field may be of particular benefit in CRC surgery, allowing for more accurate resections, minimizing recurrence rates, and preserving healthy tissue.

Integrating Raman Spectroscopy with Fluorescence Imaging

As research continues to advance, new fluorescent agents, imaging devices, applications and standardizing protocols are being developed, each with the potential to further refine the implementation of FGS in clinical practice. Crucially, the integration of fluorescence imaging with other modalities represents just one avenue through which the landscape of surgical oncology can be reshaped.

Raman Spectroscopy (RS) involves the inelastic scattering of light, known as Raman scattering, resulting in an energy exchange between the incident light and the molecules in a sample. This energy exchange alters the vibrational state of the molecule, producing a Raman spectrum that shows the intensity of scattered photons as a function of energy level, expressed as a Raman shift. In cancer surgery, RS aids in distinguishing cancerous from healthy tissues by analyzing these specific vibrational states.

This thesis explores the complementary value of combining fluorescence imaging with RS to achieve superior intraoperative diagnostic accuracy. While fluorescence imaging provides real-time, whole-field imaging, RS delivers uniquely high specificity, albeit with weaker signal intensity and constrained to point measurements (Figure 2).

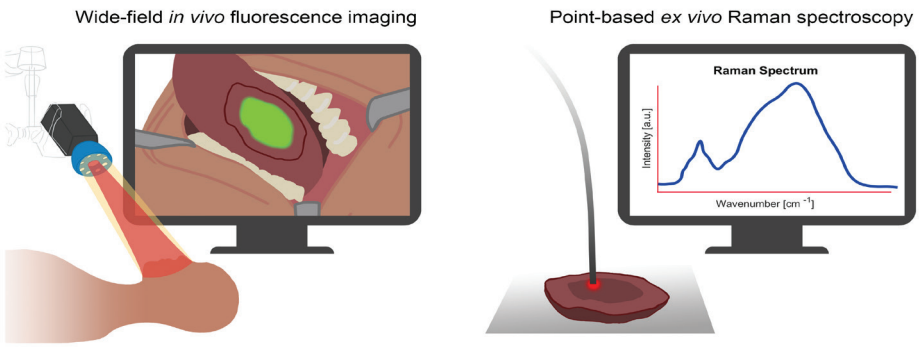

Figure 2. The integration of wide-field in vivo fluorescence imaging (left) with point-based ex vivo Raman Spectroscopy (right) for margin assessment in oral cancer surgery

Although traditionally considered mutually exclusive due to spectral overlap, we aimed to explore complementarity. The development of an RS setup capable of recording high-quality Raman spectra from tissue containing NIR fluorescent agents, and identifying an optimal wavelength interval for Raman excitation, has enabled this integration. Clinical evaluations using specimens from oral and rectal cancer trials suggest the effectiveness of combining fluorescence imaging to identify suspicious areas with RS for detailed tissue examination. This integration addresses the challenge of indeterminate margins identified with fluorescence imaging, potentially offering a more refined surgical technique.

By correlating Raman metrics with both fluorescence imaging and histopathological findings, this integration provides a comprehensive assessment of tumor margins and tissue specifics, potentially enhancing the accuracy of surgical decisions. This approach has the potential to reduce the occurrence of both incomplete and over extensive tumor resection, thereby improving patient outcomes. The novel combination of fluorescence imaging and RS in cancer surgery exemplifies a forward step in surgical oncology, aiming to redefine standards for intraoperative margin assessment across various types of cancer surgeries.

OUTLINE OF THESIS

Establishing the scope of fluorescence imaging and its applications, **Part I** systematically reviews current intraoperative imaging technologies across a spectrum of cancers. *Chapter 2* identifies current imaging modalities' limitations in assessing deep margins in laryngeal cancer surgery and suggests future directions for the application of optical imaging. *Chapter 3* explores the use of FGS in colorectal cancer, outlining its benefits for improving surgical precision and patient outcomes, thereby highlighting the potential of fluorescence imaging to transform oncologic surgery.

P**art II** of the thesis lays the groundwork for understanding the role of fluorescence imaging in cancer surgery, focusing on its critical impact on intraoperative decision-making. *Chapter 4* begins by delving into the potential of fluorescence imaging to influence surgical strategies, stressing the need for refined study methodologies and reporting standards to assess its clinical effectiveness thoroughly. Following this, *Chapter 5* presents our response to a correspondence letter ("*a pathologist's perspective*"), reinforcing the argument that FGS's influence on surgical decisions is the most direct indicator of its clinical value.

Part III focuses on the application of FGS in HNC. *Chapter 6* investigates potential targets for NIR fluorescence imaging in this area through an immunohistochemical study performed on oral, laryngeal and thyroid cancer tissue samples. Integrin αvβ6, in particular, was found to provide significant contrast for tumor margin delineation in oral and laryngeal cancer. *Chapter 7* moves into clinical application, demonstrating the safety, feasibility and efficacy

of cRGD-ZW800-1, an integrin-targeted fluorescent agent, in detecting clinically relevant inadequate margins and enhancing the rate of adequate surgical resection margins in oral squamous cell carcinoma (OSCC). This chapter highlighted FGS's crucial role in OSCC surgery, showcasing its influence on surgical decisions by identifying inadequate margins overlooked during routine intraoperative assessment, enabling additional resections in five patients (16%) thereby preventing the need for adjuvant radiotherapy in 3 patients.

Part IV proposes the integration of FGS with RS to overcome the limitations of fluorescence imaging, presenting a novel approach to achieve clearer surgical margins. *Chapter 8* discusses the complementary benefits of fluorescence imaging and RS, while *Chapter 9* introduces a NIR RS setup designed to work in harmony with FGS, effectively managing the spectral overlap issues. *Chapter 10* extends this discussion by clinically evaluating the advantages of combining *ex vivo* RS with fluorescence imaging in OSCC and rectal cancer surgery, outlining RS's role in providing precise, depth-specific measurements and reducing false positives for more accurate intraoperative decision-making.

The thesis concludes in **Part V** with *Chapters 11* and *12*, which summarize and synthesize the findings and discuss their broader implications for surgical oncology. This section highlights FGS's significant potential in cancer surgery and points towards future directions in surgical imaging and oncology, underscoring the thesis' contributions to the field.

REFERENCES

1. Woolgar, J.A. and A. Triantafyllou, *A histopathological appraisal of surgical margins in oral and oropharyngeal cancer resection specimens.* Oral Oncol, 2005. **41**(10): p. 1034-43.
2. Smits, R.W., et al., *Resection margins in oral cancer surgery: Room for improvement.* Head Neck, 2016. **38 Suppl 1**: p. E2197-203.
3. Orosco, R.K., et al., *Positive Surgical Margins in the 10 Most Common Solid Cancers.* Sci Rep, 2018. **8**(1): p. 5686.
4. Dik, E.A., et al., *Resection of early oral squamous cell carcinoma with positive or close margins: relevance of adjuvant treatment in relation to local recurrence: margins of 3 mm as safe as 5 mm.* Oral Oncol, 2014. **50**(6): p. 611-5.
5. Varvares, M.A., et al., *Surgical margins and primary site resection in achieving local control in oral cancer resections.* Laryngoscope, 2015. **125**(10): p. 2298-307.
6. Barroso, E.M., et al., *Performance of Intraoperative Assessment of Resection Margins in Oral Cancer Surgery: A Review of Literature.* Front Oncol, 2021. **11**: p. 628297.
7. Smits, R.W.H., et al., *Intraoperative Assessment of the Resection Specimen Facilitates Achievement of Adequate Margins in Oral Carcinoma.* Front Oncol, 2020. **10**: p. 614593.
8. St John, E.R., et al., *Diagnostic Accuracy of Intraoperative Techniques for Margin Assessment in Breast Cancer Surgery: A Meta-analysis.* Ann Surg, 2017. **265**(2): p. 300-310.
9. Cendan, J.C., D. Coco, and E.M. Copeland, 3rd, *Accuracy of intraoperative frozen-section analysis of breast cancer lumpectomy-bed margins.* J Am Coll Surg, 2005. **201**(2): p. 194-8.
10. Jang, J.Y., N. Choi, and H.S. Jeong, *Surgical Extent for Oral Cancer: Emphasis on a Cut-Off Value for the Resection Margin Status: A Narrative Literature Review.* Cancers (Basel), 2022. **14**(22).
11. Aaboubout, Y., et al., *Intraoperative Assessment of Resection Margins in Oral Cavity Cancer: This is the Way.* J Vis Exp, 2021(171).
12. van Lanschot, C.G.F., et al., *Relocation of inadequate resection margins in the wound bed during oral cavity oncological surgery: A feasibility study.* Head Neck, 2019. **41**(7): p. 2159-2166.
13. Nagtegaal, I.D. and P. Quirke, *What is the role for the circumferential margin in the modern treatment of rectal cancer?* J Clin Oncol, 2008. **26**(2): p. 303-12.
14. Elias, D., et al., *Peritoneal colorectal carcinomatosis treated with surgery and perioperative intraperitoneal chemotherapy: retrospective analysis of 523 patients from a multicentric French study.* J Clin Oncol, 2010. **28**(1): p. 63-8.
15. Amri, R., et al., *Association of Radial Margin Positivity With Colon Cancer.* JAMA Surg, 2015. **150**(9): p. 890-8.
16. Gild, P., et al., *Adult iatrogenic ureteral injury and stricture-incidence and treatment strategies.* Asian J Urol, 2018. **5**(2): p. 101-106.
17. Sparreboom, C.L., et al., *A multicentre cohort study of serum and peritoneal biomarkers to predict anastomotic leakage after rectal cancer resection.* Colorectal Dis, 2020. **22**(1): p. 36-45.
18. Angeramo, C.A., et al., *Postoperative outcomes in patients undergoing colorectal surgery with anastomotic leak before and after hospital discharge.* Updates Surg, 2020. **72**(2): p. 463-468.

Part I

Reviewing Intraoperative Imaging Technologies


2

Chapter 2

Current Intraoperative Imaging Techniques to Improve Surgical Resection of Laryngeal Cancer: A Systematic Review

Lorraine J. Lauwerends, Hidde A. Galema, José A.U. Hardillo, Aniel Sewnaik, Dominiek Monserez, Pieter B.A.A. van Driel, Cornelis Verhoef, Robert J. Baatenburg de Jong, Denise E. Hilling and Stijn Keereweer

Cancers (Basel). 2021 Apr 15;13(8):1895

ABSTRACT

Laryngeal cancer is a prevalent head and neck malignancy, with poor prognosis and low survival rates for patients with advanced disease. Treatment consists of unimodal therapy through surgery or radiotherapy in early staged tumors, while advanced stage tumors are generally treated with multimodal chemoradiotherapy or (total) laryngectomy followed by radiotherapy. Still, the recurrence rate for advanced laryngeal cancer is between 25 and 50%. In order to improve surgical resection of laryngeal cancer and reduce local recurrence rates, various intraoperative optical imaging techniques have been investigated. In this systematic review, we identify these technologies, evaluating the current state and future directions of optical imaging for this indication. Narrow-band imaging (NBI) and autofluorescence (AF) are established tools for early detection of laryngeal cancer. Nonetheless, their intraoperative utility is limited by an intrinsic inability to image beyond the (sub-)mucosa. Likewise, contact endoscopy (CE) and optical coherence tomography (OCT) are technically cumbersome and only useful for mucosal margin assessment. Research on fluorescence imaging (FI) for this application is sparse, dealing solely with nonspecific fluorescent agents. Evidently, the imaging modalities that have been investigated thus far are generally unsuitable for deep margin assessment. We discuss two optical imaging techniques that can overcome these limitations and suggest how they can be used to achieve adequate margins in laryngeal cancer at all stages.

INTRODUCTION

With almost 40,000 cases in Europe in 2018 [1], laryngeal cancer is the second most common malignancy of the head and neck region. Early diagnosis and adequate preoperative assessment increase the likelihood to cure disease while preserving functionality. Outcomes for patients with early stage (T1 and T2) tumors are favorable, with cure rates of 80–90% [2,3]. More advanced staged laryngeal squamous cell carcinoma (SCC) have been reported to have recurrence rates ranging between 25 and 50% [4]. These tumors are associated with loss of laryngeal function and poor prognosis, with 5-year survival rates dropping to 40% for patients with stage IV disease [2].

In head and neck cancer, margin status remains one of the most important factors for local recurrence and overall survival, demonstrating the need to improve surgical resection. In patients undergoing (total) laryng(-opharyng)ectomy, inadequate margins are clearly associated with poor survival [5,6]. In patients that are treated with laser surgery (generally early stage laryngeal cancer), the relationship between resection margin and patient outcome is less evident. Numerous studies on laryngeal cancer produce inconsistent results with regards to margin status and local control or relapse rate [7–10]. This is caused by both post-resection and -fixation shrinkage of the tissue specimen and cauterization artefacts associated with laser carbonization, which hamper an adequate histological evaluation of the surgical margins in those cases [11]. Consequently, a positive margin on the tissue specimen may not always indicate that there are residual tumor cells in the wound bed [12].

Importantly, it was clearly demonstrated that tumor-positive additional wound bed biopsies, taken after transoral CO2 laser microsurgery (TLM) of laryngeal cancer, significantly impacted local control [12]. This finding illustrates that there is a clear clinical need for improved intraoperative margin assessment during laser surgery. Extensive wound bed sampling is no good alternative because this only allows analysis of a fraction of the wound bed, making it prone to sampling error.

In addition, margin adequacy cannot be determined from sampling the wound bed. When a total laryng(-opharyng)ectomy is performed in advanced stage laryngeal cancer, a specimen-driven analysis of the surgical margins will likely be better, as has been shown in similar cases of oral cancer surgery [13, 14]. Ideally, margin status would be assessed during surgery through less invasive and more thorough inspection measures. Improved intraoperative margin assessment may also facilitate more conservative resection during partial laryngectomies and prevent superfluous biopsies, which are important considerations in improving final functional outcome and organ preservation [11].

The surgeon's ability to distinguish between malignant and healthy tissue during laryngeal surgery remains suboptimal, elucidating the need for objective intraoperative tools for margin assessment that facilitate both specimen and wound bed evaluation. Optical imaging has long been investigated and implemented for the early diagnosis of laryngeal cancer. Over the years, a number of these imaging modalities have been suggested as intraoperative tools to facilitate real-time enhanced visualization of resection margins [15,16]. This systematic review provides an overview of the intraoperative imaging modalities that have been studied to improve surgical resection of laryngeal tumors.

MATERIALS AND METHODS

This systematic review is reported according to the Preferred Reporting Items for Systematic Reviews and Meta-Analyses (see PRISMA checklist, Supplementary Table S2), and was registered in the PROSPERO database for systematic reviews (CRD42020187479).

Literature Search and Study Selection

A systematic search was conducted in the Embase, Medline, Web of Science Core Collection, Cochrane, and Google Scholar databases. A search strategy was constructed using the terms 'laryngeal cancer' and 'intraoperative imaging'. Supplementary File S1 shows the full search strings per database. The last search was conducted on October 26, 2020. Based on the title and abstract, all clinical studies concerning intraoperative imaging techniques in laryngeal cancer surgery and diagnosis were included. Only journal articles in English with the full text available were considered. Next, articles were screened on full text for final inclusion. Articles that did not explicitly describe imaging techniques for margin assessment during laryngeal cancer surgery were excluded. Screening on title and abstract and on full text was done by two independent authors (L.J.L. and H.A.G.). Disagreements were discussed with a third author (S.K.).

Data Extraction

The following data were extracted from Tables and text: imaging technique, application of imaging technique (image-guided resection and wound bed assessment), T-stage, surgical procedure, negative margin definition, negative margin rates, extra resection rate, patient-related outcomes (recurrence rate, disease specific survival, recurrence free survival), and diagnostic outcomes (sensitivity, specificity, positive predictive value, and negative predictive value).

Quality Assessment

The 'methodological index for non-randomized studies' (MINORS) was applied to all studies in the final inclusion [17]. The MINORS is a validated methodological index for non-randomized studies in which the included studies are rated on 8 (non-comparative studies) or 12 items (comparative studies). All items can obtain a score between 0 and 2 points. A 0 points score indicates that it was not reported in the article, 1 point if it was inadequately reported, and 2 points if it was adequately reported. Hence, a maximum score of 16 (non-comparative studies) or 24 points (comparative studies) could be obtained.

RESULTS

Through the search strategies, 4128 articles were identified. A total of seven additional articles were found through snowballing. After removing duplicates, 2644 articles were screened on title and abstract. Then, 68 articles were screened on full text and 19 articles were included for qualitative assessment in the systematic review. After careful consideration, the contributions from articles with a MINORS score of 4 and lower were deemed of insufficient quality, and were excluded from the systematic review. This additional screening resulted in 18 studies for final inclusion. Supplementary File S2 shows the PRISMA flow diagram. All studies were non-randomized studies. Study characteristics and main outcomes are shown in Table 1. These studies reported on the following imaging techniques: narrow-band imaging (10), autofluorescence (3), fluorescence (2), contact endoscopy (2), and optical coherence tomography (1). MINORS-index from the included articles ranged from 5 to 19. The full MINORS of the included articles is shown in Supplementary Table S1.

Table 1. Included articles.

First author	Year	Imaging Technique[4]	Control group	Study design	T-stage	*n* = (imaging)	*n* = (control)	Surgical procedure	Application of imaging	Negative margin definition
Fiz [3]	2017	NBI	WL[2]	Retrospective	Tis-T2	311	323	TLM	Pre-resection	≥ 1 mm
Garofolo [18]	2014	NBI	WL[2]	Prospective	Tis-T1a	82	152	TLM	Pre-resection	≥ 1 mm
Hainarosie [19]	2019	NBI	WL[1]	nr	nr	23	23[1]	TLM	Post-resection	nr
Klimza [20]	2019	NBI	na	Retrospective	T1-T2	44	na	TLM	Pre-resection	≥ 5 mm
Piersiala [21]	2018	NBI	na	Prospective	T2-T3	98	na	TLM	Pre- and post-resection	≥ 3 mm
Plaat [22]	2017	NBI	WL[2]	Retrospective	Tis-T2	42	51	TLM	Pre- and post-resection	nr
Šifrer [23]	2017	NBI	WL[2]	Prospective	nr[3]	14	8	Laryngectomy	Pre- and post-resection	nr
Srivastava [24]	2016	NBI	na	Retrospective	Tis-T2	30	na	TLM	Pre-resection	nr
Vicini [25]	2015	NBI	WL	Prospective	T1-T4	7	4	Transoral surgery	Pre- and post-resection	≥ 2 mm
Zwakenberg [26]	2021	NBI	WL[1]	Prospective	Tis-T4	89	89[1]	TLM, TLE	Pre-resection	nr
Fielding [27]	2006	AF	na	Prospective	nr	48	na	TLM	Pre-resection	nr
Paczona [28]	2003	AF	WL[1]	Prospective	nr	10	10[1]	TLM	Pre- and post-resection	nr
Succo [29]	2014	AF	WL[1]	Prospective	T1-T2	73	73[1]	TLM	Pre-resection	≥ 1 mm

Table 1. Included articles. (*continued*)

First author	Year	Imaging Technique[4]	Control group	Study design	T-stage	*n* = (imaging)	*n* = (control)	Surgical procedure	Application of imaging	Negative margin definition
Csanády [30]	2004	FI (5-ALA)	na	nr	T1-T2	13	na	TLM	Pre- and post-resection	nr
Digonnet [31]	2016	FI (ICG)	na	Prospective	T1-T4	3	na	Laryngectomy	Pre- and post-resection	nr
Dedivitis [32]	2009	CE	na	Prospective	T1b-T2	10	na	Open surgery	Pre-resection	≥ 2 mm
Stefanescu [33]	2016	CE	na	nr	T1-T2	43	na	TLM	Pre-resection	nr
Shakhov [34]	2001	OCT	na	nr	Tis-T2	26	na	TLM	Pre-resection	nr

NBI = narrow-band imaging; AF = autofluorescence; FI = fluorescence imaging; 5-ALA = 5-aminolevulinic acid; ICG = indocyanine green; CE = contact endoscopy; OCT = optical coherence tomography; WL = white light; TLE = total laryngectomy; TLM = transoral laser microsurgery; na = not applicable; nr = not reported. [1]The patients served as their own controls: first the regular treatment was performed, followed by extra imaging. Based on extra imaging, extra resection was done. [2]Historical control group. [3]T-stage was not specified, but article text indicates that only patients with advanced cancer treated by laryngectomy were included. [4]For NBI, the separate outcomes are further described and compared in Table 2.

Table 2. Narrow-band imaging (NBI) trial data.

Article	T-stage	*n* = NBI[1]/WL	Negative margin rate[2] NBI (vs. WL)	Patient-related outcome NBI (vs. WL)	Diagnostic outcome NBI (vs. WL)	Other findings related to NBI
Fiz [3]	Tis-T2	311/323	50% (30%)	*RFS*[3]: 83.9% (78.9%) *DSS*[4]: 98.7% (98.8%)	nr	nr
Garofolo [18]	Tis-T1a	82/152	96.4% (76.3%)	nr	nr	nr
Hainarosie [19]	nr	23/23	98% (58.8%)	nr	nr	nr
Klimza [20]	T1-T2	44/na	100%	*Local recurrence:* 3/44: 6.8%	nr	Additional lesions not seen with WL
Piersiala [21]	T2-T3	98/na	100%	*Local recurrence:* 5/98: 5.10%	*NBI+WL:* Sens[5]: 100% Spec[6]: 98.88% PPV[7]: 90% NPV[8]: 100% Accuracy: 98.98%	Additional lesions not seen with WL in 10.2% of patients
Plaat [22]	Tis-T2	42/51	nr	*Local recurrence:* 2% (24%) *Two-year RFS:* 98% (82%)	nr	nr
Šifrer [23]	T3-T4	14/8	88.9% (70.9%)	nr	*NPV*: 95.9% (88.4%)	nr
Srivastava [24]	Tis-T2	30/na	nr	nr	nr	Upstaging TNM class

Table 2. Narrow-band imaging (NBI) trial data. (*continued*)

Article	T-stage	*n* = NBI[1]/WL	Negative margin rate[2] NBI (vs. WL)	Patient-related outcome NBI (vs. WL)	Diagnostic outcome NBI (vs. WL)	Other findings related to NBI
Vicini [25]	T1-T4	7/4	87.9% (57.9%)	nr	Sens: 72.5% Spec: 66.7% NPV: 87.9%	nr
Zwakenberg [26]	Tis-T4	89/89	nr	nr	Sens: 95% Spec: 82% PPV: 87% NPV: 92% Accuracy: 89%	5.7% increase in identified tumor extent with NBI compared to WL ($P = 0.02$)

nr = not reported; na = not applicable; WL = white light. [1] NBI: narrow-band imaging. [2] Percentage of negative resection margins obtained with NBI (vs. with WL). [3] RFS: recurrence-free survival. [4] DSS: disease-specific survival. [5] Sens: sensitivity. [6] Spec: specificity. [7] PPV: positive predictive value. [8] NPV: negative predictive value.

Intraoperative Narrow-Band Imaging

Narrow-band imaging (NBI) is an endoscopic technique that uses selective light wavelengths to visualize the abnormal vascular patterns of the mucosa associated with premalignant or neoplastic lesions. NBI uses optical filters to select blue and green light (wavelengths of 415 and 540 nm, respectively). Narrow-band blue light, because of its low penetration depth, highlights mainly the mucosal surface, making subjacent capillaries appear brown. At the same time, the narrow-band green light with its higher penetration depth, allows it to enhance visibility of vessels in the submucosa, making them appear dark green (Figure 1A, 2A–B).

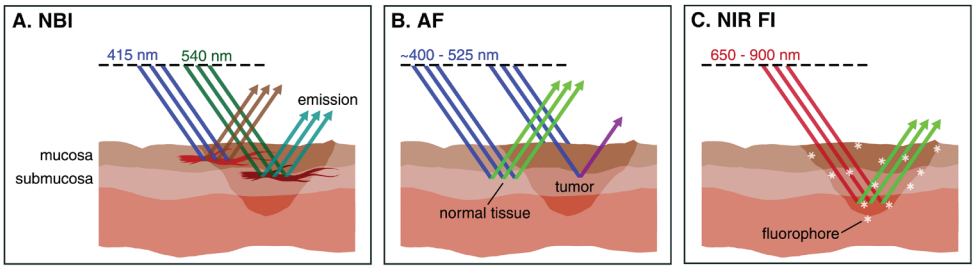

Figure 1. Schematic representation of fluorescence-based imaging working principles. (**A**) Narrow-band imaging (NBI): NBI light consists of two wavelengths: 415 nm blue and 540 nm green light. The blue light penetrates the mucosa, increasing contrast in these capillaries (appearing brown), whereas the green light reaches the submucosa, visualizing the vasculature in these deeper layers (appearing dark green). (**B**) Autofluorescence (AF) imaging: When exposed to blue light, healthy laryngeal mucosa emits green fluorescence, whereas neoplastic mucosa emits both light of lower energy (red-violet) and heat. (**C**) Near-infrared (NIR) fluorescence imaging (FI): When exposed to NIR light, previously administered fluorophores emit light of a wavelength, which is specific to the fluorophore (e.g., excitation and emission wavelengths for ICG: ~780 and 820 nm, respectively). Penetration depth of light in the NIR spectrum ranges from 0.5 to more than 10 mm, contingent to the wavelength.

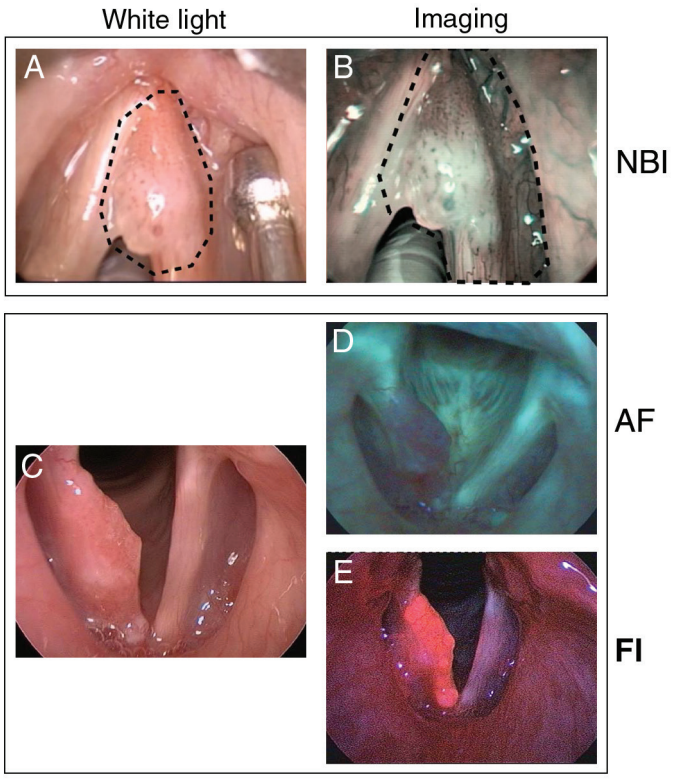

Figure 2. Clinical examples of fluorescence-based imaging modalities in laryngeal cancer. (**A**) White light image of cT1a of the anterior third of the right vocal fold and its presumptive resection margins (dotted line) compared to (**B**) Narrow-Band Imaging (NBI), showing thick dark spots typically associated with carcinoma in situ. The planned superficial resection margins of type II cordectomy (**A**) were extended on the basis thereof (**B**). (**C**) White-light laryngoscopy demonstrating a bulging small squamous cell carcinoma of the right vocal fold with extension from the anterior commissure to the vocal process. (**D**) Autofluorescence (AF) laryngoscopy shows a reddish-violet fluorescence of the cancerous right vocal fold and green fluorescence of the normal mucosa. (**E**) Protoporphyrin IX accumulates in the cancerous tissue demonstrating a bright orange-red fluorescence signal during indirect laryngoscopy. A and B are adapted and reproduced from Garofolo et al. by permission of SAGE Publications [18]. C–E are adapted and reproduced from Arens et al. by permission of Springer Nature [43].

The value of NBI during the diagnostic phase for early detection of laryngeal cancer and its precursor lesions is undisputed [35]. Various studies have demonstrated that a combination of NBI and white light (WL) endoscopy is superior to WL alone for its diagnostic capability [35–39]. Ni et al., for example, reported a diagnostic accuracy of 91% for NBI, compared with 71% for standard endoscopy [38]. Detection sensitivity of laryngeal cancer and its precursor lesions in particular is increased in multiple studies, with values ranging between 95 and 100%, confirming its ability to easily distinguish (pre)malignant from benign lesions [22,35–40]. NBI has been reported to identify malignant lesions that were missed by WL alone [26,39], and, conversely, has also been reported to reduce the amount of suspicious

lesions compared to WL [36]. NBI is redundant for diagnosing advanced tumors, as those can be adequately visualized with conventional WL endoscopy. Nevertheless, NBI can still define tumor borders with a diagnostic gain of 11% [37], which is an important quality when considering NBI for intraoperative margin assessment.

Beyond the diagnostic phase, NBI holds a lot of promise for achieving more accurate margin delineation during TLM for early glottic cancer (Table 2, 3) [41]. It has been reported that NBI was able to, statistically, significantly reduce [3,18,19,23,25], or completely prevent, the occurrence of positive superficial margins [20,21]. Overall, two studies reported the detection of additional lesions that were not seen with WL alone [20,21]. Additionally, four studies show significantly lower recurrence rates and better recurrence-free survival (RFS) with NBI as compared to WL alone [3,20–22]. The majority of studies conclude superiority of NBI over WL endoscopy in patients with early laryngeal cancer, with Klimza et al. suggesting that the added value of NBI is higher in T2 tumors, as compared to T1 tumors [20]. Then, one study included 3 patients with advanced (T3–T4) cancer, without differentiating the results according to tumor stage [25]. Despite the anatomical restraints present in the resection of advanced laryngeal tumors, Šifrer et al. reported a significantly higher rate of resection margins that were initially tumor negative in patients treated with NBI compared to their historical control group, comprising all patients previously operated by the same surgeon, before availability of NBI instrumentation [23]. The proportion of patients with T3 or T4 stage tumors, however, was not specified. Piersala et al. evaluated intraoperative NBI in patients with T2–T3 cancer, successfully achieving more accurate superficial resection margins [21]. Finally, Zwakenberg et al. recently reported that they were able to identify tumor extent by an increase of 5.7% with NBI compared to WL ($P = 0.02$) [26]. Nonetheless, these findings were not biopsy confirmed. Additionally, while this study reported inclusion of patients with Tcis-T4 tumors, the proportions were left unspecified and outcomes were not correlated with the tumor stage.

Overall, NBI was found to modify intraoperative decision-making in several ways: better visualization of tumor borders led to more secure resection margins, detection of additional lesions prompted additional biopsies, and NBI-led upstaging resulted in changes to the surgical plan [24]. With its established position in current clinical practice for early diagnosis of laryngeal cancer, NBI is the most prominently featured modality in research of optical modalities for intraoperative margin detection. An important benefit of NBI is that it is not a labeling technique requiring exogenous agents, therefore side effects or complications are of no concern, nor does it require laborious agent development. Nevertheless, NBI is specifically suited to identification of superficial carcinomas due to their aberrant vascular pattern, thus limited to detection of mucosal margins [8, 42].

Table 3. Working principles and clinical usability of all imaging techniques for intraoperative margin assessment in laryngeal cancer.

Imaging Technique	Working principle	Clinical usability for intraoperative margin assessment: pros (+) and cons (-)
Narrow-Band Imaging (NBI)	NBI uses blue (415 nm) and green (540 nm) light corresponding with the main peak absorbance of hemoglobin, to enhance visibility of mucosal and submucosal capillaries, respectively.	+ widely studied + provides real-time information + does not require exogenous agents + can be used to scan large surfaces for occult tumors + suitable for mucosal margin delineation (pre-resection) - not suitable for deep margin assessment
Autofluorescence (AF)	AF detects changes in tissue morphology and optical properties as a result of neoplasia. Using blue light, AF can differentiate between healthy and neoplastic laryngeal mucosa.	+ provides real-time information + does not require exogenous agents + can be used to scan large surfaces for occult tumors - not suitable for deep margin assessment
Fluorescence Imaging (FI)	FI uses a systemically administered fluorescent agent that 'targets' tumor cells over healthy cells. A dedicated camera system is required to detect these fluorescent agents, facilitating real-time image-guided surgery.	+ suitable for deep margin assessment (i.e., wound bed inspection) + provides real-time information + can be used to scan large surfaces for occult tumors + Near-infrared (NIR) FI has high penetration depth (up to 10 mm) - requires administration of fluorescent agents - tumor-specific fluorescent agents have not been studied in laryngeal cancer yet
Contact Endoscopy (CE)	After staining of superficial mucosal cells with methylene blue, a microscopic endoscope is placed in direct contact with the surface, distinguishing tumor from healthy cells in vivo.	+ Suitable to detect residual or recurrent cancer after radiotherapy - not suitable for deep margin assessment - requires topical staining - requires direct tissue contact - steep learning curve for image interpretation
Optical Coherence Tomography (OCT)	OCT is based on changes in refractive index of tumor cells, by detecting light that is backscattered off tissue boundaries. It is thus capable of imaging cross-sectional anatomy at high resolution in living tissue.	+ provides real-time information + does not require exogenous agents - maximum penetration depth of ~2 mm - requires direct tissue contact
Raman Spectroscopy (RS)	RS uses spectral differences between normal and malignant tissue, and is capable of near-instant, accurate and non-invasive analysis of a tissue's molecular composition.	+ able to characterize tissues other than mucosa + suitable for deep margin assessment + high specificity + does not require exogenous agents - limited to point measurements - requires direct tissue contact - does not provide real-time information (although near-instant) - Intraoperative RS for margin assessment in laryngeal cancer has not been studied yet

Intraoperative Autofluorescence Imaging

Autofluorescence (AF) is the natural fluorescence emission of tissue when exposed to light of a suitable wavelength (Table 3). AF is based on the common presence of intrinsic biomolecules acting as endogenous fluorophores [44]. Upon illumination, the electrons of a fluorophore are elevated to a higher energy level. The fluorophore is unstable in this excited state, and will rapidly revert to a slightly lower, more stable energy level by expelling heat. With some of the energy already released, the emitted light has a longer wavelength and is of lower energy than that of the illuminating light [15].

The fundamental principle of AF is related to changes in tissue morphology, optical properties, and the concentration of endogenous fluorophores in tissue as a result of neoplasia. When exposed to blue light, healthy laryngeal mucosa emits green fluorescence, whereas neoplastic mucosa fluoresces red-violet (Figure 1B, 2C–D). The advantage of AF over conventional WL endoscopy stems from the fact that (pre)malignant lesions can be differentiated from normal tissue because of decreased AF [15,16,45]. AF has previously been widely evaluated for the early diagnosis of laryngeal cancer [46], demonstrating demarcation of tumor borders and high sensitivity compared to standard technique (97.5 vs. 82.5%) [47].

In total, three clinical studies evaluate the intraoperative benefit of AF for margin assessment. Succo et al. reported high sensitivity and specificity (96.8 and 98.5%), stating an improvement in diagnostic accuracy over WL alone in 12 out of 73 cases (16.4%) [29]. Paczona et al. performed a more extensive excision based on AF in 2 of 10 cases, and reported a sensitivity and specificity of 97.4 and 60%, respectively [28]. In 2006, Fielding et al. reported the finding of additional malignant lesions in 5 out of 48 patients with laryngeal cancer, noting that AF may have potential for detecting unknown primaries and limiting the amount of sites requiring biopsies [27].

These studies suggest that direct AF can have a positive impact on disease-free survival and local control. However, more substantive studies are warranted to examine the added benefit of AF for more discrete identification of tumor presence, or positive margin reduction. AF is limited to examination of surface tissues. The illuminating light does not penetrate diseased epithelium, so that neoplastic changes within the basal mucosal layer may be hidden by epithelial hyperkeratosis. The presence of necrosis, scar tissue, bleeding, and inflammation can alter mucosal fluorescence in an unpredictable manner [15].

Intraoperative Fluorescence Imaging

Fluorescence Imaging (FI) is an emerging optical modality that facilitates intraoperative guidance aimed at complete resection of tumor tissue [48]. After systemic administration of a fluorescent agent and an appropriate dispersion time interval, FI is performed real-time using an intraoperative camera system (Figure 1C, 2C, E).

The application of FI for intraoperative margin detection in laryngeal cancers is thus far underexplored. A 2004 trial reported a sensitivity of 96% for 5-aminolevulinic acid-induced protoporphyrin-IX (5-ALA Pp-IX) fluorescence in the control of pharyngo-laryngeal cancer [30]. In this study including 13 patients with T1–T2 laryngeal cancer, Pp-IX fluorescence better visualized the borderline of superficial neoplastic tissue, facilitating more precise diagnosis and excision.

The attenuating effects of light scattering, non-specific autofluorescence and absorption are relatively low for fluorescence in the near-infrared (NIR) range [49]. In a study on the use of intravenous administration of NIR agent indocyanine green (ICG) for therapeutic lymph node dissection, Digonnet et al. briefly described primary tumor examination 3 patients with laryngeal cancer, reporting a fluorescent signal in 2 patients [31]. FI with tumor-specific NIR fluorescent agents has not yet been investigated in laryngeal cancer (Table 3).

Contact Endoscopy

Contact endoscopy (CE) is a technique that allows for in vivo visualization in cellular detail. After staining superficial cells of the mucosa with methylene blue, a microscopic endoscope is placed in direct contact with the surface, providing images of the suspected area at x60 or x150 magnification (Figure 3A–B, Table 3). Contact laryngomicroscopy is a non-invasive method capable of obtaining detailed information of cells and blood vessels in the live epithelium without biopsy, distinguishing malignant from benign tissue. CE has been shown to detect post-radiotherapy residual and recurrent cancer in the upper aerodigestive tract with similar sensitivity and specificity compared to in non-irradiated tissues [50].

CE has been studied for the detection of microscopic margins during surgery in 10 patients with early glottic SCC, yielding histopathologically confirmed complete excision (negative margins defined as ≥ 2 mm) by Dedivitis et al., without local recurrence after a minimum follow-up period of 5 years [32]. This survival benefit in early laryngeal cancer patients is promising, but needs confirmation from larger scale, adequately powered studies. A more recent study in 43 patients with T1–T2 vocal fold carcinoma finds a similar, if slightly lower, negative resection rate for CE compared to frozen sections after histopathological examination of paraffin sections: 92 vs. 98.3% [33]. While these results are indicative of its reliability for early laryngeal cancer, studies including patients with advanced laryngeal lesions are absent. Additionally, CE requires topical staining and is associated with considerable instrumentation costs, requires a steep learning curve for the interpretation of the vascular network, and is solely capable of characterizing the superficial layers of the mucosa [51].

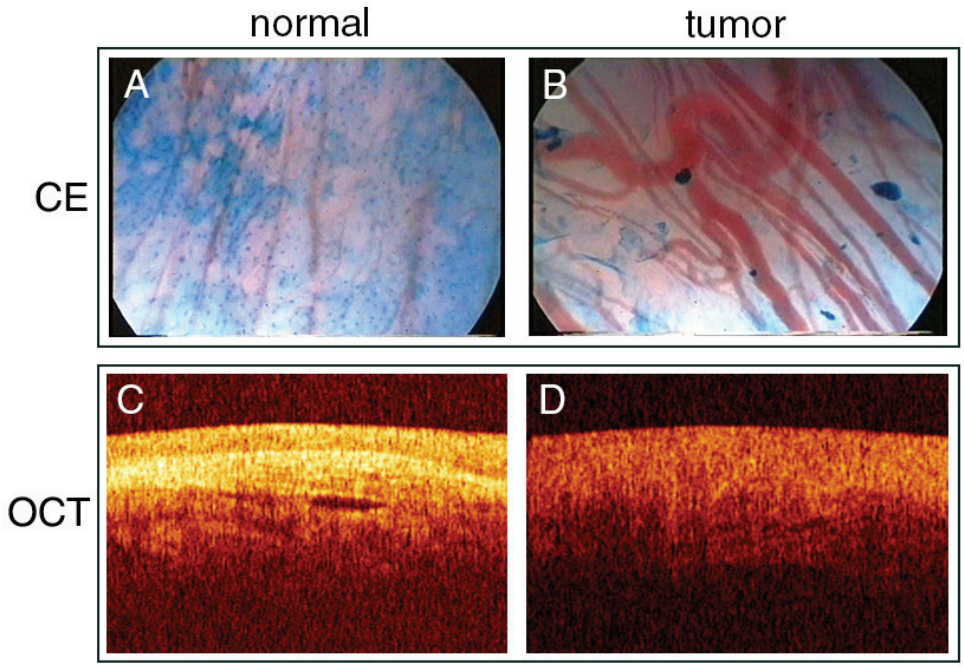

Figure 3. Clinical examples of contact endoscopy (CE) and optical coherence tomography (OCT) in laryngeal cancer. (**A**) Normal vascular network of the vocal fold in CE. (**B**) Vascular network of the vocal fold carcinoma in CE. (**C**) OCT image of healthy portion of larynx. (**D**) OCT image of exophytic tumor of larynx. A and B were adapted and reproduced from Stefanescu et al. (CC BY 4.0) [33]. C and D were adapted and reproduced from Sergeev et al. (CC BY 4.0) [52].

Optical Coherence Tomography

Optical coherence tomography (OCT) is the optical counterpart of ultrasound, and is capable of imaging cross-sectional anatomy at high resolutions in living tissue (Figure 3C–D, Table 3). OCT is based on changes in refractive index, by detecting light that is backscattered off tissue boundaries [15]. It is a noninvasive imaging method that allows in vivo use, provides real time information, and does not cause any side effects.

OCT has only been studied for intraoperative margin assessment during TLM by Shakhov et al. in 26 patients with early laryngeal carcinoma [34]. While they reported tumor margins extending beyond those seen with WL alone, no data were provided on diagnostic accuracy.

DISCUSSION

There is a paucity of trials that analyze intraoperative imaging as a surgical adjunct during procedures for laryngeal cancer. The diagnostic value of NBI and AF in early laryngeal cancer is known. Their intraoperative application as an aid in defining surgical margins has

not yet been studied as extensively, with most data available on NBI in this setting. As NBI visualization is limited to microvascular changes of the (sub)mucosa, evaluation of deep margin infiltration is impossible. Nevertheless, some recent studies report encouraging results of intraoperative NBI in patients with moderate-advanced laryngeal tumors. Distinct from intraoperative margin assessment, an interesting application for NBI is the follow-up of patients with early to moderate stage glottic cancer after curative treatment. Witkiewicz et al. recently reported that NBI after TLM is a good predictor of margin positivity, supporting clinical decision-making regarding the need for second-look surgery [53]. NBI during outpatient transnasal endoscopy was found to be an excellent follow-up tool of laryngeal cancer patients after radiotherapy to screen for recurrent disease [54]. Still, caution is warranted in the interpretation of NBI images. Post-radiotherapy nonspecific inflammation often presents as brownish spots similar to those that are typical for early cancer, and may thus be mistaken for recurrence [39,55]. More clinical studies are required to make conclusive statements about NBI for TLM of moderate-advanced laryngeal tumors. AF has been demonstrated to be useful in early laryngeal cancer detection, although intrinsic mucosal fluorescence can unpredictably be altered by numerous tissue properties [15].

Both OCT and CE are associated with various technical impracticalities. CE requires topical staining and is only able to clearly image the superficial layers of the epithelium [45]. Previous ex vivo and probe-based in vivo diagnostic efforts using OCT for laryngeal cancer have demonstrated the technique's performance in distinguishing normal from cancerous tissue [52,56–59]. Nevertheless, its maximum penetration depth of ~2 mm restricts its use to peripheral margin assessment. This inherent limited applicability likely explains the apparent shortage of studies using AF, OCT, and CE for intraoperative margin assessment in the larynx. This systematic evaluation of imaging techniques for intraoperative margin assessment reveals a prevailing incompatibility of the studied modalities in their utility for advanced stage laryngeal cancer, primarily attributable to imaging depth limitations. Furthermore, our assessment based on the MINORS criteria has revealed that the methodology and scientific evidence of a sizable portion of included studies are of suboptimal quality (Table S1). In view of this apparent research gap, it may be useful to investigate other, more widely applicable imaging techniques to improve surgical resection of both early and advanced laryngeal cancer.

Although only 2 studies employing FI for margin assessment were identified, laryngeal cancer surgery might be amenable to the more prevailing developments in FI. An important advantage of FI is that it can be used to scan large surfaces. In addition to the possibility to image fluorescence at considerable depths and tissues other than the mucosa, FI is thus ideally suited for wound bed inspection and detection of clinically occult lesions. An interesting area to explore for FI would be to identify suitable tumor-specific tracers for intraoperative imaging of early to advanced laryngeal cancer [60]. Previous research on the diagnostic value of FI for laryngeal cancer is scarce, and, thus far, only features 5-ALA and ICG [46,61,62].

While these agents are easily available and FDA-approved, they are both nonspecific. Furthermore, 5-ALA-induced Pp-IX fluorescence is outside the NIR-range, such that the signal is prone to significant interference due to the tissue's optical characteristics [30]. The compatibility of FI with CO2 laser surgery in head and neck cancer was recently validated by Odenthal and colleagues [63]. In vitro and preclinical results from this study suggest the effectiveness of fluorescence-guided surgery (FGS) using NIR dyes. Moreover, they demonstrated that laser cauterization and its associated autofluorescence are unlikely to interfere with the fluorescence signal of the injected tumor-specific tracer. Additionally, FI for intraoperative margin assessment in head and neck cancers is currently a prolific field of research, with numerous phase I/II trials on oral cancer completed and ongoing (Figure 4) [64–67]. Oral cancer is well-suited to FGS, as the oral cavity is easily accessible to the NIR camera. However, with the rapidly evolving FI cameras it is only a matter of time before FGS can be adopted to treat a wider variety of cancers. This notwithstanding, tumor-specific FI is still under development and not without pitfalls. Signal processing for FI is complex, and objective evaluation and quantification of both fluorescence and its influencing factors is challenging [49]. Development of suitable fluorescent agents is costly and time-consuming, with a lot of work left before regulatory approval and clinical implementation can be realized. Altogether, yet undiscovered potential for FI in laryngeal cancer surgery at all stages is strongly hinted at, encouraging dedicated research for this indication.

As per the confines of this systematic review, there currently is no real-time application for Raman spectroscopy (RS) in margin assessment of laryngeal cancer. However, its demonstrated potential for both in and ex vivo tissue discrimination is worth noting. RS is a technique based on spectral differences between normal and malignant tissue, and is capable of near-instant, accurate, and non-invasive analysis of a tissue's molecular composition (Table 3). In oral cancer specimen, water concentration analysis with RS has been demonstrated to objectively localize tumor borders [68]. The capacity of RS to differentiate tumor from healthy cells has been thoroughly demonstrated using laryngeal tissue samples, producing significant differences in Raman spectra between malignant and normal tissue [69–72]. Bergholt et al. were the first to demonstrate the feasibility of RS in transnasal endoscopic applications [73]. In their 2012 study, they acquired near-instant information of the endogenous biomolecular tissue composition from the larynx in healthy subjects, using a fiber-optic Raman probe. In 2016, Lin et al. conducted a similar study for in vivo probe-based RS during endoscopic examination, reporting improved diagnosis [74]. In a recent study of Stimulated Raman Scattering (SRS), Zhang et al. demonstrate the efficacy of deep-learning based SRS microscopy for margin assessment through simulated resection margins on completely removed larynx specimen [75]. Contrary to NBI and AF, RS is able to characterize tissue other than the mucosa. This is an important advantage allowing for post-resection assessment of tumor extension in the deep plane [8]. Nonetheless, RS is limited to point measurements, requiring direct tissue contact. As wide-field imaging is impossible, RS cannot be employed to screen for occult lesions and second primary tumors, and resection guidance and complete

wound bed inspection are not currently feasible. The strength of RS lies in its application for specimen-driven margin assessment, at uniquely high specificity.

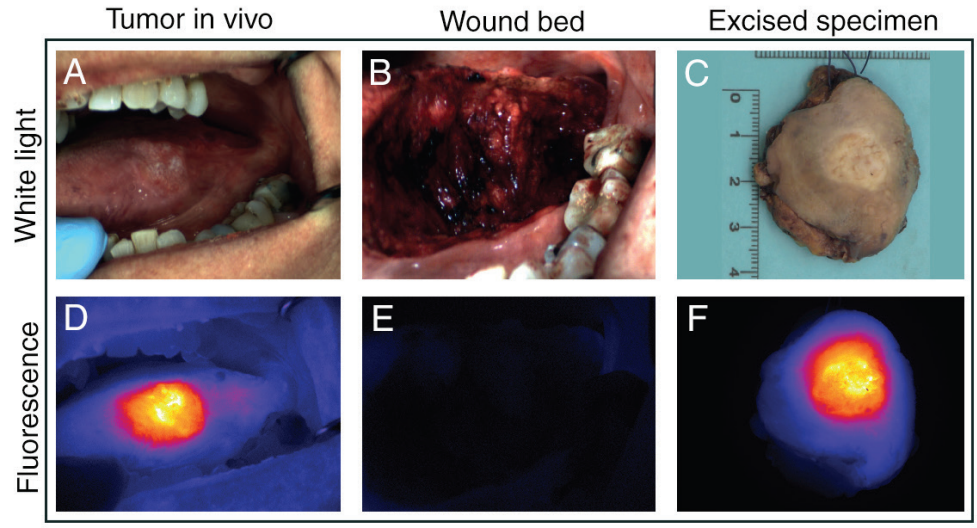

Figure 4. FI using pH-activatable nanoprobe ONM-100 in head and neck squamous cell carcinoma of the tongue. In vivo (**A,B,D,E**) and ex vivo (**C,F**) visualization of high fluorescence signal in the tumor and low fluorescence signal in tumor-free margin and wound bed. Adapted and reproduced from Voskuil et al. (CC BY 4.0) [67].

CONCLUSIONS

The demonstrated effectiveness of NBI in the early diagnosis has led to reasonable evidence for its application in intraoperative margin detection, although inclusion of patients with T3–T4 laryngeal cancer is rare. An important disadvantage remains the technique's intrinsic inability to image structures other than the (sub-)mucosa. Similar limitations hold for AF, OCT, and CE. Finally, FI has scarcely been studied for intraoperative margin assessment in laryngeal cancer. Indeed, one might need to consider optical imaging advancements in adjacent anatomical regions and similar applications to gain insight into which modalities warrant further exploration in achieving adequate margins. NIR FI with tumor-specific fluorescent agents and RS are emerging technologies that overcome many of the limitations associated with NBI, AF, CE, and OCT. With evidence supporting their value in assessing tumor depth infiltration, we believe it is worthwhile to pursue their clinical development for margin assessment in laryngeal cancer.

REFERENCES

1. Bray, F., et al., *Global cancer statistics 2018: GLOBOCAN estimates of incidence and mortality worldwide for 36 cancers in 185 countries*. CA Cancer J. Clin. **2018**, 68, 394–424.
2. Obid, R.; Redlich, M.; Tomeh, C. *The Treatment of Laryngeal Cancer.* Oral Maxillofac. Surg. Clin. North Am. **2019**, 31, 1–11, doi:10.1016/j.coms.2018.09.001.
3. Fiz, I., et al., *Impact of Close and Positive Margins in Transoral Laser Microsurgery for Tis–T2 Glottic Cancer.* Front. Oncol. **2017**, 7, 245, doi:10.3389/fonc.2017.00245.
4. Brandstorp-Boesen, J., et al., *Risk of Recurrence in Laryngeal Cancer.* PLOS ONE **2016**, 11, e0164068, doi:10.1371/journal.pone.0164068.
5. Tassone, P., et al., *Association of Positive Initial Margins With Survival Among Patients With Squamous Cell Carcinoma Treated With Total Laryngectomy.* JAMA Otolaryngol. Neck Surg. **2018**, 144, 1030, doi:10.1001/jamaoto.2018.1095.
6. Zhu, X., et al., *A prognostic nomogram for predicting risk of recurrence in laryngeal squamous cell carcinoma patients after tumor resection to assist decision making for postoperative adjuvant treatment.* J. Surg. Oncol. **2019**, 120, 698–706, doi:10.1002/jso.25614.
7. Saraniti, C., et al., *Prognostic role of resection margin in open oncologic laryngeal surgery: survival analysis of a cohort of 139 patients affected by squamous cell carcinoma.* Braz. J. Otorhinolaryngol. **2019**, 85, 603–610, doi:10.1016/j.bjorl.2018.04.012.
8. Sjögren, E. *Transoral Laser Microsurgery in Early Glottic Lesions.* Curr. Otorhinolaryngol. Rep. **2017**, 5, 56–68, doi:10.1007/s40136-017-0148-2.
9. Chiesa-Estomba, C.M., et al., *CO2 Transoral Laser Microsurgery in Benign, Premalignant and Malignant (Tis, T1, T2) Lesion of the Glottis. A Literature Review.* Med. **2019**, 6, 77, doi:10.3390/medicines6030077.
10. Michel, J., et al., *Prognostic value of the status of resection margins after endoscopic laser cordectomy for T1a glottic carcinoma.* Eur. Ann. Otorhinolaryngol. Head Neck Dis. **2011**, 128, 297–300, doi:10.1016/j.anorl.2011.05.006.
11. Fiz, I.; Koelmel, J.C.; Sittel, C. *Nature and role of surgical margins in transoral laser microsurgery for early and intermediate glottic cancer.* Curr. Opin. Otolaryngol. Head Neck Surg. **2018**, 26, 78–83, doi:10.1097/moo.0000000000000446.
12. Hendriksma, M., et al., *Evaluation of surgical margin status in patients with early glottic cancer (Tis-T2) treated with transoral CO2 laser microsurgery, on local control.* Eur. Arch. Oto-Rhino-Laryngology **2018**, 275, 2333–2340, doi:10.1007/s00405-018-5070-9.
13. Amit, M., et al., *Improving the rate of negative margins after surgery for oral cavity squamous cell carcinoma: A prospective randomized controlled study.* Head Neck **2016**, 38, E1803–E1809, doi:10.1002/hed.24320.
14. Van Lanschot, C.G., et al., *Relocation of inadequate resection margins in the wound bed during oral cavity oncological surgery: A feasibility study.* Head Neck **2019**, 41, 2159–2166, doi:10.1002/hed.25690.
15. Hughes, O.R., et al., *Optical and molecular techniques to identify tumor margins within the larynx.* Head Neck **2010**, 32, 1544–1553, doi:10.1002/hed.21321.
16. Mannelli, G.; Cecconi, L.; Gallo, O. *Laryngeal preneoplastic lesions and cancer: challenging diagnosis. Qualitative literature review and meta-analysis.* Crit. Rev. Oncol. **2016**, 106, 64–90, doi:10.1016/j.critrevonc.2016.07.004.
17. Slim, K., et al., *Methodological index for non-randomized studies (MINORS): development and validation of a new instrument.* ANZ J. Surg. **2003**, 73, 712–716, doi:10.1046/j.1445-2197.2003.02748.x.

18. Garofolo, S., et al., *Intraoperative Narrow Band Imaging Better Delineates Superficial Resection Margins During Transoral Laser Microsurgery for Early Glottic Cancer.* Ann. Otol. Rhinol. Laryngol. **2014**, 124, 294–298, doi:10.1177/0003489414556082.
19. Hainăroșie, R., et al., *The utility of Narrow Band Imaging in obtaining disease free resection margins during endo-scopic surgery of the larynx.* Romanian Biotechnol. Lett. **2019**, 24, 360–365, doi:10.25083/rbl/24.2/360.365.
20. Klimza, H., et al., *The role of intraoperative narrow-band imaging in transoral laser microsurgery for early and moderately advanced glottic cancer.* Braz. J. Otorhinolaryngol. **2019**, 85, 228–236, doi:10.1016/j.bjorl.2018.01.004.
21. Piersiala, K., et al., *Narrow band imaging in transoral laser microsurgery (TLM) in moderately advanced (T2, T3) glottic cancer.* Otolaryngol. Polska **2018**, 72, 17–23, doi:10.5604/01.3001.0012.0486.
22. Plaat, B.E.C., et al., *Narrow-band imaging in transoral laser surgery for early glottic cancer in relation to clinical outcome.* Head Neck **2017**, 39, 1343–1348, doi:10.1002/hed.24773.
23. Šifrer, R., et al., *The assessment of mucosal surgical margins in head and neck cancer surgery with narrow band imaging.* Laryngoscope **2017**, 127, 1577–1582, doi:10.1002/lary.26405.
24. Srivastava, R. *Narrow band imaging during transoral laser surgery for premalignant and early malignant glottic lesions.* J. Head Neck Physicians Surg. **2016**, 4, 35, doi:10.4103/2347-8128.182849.
25. Vicini, C., et al., *A novel approach emphasising intra-operative superficial margin enhancement of head-neck tumours with narrow-band imaging in transoral robotic surgery.* Acta Otorhinolaryngol. Ital. **2015**, 35, 157–161.
26. Zwakenberg, M.A., et al., *Evaluating Laryngopharyngeal Tumor Extension Using Narrow Band Imaging Versus Conventional White Light Imaging.* Laryngoscope **2021**, doi:10.1002/lary.29361.
27. Fielding, D., et al., *DAFE autofluorescence assessment of oral cavity, larynx and bronchus in head and neck cancer patients.* Photodiagnosis Photodyn. Ther. **2006**, 3, 259–265, doi:10.1016/j.pdpdt.2006.07.004.
28. Paczona, R.; Marandas, P.; Luboinski, B. *Autofluorescence videoendoscopy for photodiagnosis of head and neck squamous cell carcinoma.* Eur. Arch. Oto-Rhino-Laryngology **2003**, 260, 544–548, doi:10.1007/s00405-003-0635-6.
29. Succo, G., et al., *Direct autofluorescence during CO2 laser surgery of the larynx: can it really help the surgeon?* Acta Otorhinolaryngol. Ital. **2014**, 34, 174–183.
30. Czigner, J., et al., *ALA (5-aminolevulinic acid)-induced protoporphyrin IX fluorescence in the endoscopic diagnostic and control of pharyngo-laryngeal cancer.* Eur. Arch. Oto-Rhino-Laryngology **2003**, 261, 262–266, doi:10.1007/s00405-003-0660-5.
31. Digonnet, A., et al., *Near infrared fluorescent imaging after intravenous injection of indocyanine green during neck dissection in patients with head and neck cancer: A feasibility study.* Head Neck **2015**, 38, E1833–E1837, doi:10.1002/hed.24331.
32. Dedivitis, R.A.; Pfuetzenreiter Jr, E.G.; Guimaraes, A.V. C*ontact endoscopy of the larynx as an auxiliary method to the surgical margins in frontolateral laryngectomy.* Acta Otorhinolaryngol Ital **2009**, 29, 16–20.
33. Stefanescu, D.C., et al., *The Use of Methylene Blue in Assessing Disease Free Margins During CO2 LASER Assisted Direct Laryngoscopy for Glottis Cancer.* Revista De Chimie **2016**, 67, 1327-1328.
34. Shakhov, A.V., et al., *Optical coherence tomography monitoring for laser surgery of laryngeal carcinoma.* J. Surg. Oncol. **2001**, 77, 253–258, doi:10.1002/jso.1105.
35. Kraft, M., et al., *Value of narrow band imaging in the early diagnosis of laryngeal cancer.* Head Neck **2015**, 38, 15–20, doi:10.1002/hed.23838.

36. Popek, B., et al., *Clinical experience of narrow band imaging (NBI) usage in diagnosis of laryngeal lesions.* Otolaryngol. Polska **2019**, 73, 18–23, doi:10.5604/01.3001.0013.3401.
37. Bertino, G., et al., *Effectiveness of narrow band imaging in the detection of premalignant and malignant lesions of the larynx: Validation of a new endoscopic clinical classification.* Head Neck **2014**, 37, 215–222, doi:10.1002/hed.23582.
38. Ni, X.-G.; Zhang, Q.-Q.; Wang, G.-Q. *Narrow band imaging versus autofluorescence imaging for head and neck squamous cell carcinoma detection: a prospective study.* J. Laryngol. Otol. **2016**, 130, 1001–1006, doi:10.1017/s0022215116009002.
39. Sikka, K., et al., *Role of narrow band imaging in the diagnosis of laryngeal lesions: Pilot study from India.* Indian J. Cancer **2018**, 55, 242–247, doi:10.4103/ijc.ijc_590_17.
40. Kimza, H.; Jackowska, J.; Wierzbicka, M. *The usefulness of the NBI – narrow band imaging for the larynx assessment.* Otolaryngol. Polska **2018**, 72, 1–5, doi:10.5604/01.3001.0011.7253.
41. Campo, F., et al., *The Prognostic Value of Adding Narrow-Band Imaging in Transoral Laser Microsurgery for Early Glottic Cancer: A Review.* Lasers Surg. Med. **2020**, 52, 301–306, doi:10.1002/lsm.23142.
42. Robbins, K.T., et al., *Surgical margins in head and neck cancer: Intra- and postoperative considerations.* Auris Nasus Larynx **2019**, 46, 10–17, doi:10.1016/j.anl.2018.08.011.
43. Arens, C., et al., *Indirect fluorescence laryngoscopy in the diagnosis of precancerous and cancerous laryngeal lesions.* Eur. Arch. Oto-Rhino-Laryngology **2007**, 264, 621–626, doi:10.1007/s00405-007-0251-y.
44. Croce, A.; Bottiroli, G. *Autofluorescence spectroscopy and imaging: a tool for biomedical research and diagnosis*. Eur. J. Histochem. **2014**, 58, 2461, doi:10.4081/ejh.2014.2461.
45. Tibbetts, K.M.; Tan, M. *Role of Advanced Laryngeal Imaging in Glottic Cancer.* Otolaryngol. Clin. North Am. **2015**, 48, 565–584, doi:10.1016/j.otc.2015.04.004.
46. Kraft, M., et al., *Value of fluorescence endoscopy for the early diagnosis of laryngeal cancer and its precursor lesions.* Head Neck **2010**, 33, 941–948, doi:10.1002/hed.21565.
47. Saetti, R., et al., *Efficacy of autofluoroscence videoendoscopy in the diagnosis of laryngeal lesions.* Acta Otorhinolaryngol. Ital. **2007**, 27, 181–185.
48. Vahrmeijer, A.L., et al., *Image-guided cancer surgery using near-infrared fluorescence.* Nat. Rev. Clin. Oncol. **2013**, 10, 507–518, doi:10.1038/nrclinonc.2013.123.
49. Keereweer, S., et al., *Optical Image-Guided Cancer Surgery: Challenges and Limitations.* Clin. Cancer Res. **2013**, 19, 3745–3754, doi:10.1158/1078-0432.ccr-12-3598.
50. Kumar, S., et al., *Contact endoscopy for detection of residual or recurrent disease after radiotherapy for squamous cell carcinoma of the upper aerodigestive tract*. J. Laryngol. Otol. **2020**, 134, 344–349, doi:10.1017/s0022215120000651.
51. Mishra, A., et al., *Contact Endoscopy - A promising tool for evaluation of laryngeal mucosal lesions.* J. Laryngol. Voice **2012**, 2, 53, doi:10.4103/2230-9748.106978.
52. Sergeev, A.M., et al., *In vivo endoscopic OCT imaging of precancer and cancer states of human mucosa.* Opt. Express **1997**, 1, 432–440, doi:10.1364/oe.1.000432.
53. Witkiewicz, J., et al., *The usefulness of the narrow band imaging (NBI) in decision-making process regarding second look procedure (SL) in laryngeal cancer follow-up after transoral laser microsurgery.* PLOS ONE **2020**, 15, e0236623, doi:10.1371/journal.pone.0236623.
54. Zabrodsky, M., et al., *The Role of Narrow Band Imaging in the Detection of Recurrent Laryngeal and Hypopharyngeal Cancer after Curative Radiotherapy.* BioMed Res. Int. **2014**, 2014, 1–9, doi:10.1155/2014/175398.
55. Wang, W.-H., et al., *Detection of Mucosal Recurrent Nasopharyngeal Carcinomas After Radiotherapy With Narrow-Band*

Imaging Endoscopy. Int. J. Radiat. Oncol. **2012**, 83, 1213–1219, doi:10.1016/j.ijrobp.2011.09.034.

56. Bibas, A., et al., *3-D optical coherence tomography of the laryngeal mucosa*. Clin. Otolaryngol. 2004, 29, 713–720, doi:10.1111/j.1365-2273.2004.00902.x.
57. Kraft, M., et al., *Technique of Optical Coherence Tomography of the Larynx During Microlaryngoscopy.* Laryngoscope **2007**, 117, 950–952, doi:10.1097/mlg.0b013e318038166d.
58. Burns, J.A. *Optical coherence tomography*. Curr. Opin. Otolaryngol. Head Neck Surg. **2012**, 20, 477–481, doi:10.1097/moo.0b013e3283582d7d.
59. Englhard, A.S., et al., *Intraoperative assessment of laryngeal pathologies with optical coherence tomography integrated into a surgical microscope.* Lasers Surg. Med. **2017**, 49, 490–497, doi:10.1002/lsm.22632.
60. Odenthal, J., et al., *Targeting CD44v6 for fluorescence-guided surgery in head and neck squamous cell carcinoma.* Sci. Rep. **2018**, 8, 1–11, doi:10.1038/s41598-018-28059-9.
61. Schmidt, F., et al., *Feasibility of real-time near-infrared indocyanine green fluorescence endoscopy for the evaluation of mucosal head and neck lesions*. Head Neck **2016**, 39, 234–240, doi:10.1002/hed.24570.
62. Mehlmann, M., et al., *Fluorescence staining of laryngeal neoplasms following topical application of 5-aminolevulinic acid: preliminary results*. Biomedical Optics **1999**, 25, 414–420,, doi:10.1364/bio.1999.ctue1.
63. Odenthal, J.; Friedl, P.; Takes, R.P. *Compatibility of CO 2 laser surgery and fluorescence detection in head and neck cancer cells*. Head Neck **2019**, 41, 1253–1259, doi:10.1002/hed.25547.
64. Moore, L.S., et al., *Characterizing the Utility and Limitations of Repurposing an Open-Field Optical Imaging Device for Fluorescence-Guided Surgery in Head and Neck Cancer Patients*. J. Nucl. Med. **2016**, 58, 246–251, doi:10.2967/jnumed.115.171413.
65. Nishio, N., et al., *Optimal Dosing Strategy for Fluorescence-Guided Surgery with Panitumumab-IRDye800CW in Head and Neck Cancer.* Mol. Imaging Biol. **2020**, 22, 156–164, doi:10.1007/s11307-019-01358-x.
66. Rosenthal, E.L., et al., *Safety and Tumor Specificity of Cetuximab-IRDye800 for Surgical Navigation in Head and Neck Cancer.* Clin. Cancer Res. **2015**, 21, 3658–3666, doi:10.1158/1078-0432.ccr-14-3284.
67. Voskuil, F.J., et al., *Fluorescence-guided imaging for resection margin evaluation in head and neck cancer patients using cetuximab-800CW: A quantitative dose-escalation study.* Theranostics **2020**, 10, 3994–4005, doi:10.7150/thno.43227.
68. Barroso, E.M., et al., *Water Concentration Analysis by Raman Spectroscopy to Determine the Location of the Tumor Border in Oral Cancer Surgery*. Cancer Res. **2016**, 76, 5945–5953, doi:10.1158/0008-5472.can-16-1227.
69. Lau, D.P., et al., *Raman spectroscopy for optical diagnosis in the larynx: Preliminary findings.* Lasers Surg. Med. **2005**, 37, 192–200, doi:10.1002/lsm.20226.
70. Pujary, P.; Maheedhar, K.; C, M.K.; Pujary, K. *Raman Spectroscopic Methods for Classification of Normal and Malignant Hypopharyngeal Tissues: An Exploratory Study*. Pathol. Res. Int. **2011**, 2011, 1–9, doi:10.4061/2011/632493.
71. Teh, S.K., et al., *Spectroscopic diagnosis of laryngeal carcinoma using near-infrared Raman spectroscopy and random recursive partitioning ensemble techniques*. Anal. **2009**, 134, 1232–1239, doi:10.1039/b811008e.
72. Stone, N., et al., *Raman Spectroscopy for Early Detection of Laryngeal Malignancy: Preliminary Results.* Laryngoscope **2000**, 110, 1756–1763, doi:10.1097/00005537-200010000-00037.
73. Bergholt, M.S., et al., *In vivo, real-time, transnasal, image-guided Raman endoscopy: defining spectral properties in the nasophar-*

ynx and larynx. J. Biomed. Opt. **2012**, 17, 077002, doi: 10.1117/1.JBO.17.7.077002.

74. Lin, K., et al., *Real-time in vivo diagnosis of laryngeal carcinoma with rapid fiber-optic Raman spectroscopy.* Biomed. Opt. Express **2016**, 7, 3705–3715, doi:10.1364/boe.7.003705.

75. Zhang, L., et al., *Rapid histology of laryngeal squamous cell carcinoma with deep-learning based stimulated Raman scattering microscopy.* Theranostics **2019**, 9, 2541–2554, doi:10.7150/thno.32655.

SUPPLEMENTARY MATERIALS

Supplementary File S1 Search Strategy

Intraoperative imaging for laryngeal cancer

Database searched	via	Years of coverage	References	After de-duplication
Embase	Embase.com	1971 - Present	2166	2146
Medline ALL	Ovid	1946 - Present	907	140
Web of Science Core Collection	Web of Knowledge	1975 - Present	754	156
Cochrane Central Register of Controlled Trials	Wiley	1992 - Present	101	54
Other sources: Google Scholar (ranked on relevance)			200	141
Total			**4128**	**2637**

Embase.com

('epiglottis tumor'/exp OR 'larynx tumor'/exp OR 'larynx'/exp OR (((epiglott* OR larynx* OR microlaryng* OR laryng* OR glott* OR postcricoid* OR subglot* OR supraglot* OR vocal-cord*) NEAR/6 (cancer* OR carcinoma* OR tumor* OR tumour* OR neoplas* OR papilloma* OR granuloma* OR lesion* OR malignan* OR premalignan* OR leukoplak* OR dysplas* OR surg* OR operat*))):ab,ti,kw) AND ('narrow band imaging'/de OR 'autofluorescence'/de OR 'Raman spectrometry'/de OR 'coherent anti Stokes Raman spectroscopy'/de OR 'fluorescence'/de OR 'confocal microscopy'/exp OR 'fluorescent dye'/de OR 'white light'/de OR (((narrowband* OR narrow-band*) NEAR/3 (imag*)) OR autofluorescence* OR auto-fluorescence* OR intrinsic-fluorescence* OR native-fluorescence* OR ((fluorescen* OR imag*) NEAR/3 guided) OR ((light* OR optical* OR molecular*) NEAR/3 (imag*)) OR near-infrared OR tracer* OR target* OR dye* OR probe* OR raman* OR confocal* OR ((contact*) NEAR/3 (endomicroscop* OR microscop* OR endoscop*))):ab,ti,kw) AND ('intraoperative period'/de OR 'intraoperative monitoring'/de OR 'surgery'/exp OR 'surgery':lnk OR 'laryngoscopy'/exp OR (intraoperativ* OR intra-operativ* OR intrasurg* OR surg* OR real-time* OR margin* OR microsurg* OR laryngoscop* OR microlaryngoscop*):ab,ti,kw)

Medline

(Laryngeal Neoplasms/ OR Granuloma, Laryngeal/ OR (((epiglott* OR larynx* OR microlaryng* OR laryng* OR glott* OR postcricoid* OR subglot* OR supraglot* OR vocal-cord*) ADJ6 (cancer* OR carcinoma* OR tumor* OR tumour* OR neoplas* OR papilloma* OR granuloma* OR lesion* OR malignan* OR premalignan* OR leukoplak* OR dysplas* OR surg* OR operat*))).ab,ti,kf.) AND (Optical Imaging/ OR Narrow Band Imaging/ OR autofluorescence/ OR Fluorescence/ OR Microscopy, Confocal/ OR Fluorescent Dyes/ OR (((narrowband* OR narrow-band*) ADJ3 (imag*)) OR autofluorescence* OR auto-fluorescence* OR intrinsic-fluorescence* OR native-fluorescence* OR ((fluorescen* OR imag*) ADJ3 guided) OR ((light* OR optical* OR molecular*) ADJ3 (imag*)) OR near-infrared OR tracer* OR target* OR dye* OR probe* OR raman* OR confocal* OR ((contact*) ADJ3 (endomicroscop* OR microscop* OR endoscop*))).ab,ti,kf.) AND (exp Intraoperative Period/ OR Monitoring, Intraoperative/ OR exp Surgical Procedures, Operative/ OR surgery.fs. OR Laryngoscopy/ OR (intraoperativ* OR intra-operativ* OR intrasurg* OR surg* OR real-time* OR margin* OR microsurg* OR laryngoscop* OR microlaryngoscop*).ab,ti,kf.)

Web of Science

TS=(((((epiglott* OR larynx* OR microlaryng* OR laryng* OR glott* OR postcricoid* OR subglot* OR supraglot* OR vocal-cord*) NEAR/5 (cancer* OR carcinoma* OR tumor* OR tumour* OR neoplas* OR papilloma* OR granuloma* OR lesion* OR malignan* OR premalignan* OR leukoplak* OR dysplas* OR surg* OR operat*)))) AND ((((narrowband* OR narrow-band*) NEAR/2 (imag*)) OR autofluorescence* OR auto-fluorescence* OR intrinsic-fluorescence* OR native-fluorescence* OR ((fluorescen* OR imag*) NEAR/2 guided) OR ((light* OR optical* OR molecular*) NEAR/2 (imag*)) OR near-infrared OR

tracer* OR target* OR dye* OR probe* OR raman* OR confocal* OR ((contact*) NEAR/2 (endomicroscop* OR microscop* OR endoscop*)))) AND ((intraoperativ* OR intra-operativ* OR intrasurg* OR surg* OR real-time* OR margin* OR microsurg* OR laryngoscop* OR microlaryngoscop*)))

Cochrane Central

((((epiglott* OR larynx* OR microlaryng* OR laryng* OR glott* OR postcricoid* OR subglot* OR supraglot* OR vocal NEXT cord*) NEAR/6 (cancer* OR carcinoma* OR tumor* OR tumour* OR neoplas* OR papilloma* OR granuloma* OR lesion* OR malignan* OR premalignan* OR leukoplak* OR dysplas* OR surg* OR operat*)):ab,ti,kw) AND ((((narrowband* OR narrow NEXT band*) NEAR/3 (imag*)) OR autofluorescence* OR auto NEXT fluorescence* OR intrinsic NEXT fluorescence* OR native NEXT fluorescence* OR ((fluorescen* OR imag*) NEAR/3 guided) OR ((light* OR optical* OR molecular*) NEAR/3 (imag*)) OR "near infrared" OR tracer* OR target* OR dye* OR probe* OR raman* OR confocal* OR ((contact*) NEAR/3 (endomicroscop* OR microscop* OR endoscop*))):ab,ti,kw) AND ((intraoperativ* OR intra NEXT operativ* OR intrasurg* OR surg* OR real NEXT time* OR margin* OR microsurg* OR laryngoscop* OR microlaryngoscop*):ab,ti,kw)

Google Scholar

"epiglottis|larynx|laryngeal cancer|carcinoma|tumor|tumour|neoplasm" "narrow band imaging"|"optical|molecular imaging"|autofluorescence|"auto|intrinsic|native fluorescence" |tracer|target|dye|probe|raman|confocal intraoperative

Extra search string: Embase.com + head and neck tumor

('epiglottis tumor'/exp OR 'larynx tumor'/exp ***OR 'head and neck tumor'/de*** OR (((epiglott* OR larynx* OR microlaryng* OR laryng* OR glott* OR postcricoid* OR subglot* OR supraglot* OR vocal-cord*) NEAR/6 (cancer* OR carcinoma* OR tumor* OR tumour* OR neoplas* OR papilloma* OR granuloma* OR lesion* OR malignan* OR premalignan* OR leukoplak* OR dysplas* OR surg* OR operat*)):ab,ti,kw) AND ('narrow band imaging'/de OR 'autofluorescence'/de OR 'Raman spectrometry'/de OR 'coherent anti Stokes Raman spectroscopy'/de OR 'fluorescence'/de OR 'confocal microscopy'/exp OR 'fluorescent dye'/de OR (((narrowband* OR narrow-band*) NEAR/3 (imag*)) OR autofluorescence* OR auto-fluorescence* OR intrinsic-fluorescence* OR native-fluorescence* OR ((fluorescen* OR imag*) NEAR/3 guided) OR ((light* OR optical* OR molecular*) NEAR/3 (imag*)) OR near-infrared OR tracer* OR target* OR dye* OR probe* OR raman* OR confocal* OR ((contact*) NEAR/3 (endomicroscop* OR microscop* OR endoscop*))):ab,ti,kw) AND ('intraoperative period'/de OR 'intraoperative monitoring'/de OR 'surgery'/exp OR 'surgery':lnk OR (intraoperativ* OR intra-operativ* OR intrasurg* OR surg* OR real-time* OR margin* OR microsurg* OR laryngoscop* OR microlaryngoscop*):ab,ti,kw)

Supplementary File S2 PRISMA 2020 flow diagram for new systematic

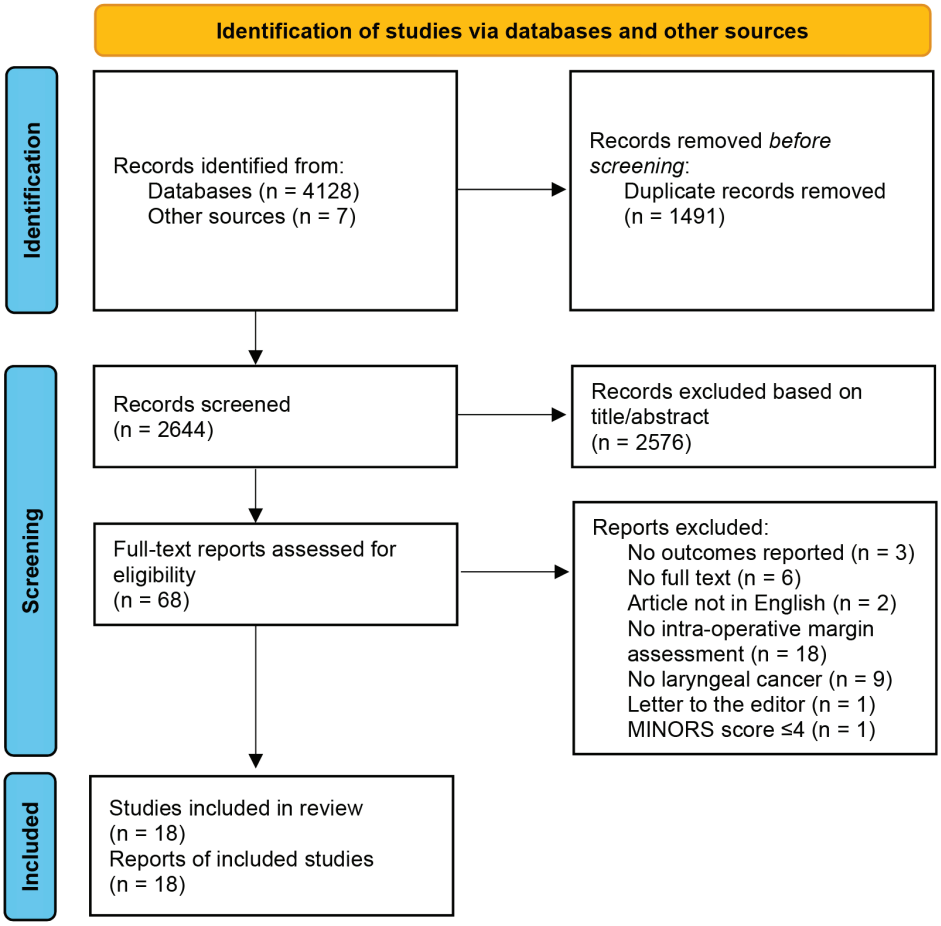

From: Page MJ, McKenzie JE, Bossuyt PM, Boutron I, Hoffmann TC, Mulrow CD, et al. The PRISMA 2020 statement: an updated

guideline for reporting systematic reviews. BMJ 2021;372:n71. doi: 10.1136/bmj.n71

For more information, visit www.prisma-statement.org.

Supplementary Table S2 – PRISMA 2020 Checklist



Supplementary Table S2 - PRISMA 2020 Checklist

Section and Topic	Item #	Checklist item	Location where item is reported
TITLE			
Title	1	Identify the report as a systematic review.	1
ABSTRACT			
Abstract	2	See the PRISMA 2020 for Abstracts checklist.	1
INTRODUCTION			
Rationale	3	Describe the rationale for the review in the context of existing knowledge.	2
Objectives	4	Provide an explicit statement of the objective(s) or question(s) the review addresses.	2
METHODS			
Eligibility criteria	5	Specify the inclusion and exclusion criteria for the review and how studies were grouped for the syntheses.	3, Supplementary File S2
Information sources	6	Specify all databases, registers, websites, organisations, reference lists and other sources searched or consulted to identify studies. Specify the date when each source was last searched or consulted.	2
Search strategy	7	Present the full search strategies for all databases, registers and websites, including any filters and limits used.	Supplementary File S1
Selection process	8	Specify the methods used to decide whether a study met the inclusion criteria of the review, including how many reviewers screened each record and each report retrieved, whether they worked independently, and if applicable, details of automation tools used in the process.	3
Data collection process	9	Specify the methods used to collect data from reports, including how many reviewers collected data from each report, whether they worked independently, any processes for obtaining or confirming data from study investigators, and if applicable, details of automation tools used in the process.	3
Data items	10a	List and define all outcomes for which data were sought. Specify whether all results that were compatible with each outcome domain in each study were sought (e.g. for all measures, time points, analyses), and if not, the methods used to decide which results to collect.	3
	10b	List and define all other variables for which data were sought (e.g. participant and intervention characteristics, funding sources). Describe any assumptions made about any missing or unclear information.	3
Study risk of bias assessment	11	Specify the methods used to assess risk of bias in the included studies, including details of the tool(s) used, how many reviewers assessed each study and whether they worked independently, and if applicable, details of automation tools used in the process.	3, Supplementary Table S1
Effect measures	12	Specify for each outcome the effect measure(s) (e.g. risk ratio, mean difference) used in the synthesis or presentation of results.	3
Synthesis methods	13a	Describe the processes used to decide which studies were eligible for each synthesis (e.g. tabulating the study intervention characteristics and comparing against the planned groups for each synthesis (item #5)).	3
	13b	Describe any methods required to prepare the data for presentation or synthesis, such as handling of missing summary statistics, or data conversions.	n/a
	13c	Describe any methods used to tabulate or visually display results of individual studies and syntheses.	n/a
	13d	Describe any methods used to synthesize results and provide a rationale for the choice(s). If meta-analysis was performed, describe the model(s), method(s) to identify the presence and extent of statistical heterogeneity, and software package(s) used.	n/a
	13e	Describe any methods used to explore possible causes of heterogeneity among study results (e.g. subgroup analysis, meta-regression).	n/a
	13f	Describe any sensitivity analyses conducted to assess robustness of the synthesized results.	n/a
Reporting bias	14	Describe any methods used to assess risk of bias due to missing results in a synthesis (arising from reporting biases).	n/a



Supplementary Table S2 - PRISMA 2020 Checklist

Section and Topic	Item #	Checklist item	Location where item is reported
assessment			
Certainty assessment	15	Describe any methods used to assess certainty (or confidence) in the body of evidence for an outcome.	n/a
RESULTS			
Study selection	16a	Describe the results of the search and selection process, from the number of records identified in the search to the number of studies included in the review, ideally using a flow diagram.	5, Supplementary File S2
	16b	Cite studies that might appear to meet the inclusion criteria, but which were excluded, and explain why they were excluded.	3
Study characteristics	17	Cite each included study and present its characteristics.	5-10, Table 1,2
Risk of bias in studies	18	Present assessments of risk of bias for each included study.	3, Supplementary Table S1
Results of individual studies	19	For all outcomes, present, for each study: (a) summary statistics for each group (where appropriate) and (b) an effect estimate and its precision (e.g. confidence/credible interval), ideally using structured tables or plots.	5-10, Table 2,3
Results of syntheses	20a	For each synthesis, briefly summarise the characteristics and risk of bias among contributing studies.	5-10
	20b	Present results of all statistical syntheses conducted. If meta-analysis was done, present for each the summary estimate and its precision (e.g. confidence/credible interval) and measures of statistical heterogeneity. If comparing groups, describe the direction of the effect.	n/a
	20c	Present results of all investigations of possible causes of heterogeneity among study results.	n/a
	20d	Present results of all sensitivity analyses conducted to assess the robustness of the synthesized results.	n/a
Reporting biases	21	Present assessments of risk of bias due to missing results (arising from reporting biases) for each synthesis assessed.	n/a
Certainty of evidence	22	Present assessments of certainty (or confidence) in the body of evidence for each outcome assessed.	n/a
DISCUSSION			
Discussion	23a	Provide a general interpretation of the results in the context of other evidence.	10-12
	23b	Discuss any limitations of the evidence included in the review.	10-12
	23c	Discuss any limitations of the review processes used.	10-12
	23d	Discuss implications of the results for practice, policy, and future research.	10-12
OTHER INFORMATION			
Registration and protocol	24a	Provide registration information for the review, including register name and registration number, or state that the review was not registered.	2-3, CRD42020187479
	24b	Indicate where the review protocol can be accessed, or state that a protocol was not prepared.	2-3, CRD42020187479
	24c	Describe and explain any amendments to information provided at registration or in the protocol.	n/a
Support	25	Describe sources of financial or non-financial support for the review, and the role of the funders or sponsors in the review.	13

Supplementary Table S2 - PRISMA 2020 Checklist

Section and Topic	Item #	Checklist item	Location where item is reported
Competing interests	26	Declare any competing interests of review authors.	13
Availability of data, code and other materials	27	Report which of the following are publicly available and where they can be found: template data collection forms; data extracted from included studies; data used for all analyses; analytic code; any other materials used in the review.	n/a

From: Page MJ, McKenzie JE, Bossuyt PM, Boutron I, Hoffmann TC, Mulrow CD, et al. The PRISMA 2020 statement: an updated guideline for reporting systematic reviews. BMJ 2021;372:n71. doi: 10.1136/bmj.n71
For more information, visit: http://www.prisma-statement.org/

Supplementary Table S3 - MINORS Score

Study	Cumulative MINORS score	Maximum MINORS score	Clearly stated aim	Consecutive patients	Prospective data collection	Appropriate endpoint	Unbiased evaluation of endpoints	Appropriate follow-up	Loss to follow-up	Prospective calculation of sample size	Gold Standard control	Contemporary groups	Baseline equivalence of groups	Statistical analysis adapted to study design
Fiz[3]	17	24	2	2	1	2	0	2	1	0	2	1	2	2
Garofolo[18]	18	24	2	2	1	2	0	2	2	0	2	1	2	2
Hainarosie[19]	9	24	0	0	0	1	0	2	2	0	2	1	1	0
Klimza[20]	11	16	2	2	1	2	0	2	2	0	na	na	na	na
Piersiala[21]	12	16	2	2	2	2	0	2	2	0	na	na	na	na
Plaat[22]	17	24	2	2	1	1	0	2	2	0	2	1	2	2
Šifrer[23]	18	24	2	2	2	0	2	2	2	0	2	1	2	1
Srivastava[24]	7	16	0	2	1	0	0	2	2	0	na	na	na	na
Vicini[25]	17	24	2	1	1	2	0	2	2	0	2	2	2	1
Zwakenberg[26]	20	24	2	0	2	2	2	2	2	0	2	2	2	2
Fielding[27]	10	16	2	1	2	1	0	2	2	0	na	na	na	na
Paczona[28]	10	24	2	0	2	0	0	0	2	0	2	1	1	0
Succo[29]	15	24	2	1	2	2	0	2	2	0	2	1	1	0
Csanády[30]	6	16	1	0	0	1	0	2	2	0	na	na	na	na
Digonnet[31]	10	16	1	2	2	1	0	2	2	0	na	na	na	na
Dedivitis[32]	9	16	2	0	2	1	0	2	2	0	na	na	na	na
Stefanescu[33]	7	16	2	0	0	1	0	2	2	0	na	na	na	na
Shakhov[34]	5	16	1	0	0	0	0	2	2	0	na	na	na	na


3

Chapter 3

Fluorescence-guided surgery in colorectal cancer; a review on clinical results and future perspectives

Hidde A. Galema* & Ruben P. J. Meijer*, Lorraine J. Lauwerends, Cornelis Verhoef, Jacobus Burggraaf, Alexander L. Vahrmeijer, Merlijn Hutteman, Stijn Keereweer* & Denise E. Hilling*

*Both authors contributed equally to the manuscript

European Journal of Surgical Oncology. 2022 Apr;48(4):810-821.

ABSTRACT

Background: Colorectal cancer is the fourth most diagnosed malignancy worldwide and surgery is one of the cornerstones of the treatment strategy. Near-infrared (NIR) fluorescence imaging is a new and upcoming technique, which uses an NIR fluorescent agent combined with a specialised camera that can detect light in the NIR range. It aims for more precise surgery with improved oncological outcomes and a reduction in complications by improving discrimination between different structures. *Methods:* A systematic search was conducted in the Embase, Medline and Cochrane databases with search terms corresponding to 'fluorescence-guided surgery', 'colorectal surgery', and 'colorectal cancer' to identify all relevant trials. *Results:* The following clinical applications of fluorescence guided surgery for colorectal cancer were identified and discussed: (1) tumour imaging, (2) sentinel lymph node imaging, (3) imaging of distant metastases, (4) imaging of vital structures, (5) imaging of perfusion. Both experimental and FDA/EMA approved fluorescent agents are debated. Furthermore, promising future modalities are discussed. *Conclusion:* Fluorescence-guided surgery for colorectal cancer is a rapidly evolving field. The first studies show additional value of this technique regarding change in surgical management. Future trials should focus on patient related outcomes such as complication rates, disease free survival, and overall survival.

INTRODUCTION

Colorectal cancer (CRC) is globally the fourth most common malignancy and the second cause of cancer related mortality with over 550 000 deaths annually[1]. In most CRC patients, surgery remains the cornerstone of treatment. Complete surgical resection of the tumour is associated with better overall survival and lower recurrence rates[2, 3]. Minimal invasive surgery, laparoscopic or robot-assisted, is increasingly used in the last two decades. Despite it its advantages, this application also brought new technical challenges as it lacks tactile feedback for tumour identification and identification of vital structures. These challenges sparked the interest in novel intraoperative visualisation techniques, such as near-infrared (NIR) fluorescence imaging.

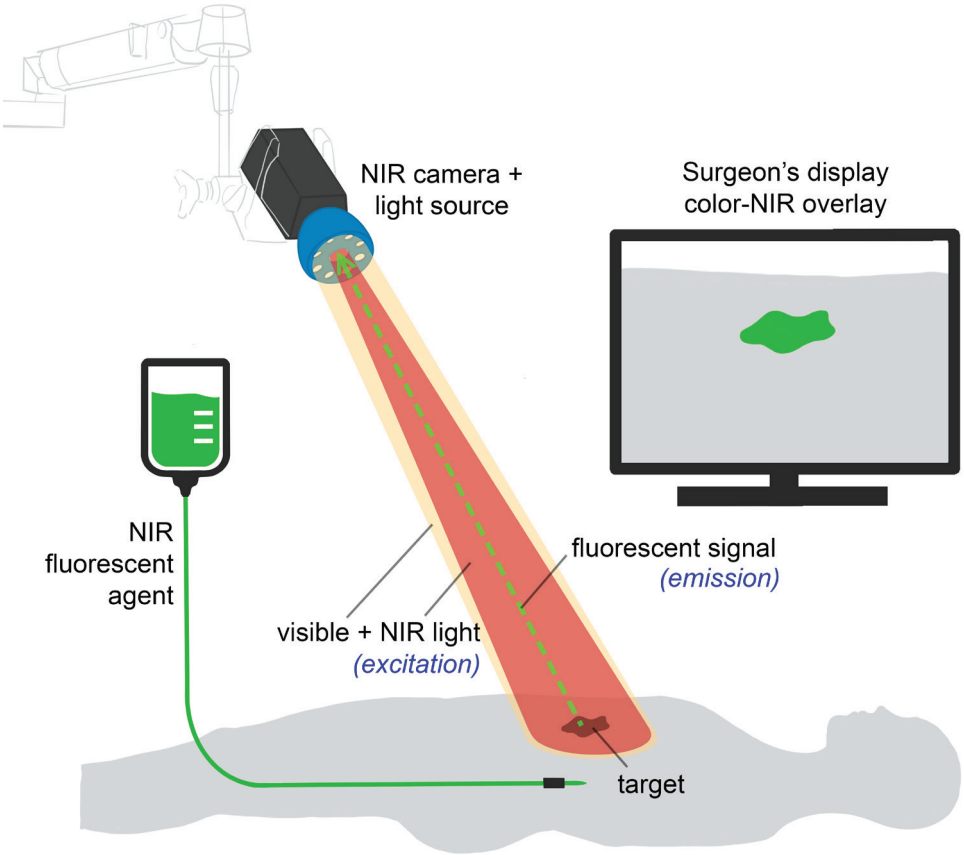

Figure 1. The basic principles of fluorescence-guided surgery NIR fluorescent agents are administered intravenously or locally. Imaging of the agent is performed using a fluorescence imaging system. Besides a white light source and camera, this system includes a dedicated NIR excitation light, collection optics and filtration, and a camera dedicated to NIR fluorescence emission light. NIR fluorescence output is displayed on a screen in the operating theatre. A simultaneous visible light image, which can be merged with the NIR fluorescence image, is desirable.

NIR fluorescence imaging is a real-time imaging technique that combines a NIR fluorescent agent with a specialised imaging system (figure 1). These systems can capture light emitted by a fluorescent agent after excitation with an appropriate light source (figure 2). NIR light (650-900 nm) is favourable for intraoperative imaging compared to visible light because of its better depth penetration in tissue (up to 10 mm). Moreover, the fluorescent agents will not interfere with the standard surgical field, as the human eye is unable to detect light within these NIR wavelengths.

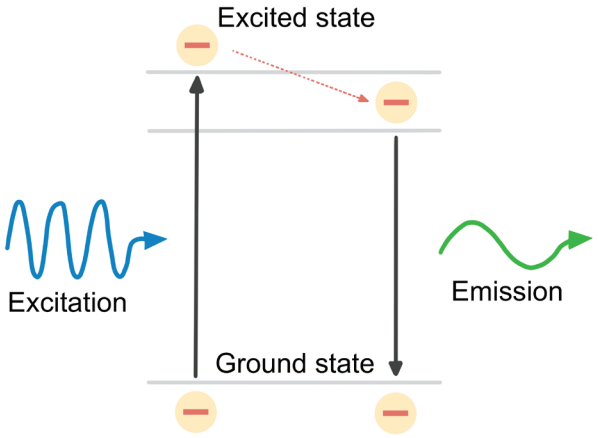

Figure 2. The basic principles of fluorescence (print in color) Photons emitted by the fluorescence imaging system are absorbed by the fluorescent agent. Subsequently, the electrons within the agent transition from their ground state to an excited state, and back to their ground state. During this last step, a photon with a lower wavelength than the photon from the imaging system, is emitted as the energy from the electron gets released. This emitted fluorescence signal is captured by the dedicated fluorescence camera.

NIR fluorescent agents are predominantly injected intravenously and can be divided into two groups: targeted (binding to a specific ligand or activated by the tumour-specific environment) and non-targeted. Currently, various targeted fluorescent agents are tested in phase I-III clinical trials[4]. In the group of non-targeted agents, indocyanine green (ICG) and methylene blue (MB) are approved by the United States Food and Drug Administration (FDA) and the European Medicines Agent (EMA), for other purposes. ICG was first used in 1957 to determine hepatic function, but its fluorescent properties (excitation peak around 800 nm), and hence other applications, became known decades later[5]. MB on the other hand, is predominantly cleared renally and has its excitation peak around 700 nm[6]. Both agents have been proven to be safe for fluorescence utilisation.

There are many applications for NIR fluorescence imaging during colorectal surgery. This review provides an overview of the currently available clinical applications and promising future modalities of fluorescence-guided surgery in the treatment of CRC patients.

METHODS

Due to heterogeneity in available literature and study phases between the several subjects, this study was not fully conducted according to the PRISMA guidelines.

Literature search and selection criteria

A systematic search was conducted in the Embase, Medline and Cochrane databases with search terms corresponding to 'fluorescence-guided surgery', 'colorectal surgery', and 'colorectal cancer'. The search strategy was expanded with terms to identify articles reporting on vital structure imaging and colorectal metastases. Supplement 1 shows the search strategies per database and its corresponding hits. The last search was conducted on December 21st, 2020. All articles were independently screened based on title and abstract by two authors (HG and RM). Next, full article screening and reference screening was performed. Inconsistencies were discussed with an additional author (DH). Regarding experimental fluorescent agents, all clinical studies were included in the final reference list. Regarding ICG and MB, the final reference list was generated based on the quality of the article and the amount of scientific evidence available per subject. Articles on the following subjects were included: fluorescence-guided surgery for CRC for the imaging of the primary tumour, lymph nodes, metastases (peritoneal, liver, extra-abdominal), vital structures (nerve, ureter, urethra), and perfusion (anastomosis, omentoplasty). Only articles in English and published after the year 2000 were considered.

Data extraction

The following data was extracted: tumour type, fluorescent agent, fluorescence imaging application, (optimal) dose, (optimal) dosing interval, optimal TBR, sensitivity, specificity, change in surgical management, and other outcomes.

Quality assessment

Quality assessment was performed for all studies assessing experimental fluorescent agents. The Methodological index for non-randomized studies (MINORS score) was used for quality assessment. A total score of 16 (for non-comparative studies) or 24 (for comparative studies) could be obtained[7].

RESULTS

A total of 14 completed clinical studies (Supplement 2) and 8 ongoing trials (Supplement 3) assessing experimental fluorescent agents for CRC surgery were identified. Figure 3 gives an overview of all clinical applications of FGS for CRC, with the assessed fluorescent agents (table 1). All 14 clinical studies regarding experimental fluorescence agents had a MINORS score of 11 or higher (Supplement 4).

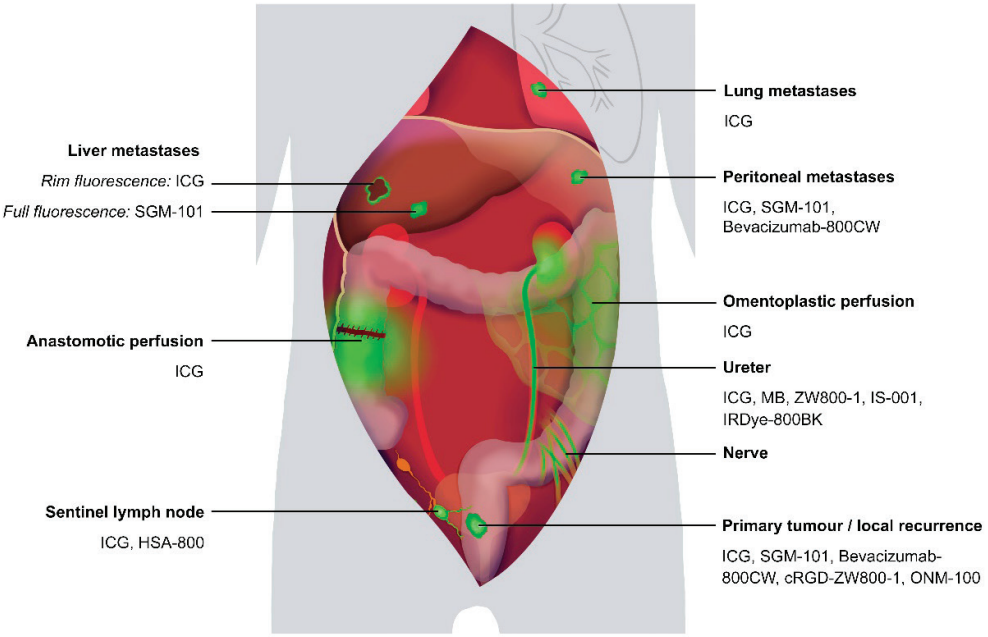

Figure 3. A schematic overview of all clinical applications of fluorescence guided surgery for colorectal cancer
Abbreviations: ICG indocyanine green, MB Methylene blue

Table 1. overview of all fluorescent agents used for colorectal cancer surgery and their optical properties

Fluorescent Agent	Molecular target	Fluorophore	~Peak absorbance wavelength	~Peak emission wavelength	Ref.
Bevacizumab-800CW	VEGF-A	IRDye-800CW	778 nm	794 nm	21
cRGD-ZW800-1	Integrins (αvβ6, αvβ3, αvβ5)	ZW800-1	785 nm	805 - 850 nm	69
HSA800	na	IRDye-800CW	778 nm	795 nm	21
ICG	na	ICG	780 nm	830 nm	5
IRDye-800BK	na	IRDye-800BK	774 nm	790 nm	72
IS-001	na	IS-001	780 nm	815 nm	70
LUM015	Cathepsins (K, L, S, B)	Cy5	650 nm	675 nm	22
MB	na	MB	667 nm	685 nm	6
ONM-100	Metabolic acidosis*	ICG	780 nm	830 nm	5
SGM-101	CEA	BM-104	685 nm	705 nm	19
ZW800-1	na	ZW800-1	785 nm	805 - 850 nm	69

*Activated in a tumour-specific PH-environment

Abbreviations: VEGF-A vascular endothelial growth factor alpha | nm nanometre | ICG indocyanine green | MB methylene blue | CEA carcinoembryonic antigen | na not applicable

Imaging of the primary tumour and local recurrence

Achieving tumour-negative resection margins is of utmost importance in the surgical treatment of CRC patients, as tumour-positive resection margins are associated with a significant decrease in overall survival[2, 8]. Tumour-positive resection margins are reported in 5% of all colon cancer cases, but occur more frequently with increasing tumour stage, with an occurrence of up to 14% in T4 colon cancer[2]. Moreover, in primary locally advanced rectal cancer the proportion of tumour-positive resection margins is 28%[8]. This rate is even higher in patients with recurrent rectal cancer, where up to 50% tumour-positive resection margins are reported[9]. These high rates in recurrent rectal cancer are likely a consequence of the distorted anatomy and treatment related fibrosis after previous resection and (re-) neoadjuvant treatment. Tumour identification is challenging in these cases due to the difficult distinction (both visual and tactile) between fibrosis and residual tumour tissue.

Preoperative endoscopic tattooing with India ink, a permanent marker injected distal to the tumour, is the current standard of care for intraoperative tumour identification in CRC, with an accuracy rate of 70-88%[10, 11]. However, India ink can leak into the abdominal cavity and thereby interfere with the surgical procedure.

In 2009, the first NIR fluorescence imaging technique to identify the primary tumour in CRC was introduced by injecting ICG peritumoural via endoscopy. It has a high tumour identification rate (100%) and minimal adverse events[12, 13]. However, a major drawback is the relatively rapid clearance of ICG, as detection rates tend to decrease two to seven days after injection[12]. Therefore, patients must undergo an additional endoscopy in the week before surgery, in contrast to the conventional injection of India ink that can be administered at the initial, diagnostic colonoscopy. Because of these drawbacks, peritumoural ICG injection has not been widely implemented for tumour identification. Moreover, this technique will not improve the tumour-negative resection margin rates because it does not differentiate between tumour tissue and benign surrounding tissue, nor does it enable the detection of additional lesions. A potential solution is the use of fluorescent agents that specifically bind to tumour cells.

The number of tumour-targeted fluorescent agents has substantially increased in the past two decades. The use of these agents is aimed to achieve complete tumour resection. This should lead to a decrease in the number of tumour-positive resection margins, detection of additional lesions and avoid unnecessary removal of benign tissue. To quantify fluorescence intensity, most studies use the signal-to-background ratio (SBR) or tumour-to-background ratio (TBR). This is a ratio of the mean fluorescence intensity of the tumour and the surrounding tissue (background). A TBR of at least 1.5 and preferably 2.0 is deemed sufficient for tumour identification. Currently, four tumour-targeted fluorescent agents have been tested in early phase clinical studies for CRC and have shown promising results: SGM-101, cRGD-ZW800-1, bevacizumab-800CW, and ONM-100[14-18].

SGM-101 consists of a monoclonal antibody targeting the carcinoembryonic antigen (CEA) bound to the fluorophore BM-104[19]. A phase II study of 37 patients showed an intraoperative TBR of 1.9. Importantly, based on fluorescence assessment, the surgical plan was changed in 9 (24%) patients. In 7 patients, fluorescence led to resection of malignant lesions that were not identified with white light only. In two patients, clinically suspected but non-fluorescent tissue was proven to be benign, which resulted in a less extensive resection[18]. These promising results have led to the initiation of 2 phase III trials using SGM-101 (NCT03659448, NCT04642924).

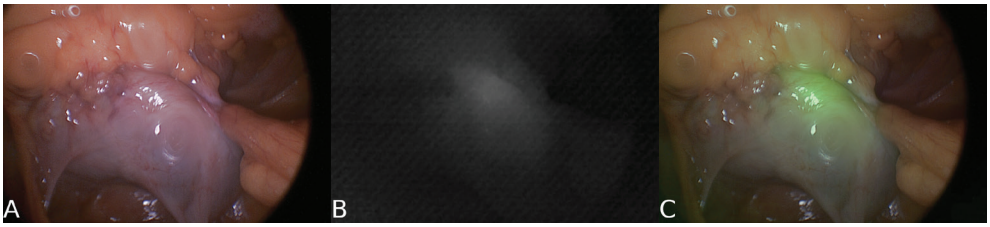

Fig. 4. Fluorescence imaging results of primary colon cancer. Intraoperative fluorescence imaging result of an adenocarcinoma of the ascending colon (TBR 1.6) using cRGD-ZW800-1. Imaging was performed using the Quest Spectrum laparoscopic imaging system. It shows an image in white light (A), near-infrared (B) and merge of A and B (C).

cRGD-ZW800-1 is a cyclic pentapeptide (cRGD) conjugated to the 800 nm zwitterionic NIR fluorophore ZW800-1. It targets various integrins that have been shown to be overexpressed on colorectal tumour cells. In the first-in-human study, 12 colon cancer patients were included. Intraoperative fluorescence imaging of the primary tumour was feasible in both open and minimal invasive surgeries (figure 4). The highest mean TBR of 1.6 was found in the highest dosing of 0.05 mg/kg[15].

Bevacizumab-800CW consists of a monoclonal antibody targeting vascular endothelial growth factor A (VEGF-A), bound to IRDye800CW[20, 21]. Bevacizumab-800CW has been studied in eight rectal cancer patients[16]. During back table fluorescence assessment of the resection margins on the surgical specimen, a tumour-positive margin was correctly identified in one out of two patients. In the six patients with a tumour-negative resection margin, one (17%) showed a false-positive signal.

ONM-100 is a pH-activatable fluorescent agent that exploits the metabolic microenvironment of solid tumours[17]. It does not bind to specific tumour receptors but is activated in the acidic tumour environment. It is a conjugation of a pH-sensitive nanoparticle to ICG, which becomes fluorescent in environments with a pH below 6.9. Thirty patients were studied with this agent, of which three underwent surgery for CRC. All three CRC patients showed a sharply demarcated fluorescent signal during back table imaging. Currently, a

phase II study using ONM-100 is ongoing in which patients undergoing surgery for CRC are also included (NCT03735680).

A phase I/II trial will be conducted using LUM015, a novel PEGylated protease-activated fluorescent imaging agent targeting cathepsins, which play a crucial role in mammalian cell turnover[22]. The first results of this study, which focuses on intraoperative imaging of CRC, are expected in 2021 (NCT02584244).

Altogether, these early phase clinical trials have shown that tumour-targeted fluorescence imaging is a feasible addition to CRC surgery. The fluorescent agents detected most of the known tumours and SGM-101 even detected additional lesions, which were not detected in white light. To assess the impact on patient related outcomes, future studies should focus on clinical endpoints like tumour-negative resection margin rate and change in surgical management.

Imaging of the sentinel lymph node

Adequate lymph node staging in CRC patients is crucial; it is an important prognostic feature and determines the need for (neo)adjuvant chemotherapy and/or radiotherapy. The sentinel lymph node (SLN) may be crucial in nodal staging, as it is defined as the first lymph node draining the tumour and is believed to be the first place for lymphogenic metastases. Moreover, one in three patients with stage I and II colon cancer, who are staged as lymph node-negative, still develop distant metastases[23]. This might be a consequence of understaging by histopathology, due to lymph nodes with occult malignant cells and micrometastases. Currently, a single paraffin embedded slide per lymph node is reviewed during routine histopathological analysis, increasing the chance of missing tumour cells away from the slide's cutting edge. More extensive histopathological analysis of all resected lymph nodes would improve nodal staging, but this process is time-consuming and expensive[24]. Extensive analysis of only the SLN is feasible, and thus unfolds a niche for SLN mapping in CRC. Moreover, tumour-negative SLNs create an opportunity for endoscopic or local resection of early stage tumours[25].

A reason for the absence of SLN mapping in the routine treatment of CRC patients might be a consequence of so-called skip metastases that are reported in up to 22% the patients[26]. In these cases, malignant cells are absent in the SLN, but present in other regional lymph nodes. Moreover, the use of blue dye for SLN mapping in CRC appears limited due to its minimal depth penetration in the mesocolic and mesorectal fat[27]. Therefore, the interest in fluorescent dyes, especially the peritumoural injection of ICG, has increased. These fluorescent dyes have already shown to be of additional value for the identification of complete lymph drainage patterns, including aberrant flow[28, 29]. Nevertheless, the identification of only the SLN would be a valuable addition.

Various techniques have been used in studies assessing fluorescence-guided SLN mapping in CRC. Agent administration and SLN mapping can be performed before or during the procedure (*in vivo*) or after resection (*ex vivo*). Although *ex vivo* imaging might be easier to adapt in the current surgical or pathological workflow, it has drawbacks. Most importantly, *ex vivo* injection of an agent and identification of the SLN lacks the possibility of finding SLNs in patients with aberrant lymph node drainage patterns[30]. Another technical consideration is the site of injection. For *in vivo* SLN mapping, submucosal injection is done endoscopically, prior to surgery. Alternatively, subserosal injection can be performed during surgery, which in laparoscopic surgery demands transcutaneous needle placement. Submucosal injection is preferred over subserosal injection because of better accuracy of injection near the tumour and easier endoscopic needle positioning[31].

ICG is the only fluorescent dye that has been reported for *in vivo* SLN mapping in CRC with cohorts up to 48 patients and success rates of SLN detection ranging from 65.5 to 100%[31-35]. The accuracy of this technique seems to diminish with increasing tumour stage[34, 36]. Which is most likely a result of the distorted drainage patterns caused by transmural growth of advanced tumours.

Ex vivo SLN mapping facilitates the use of experimental agents, like HSA800 (IRDye 800CW conjugated to human serum albumin). HSA800 has shown a potential advantage over ICG, due to its bigger hydrodynamic diameter that results in better retention in the SLN[37]. HSA800 has demonstrated successful identification of the SLN in 95-100% of 96 patients[38-40].

Despite high fluorescence-guided SLN identification rates, the SLN itself was associated with a relatively low negative predictive value (74 – 100%) in general, mainly as a result of high false-negative rates (when the SLN did not contain tumour tissue, but other regional lymph nodes did)[31-35, 38, 39]. This can be a result of the occurrence of skip metastases[26].

Correct staging is essential for treatment planning in CRC patients and may be improved with SLN mapping. A patient is upstaged when no tumour deposits were seen during conventional histopathology of all lymph nodes, but the SLN showed malignant cells at advanced histopathological analysis using serial sectioning and immunohistochemistry. SLN mapping with ICG and subsequent advanced histopathology resulted in upstaging in 6-23% of the patients[31-33]. Although plausible, it is yet unknown whether upstaged patients with micrometastatic lymph nodes will benefit from subsequent neoadjuvant treatment.

Overall, it can be concluded that fluorescence-guided identification of the SLN is feasible and potentially of additional clinical value. However, a wide variety of techniques for fluorescence-guided SLN identification are currently used. It is recommended to first determine the optimal agent, injection technique and patient population. The high false-negative rate (tumour-negative SLN with tumour-positive regional nodes) remains a major drawback for SLN mapping in CRC in general. Nevertheless, its value in terms of upstaging and the consequence of adjuvant treatment seems enough reason to further explore this field.

Imaging of distant metastases

Peritoneal metastases

Approximately 10% of all CRC patients develop peritoneal metastases during the course of the disease[41]. In the past, this diagnosis was considered non-curable with a median overall survival of approximately 12 months[42]. These survival rates have improved with the introduction of cytoreductive surgery followed by intraoperative hyperthermic intraperitoneal chemotherapy (HIPEC)[3, 43]. Studies have shown that in particular complete cytoreduction plays a major role as it prolongs the long-term survival of patients with peritoneal metastases[3]. However, identification of small peritoneal lesions can be challenging, especially after previous abdominal surgery or neoadjuvant therapy with subsequent fibrosis. An accurate PCI is essential as this score plays a crucial role in the decision to perform a HIPEC procedure or not[44]. Fluorescence imaging can potentially lead to more complete cytoreductive surgery by more accurately identifying peritoneal lesions.

Intravenous injection of ICG and subsequent fluorescence imaging of peritoneal metastases is primarily based on the enhanced permeability and retention (EPR) effect. The EPR effect is dependent on the porous nature of tumour vasculature and the extended circulation of the fluorescent agent, leading to accumulation in the tumour[45]. ICG is administered at the start of the surgical procedure and has shown good intraoperative imaging of peritoneal metastases, which has led to a modification of the surgical plan in 4 out of 14 patients (29%) solely based on the fluorescence assessment[46]. Nevertheless, the authors reported limited ability to assess fluorescence in areas with high physiological ICG accumulation such as the liver, as well as a sensitivity of 0% in patients with mucinous tumours[46]. Moreover, neoadjuvant treatment resulted in a higher false-negative rate (53.8% vs. 42.9%) and lower sensitivity (65.0% vs 76.3%) compared to patients who did not receive neoadjuvant treatment[47].

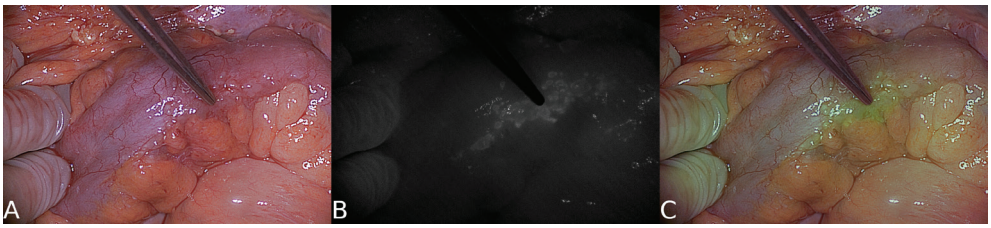

Figure 5. Fluorescence imaging result of colorectal peritoneal metastases. Intraoperative fluorescence imaging result of peritoneal metastases of a mucinous carcinoma with signet ring cell differentiation (TBR 1.8) using SGM-101. Imaging was performed using the Quest Spectrum open imaging system. It shows an image in white light (A), near-infrared (B) and merge of A and B (C)

To date, two tumour-targeted agents have been used for *in vivo* detection of peritoneal metastases in CRC: bevacizumab-800CW and SGM-101. Bevacizumab-800CW was the first tumour-targeted fluorescent agent that was reported to yield promising results, identifying additional peritoneal metastases in two out of seven (29%) patients[48]. Similar results were achieved in a study with SGM-101, where fluorescence imaging led to a change in PCI in 5 out of 12 (42%) patients (figure 5). Four patients had a higher PCI and one patient a lower PCI, all confirmed by histopathology[49]. It is noteworthy that both studies reported a high false-positive rate (38% and 47%, respectively). This could be a result of non-specific localisation of the fluorescent agent or autofluorescence of collagen-rich structures and calcifications[50].

One clinical trial is currently ongoing using LUM015, including patients with peritoneal metastases of gastrointestinal cancer, ovarian cancer, and mesothelioma (NCT03834272). The aforementioned phase III study with SGM-101 will also include patients with peritoneal metastases (NCT03659448).

The feasibility of fluorescence-guided detection of peritoneal metastases has been demonstrated, allowing for detection of peritoneal deposits and potentially also of occult lesions. This is especially valuable knowing that treatment success is primarily determined by complete cytoreduction.

Liver metastases

Over the course of the disease, 20 – 30% of CRC patients develop liver metastases (CRLM) [51]. Complete resection of these metastases is an important treatment option, with positive resection margins being associated with a two- to three-fold decrease in 5-year survival compared to negative margins. However, positive resection margins occur in approximately 13% of patients[52]. In the past, the hepatic surface was palpated for superficial lesions during surgery. With minimal invasive surgery this has become challenging. Nowadays, preoperative magnetic resonance imaging (MRI), computed tomography (CT) and intraoperative ultrasound (IOUS) are the most frequently used imaging modalities for the identification

of CRLM[53]. Fluorescence imaging offers surgeons another tool for detecting CRLM. It is suitable for detecting small superficial metastases (up to eight mm deep), but also for resection margin assessment. Intravenous ICG doses between 10 - 50 mg are described with injection windows of 1 – 14 days prior to surgery[54]. After intravenous injection, ICG is exclusively cleared by the liver. Immature hepatocytes, located at the transition zone between healthy and malignant liver cells, are unable to excrete ICG into bile due to down-regulation of anion transporters, resulting in an accumulation of ICG. This causes CRLM to show a rim of fluorescence (figure 6)[55].

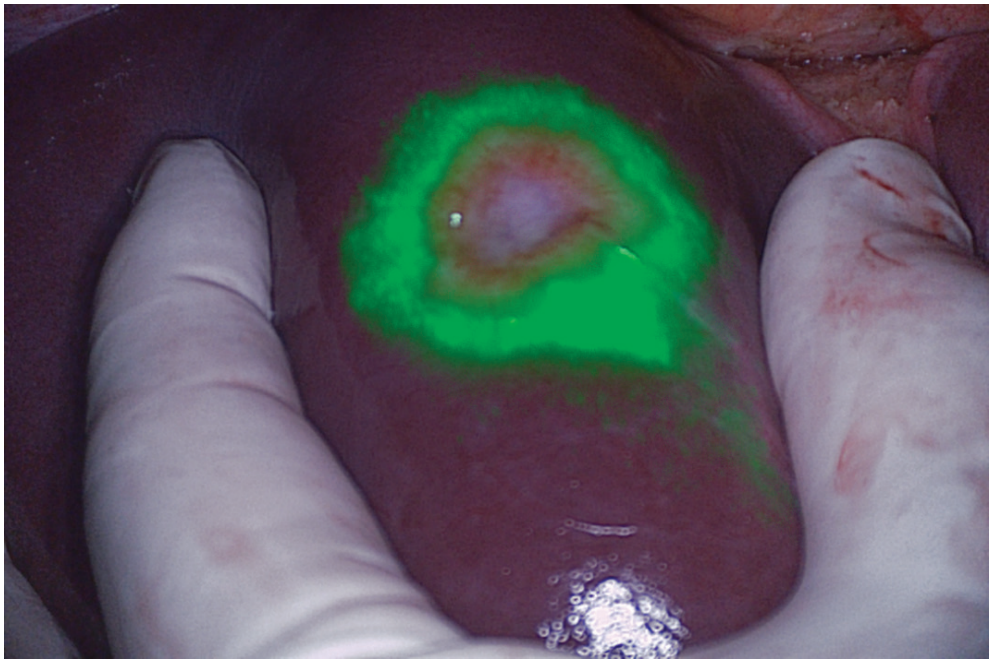

Figure 6. Fluorescence imaging result of a liver metastasis. A colorectal liver metastasis showing clear 'rim fluorescence' after intravenous injection of 10 mg indocyanine green 24 hours prior to surgery. Imaging was performed using the Quest Spectrum open imaging system.

Various studies have reported on fluorescence imaging with ICG for the detection of occult CRLM, but none were randomised[55-57]. In one systematic review, six out of nine studies reported a sensitivity exceeding 94%[54]. Furthermore, when fluorescence imaging was added to conventional imaging, extra metastases were found and resected in 20 out of 148 patients (13.5%). Tumour-targeted fluorescence identification of CRLM was previously reported in one study using SGM-101. SGM-101 provided visualisation of all 12 malignant lesions in eight patients with a mean in *vivo* TBR of 1.7[58].

It is widely debated if additional resection of small superficial CRLM improves overall survival. One study has retrospectively assessed (disease-free) survival of 86 patients after

ICG-guided resection of CRLM[59]. Significantly more additional lesions were found when fluorescence-guided resection with ICG was added compared to standard care (25% vs. 13%, p=0.04). However, this was not associated with a significant decrease in local recurrence-free survival (HR: 0.74; 95% CI: 0.42 – 1.28), and overall survival (HR: 0.94; 95% CI: 0.50 – 1.76).

Besides detection of CRLM, fluorescence imaging can also be used for margin assessment and aiding in tumour delineation for CRLM resection. Two small case series with a total of 52 patients achieved 100% tumour-negative resection margins using ICG to determine the precise tumour border[56, 57]. Recently, a systematic workflow was proposed to detect or prevent tumour positive margins in CRLM surgery[60]. In a selected group of eight patients with initial tumour positive resection margins, the surgeons were able to correctly identify seven out of eight positive margins by using the proposed surgical workflow. The currently ongoing prospective MIMIC-trial will assess whether this surgical workflow can lead to a decrease of tumour-positive resection margins in 186 patients with CRLM (Netherlands trial register: NL7674).

Fluorescence imaging with ICG has been demonstrated to improve intraoperative detection of CRLM. It can also be used for margin assessment and aiding in tumour delineation for CRLM resection. Future trials must confirm this potential and demonstrate whether this technique will improve patient survival.

Extra-abdominal metastases

A feasibility study with SGM-101 to identify colorectal lung metastases is currently recruiting (NCT04737213). A similar study with SGM-101 to identify colorectal brain metastases will be conducted soon (NCT04755920).

Imaging of vital structures

Ureters

Iatrogenic ureteral injury is a severe complication in abdominal surgery and has an incidence of up to 5.7% in colorectal surgery. Surgeries on the distal colon and rectum bear the highest risk for ureteral injury[61]. Depending on the time of diagnosis, location, and extent of the injury, treatment ranges from minimal invasive transurethral procedures to complex surgical reconstruction. Consequences of (undiagnosed) iatrogenic ureteral injury include kidney failure, sepsis, ureteral stenosis, urinoma, and fistulas[62]. The ureter is usually identified through visual inspection and palpation, which can be difficult due to its retroperitoneal location. The introduction of minimal invasive surgery in the last decades has further increased this challenge[61]. Intraoperative fluorescence imaging can guide the surgeon in identification of the ureter, which could result in less ureteral injury. ICG and MB have both been studied for ureteral identification. Due to the hepatic clearance of ICG, retrograde intra-ureteral

injection is needed, which makes ureteral identification with ICG a complex procedure[63]. Successful ureteral identification using ICG is reported in 94 – 100% of procedures[63-65]. As MB is cleared renally, intravenous injection is possible for intraoperative identification of ureters. Outcomes of intravenous MB administration for ureteral identification show variable results[66-68]. Fluorescence of the ureters is reported in 50 – 100% of cases and usually between 10 – 90 minutes after injection of MB. Optimal visualisation is achieved with doses between 0.5 mg/kg and 1.0 mg/kg. Most important, in most cases, the ureter could only be identified with fluorescence after it was already adequately identified in white light, thus the clinical benefit was minimal. Overall, MB appears to be suboptimal for ureteral identification.

To date, three experimental fluorophores have been used in clinical studies to image the ureter: ZW800-1, IS-001, and IRDye800BK[69-71]. These experimental fluorophores are all fluorescent dyes with peak emission around 800 nm. ZW800-1 is a zwitterionic molecule that shows low non-specific binding and is exclusively renally cleared. ZW800-1 was intravenously administered during abdominopelvic surgery in 12 patients. Using ZW800-1, all ureters became fluorescent within 10 minutes, without dissecting the peritoneum[69]. The SBR was 2.7 in the group with 2.5 mg throughout the first hour. The ureters remained visible with NIR during the whole procedure, with the longest procedure being over 3.5 hours. The first clinical study assessing the safety and efficacy of IS-001 included 24 patients who underwent laparoscopic gynaecological surgery[70]. The ureters could be identified in all patients, the highest SBR (3.6) was observed with a dose of 20 mg. Signal intensity decreased rapidly over time, with the peak SBR occurring 30 minutes after injection. The third experimental fluorescent dye that was studied for ureter identification is IRDye800BK, a hydrophilic dye [72]. In this trial, the optimal dose of 0.06 mg/kg was administered in 25 patients[71]. In all patients, the ureter was visualised within ten minutes. After 90 minutes the ureter was still visible in 89% of the patients. Currently, another clinical trial is ongoing using IRDye800BK, including 40 patients undergoing laparoscopic surgery. (NCT03387410)

ZW800-1, IS-001, and IRDye-800BK appear suitable for ureter identification with NIR fluorescence imaging and have advantages over MB and ICG. Future clinical trials are needed to confirm the promising early results of these experimental fluorescent agents. However, large sample sizes are required for such studies due to relatively low incidence of iatrogenic ureteral injury. Therefore, phase III studies should focus on patients with high risk for intraoperative ureteral injury.

Urethra

Besides ureteral injury, the urethra is also at risk for injury during pelvic surgery. Perineal dissection in (low) rectal surgery is an especially high-risk step for urethral injury. One clinical study with urethral administration of ICG during prostatectomies in 12 patients has been published[73]. No intraoperative urethra injury occurred. In another study, ICG was injected

in the urethra during a transanal total mesorectal excision in one patient, resulting in successful identification of the urethra[74].

Nerves

Sexual and urological dysfunction due to iatrogenic nerve injury are complications of rectal surgery, significantly affecting quality of life. Up to 79% of the patients undergoing rectal surgery acquire some sort of sexual or urological dysfunction[75]. The hypogastric, splanchnic, and levator ani nerves are at risk during (colo)rectal surgery[76]. Nerve targeted fluorescence-guided surgery has the potential to improve nerve identification, and therefore prevent injury. Although promising pre-clinical results of nerve specific fluorescence imaging have been reported, the translation to clinical studies has yet to be made[77-79]. The main difficulties include fluorescent agents not being able to pass the nerve-blood barrier, and relatively high nonspecific uptake of nerve targeted agents by fat and muscle[79].

Imaging of perfusion

Anastomotic perfusion

Anastomotic leakage is one of the most severe complications in CRC surgery. It often requires additional surgical or radiological intervention, leading to a prolonged hospital stay. Anastomotic leakage is reported up to 13% of patients undergoing CRC surgery with subsequent mortality rates of up to 27%[80, 81]. Poor bowel perfusion is thought to play an important role in anastomotic leakage. ICG fluorescence-angiography can provide real-time feedback of bowel perfusion and aid the surgeon in determining the optimal location for the anastomosis. ICG doses between 2 – 20 mg have been reported[82, 83]. In general, bowel perfusion can be assessed within 60 seconds after intravenous injection.

Over the years, several cohort studies have been published on the effect of ICG fluorescence angiography use on anastomotic leakage. Studies specifically addressing colonic anastomoses are sporadic and fail to show a significant decrease in anastomotic leakage rates when using ICG fluorescence angiography[84, 85]. More data has been reported on rectal surgery. Song et al. published the most recent and complete meta-analysis on rectal anastomoses including 2088 patients from nine retrospective studies[86]. Their pooled analysis showed an odds ratio for anastomotic leakage of 0.34 (95% CI: 0.22 – 0.52) in favour of ICG fluorescence angiography over standard of care.

Recently, the first randomised controlled trials (RCTs) on ICG fluorescence angiography have been published. One study included 240 patients undergoing left-sided colon or rectal resection and failed to show a significant difference in anastomotic leakage rate between the ICG fluorescence angiography group and the control group (5% vs 9%; p = 0.2)[87]. The second study investigated the value of ICG fluorescence angiography on the occurrence of anastomotic leakage in 377 patients undergoing sigmoid or rectal resection. A significantly

lower anastomotic leakage rate was found in the ICG fluorescence angiography group (9.1% vs 16.3%; p = 0.04)[88]. However, this difference was predominantly based on the occurrence of anastomotic leakage grade A, which does not alter patient management[89]. Thus, minimal clinical benefit was demonstrated as no difference was observed in the number of re-operations or the length of postoperative hospital stay. The third RCT also failed to report a significant decrease of anastomotic leakage in the ICG fluorescence angiography group compared to the control group (9.0% vs 9.6%; p = 0.37)[90]. It should be noted that the pre-determined sample size was not achieved due to a decrease in accrual rates. More RCTs have been registered that will include similar or higher amount of patients (NCT02598414, NCT04012645). Noteworthy are the INTACT-trial and the AVOID-trial, both planning to include up to 1000 patients (ISCRN: 13334746, NCT04712032). Also, the prospective IMARI trial is assessing a series of interventions, including ICG fluorescence angiography, and its influence on anastomotic leakage in rectal cancer surgery (Netherlands trial register: NL8261).

In conclusion, ICG fluorescence angiography has potential in the prevention of anastomotic leakage in a safe and simple way. Pooled analysis of cohort studies has demonstrated that ICG fluorescence angiography reduces anastomotic leakage, but high-quality evidence is currently lacking. RCTs with inclusion up to 1000 patients are currently ongoing and might provide with the answer if ICG fluorescence angiography prevents anastomotic leakage in CRC surgery.

Omentoplastic perfusion

Perineal wound bed complications occur in almost 50% of the patients undergoing abdominoperineal resection (APR) and carry major morbidity[91]. Omentoplasty can be performed for the prevention and management of these complications. It is hypothesised that the transferred omentum prevents dead space formation, has an anti-inflammatory and antibacterial effect, and provides excellent vascularisation to the wound bed[92]. However, its clinical benefit in rectal cancer surgery has been disputed. A meta-analysis of 1894 patients showed that omentoplasty did not reduce the risk of postoperative presacral abscesses or perineal complications[93]. ICG fluorescence angiography of the transferred omentum was recently assessed in a pilot study[94]. Remarkably, ICG fluorescence angiography led to a change in surgical management in 80% of the patients. A follow up study by the same group showed a decrease in pelviperineal non-healing in the ICG group compared to the control group (22% vs 42%; p = 0.051)[95]. However non-significant, this study showed a trend towards improved outcomes after ICG fluorescence angiography guided omentoplasty. The reported alteration of the surgical plan in 80% of cases suggests that 'standard' omentoplasty is vulnerable to poor omental perfusion. Further research on ICG fluorescence angiography for omentoplasty is therefore warranted.

DISCUSSION AND FUTURE PERSPECTIVES

NIR fluorescence-guided surgery is a rapidly evolving technique with various clinical applications in CRC surgery. This review provides an overview of the clinical applications of all fluorescent agents for CRC surgery. ICG, the nonspecific FDA/EMA approved fluorescent agent is already used in a variety of clinical applications of which CRLM resection and ICG fluorescence angiography show the most potential. However, no unequivocal benefits in relevant outcome measures have yet been reported. Over the past years, promising experimental fluorescent agents (targeted and non-targeted) have been investigated. These agents could potentially improve intraoperative fluorescence imaging, ultimately leading to improved detection of tumour tissue, vital structures, and vascularisation. Improving intraoperative detection of tumour could not only lead to more complete resections, but can also lead to better patient selection, as unnecessary surgery could be prevented if the disease is found to be too advanced. On the other hand, false-positive lesions would lead to unnecessary resection of healthy tissue which makes tumour-binding specificity of the fluorescent agent crucial.

Quantification of the fluorescence signal is challenging, with numerous factors such as scattering, absorption, camera angulation and distance, and background light influencing the signal intensity[96]. The latest studies on ICG fluorescence angiography for the prevention of anastomotic leakage focus on less subjective perfusion assessment by analysing time-dependent inflow parameters[97, 98]. Real-time quantification of the fluorescence signal of tumour-targeted agents, aiding surgeons in deciding whether tissue is malignant or not, has not been reported yet. Most clinical studies report the SBR (or TBR) and change in surgical management as the main parameters in early phase studies. Eventually, trials should report on clinically significant events such as the tumour-negative resection margin rate, detection of occult lesions, surgical complications, and (disease free) survival[99].

Nowadays, a variety of fluorescence camera systems is available in clinical practice. It is important to keep in mind that these camera systems can influence imaging results[100]. This also counts for the difference between open- and laparoscopic cameras. Most laparoscopes that are currently clinically available are optimised for ICG at 830 nm. This wavelength is slightly too high for optimal imaging of most experimental fluorescent agents, which have peak emission wavelengths around 800 nm (table 1). Therefore, there is a need for high-quality laparoscopes that are optimised for imaging of specific tumour-targeted fluorescent agents. Fluorescence imaging could account for the lack of tactile feedback in minimal invasive surgery, as it has the potential to improve visualisation of vital structures (e.g. the ureter, nerves) and tumours. Moreover, fluorescence imaging can be integrated in the laparoscopic field with an overlay view, which is an advantage over open surgery, where an additional handheld camera is needed. Especially in rectal surgery, in the conically shaped (male) pelvis, difficulties are experienced with optimal positioning due to the size of most open cameras. A

laparoscope is much smaller and therefore easier to manoeuvre towards an optimal imaging angle.

CONCLUSION

In conclusion, the field of fluorescence-guided surgery is rapidly evolving with already several clinical applications in CRC surgery. ICG is widely used, and its use appears to be beneficial in specific applications. Many experimental fluorescent agents have been developed and several of these agents are currently being assessed in late phase clinical studies. The most promising applications of these experimental fluorescent agents in CRC surgery are distinguishing between fibrotic and tumour tissue after neo-adjuvant treatment, improving the rate of tumour-negative resection margins in locally advanced and recurrent rectal cancer, detection of occult metastases in cytoreductive surgery for peritoneal metastases, and ureteral imaging in high-risk cases. An essential next step for the implementation of these agents in clinical practice is to show direct patient benefit in terms of change in surgical management, surgical complications, recurrence-free survival, and overall survival.

Acknowledgements: The authors wish to thank S.T.G. Meertens-Gunput of the Erasmus MC Medical Library for developing and updating the search strategies. Moreover, we thank K.S. de Valk for supplying figure 4 and O.D. Bijlstra for supplying figure 6.

REFERENCES

1. Bray, F., et al., *Global cancer statistics 2018: GLOBOCAN estimates of incidence and mortality worldwide for 36 cancers in 185 countries.* CA Cancer J Clin, 2018. **68**(6): p. 394-424.
2. Amri, R., et al., *Association of Radial Margin Positivity With Colon Cancer.* JAMA Surg, 2015. **150**(9): p. 890-8.
3. Elias, D., et al., *Peritoneal colorectal carcinomatosis treated with surgery and perioperative intraperitoneal chemotherapy: retrospective analysis of 523 patients from a multicentric French study.* J Clin Oncol, 2010. **28**(1): p. 63-8.
4. Hernot, S., et al., *Latest developments in molecular tracers for fluorescence image-guided cancer surgery.* Lancet Oncol, 2019. **20**(7): p. e354-e367.
5. Fox, I.J., et al., *A tricarbocyanine dye for continuous recording of dilution curves in whole blood independent of variations in blood oxygen saturation.* Proc Staff Meet Mayo Clin, 1957. **32**(18): p. 478-84.
6. Ginimuge, P.R. and S.D. Jyothi, *Methylene blue: revisited.* J Anaesthesiol Clin Pharmacol, 2010. **26**(4): p. 517-20.
7. Slim, K., et al., *Methodological index for non-randomized studies (minors): development and validation of a new instrument.* ANZ J Surg, 2003. **73**(9): p. 712-6.
8. Nagtegaal, I.D. and P. Quirke, *What is the role for the circumferential margin in the modern treatment of rectal cancer?* J Clin Oncol, 2008. **26**(2): p. 303-12.
9. Holman, F.A., et al., *Results of a pooled analysis of IOERT containing multimodality treatment for locally recurrent rectal cancer: Results of 565 patients of two major treatment centres.* Eur J Surg Oncol, 2017. **43**(1): p. 107-117.
10. Conaghan, P.J., et al., *Leaving a mark: the frequency and accuracy of tattooing prior to laparoscopic colorectal surgery.* Colorectal Dis, 2011. **13**(10): p. 1184-7.
11. Feingold, D.L., et al., *Safety and reliability of tattooing colorectal neoplasms prior to laparoscopic resection.* J Gastrointest Surg, 2004. **8**(5): p. 543-6.
12. Satoyoshi, T., et al., *Timing of indocyanine green injection prior to laparoscopic colorectal surgery for tumor localization: a prospective case series.* Surg Endosc, 2020.
13. Watanabe, M., et al., *Colonic tattooing using fluorescence imaging with light-emitting diode-activated indocyanine green: A feasibility study.* Surg Today, 2009. **39**(3): p. 214-218.
14. Boogerd, L.S.F., et al., *Safety and effectiveness of SGM-101, a fluorescent antibody targeting carcinoembryonic antigen, for intraoperative detection of colorectal cancer: a dose-escalation pilot study.* Lancet Gastroenterol Hepatol, 2018. **3**(3): p. 181-191.
15. de Valk, K.S., et al., *First-in-Human Assessment of cRGD-ZW800-1, a Zwitterionic, Integrin-Targeted, Near-Infrared Fluorescent Peptide in Colon Carcinoma.* Clin Cancer Res, 2020. **26**(15): p. 3990-3998.
16. de Jongh, S.J., et al., *Back-Table Fluorescence-Guided Imaging for Circumferential Resection Margin Evaluation Using Bevacizumab-800CW in Patients with Locally Advanced Rectal Cancer.* J Nucl Med, 2020. **61**(5): p. 655-661.
17. Voskuil, F.J., et al., *Exploiting metabolic acidosis in solid cancers using a tumor-agnostic pH-activatable nanoprobe for fluorescence-guided surgery.* Nat Commun, 2020. **11**(1): p. 3257.
18. de Valk, K.S., et al., *Dose-Finding Study of a CEA-Targeting Agent, SGM-101, for Intraoperative Fluorescence Imaging of Colorectal Cancer.* Ann Surg Oncol, 2020.
19. Gutowski, M., et al., *SGM-101: An innovative near-infrared dye-antibody conjugate that targets CEA for fluorescence-guided surgery.* Surg Oncol, 2017. **26**(2): p. 153-162.
20. Lv, W., et al., *Long-term tracking of cancer cell nucleus and identification of colorectal cancer with an aggregation-induced*

emission-based fluorescent probe. J Biomed Nanotechnol, 2019. **15**(5): p. 1033-1042.
21. El Zoghbi, M., et al., *Artificial Intelligence-Assisted Optical Diagnosis: A Comprehensive Review of Its Role in Leave-In-Situ and Resect-and-Discard Strategies in Colonoscopy.* Clin Transl Gastroenterol, 2023. **14**(10): p. e00640.
22. Whitley, M.J., et al., *A mouse-human phase 1 co-clinical trial of a protease-activated fluorescent probe for imaging cancer.* Sci Transl Med, 2016. **8**(320): p. 320ra4.
23. Figueredo, A., M.E. Coombes, and S. Mukherjee, *Adjuvant therapy for completely resected stage II colon cancer.* Cochrane Database Syst Rev, 2008(3): p. CD005390.
24. Yamamoto, H., et al., *Micrometastasis Volume in Lymph Nodes Determines Disease Recurrence Rate of Stage II Colorectal Cancer: A Prospective Multicenter Trial.* Clin Cancer Res, 2016. **22**(13): p. 3201-8.
25. Cahill, R.A., J. Leroy, and J. Marescaux, *Localized resection for colon cancer.* Surg Oncol, 2009. **18**(4): p. 334-42.
26. Bao, F., et al., *Prognostic impact of lymph node skip metastasis in Stage III colorectal cancer.* Colorectal Dis, 2016. **18**(9): p. O322-9.
27. Bembenek, A.E., et al., *Sentinel lymph node biopsy in colon cancer: a prospective multicenter trial.* Ann Surg, 2007. **245**(6): p. 858-63.
28. Chand, M., et al., *Feasibility of fluorescence lymph node imaging in colon cancer: FLICC.* Tech Coloproctol, 2018. **22**(4): p. 271-277.
29. Nishigori, N., et al., *Visualization of Lymph/Blood Flow in Laparoscopic Colorectal Cancer Surgery by ICG Fluorescence Imaging (Lap-IGFI).* Ann Surg Oncol, 2016. **23 Suppl 2**: p. S266-74.
30. Tuech, J.J., et al., *Sentinel lymph node mapping in colon cancer.* Surg Endosc, 2004. **18**(12): p. 1721-9.
31. Ankersmit, M., et al., *Near-infrared fluorescence imaging for sentinel lymph node identification in colon cancer: a prospective single-center study and systematic review with meta-analysis.* Tech Coloproctol, 2019. **23**(12): p. 1113-1126.
32. Andersen, H.S., et al., *In vivo and ex vivo sentinel node mapping does not identify the same lymph nodes in colon cancer.* Int J Colorectal Dis, 2017. **32**(7): p. 983-990.
33. Hirche, C., et al., *Ultrastaging of colon cancer by sentinel node biopsy using fluorescence navigation with indocyanine green.* Int J Colorectal Dis, 2012. **27**(3): p. 319-324.
34. Nagata, K., et al., *Laparoscopic sentinel node mapping for colorectal cancer using infrared ray laparoscopy.* Anticancer Res, 2006. **26**(3 B): p. 2307-2311.
35. Cahill, R.A., et al., *Near-infrared (NIR) laparoscopy for intraoperative lymphatic road-mapping and sentinel node identification during definitive surgical resection of early-stage colorectal neoplasia.* Surg Endosc Interv Tech, 2012. **26**(1): p. 197-204.
36. Burghgraef, T.A., et al., *In vivo sentinel lymph node identification using fluorescent tracer imaging in colon cancer: A systematic review and meta-analysis.* Crit Rev Oncol Hematol, 2021. **158**: p. 103149.
37. Ohnishi, S., et al., *Organic alternatives to quantum dots for intraoperative near-infrared fluorescent sentinel lymph node mapping.* Mol Imaging, 2005. **4**(3): p. 172-81.
38. Schaafsma, B.E., et al., *Ex vivo sentinel node mapping in colon cancer combining blue dye staining and fluorescence imaging.* J Surg Res, 2013. **183**(1): p. 253-257.
39. Hutteman, M., et al., *Clinical translation of ex vivo sentinel lymph node mapping for colorectal cancer using invisible near-infrared fluorescence light.* Ann Surg Oncol, 2011. **18**(4): p. 1006-1014.
40. Weixler, B., et al., *Sentinel Lymph Node Mapping with Isosulfan Blue or Indocyanine Green in Colon Cancer Shows Comparable Results and Identifies Patients with Decreased Survival: A Prospective Single-Center Trial.* World J Surg, 2017. **41**(9): p. 2378-2386.
41. Koppe, M.J., et al., *Peritoneal carcinomatosis of colorectal origin: incidence and current*

treatment strategies. Ann Surg, 2006. **243**(2): p. 212-22.
42. Razenberg, L.G., et al., *Challenging the dogma of colorectal peritoneal metastases as an untreatable condition: Results of a population-based study.* Eur J Cancer, 2016. **65**: p. 113-20.
43. Simkens, G.A., et al., *Development of a Prognostic Nomogram for Patients with Peritoneally Metastasized Colorectal Cancer Treated with Cytoreductive Surgery and HIPEC.* Ann Surg Oncol, 2016. **23**(13): p. 4214-4221.
44. Faron, M., et al., *Linear Relationship of Peritoneal Cancer Index and Survival in Patients with Peritoneal Metastases from Colorectal Cancer.* Ann Surg Oncol, 2016. **23**(1): p. 114-9.
45. Maeda, H., *Tumor-selective delivery of macromolecular drugs via the EPR effect: background and future prospects.* Bioconjug Chem, 2010. **21**(5): p. 797-802.
46. Liberale, G., et al., *Fluorescence imaging after indocyanine green injection for detection of peritoneal metastases in patients undergoing cytoreductive surgery for peritoneal carcinomatosis from colorectal cancer: A pilot study.* Ann Surg, 2016. **264**(6): p. 1110-1115.
47. Filippello, A., et al., *Affinity of Indocyanine Green in the Detection of Colorectal Peritoneal Carcinomatosis.* Surg Innov, 2017. **24**(2): p. 103-108.
48. Harlaar, N.J., et al., *Molecular fluorescence-guided surgery of peritoneal carcinomatosis of colorectal origin: a single-centre feasibility study.* Lancet Gastroenterol Hepatol, 2016. **1**(4): p. 283-290.
49. Schaap, D.P., et al., *Carcinoembryonic antigen-specific, fluorescent image-guided cytoreductive surgery with hyperthermic intraperitoneal chemotherapy for metastatic colorectal cancer.* Br J Surg, 2020. **107**(4): p. 334-337.
50. Kobayashi, H., R. Watanabe, and P.L. Choyke, *Improving conventional enhanced permeability and retention (EPR) effects; what is the appropriate target?* Theranostics, 2013. **4**(1): p. 81-9.
51. Manfredi, S., et al., *Epidemiology and management of liver metastases from colorectal cancer.* Ann Surg, 2006. **244**(2): p. 254-9.
52. Nierop, P.M.H., et al., *Histopathological growth patterns and positive margins after resection of colorectal liver metastases.* HPB (Oxford), 2020. **22**(6): p. 911-919.
53. Elfrink, A.K.E., et al., *Preoperative imaging for colorectal liver metastases: a nationwide population-based study.* BJS Open, 2020. **4**(4): p. 605-621.
54. Liberale, G., et al., *Indocyanine green fluorescence-guided surgery after IV injection in metastatic colorectal cancer: A systematic review.* Eur J Surg Oncol, 2017. **43**(9): p. 1656-1667.
55. Van Der Vorst, J.R., et al., *Near-infrared fluorescence-guided resection of colorectal liver metastases.* Cancer, 2013. **119**(18): p. 3411-3418.
56. Peloso, A., et al., *Combined use of intraoperative ultrasound and indocyanine green fluorescence imaging to detect liver metastases from colorectal cancer.* HPB, 2013. **15**(12): p. 928-934.
57. Aoki, T., et al., *Determination of the surgical margin in laparoscopic liver resections using infrared indocyanine green fluorescence.* Langenbecks Arch Surg, 2018. **403**(5): p. 671-680.
58. Meijer, R.P.J., et al., *Intraoperative detection of colorectal and pancreatic liver metastases using SGM-101, a fluorescent antibody targeting CEA.* Eur J Surg Oncol, 2020.
59. Handgraaf, H.J.M., et al., *Long-term follow-up after near-infrared fluorescence-guided resection of colorectal liver metastases: A retrospective multicenter analysis.* Eur J Surg Oncol, 2017. **43**(8): p. 1463-1471.
60. Achterberg, F.B., et al., *Real-time surgical margin assessment using ICG-fluorescence during laparoscopic and robot-assisted resections of colorectal liver metastases.* Ann Transl Med, 2020. **8**(21): p. 1448.
61. Gild, P., et al., *Adult iatrogenic ureteral injury and stricture-incidence and treatment*

strategies. Asian J Urol, 2018. **5**(2): p. 101-106.
62. Blackwell, R.H., et al., *Complications of Recognized and Unrecognized Iatrogenic Ureteral Injury at Time of Hysterectomy: A Population Based Analysis.* J Urol, 2018. **199**(6): p. 1540-1545.
63. White, L.A., et al., *Intraureteral indocyanine green augments ureteral identification and avoidance during complex robotic-assisted colorectal surgery.* Colorectal Dis, 2020.
64. Mandovra, P., V. Kalikar, and R.V. Patankar, *Real-Time Visualization of Ureters Using Indocyanine Green During Laparoscopic Surgeries: Can We Make Surgery Safer?* Surg Innov, 2019. **26**(4): p. 464-468.
65. Cabanes, M., et al., *Intra-operative identification of ureters using indocyanine green for gynecological oncology procedures.* Int J Gynecol Cancer, 2019.
66. Al-Taher, M., et al., *Fluorescence Ureteral Visualization in Human Laparoscopic Colorectal Surgery Using Methylene Blue.* J Laparoendosc Adv Surg Techn, 2016. **26**(11): p. 870-875.
67. Barnes, T.G., et al., *Methylene blue fluorescence of the ureter during colorectal surgery.* 2018. **32**(9): p. 4036-4043.
68. Verbeek, F.P.R., et al., *Intraoperative near infrared fluorescence guided identification of the ureters using low dose methylene blue: A first in human experience.* J Urol, 2013. **190**(2): p. 574-579.
69. de Valk, K.S., et al., *A zwitterionic near-infrared fluorophore for real-time ureter identification during laparoscopic abdominopelvic surgery.* Nat Commun, 2019. **10**(1).
70. Farnam, R.W., et al., *Intraoperative ureter visualization using a near-infrared imaging agent.* J Biomed Opt, 2019. **24**(6): p. 1-8.
71. Huh, W.K., et al., *Fluorescence Imaging of the Ureter in Minimally Invasive Pelvic Surgery.* J Minimally Invasive Gynecol, 2020.
72. Al-Taher, M., et al., *Evaluation of a novel dye for near-infrared fluorescence delineation of the ureters during laparoscopy.* BJS Open, 2018. **2**(4): p. 254-261.
73. Simone, G., et al., *Urethra and Ejaculation Preserving Robot-assisted Simple Prostatectomy: Near-infrared Fluorescence Imaging-guided Madigan Technique.* Eur Urol, 2019. **75**(3): p. 492-497.
74. Nitta, T., et al., *Novel technique with the IRIS U kit to prevent urethral injury in patients undergoing transanal total mesorectal excision.* Ann Med Surg, 2019. **46**: p. 1-3.
75. Lange, M.M., et al., *Risk factors for sexual dysfunction after rectal cancer treatment.* Eur J Cancer, 2009. **45**(9): p. 1578-88.
76. Lange, M.M. and C.J. van de Velde, *Urinary and sexual dysfunction after rectal cancer treatment.* Nat Rev Urol, 2011. **8**(1): p. 51-7.
77. Gonzales, J., et al., *Fluorescence labeling of a NaV1.7-targeted peptide for near-infrared nerve visualization.* EJNMMI Res, 2020. **10**(1).
78. Hingorani, D.V., et al., *Nerve-targeted probes for fluorescence-guided intraoperative imaging.* Theranostics, 2018. **8**(15): p. 4226-4237.
79. Wang, L.G., et al., *Near-infrared nerve-binding fluorophores for buried nerve tissue imaging.* Sci Transl Med, 2020. **12**(542).
80. Sparreboom, C.L., et al., *A multicentre cohort study of serum and peritoneal biomarkers to predict anastomotic leakage after rectal cancer resection.* Colorectal Dis, 2020. **22**(1): p. 36-45.
81. Angeramo, C.A., et al., *Postoperative outcomes in patients undergoing colorectal surgery with anastomotic leak before and after hospital discharge.* Updates Surg, 2020. **72**(2): p. 463-468.
82. van Manen, L., et al., *A practical guide for the use of indocyanine green and methylene blue in fluorescence-guided abdominal surgery.* J Surg Oncol, 2018. **118**(2): p. 283-300.
83. Watanabe, J., et al., *Indocyanine green fluorescence imaging to reduce the risk of anastomotic leakage in laparoscopic low anterior resection for rectal cancer: a propensity*

score-matched cohort study. Surg Endosc, 2020. **34**(1): p. 202-208.

84. Kin, C., et al., *Equivocal effect of intraoperative fluorescence angiography on colorectal anastomotic leaks.* Dis Colon Rectum, 2015. **58**(6): p. 582-587.
85. Kudszus, S., et al., *Intraoperative laser fluorescence angiography in colorectal surgery: a noninvasive analysis to reduce the rate of anastomotic leakage.* Langenbeck's Arch Surg, 2010: p. 1-6.
86. Song, M., et al., *Assessment of intraoperative use of indocyanine green fluorescence imaging on the incidence of anastomotic leakage after rectal cancer surgery: a PRISMA-compliant systematic review and meta-analysis.* Tech Coloproctol, 2020.
87. De Nardi, P., et al., *Intraoperative angiography with indocyanine green to assess anastomosis perfusion in patients undergoing laparoscopic colorectal resection: results of a multicenter randomized controlled trial.* Surg Endosc, 2020. **34**(1): p. 53-60.
88. Alekseev, M., et al., *A study investigating the perfusion of colorectal anastomoses using fluorescence angiography: results of the FLAG randomized trial.* Colorectal Dis, 2020.
89. Rahbari, N.N., et al., *Definition and grading of anastomotic leakage following anterior resection of the rectum: a proposal by the International Study Group of Rectal Cancer.* Surgery, 2010. **147**(3): p. 339-51.
90. Jafari, M.D., et al., *Perfusion Assessment in Left-Sided/Low Anterior Resection (PILLAR III): A Randomized, Controlled, Parallel, Multicenter Study Assessing Perfusion Outcomes with PINPOINT Near-Infrared Fluorescence Imaging in Low Anterior Resection.* Dis Colon Rectum, 2021.
91. Musters, G.D., et al., *Biological Mesh Closure of the Pelvic Floor After Extralevator Abdominoperineal Resection for Rectal Cancer: A Multicenter Randomized Controlled Trial (the BIOPEX-study).* Ann Surg, 2017. **265**(6): p. 1074-1081.
92. Chandra, A., et al., *The anti-inflammatory and antibacterial basis of human omental defense: selective expression of cytokines and antimicrobial peptides.* PLoS One, 2011. **6**(5): p. e20446.
93. Blok, R.D., et al., *A Systematic Review and Meta-analysis on Omentoplasty for the Management of Abdominoperineal Defects in Patients Treated for Cancer.* Ann Surg, 2020. **271**(4): p. 654-662.
94. Slooter, M.D., et al., *Near-infrared fluorescence angiography for intra-operative assessment of pedicled omentoplasty for filling of a pelvic cavity: a pilot study.* Tech Coloproctol, 2019. **23**(8): p. 723-728.
95. Slooter, M.D., et al., *Optimizing omentoplasty for management of chronic pelvic sepsis by intra-operative fluorescence angiography: a comparative cohort study.* Colorectal Dis, 2020. **22**(12): p. 2252-9.
96. Keereweer, S., et al., *Optical image-guided cancer surgery: challenges and limitations.* Clin Cancer Res, 2013. **19**(14): p. 3745-54.
97. Lütken, C.D., et al., *Optimizing quantitative fluorescence angiography for visceral perfusion assessment.* Surg Endosc, 2020. **34**(12): p. 5223-5233.
98. Goncalves, L.N., et al., *Perfusion Parameters in Near-Infrared Fluorescence Imaging with Indocyanine Green: A Systematic Review of the Literature.* Life, 2021. **11**(5): p. 433.
99. Lauwerends, L.J., et al., *Real-time fluorescence imaging in intraoperative decision making for cancer surgery.* Lancet Oncol, 2021.
100. Zhu, B. and E.M. Sevick-Muraca, *A review of performance of near-infrared fluorescence imaging devices used in clinical studies.* Br J Radiol, 2015. **88**(1045): p. 20140547.

SUPPLEMENTARY MATERIALS

Supplement 1: search strategies per database and the corresponding hits after removal of duplicates

Embase.com (1123 articles)

('fluorescence guided surgery'/de OR (('fluorescence angiography'/de OR 'fluorescence imaging system'/de OR 'indocyanine green angiography'/de OR 'indocyanine green'/de OR 'near infrared spectroscopy'/exp OR 'near infrared imaging system'/de OR 'fluorescence imaging'/de) AND ('surgery'/exp OR surgery:lnk OR 'laparoscope'/exp)) OR (((fluorescen* OR indocyanine-green* OR ICG OR near-infrared* OR near-infra-red*) NEAR/9 (surg* OR operat* OR intraoperat* OR resect* OR microsurg* OR laparoscop*))):ab,ti,kw) ***AND*** ('large intestine tumor'/exp OR 'large intestine cancer'/exp OR 'large intestine carcinoma'/exp OR 'colorectal surgery'/exp OR 'ureter'/de OR 'ureter injury'/de OR 'ureter surgery'/exp OR 'urethra'/exp OR 'urethra injury'/de OR 'urethra surgery'/exp OR 'peripheral nerve'/de OR (((rect* OR colorect* OR colon* OR appendi* OR anal* OR anus OR cecum OR caecum OR large-intestin* OR sigmoid* OR bowel*) NEAR/3 (carcinoma* OR neoplas* OR tumor* OR tumour* OR cancer* OR surger* OR resect*)) OR ureter* OR urethr* OR (nerve* NEAR/3 (imag* OR detect* OR locali*))):ab,ti,kw) *NOT [conference abstract]/lim AND [english]/lim*

Medline Ovid (198 articles)

(((Fluorescein Angiography/ OR Optical Imaging/ OR Indocyanine Green/ OR Spectroscopy, Near-Infrared/) AND (exp Surgical Procedures, Operative/ OR surgery.fs. OR Laparoscopy/)) OR (((fluorescen* OR indocyanine-green* OR ICG OR near-infrared* OR near-infra-red*) ADJ9 (surg* OR operat* OR intraoperat* OR resect* OR microsurg* OR laparoscop*))).ab,ti,kf.) ***AND*** (exp Colorectal Neoplasms/ OR Colorectal Surgery/ OR Urethra/ OR Ureter/ OR Peripheral Nerves/ OR (((rect* OR colorect* OR colon* OR appendi* OR anal* OR anus OR cecum OR caecum OR large-intestin* OR sigmoid* OR bowel*) ADJ3 (carcinoma* OR neoplas* OR tumor* OR tumour* OR cancer* OR surger* OR resect*)) OR ureter* OR urethr* OR (nerve* ADJ3 (imag* OR detect* OR locali*))).ab,ti,kf.) *NOT (letter* OR news OR comment* OR editorial* OR congres* OR abstract* OR book* OR chapter* OR dissertation abstract*).pt. AND english.lg.*

Cochrane Central Register of Controlled Trials (73 articles)

((((fluorescen* OR indocyanine-green* OR ICG OR "near-infrared*" OR "near-infra-red*") NEAR/9 (surg* OR operat* OR intraoperat* OR resect* OR microsurg* OR laparoscop*))):ab,ti,kw) ***AND*** ((((rect* OR colorect* OR colon* OR appendi* OR anal* OR anus OR cecum OR caecum OR large-intestin* OR sigmoid* OR bowel*) NEAR/3 (carcinoma* OR neoplas* OR tumor* OR tumour* OR cancer* OR surger* OR resect*)) OR ureter* OR urethr* OR (nerve* NEAR/3 (imag* OR detect* OR locali*))):ab,ti,kw)

Supplement 2: overview of all clinical studies on colorectal cancer surgery assessing experimental fluorescent agents.

Primary tumour													
First author	**Tumour type**	**Year**	**Fluorescent agent**	**Study design**	**Fluorescence imaging application**	**Number of patients**	**(Optimal) dose**	**(Optimal) dosing interval**	**Optimal TBR (mean)**	**Sensitivity**	**Specificity**	**Change in surgical management**	**Other outcomes**
Boogerd[13]	CC + RC	2018	SGM-101	Open-label, dose escalation	In vivo and PEARL MSI	26*	10 mg	4 days	1.64 (*in vivo*) 6.1 (*ex vivo*: PEARL MSI)	98%	62%	35%	ppv: 81% | npv: 94% | acc: 84%
De Jongh[15]	RC	2020	Bevacizumab-800CW	Open-label, fixed dose, pilot study	1 = Back table imaging for CRM evaluation 2 = Odyssey imaging to determine sens / spec for tumour detection	1 = 8 2 = 17	4.5 mg	2-3 days	4.7 (*ex vivo*: Odyssey)	96.19%**	80.39%**	na	Tumour positive CRM correctly identified in 1 out of 2 patients (50%)
De Valk[14]	CC	2020	cRGD-ZW800-1	Open-label, dose escalation	In vivo and PEARL MSI	12	0.05 mg/kg	18 hours	1.6 (*in vivo*) 6.2 (*ex vivo*: PEARL MSI)	nr	nr	nr	Lymph nodes: sens 100% | spec: 87% | ppv: 33% | npv: 100% | acc: 88%

Supplement 2: overview of all clinical studies on colorectal cancer surgery assessing experimental fluorescent agents. *(continued)*

Primary tumour												
De Valk[17]	CC + RC	2020	SGM-101	Open-label, dose escalation	In vivo and back table	37*	10 mg	4 days	1.9 (*in vivo*) 3.5 (*ex vivo*: back table)	96%	63%	24%	ppv: 70% | npv: 94% | acc: 78%
Voskuil[16]	nr***	2020	ONM-100	Open-label, dose escalation	PEARL MSI	3	1.2 mg/kg	24 hours	nr***	nr***	nr***	nr***	-

* 21 out of 26 patients from Boogerd et al were also included in the study by de Valk et al

** Based on microscopy determined optimal mean fluorescence intensity cut off values for tumour detection

*** Results of interest not separately specified for colorectal cancer patients

Sentinel lymph node											
First author	**Year**	**Fluorescent agent**	**Study design**	**Fluorescence imaging application**	**Number of patients**	**(Optimal) dose**	**(Optimal) dosing interval**	**SBR**	**Sensitivity**	**Specificity**	**Change in surgical management**	**Other outcomes**
Hutteman[36]	2011	HSA800	Pilot study	Ex vivo	24	1cc 50 µM	post-operative in specimen	nr	nr	na	nr	SLN's detected: 100% | avg SLN's: 3
Schaafsma[35]	2013	HSA800	Pilot study	Ex vivo	22	1cc 50 µM	post-operative in specimen	nr	80%	na	nr	SLN's detected: 95% | avg SLN's: 3.5

Supplement 2: overview of all clinical studies on colorectal cancer surgery assessing experimental fluorescent agents. *(continued)*

Primary tumour												
Weixler[37]	2017	HSA800	Prospective single-centre	Ex vivo	50	1cc 50 μM	post-operative in specimen	nr	64%	na	10%	SLN's detected: 100% | avg SLN's: 4.4
(C) Peritoneal metastases												
First author	**Year**	**Fluorescent agent**	**Study design**	**Fluorescence imaging application**	**Number of patients**	**(Optimal) dose**	**(Optimal) dosing interval**	**Optimal TBR (mean)**	**Sensitivity**	**Specificity**	**Change in surgical management**	**Other outcomes**
Harlaar[45]	2016	Bevacizumab-800CW	Open-label, feasibility study	In vivo and back table	7	4.5 mg	2 days	6.92 (ex vivo: back table)	nr	nr	29%	ppv: 53% | npv: 100%
Schaap[46]	2020	SGM-101	Open-label, pilot study	In vivo and back table	14	10-15 mg	4-6 days	nr	98.5%	62.2%	50%	ppv: 82.3%| npv: 95.8%| acc: 85.4%
(D) Liver metastases												
First author	**Year**	**Fluorescent agent**	**Study design**	**Fluorescence imaging application**	**Number of patients**	**Optimal dose**	**Optimal dosing interval**	**Optimal TBR (median)**	**Sensitivity**	**Specificity**	**Change in surgical management**	**Other outcomes**

Supplement 2: overview of all clinical studies on colorectal cancer surgery assessing experimental fluorescent agents. *(continued)*

Primary tumour											
Meijer[55]	2020	SGM-101	Open label, dose finding	In vivo (occult lesions and resection margin)	8	10 mg	4 days	2.0 (in vivo)	nr	nr	0%	ppv: 89% | positive CRM: 9%
(E) Ureter												
First author	**Year**	**Fluorescent agent**	**Study design**	**Fluorescence imaging application**	**Number of patients**	**Optimal dose**	**Dosing interval**	**Optimal SBR**	**Ureters identified**	**Duration of visualisation**		
De Valk[67]	2019	ZW800-1	Open label, dose finding	In vivo	12	2.5 mg	per-operative	2.7	100%	3.5 hours		
Farnam[68]	2019	IS-001	Open label, dose finding	In vivo	24	20 - 40 mg	per-operative	3.6	100%	nr		
Huh[69]	2020	IRDye-800BK	Open label, dose finding	In vivo	41	0.06 mg/kg	per-operative	nr	100%	1.5 hours		

Abbreviations: *TBR* tumour-to-background ratio | *CC* colon cancer | *RC* rectal cancer | *ppv* positive predictive value | *npv* negative predictive value | *acc* accuracy | *CRM* circumferential resection margin | *na* not applicable | *nr* not reported | *sens* sensitivity | *spec* specificity | *SLN* sentinel lymph node | *avg* average

Supplement 3: overview of all ongoing clinical trials on colorectal cancer surgery assessing experimental fluorescent agents

Principal investigator	Fluorescent agent	Study phase	Imaging target	Tumour type	Planned inclusion FI (n)	Control group (n)	Recruitment status	(Estimated) study completion date	NCT number
Barnes, T.G.	IRDYe-800BK	Phase I/II	Ureter	na	40	na	Completed	nov-18	NCT03387410
Chan, A.T.	LUM015	Phase I	Primary tumour	All stage colorectal cancer	11	na	Recruiting	dec-20	NCT02584244
Cusack, J.C.	LUM015	nr	Peritoneal metastases	Peritoneal metastases of CRC	nr*	na	Not yet recruiting	feb-21	NCT03834272
OncoNano Medicine, Inc.	ONM-100	Phase II	Primary tumour	Colorectal cancer, not specified	nr*	na	Recruiting	dec-20	NCT03735680
Vahrmeijer, A.L.	SGM-101	Phase III	Primary tumour and peritoneal metastases	LARC & LRRC, T4 colon cancer, locally recurrent colon cancer, and peritoneal metastases of CRC	240	60	Recruiting	dec-21	NCT03659448
Vahrmeijer, A.L	SGM-101	Phase II	Extra abdominal metastases	Colorectal lung metastases	10	na	Recruiting	dec-21	NCT04737213
Vahrmeijer, A.L	SGM-101	Phase II	Extra abdominal metastases	Colorectal brain metastases	10	na	Not yet recruiting	dec-22	NCT04755920
Vahrmeijer, A.L	SGM-101	Phase III	Primary tumour	LARC & LRRC	203	na	Recruiting	oct-23	NCT04642924

* Study assessing various tumour types, amount of patient undergoing surgery for colorectal cancer is not specified.

Abbreviations: *na* not applicable | *nr* not reported |*CRC* colorectal cancer | *LARC* locally advanced rectal cancer | *LRRC* locally recurrent rectal cancer

Part II

Conceptual Foundations of Fluorescence Imaging in Cancer Surgery


4

Chapter 4

Real-time fluorescence imaging in intraoperative decision making for cancer surgery

Lorraine J Lauwerends, Pieter B A A van Driel, Robert J Baatenburg de Jong, José A U Hardillo, Senada Koljenovic, Gerwin Puppels, Laura Mezzanotte, Clemens W G M Löwik, Eben L Rosenthal, Alexander L Vahrmeijer, Stijn Keereweer

Lancet Oncology. 2021 May;22(5):e186–e195.

ABSTRACT

Fluorescence-guided surgery is an intraoperative optical imaging method that provides surgeons with real-time guidance for the delineation of tumours. Currently, in phase 1 and 2 clinical trials, evaluation of fluorescence-guided surgery is primarily focused on its diagnostic performance, although the corresponding outcome variables do not inform about the added clinical benefit of fluorescence-guided surgery and are challenging to assess objectively. Nonetheless, the effect of fluorescence-guided surgery on intraoperative decision making is the most objective outcome measurement to assess the clinical value of this imaging method. In this Review, we explore the study designs of existing trials of fluorescence-guided surgery that allow us to extract information on potential changes in intraoperative decision making, such as additional or more conservative resections. On the basis of this analysis, we offer recommendations on how to report changes in intraoperative decision making that result from fluorescence imaging, which is of utmost importance for the widespread clinical implementation of fluorescence-guided surgery.

INTRODUCTION

Surgeons often rely on experience, training, visual, and tactile information when delineating and resecting most solid tumours. However, identifying tumour margins based on these subjective parameters is challenging and can result in residual disease, which is a prevalent cause of local recurrence and ultimately affects patient prognosis. Complete resection of malignant tissue with adequate tumour-free margins must also be balanced with preservation of the surrounding structures to minimise functional impairment. Histopathological examination of the resected specimen is the current gold standard for margin assessment, but, for many oncological surgeries, it is technically and logistically unrealistic to intraoperatively assess the complete surgical margin by histopathology [1]. Although selective frozen section analysis of suspected regions during surgery is feasible, this technique is time-consuming, can only examine a small part of the specimen, and is subject to sampling errors [2]. Therefore, frozen section analysis is associated with a high false-negative rate [3]. A labour-intensive and still subjective improvement would be extensive intraoperative assessment of the resection margins on the specimen by the surgeon and a pathologist [4], with efforts to base such an assessment on objective optical methods [5]. There is a clear need for highly accurate, intraoperative, real-time methods for tumour margin identification. The increasing interest and preclinical and clinical findings in the field of fluorescence imaging emphasise its potential for intraoperative management.

Fluorescence-guided surgery is an optical imaging method that provides real-time guidance for the delineation of tumours during surgery, with higher sensitivity than direct visual inspection and palpation[6]. An additional benefit of this imaging technique is that it allows for scanning of large surfaces, which might result in the detection of clinically occult tumour lesions.

5-aminolevulinic acid has been well established for its use in fluorescence-guided neurosurgery and has been studied since 1998, leading to a landmark multicentre, randomised controlled trial of fluorescence-guided surgery in 2006 [7-9]. This study showed higher rates of gross total resection for patients in the 5-aminolevulinic acid group, and significantly improved progression-free survival after 6 months. In the past decade, several groups have started to report on the clinical impact of using 5-aminolevulinic acid to adapt the surgical plan, improving the intraoperative extent of resection [10-12]. Fluorescence imaging with indocyanine green, which is analogous to 5-aminolevulinic acid, was introduced in 2007 for the realtime identification of liver cancers, and remains a commonly used technique in various settings, including hepatic resection and vascular perfusion assessment [13, 14]. Clinical implementation of 5-aminolevulinic acid and indocyanine green was facilitated by the fact that these compounds were already approved for clinical use by the US Food and Drug Administration. Considering the enormous costs associated with drug development, offlabel use of already approved agents was the logical next step [15].

These conventional fluorescence imaging agents led to the development of many near-infrared fluorescent agents with improved molecular specificity and image contrast. Indeed, imaging in the near-infrared region of the electromagnetic spectrum has optimal characteristics that limit the effects of autofluorescence and light scattering and increase tissue penetration [16]. These tumour-specific fluorescent agents consist of fluorophores attached to various targeted ligands, including peptides, antibodies, affibodies, activatable tracers, and small molecules [17, 18]. So far, clinical studies on intraoperative fluorescence imaging with several fluorescent targeting agents show promising results for various cancer types [18].

To date, most studies on intraoperative fluorescence imaging have been proof-of-principle studies [1, 19-54]. In addition to safety considerations, the technical and diagnostic performances of combinations of fluorescent targeting agents and imaging devices have been evaluated for tumour-to-background ratio and for the sensitivity and specificity of the fluorescent signal. These factors provide essential information about the quality of the imaging strategy, and these data are indispensable for further development of this new technology. However, the purpose of fluorescence-guided surgery is to improve oncological and functional outcomes. Therefore, when evaluating the clinical value of fluorescence-guided surgery, this technique could be considered not only as an imaging method, but also as a tool for decision making. In other words, how does surgical management change when fluorescence-guided surgery is added to the surgical procedure? Additionally, in how many cases does this change in management result in an improved oncological or functional outcome?

Providing insight into how intraoperative fluorescence imaging affects patient care is essential for funding agencies and regulatory bodies, which weigh costs and safety risks against clinical benefit—a crucial step towards approval and widespread clinical implementation[55]. Although US Food and Drug Administration guidance documents for approval of imaging products state that an agent's ability to locate and outline normal structures, or distinguish between normal and abnormal anatomy, are sufficient evidence of its clinical usefulness, some health-care funders frequently enforce strict requirements regarding efficacy [55]. Thus, to evaluate the added clinical value of fluorescence-guided surgery, its effect on clinical decision making needs to be identified. Most early-stage studies report on diagnostic performance and do not aim to assess the effect of fluorescence-guided surgery on surgical decision making. However, they can still provide an indication of the number of cases in which surgical management would potentially have changed if clinical follow through had been done. In this Review, we present an overview of the current reporting methods of clinical studies that mainly focus on diagnostic performance. We then explain why change in surgical management is an essential outcome measurement to evaluate the effect of fluorescence imaging on cancer surgery. Finally, we establish metrics to define changes in intraoperative decision making that result from intraoperative fluorescence imaging.

Limitations of current reports on intraoperative fluorescence imaging

The tumour-to-background ratio shows the ability of an imaging strategy to provide contrast between tumour and surrounding tissue for accurate tumour delineation or identification of clinically occult lesions. It is a routinely reported endpoint in preclinical and clinical studies to establish the ideal dose of an imaging agent. Sensitivity and specificity, requiring large sample sizes for powered calculation, are generally evaluated in phase 2 and 3 clinical trials[56]. These test characteristics provide insight into the fluorescent agent's targeting efficacy: does the fluorescence colocalise with the tumour, and is a non-fluorescent area free of tumour[57]?

Direct comparison between the results of such clinical studies of fluorescence-guided surgery is difficult [18], partly because there is no consensus on standardised protocols for the clinical evaluation of fluorescent targets. Equally important is the nature of the outcome parameters. For example, calculations of the tumour-to-background ratio, an important determinant for the evaluation of the efficacy of a fluorescent tracer, can be influenced by selection bias for relevant regions of interest, tissue optical properties that are generally variable and unknown in each individual patient, and the technical specifications and performance of the chosen imaging instrument[16]. Interobserver variation, learning curves for technology use, tumour size, and antigen expression are just a few of many other variables that are challenging to quantify. Moreover, whereas the ex-vivo tumour-to-background ratio is often not reported, the more clinically relevant in-vivo tumour-to-background ratio is even less so.

We advocate for the reporting of all changes to intraoperative decision making precisely because of the challenge of objectively evaluating all possible influencing factors. Overall, the impact of fluorescence-guided surgery on intraoperative decision making is the most effective and objective outcome measurement that is independent of interinstitution and intrainstitution variance and can be compared across all cancer types, imaging systems, and fluorescent tracers.

Although tumour-to-background ratio, sensitivity, and specificity are important markers of the diagnostic performance of fluorescence-guided surgery, they do not provide information on how frequently fluorescence imaging information leads to a change in conventional surgical practice. Additionally, such changes brought on by fluorescence-guided surgery must be evaluated for their efficacy so that an improved clinical outcome can be attributed to it; disclosing the frequency of these changes is necessary to gain insight into how fluorescence-guided surgery contributes to clinical outcome. Data obtained from consistent recording and quantification of adjustments made to the standard workflow in current and future clinical trials of fluorescence-guided surgery will exemplify its effect on clinical decision making, and are essential to establish an eventual correlation with patient outcomes in the long term.

Four basic applications of fluorescence imaging during cancer surgery

To describe a change in surgical management, the four basic applications of intraoperative fluorescence imaging need to be acknowledged. Each application brings a different benefit, having a slightly distinct standard surgical management (figure 1), and is therefore evaluated by different clinical trial endpoints [58]. Clinical examples of each application are illustrated in figure 2.

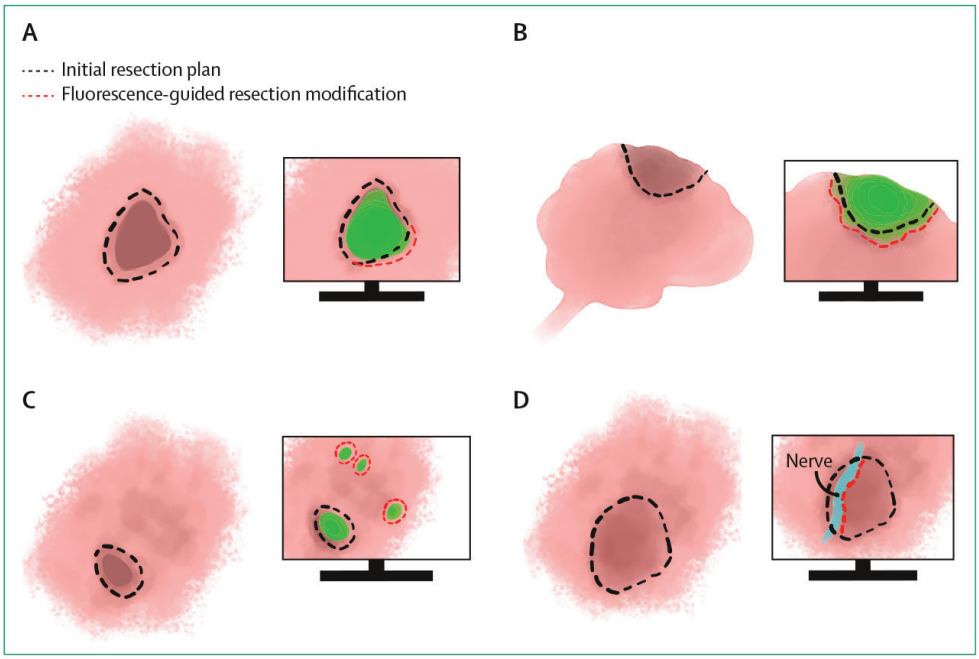

Figure 1: Schematic representations of the four basic applications of fluorescence-guided surgery

Green shaded areas represent fluorescence emitted by tumour cells. (A) Excision with tumour-free margins. (B) Debulking procedures. (C) Identification of clinically occult lesions. (D) Identification of vital structures and vascular perfusion (blue shaded area represents fluorescence emitted by nerve).

The first application for which fluorescence-guided surgery is suitable is excision aimed at achieving adequate tumour-free margins, which is the mainstay of surgical treatment for many solid tumours, including breast, colon, skin, prostate, lung, head and neck, and many others (figures 1A, 2A). In most cases, an adequate surgical margin is an important surrogate marker for overall survival [62]. Fluorescence imaging can be used in vivo during surgery or ex vivo on the specimen, to decide where to do a frozen section assessment, additional resection, or both [24, 36, 63]. The main oncological outcome parameter for fluorescence-guided surgery, compared with the standard of care, is an increase in the percentage of patients with adequate surgical margins. Additionally, precise margin delineation is imperative in delicate regions, where wider resection inevitably leads to increased morbidity and loss of functionality (eg, in head and neck cancer). For these cases, the extent of the resection might decrease

when guided by the fluorescence signal. These parameters should be reported as a percentage of cases in which the conventional surgical management was changed, on the basis of intraoperative fluorescence imaging findings on the resected specimen (ie, ex vivo) or wound bed (ie, in situ). Importantly, efficacy should then be objectified by reporting the percentage of additional resections that are histopathologically confirmed true positives or false positives for tumour cells.

The second application of fluorescence-guided surgery is as a debulking procedure aimed at decreasing the tumour load as much as possible without compromising vital structures (figures 1B, 2B). In ovarian cancer and some brain tumours, debulking or cytoreductive surgery is done to increase the efficacy of adjuvant radiotherapy or chemotherapy [64]. For incurable disease, debulking can be done to improve quality of life. In these procedures, the main oncological outcome benefit of fluorescence-guided surgery is its ability to identify the perimeter of the tumour or additional clinically occult lesions [8, 49, 65]. This outcome should be reported as the percentage of cases in which additional resection is done to remove more tumour tissue based on the fluorescence signal. Again, the percentage of additional resections that are histopathologically confirmed true positives or false positives should be reported.

The third application in which fluorescence-guided surgery can be beneficial is in the identification of clinically occult lesions (figures 1C, 2C). There are many examples of the utility of fluorescence-guided surgery in this context, including identification of occult pulmonary [66] or abdominal [67] lesions, sentinel lymph nodes [68], and use in multifocal or multicentric tumours where multiple tumours might be present within a single organ (eg, breast, liver, kidney, and thyroid), separate from the lesion that is clinically evident. In these cases, fluorescence-guided surgery might aid in identifying secondary, separately located, clinically occult tumours [58]. Reporting should be consistent with that of debulking procedures, whereby the percentage of additional resected lesions and histopathologically confirmed true-positive or false-positive rates are included. An additional element needs to be considered when fluorescence-guided surgery is evaluated as a diagnostic tool for sentinel lymph node detection, in that a false-negative sentinel lymph node can translate to more conservative treatment; hence, the incidence of false negatives should also be reported.

The fourth application of fluorescence-guided surgery considers the non-oncological aspects of cancer surgery (figures 1D, 2D). Fluorescence imaging can be applied to aid in the identification of relevant vital structures that need to be spared during oncological surgery. These structures can be identified and imaged during the operation, and the trial endpoints in these studies focus on reducing the rate of iatrogenic injury and related morbidity. Examples include imaging of the biliary tract during hepatobiliary surgery [69], and of nerves [70] or ureters during abdominopelvic surgery [60]. However, in these studies, objectively establishing the change in surgical management can be challenging because the surgeon is

not masked to the fluorescence signal and is very likely to follow the fluorescent signal to prevent iatrogenic injury.

Another non-oncological application of fluorescence-guided surgery in cancer surgery is the assessment of vascular perfusion. Examples include the use of fluorescence-guided surgery to evaluate the perfusion of free-flap reconstructions [71], peritoneum [72], or skin [73]. Similarly, indocyanine green has been used to identify segmental and subsegmental boundaries to facilitate anatomical resection during liver and lung surgery [74, 75]. Moreover, anastomotic leakage, the complication in colorectal surgery that is most associated with increased morbidity and mortality, has been shown to be reduced with the use of fluorescence-guided surgery in randomised controlled trials [76]. The clinical benefit of fluorescence-guided surgery for such applications needs to be concluded from improved surgical outcome (eg, reduction of iatrogenic injury, tissue sparing, flap failure, or anastomotic leakage) [58].

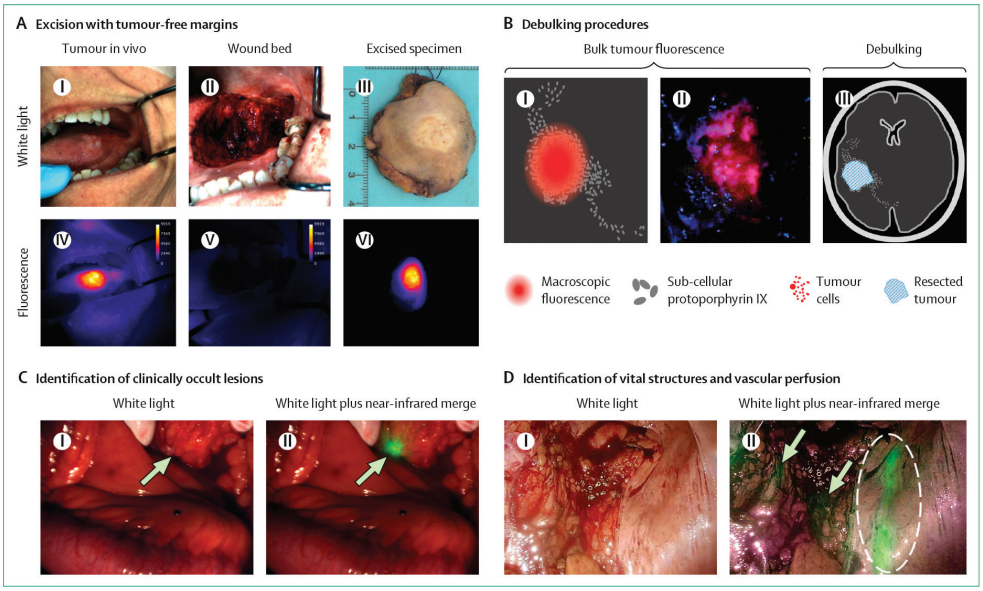

Figure 2: Clinical examples of the four basic applications of fluorescence-guided surgery

(A) Fluorescence imaging using pH-activatable nanoprobe ONM-100 in head and neck squamous cell carcinoma of the tongue. In-vivo (I, II, IV, and V) and ex-vivo (III and VI) visualisation of high-fluorescence signal in the tumour and low-fluorescence signal in the tumour-free margin and wound bed. Reproduced from Voskuil and colleagues[39], by permission of Nature. (B) 5-aminolevulinic acid-based fluorescence imaging in neurosurgery. (I) Macroscopic protoporphyrin IX fluorescence is visible at the central portion of a high-grade glioma, but not at the infiltrative margins. (II) Example fluorescence microscopy image of protoporphyrin IX expression in the tumour. (III) Debulking guided by macroscopic protoporphyrin IX fluorescence resulting in residual tumour burden. Reproduced from Wei and colleagues[59], by permission of Frontiers. (C) Intraoperative detection with fluorescent tracer bevacizumab-IRDye800CW of a peritoneal metastasis (arrow) detected by white light alone (I) and fluorescence-guided surgery using the near-infrared signal merged with white light (II). Reproduced from Harlaar and colleagues[60], by permission of Elsevier. (D) Visualisation

of ureter residing under peritoneum with fluorophore ZW800-1 using white light alone (I) and the near-infrared fluorescence signal merged with white light (II). The ureter (dashed circle) is captured during a pulse of urine flow during surgery. The darker green areas (arrows) show background fluorescence from vessels in the surrounding tissue. Reproduced from de Valk and colleagues[61], by permission of Nature.

Current clinical trial designs for fluorescence-guided surgery

Several completed and ongoing clinical trials of fluorescent agents were analysed to identify studies that report a change in surgical management as an outcome parameter. Studies were categorised according to their design, focusing on how and when fluorescence-guided surgery was introduced into the standard of care (table, showing the lowest [type A] to the highest [types E and F] potential for reporting the effect of fluorescence-guided surgery on intraoperative decision making). This categorisation allowed for the identification of study designs that can provide information on (potential) changes in intraoperative decision making. The following questions regarding steps taken as a result of fluorescence imaging were assessed: did fluorescence imaging influence intraoperative decision making and, if so, to what degree? Were biopsies or additional resections done as a result of residual fluorescence in the wound bed, the resected specimen, or both, or was resection (also) guided by fluorescence imaging beforehand?

In type A studies, fluorescence and white light images or videos are collected before resection, after which fluorescence intensity is compared with the surrounding background tissue, fluorescence is correlated with tumour presence, and results are analysed offline. The primary motivation for these studies is to assess the sensitivity and specificity of the fluorescent agent. This study type could be thus adapted to evaluate potential changes in intraoperative decision making (not yet been done in published reports): first, delineate the conventional tumour resection, then use fluorescence imaging, and report whether the tumour outline changed. This procedure would thus still provide insight into how fluorescence imaging might have altered the surgical plan.

Studies of type B, C, and D describe cases in which observations by fluorescence imaging indicate potential for a change in intraoperative decision making. Unfortunately, the percentage of cases in which this potential change happens is seldom reported. In type B studies, fluorescence imaging of the resected specimen is done. Fluorescence on the specimen surface might indicate a close or positive resection margin. Although the surgical management is not altered, this finding clearly highlights the clinical impact that fluorescence imaging would have had if acted on.

Table: Types of clinical trial designs for fluorescence-guided surgery

	Timing of fluorescence imaging	Design	Reported changes in intraoperative decision making
Type A	Preresection [24–27]	Fluorescence imaging and white light imaging of lesions; standard removal of lesions	None (data might be available)*
Type B	On the resected specimen [28–32]	Standard identification and removal of lesions; fluorescence imaging of specimen	None (data available)†
Type C	Preresection; on the resected specimen, wound bed, or both [1,33–36]	Fluorescence imaging and white light imaging of lesions; standard removal of lesions; fluorescence imaging of wound bed, specimen, or both	None (data available)†
Type D	Type C with biopsies of fluorescent lesions [37–43]	Fluorescence imaging and white light imaging of lesions; standard removal of lesions; fluorescence imaging of wound bed, specimen, or both; biopsies of fluorescent lesions	None (data available)†
Type E	Preresection; on the resected specimen, wound bed, or both [44–53]	Fluorescence imaging and white light imaging of lesions; standard removal of lesions; fluorescence imaging of wound bed, specimen, or both; additional resection of residual fluorescent lesions, or other change in surgical plan	Yes; reporting not always comprehensive
Type F	Throughout the entire procedure [10,35,54–58]	Removal of lesions guided by fluorescence imaging and visual inspection or palpation	Yes; reporting not always comprehensive

*Study design that could be adapted to provide data to inform on how often fluorescence imaging would have led to a change in intraoperative decision making. †Study design that provides data to inform on how often fluorescence imaging would have led to a change in intraoperative decision making.

In type C studies, fluorescence imaging is done before resection, followed by fluorescence imaging of the resected specimen, wound bed, or both. Regardless of the findings of fluorescent signals, no additional resections are done during the operation. Because no biopsies are taken from the fluorescent lesions in the wound bed in these studies, whether fluorescence correlates with tumour presence (ie, whether these lesions are true or false positives) is unclear. However, the finding of residual fluorescent lesions still suggests that if the resection is directed by fluorescence imaging, the surgical management might be different from standard practice.

Type D studies are similar to type C studies, except that biopsies of residual fluorescent lesions are taken, providing additional essential information on true-positive and false-positive detection rates. Despite the outcome of these biopsies, no additional resection is done, and surgical management is therefore not changed. This approach does, however, allow the researcher to report the percentage of cases in which a change in surgical management

is occasioned by the fluorescence imaging results. In some surgical cases in which areas with residual fluorescence are not also clinically suspect, and specificity of the targeting agent is not yet well established, limiting disruption of the standard of care by only taking biopsies for retrospective correlation with histopathology is ethically justified.

Type E includes studies in which resection is primarily based on standard-of-care palpation and visual inspection, with further resection of fluorescent lesions. This design is ideal for reporting the altered management of fluorescence-guided surgery compared with standard surgical practice. The resected lesions undergo pathological examination, so true and false positives can be reported. Although these studies suggest changes in intraoperative decision making, they do not always report in how many cases the standard of care was altered.

A type F study design implies true fluorescence-guided surgery, wherein the initial resection is based on the combination of fluorescence imaging and standard-of-care visual inspection and palpation. Fluorescence imaging and traditional cues are complementary and assessed simultaneously: fluorescence signals provide additional information to aid the surgeon in intraoperative decision making, without the intention to overrule a surgeon's judgment. Different from a type E study, where fluorescence-guided surgery might guide the resection of additional lesions that would have been missed otherwise, a type F design can also result in more restricted resection than would current standard practice (ie, the surgeon can decide to more conservatively resect lesions based on how they fluoresce).

Insufficient reporting of the potential clinical effect of fluorescence-guided surgery

As can be concluded from the table, only a few clinical trials currently report changes in surgical management as a separate outcome parameter. However, many of the type E and F trials suggest that fluorescence imaging information might (or did) alter the standard surgical procedure, although in how many surgical cases a change actually occurred is not generally reported. Several studies mention malignant lesions that were only identified with fluorescence imaging [31, 39, 40, 43-46, 48, 51, 53, 54], but the number of cases in which the management would have been changed is often not specified. This underreporting represents missed opportunities because, on the basis of their study design, it can be deduced that these data should be available to the researcher. If changes to surgical management were clearly reported, much information about the potential clinical impact of fluorescence-guided surgery would become available to the field.

The few trials that do report this specific parameter illustrate its clinical usefulness. One type F study reported that this parameter "improved surgical decision making", showing that fluorescence imaging led to an improvement in surgical outcome in 21% of cases [50]. Several other studies describe additional action as a result of fluorescence imaging[31, 43-47, 54].

In the only completed randomised controlled trial of fluorescence imaging for primary tumour surgery, true fluorescence-guided resection with 5-aminolevulinic acid was done in patients with malignant gliomas[8]. In this phase 3 study, in which 322 patients were randomly assigned to either fluorescence-guided surgery or conventional microsurgery with white light, endpoints were solely concerned with differences in outcome (eg, amount of residual contrast-enhancing tumour and progression-free survival); the results showed higher rates of gross total resection for patients in the 5-aminolevulinic acid group and significantly improved progression-free survival after 6 months. There is a need to quantitatively assess also overall survival and quality of life attributable to fluorescence-guided surgery, but such endpoints require costly, time-consuming, and logistically cumbersome randomised controlled trials, and require long follow-up periods. The ability to draw conclusions on the potential clinical impact of fluorescence-guided surgery from earlier, smaller scale studies would facilitate the decision to proceed from phase 1 and phase 2 studies to new randomised controlled trials.

Reporting changes in surgical management guided by fluorescence imaging

To show (potential) deviations from the standard of care as a result of fluorescence-guided surgery, it is important that comparisons can be made between standard-of-care surgery with and without fluorescence. For this comparison to be possible, it is necessary that more attention is given to the description of the method, as the study type (table) determines how and to what degree this effect can be analysed. The key factor in reporting the effect of fluorescence-guided surgery on intraoperative decision making is to describe clearly whether additional steps (eg, biopsy or resection) are taken as a result of fluorescence-guided surgery and in how many cases this decision was justified (true or false positive). Besides prompting additional resections, fluorescence imaging findings could also lead to abortion of the procedure in cases in which clinically occult, distant, and inoperable metastases are discovered [43]. Importantly, any complications or morbidity related to additional resection need to be reported. The usefulness of this parameter as a primary outcome measurement is underlined by the phase 3 trial on ovarian cancer (NCT03180307) assessing the efficacy of OTL38 (a folate-indole-cyanine green-like conjugate to folate receptor alpha). In this trial, efficacy was defined as the proportion of patients in which fluorescence imaging yields at least one additional tumour-positive lesion compared with normal conditions. Change in surgical management is also a secondary outcome in an ongoing randomised controlled trial of SGM-101, a fluorochrome-labelled anti-carcinoembryonic antigen monoclonal antibody, in colorectal cancer patients (NCT03659448).

Another important implication of fluorescence-guided surgery is its potential for more conservative surgical excision: to reduce unnecessary resection of non-malignant tissue (ie, retention of normal tissue). This objective is particularly important for tumours located in functionally or aesthetically delicate areas. When evaluating the added value of fluorescence-

guided surgery, it is important to also provide insight into these changes in intraoperative decision making that lead to reduced unnecessary resection.

We propose a checklist of recommendations that are relevant for the evaluation of changes in intraoperative clinical decision making (panel; see table for study type details).

Panel: Recommendations for the evaluation of changes in intraoperative decision making

Fluorescence imaging preresection
- Report whether the intended resection was, or could have been, altered on the basis of fluorescence imaging
- Include a fluorescence imaging step between delineation and resection of the tumour

Fluorescence imaging sequence during resection
- Report whether resection is done as per standard of care (without fluorescence imaging)
- Report whether and how surgical management changes when fluorescence imaging is turned on and off during resection

Fluorescence imaging of specimen
- Report the percentage of cases in which a fluorescent lesion on the specimen surface, corresponding to a close or positive surgical margin, would have caused a change in surgical management (types B or C study design), results in an additional biopsy (type D study design), or results in additional resection (type E study design)
- Compare standard-of-care sampling to fluorescence imaging-based sampling

Fluorescence imaging of wound bed
- Report the percentage of cases where a fluorescent lesion in the wound bed would have caused a change in surgical management (types B or C study design), results in an additional biopsy (type D study design), or results in additional resection (type E study design)

Fluorescence imaging of other scanned surfaces

Report the percentage of cases in which clinically occult lesions are detected and whether this detection changed intraoperative decision making, postoperative clinical management, outcome, or all (types E and F study design)

In general, report:
- Detection rate of true positives (fluorescent malignant lesions)
- Detection rate of false positives (fluorescent lesions without malignancy)
- Detection rate of false negatives* (non-fluorescent malignant lesions)
- Any complications or morbidity related to fluorescence-guided additional resections
- Change in duration of the surgical procedure as a result of fluorescence-guided surgery
- Changes in postoperative clinical management and outcome related to fluorescence-guided surgery

*The true negative rate is omitted because it would require histopathological evaluation of 100% of the imaged surface, which is unfeasible in the clinical setting. Conclusions on the true negative rate of fluorescence imaging can most likely be drawn only on the basis of patient outcomes, although there are many possible confounders, such as postsurgical therapy (eg, radiation).

DISCUSSION

The need for more uniformity in reporting results of fluorescence-guided surgery has been extensively discussed [55, 57, 77-79]. We believe that the effect of fluorescence-guided surgery on intraoperative decision making should be added as a standardised part of reporting. Our recommendations for reporting the change in intraoperative management aim to make this effect quantifiable and easy to evaluate and compare.

Phase 1 and phase 1/2 studies are frequently designed not to interfere with the standard of clinical care, but fluorescence imaging-related observations can still indicate the clinical potential of fluorescence imaging. Study types A and B are typical for phase 1 and 1/2 trials, wherein safety, feasibility, and efficacy of the imaging strategy (fluorescent agent, camera,

or both) are measured simultaneously. These studies are generally required for medical and ethical reasons before alteration of the standard of care (ie, types E and F studies) can be approved. Type D studies provide a good alternative by incorporating the possibility of taking biopsies from fluorescent areas in the wound bed, specimen, or both for correlation with histopathology. Such biopsies add essential information about the potential impact of fluorescence-guided surgery on intraoperative decision making and whether additional resection would have been justified. In cases where areas with residual fluorescence are also clinically suspect, intraoperative frozen sections would be preferable to biopsies because these lesions can then readily be resected, which increases the likelihood of clinical benefit.

Introducing a new technique into the operating room might be initially associated with incremental operating time, more biopsies, and potentially higher morbidity in cases with additional resections. These changes can be associated with higher costs. However, there have been studies reporting a reduction in operation time because fluorescence-guided surgery allowed a clearer delineation of vascular structures, expediting dissection and preventing injury [80]. Moreover, fluorescence-guided surgery is anticipated to eventually replace the role of fresh frozen analysis, which would substantially reduce operating time. Finally, the use of fluorescence-guided surgery could increase the rate of clear resection margins or result in more personalised adjuvant treatment regimens. When resulting in improved oncological outcome, fluorescence-guided surgery will also lead to a reduction in costs related to diagnosis and salvage treatment of recurrent disease. Analyses have shown that fluorescence-guided surgery appears to be cost-effective in surgery for high-grade gliomas [81] and breast cancer [82]. Future cost-effectiveness studies are required to further elucidate the weight of all these variables. Therefore, it is important that these factors are reported.

The clinical impact of fluorescence-guided surgery encompasses more than changes to surgical decision making. Unanticipated intraoperative findings can also have an effect on postoperative clinical management and outcome. For example, fluorescence imaging might show occult tumour lesions, which can result in changed adjuvant therapy, potentially affecting tumour recurrence and patient survival. Another advantage of fluorescence-guided surgery is its ability to reflect biological characteristics of viable cancer cells. Fluorescence signal intensity can visualise molecular expression patterns, which might have prognostic value [83]. Both surgical changes and additional intraoperative findings (that do not necessarily lead to immediate action) gained from intraoperative fluorescence imaging should be reported. Evidence supporting the clinical impact of fluorescence-guided surgery in a broader sense can be obtained much more effectively when early, smaller scale studies also report on potential clinical consequences: it is the first step towards correlation of intraoperative decision making and findings with patient outcomes.

The most scientifically robust study design to assess the clinical impact of fluorescence-guided surgery is a multicentre, randomised controlled trial with functional outcome and

disease-specific survival as primary endpoints. To minimise surgeon bias, initial inspection and delineation of the tumour by the surgeon should be done while the surgeon is masked to the fluorescence signal—that is, before the first intraoperative imaging sequence. Under these semiblinded circumstances, the standard operating procedure is the control situation, and each patient is his or her own control [78]. Depending on the application and cancer type, numerous secondary endpoints could be considered. Examples include the change in rate of positive margins; retention of normal tissue; preservation of tissue function; occurrence of complications; prediction of postoperative outcomes (eg, risk of recurrence and sensitivity to chemotherapy); and change in the need for adjuvant therapies or salvage surgery [55].

CONCLUSION

Current evaluations of fluorescence-guided surgery mainly focus on diagnostic performance through outcome parameters that are notoriously difficult to objectively evaluate and quantify, and that do not inform about the clinical implications of the technique. Without adequate reporting of the impact of fluorescent findings on intraoperative decision making, there is a serious risk that the field of fluorescence-guided surgery will not progress towards widespread clinical implementation. These relevant insights can be obtained by reporting how (and how frequently) fluorescence-guided surgery leads to changes in intraoperative decision making (eg, additional or more limited resections) compared with current practice. In addition, these changes need to be evaluated for the efficacy and safety attributed to fluorescence-guided surgery to be correlated with patient outcomes in the long term. The impact of fluorescence-guided surgery on intraoperative decision making is the most effective and objective outcome measurement to evaluate the clinical value of fluorescence-guided surgery and to compare study results across all cancer types, imaging systems, and fluorescent tracers.

SEARCH STRATEGY AND SELECTION CRITERIA

Relevant studies were collated by searching clinicaltrials.gov, cinicaltrialsregister.eu, the Dutch Trial Register, and the International Standard Randomised Controlled Trial Number Registry with the search terms “cancer” or “tumo(u)r”, combined with “fluorescence”, “fluorescence-guided surgery”, “image guided surgery”, “molecular imaging”, and “optical imaging”. References for this review were then identified by searching PubMed using the same terms as mentioned above, as well as National Clinical Trial numbers. Only papers published in English between Jan 1, 2006, and July 1, 2020, were considered. The final reference list was generated on the basis of originality and was limited to papers presenting results from clinical trials of fluorescence-guided surgery.

REFERENCES

1. Koller, M., et al., *Implementation and benchmarking of a novel analytical framework to clinically evaluate tumor-specific fluorescent tracers.* Nat Commun, 2018. **9**(1): p. 3739.
2. St John, E.R., et al., *Diagnostic Accuracy of Intraoperative Techniques for Margin Assessment in Breast Cancer Surgery: A Meta-analysis.* Ann Surg, 2017. **265**(2): p. 300-310.
3. Cendan, J.C., D. Coco, and E.M. Copeland, 3rd, *Accuracy of intraoperative frozen-section analysis of breast cancer lumpectomy-bed margins.* J Am Coll Surg, 2005. **201**(2): p. 194-8.
4. van Lanschot, C.G.F., et al., *Relocation of inadequate resection margins in the wound bed during oral cavity oncological surgery: A feasibility study.* Head Neck, 2019. **41**(7): p. 2159-2166.
5. Barroso, E.M., et al., *Water Concentration Analysis by Raman Spectroscopy to Determine the Location of the Tumor Border in Oral Cancer Surgery.* Cancer Res, 2016. **76**(20): p. 5945-5953.
6. Vahrmeijer, A.L., et al., *Image-guided cancer surgery using near-infrared fluorescence.* Nat Rev Clin Oncol, 2013. **10**(9): p. 507-18.
7. Stummer, W., et al., *Intraoperative detection of malignant gliomas by 5-aminolevulinic acid-induced porphyrin fluorescence.* Neurosurgery, 1998. **42**(3): p. 518-25; discussion 525-6.
8. Stummer, W., et al., *Fluorescence-guided surgery with 5-aminolevulinic acid for resection of malignant glioma: a randomised controlled multicentre phase III trial.* Lancet Oncol, 2006. **7**(5): p. 392-401.
9. Georges, J.F., et al., *Delta-Aminolevulinic Acid-Mediated Photodiagnoses in Surgical Oncology: A Historical Review of Clinical Trials.* Front Surg, 2019. **6**: p. 45.
10. Cornelius, J.F., et al., *Impact of 5-aminolevulinic acid fluorescence-guided surgery on the extent of resection of meningiomas--with special regard to high-grade tumors.* Photodiagnosis Photodyn Ther, 2014. **11**(4): p. 481-90.
11. Hollon, T., et al., *Surgical Adjuncts to Increase the Extent of Resection: Intraoperative MRI, Fluorescence, and Raman Histology.* Neurosurg Clin N Am, 2019. **30**(1): p. 65-74.
12. Foster, N. and S. Eljamel, *ALA-induced fluorescence image guided surgery of meningiomas: A meta-analyses.* Photodiagnosis Photodyn Ther, 2016. **15**: p. 73-8.
13. Ishizawa, T., et al., *Real-time identification of liver cancers by using indocyanine green fluorescent imaging.* Cancer, 2009. **115**(11): p. 2491-504.
14. Purich, K., et al., *Intraoperative fluorescence imaging with indocyanine green in hepatic resection for malignancy: a systematic review and meta-analysis of diagnostic test accuracy studies.* Surg Endosc, 2020. **34**(7): p. 2891-2903.
15. Samkoe, K.S., et al., *Application of Fluorescence-Guided Surgery to Subsurface Cancers Requiring Wide Local Excision: Literature Review and Novel Developments Toward Indirect Visualization.* Cancer Control, 2018. **25**(1): p. 1073274817752332.
16. Keereweer, S., et al., *Optical image-guided cancer surgery: challenges and limitations.* Clin Cancer Res, 2013. **19**(14): p. 3745-54.
17. Joshi, B.P. and T.D. Wang, *Targeted Optical Imaging Agents in Cancer: Focus on Clinical Applications.* Contrast Media Mol Imaging, 2018. **2018**: p. 2015237.
18. Hernot, S., et al., *Latest developments in molecular tracers for fluorescence image-guided cancer surgery.* The Lancet Oncology, 2019. **20**(7): p. e354-e367.
19. Sturm, M.B., et al., *Targeted imaging of esophageal neoplasia with a fluorescently labeled peptide: first-in-human results.* Sci Transl Med, 2013. **5**(184): p. 184ra61.
20. Joshi, B.P., et al., *Multimodal endoscope can quantify wide-field fluorescence detection*

of Barrett's neoplasia. Endoscopy, 2016. **48**(2): p. A1-A13.
21. Joshi, B.P., et al., *Detection of Sessile Serrated Adenomas in the Proximal Colon Using Wide-Field Fluorescence Endoscopy.* Gastroenterology, 2017. **152**(5): p. 1002-1013 e9.
22. van Keulen, S., et al., *Intraoperative Tumor Assessment Using Real-Time Molecular Imaging in Head and Neck Cancer Patients.* J Am Coll Surg, 2019. **229**(6): p. 560-567 e1.
23. Hsiung, P.L., et al., *Detection of colonic dysplasia in vivo using a targeted heptapeptide and confocal microendoscopy.* Nat Med, 2008. **14**(4): p. 454-8.
24. van Keulen, S., et al., *Rapid, non-invasive fluorescence margin assessment: Optical specimen mapping in oral squamous cell carcinoma.* Oral Oncol, 2019. **88**: p. 58-65.
25. Dintzis, S.M., et al., *Real-time Visualization of Breast Carcinoma in Pathology Specimens From Patients Receiving Fluorescent Tumor-Marking Agent Tozuleristide.* Arch Pathol Lab Med, 2019. **143**(9): p. 1076-1083.
26. Slooter, M.D., et al., *Detecting tumour-positive resection margins after oral cancer surgery by spraying a fluorescent tracer activated by gamma-glutamyltranspeptidase.* Oral Oncol, 2018. **78**: p. 1-7.
27. Whitley, M.J., et al., *A mouse-human phase 1 co-clinical trial of a protease-activated fluorescent probe for imaging cancer.* Sci Transl Med, 2016. **8**(320): p. 320ra4.
28. Fakurnejad, S., et al., *Intraoperative Molecular Imaging for ex vivo Assessment of Peripheral Margins in Oral Squamous Cell Carcinoma.* Front Oncol, 2020. **9**: p. 1476.
29. Hekman, M.C., et al., *Tumor-targeted Dual-modality Imaging to Improve Intraoperative Visualization of Clear Cell Renal Cell Carcinoma: A First in Man Study.* Theranostics, 2018. **8**(8): p. 2161-2170.
30. Rosenthal, E.L., et al., *Safety and Tumor Specificity of Cetuximab-IRDye800 for Surgical Navigation in Head and Neck Cancer.* Clin Cancer Res, 2015. **21**(16): p. 3658-66.
31. Tummers, Q.R.J.G., et al., *Intraoperative imaging of folate receptor alpha positive ovarian and breast cancer using the tumor specific agent EC17.* Oncotarget, 2016. **7**(22).
32. de Valk, K.S., et al., *First-in-Human Assessment of cRGD-ZW800-1, a Zwitterionic, Integrin-Targeted, Near-Infrared Fluorescent Peptide in Colon Carcinoma.* Clin Cancer Res, 2020. **26**(15): p. 3990-3998.
33. Cho, S.S., et al., *Intraoperative near-infrared imaging with receptor-specific versus passive delivery of fluorescent agents in pituitary adenomas.* J Neurosurg, 2018: p. 1-11.
34. Guzzo, T.J., et al., *Intraoperative Molecular Diagnostic Imaging Can Identify Renal Cell Carcinoma.* J Urol, 2016. **195**(3): p. 748-55.
35. Lee, J.Y.K., et al., *Folate receptor overexpression can be visualized in real time during pituitary adenoma endoscopic transsphenoidal surgery with near-infrared imaging.* J Neurosurg, 2018. **129**(2): p. 390-403.
36. Gao, R.W., et al., *Determination of Tumor Margins with Surgical Specimen Mapping Using Near-Infrared Fluorescence.* Cancer Res, 2018. **78**(17): p. 5144-5154.
37. Liu, J., et al., *In vivo molecular imaging of epidermal growth factor receptor in patients with colorectal neoplasia using confocal laser endomicroscopy.* Cancer Lett, 2013. **330**(2): p. 200-7.
38. Nishio, N., et al., *Optimal Dosing Strategy for Fluorescence-Guided Surgery with Panitumumab-IRDye800CW in Head and Neck Cancer.* Mol Imaging Biol, 2020. **22**(1): p. 156-164.
39. Voskuil, F.J., et al., *Exploiting metabolic acidosis in solid cancers using a tumor–agnostic pH-activatable nanoprobe for fluorescence-guided surgery.* Nat Commun, 2020. **11**(1): p. 3257.
40. Burggraaf, J., et al., *Detection of colorectal polyps in humans using an intravenously administered fluorescent peptide targeted*

against c-Met. Nat Med, 2015. **21**(8): p. 955-61.

41. Hoogstins, C.E.S., et al., *Image-Guided Surgery in Patients with Pancreatic Cancer: First Results of a Clinical Trial Using SGM-101, a Novel Carcinoembryonic Antigen-Targeting, Near-Infrared Fluorescent Agent.* Ann Surg Oncol, 2018. **25**(11): p. 3350-3357.
42. Lamberts, L.E., et al., *Tumor-Specific Uptake of Fluorescent Bevacizumab-IRDye800CW Microdosing in Patients with Primary Breast Cancer: A Phase I Feasibility Study.* Clin Cancer Res, 2017. **23**(11): p. 2730-2741.
43. Lu, G., et al., *Tumour-specific fluorescence-guided surgery for pancreatic cancer using panitumumab-IRDye800CW: a phase 1 single-centre, open-label, single-arm, dose-escalation study.* Lancet Gastroenterol Hepatol, 2020. **5**(8): p. 753-764.
44. Moore, L.S., et al., *Characterizing the utility and limitations of repurposing an open-field optical imaging device for fluorescence-guided surgery in head and neck cancer patients.* J Nucl Med, 2017. **58**(2): p. 246-251.
45. Okusanya, O.T., et al., *Intraoperative molecular imaging can identify lung adenocarcinomas during pulmonary resection.* J Thorac Cardiovasc Surg, 2015. **150**(1): p. 28-35 e1.
46. Predina, J.D., et al., *Intraoperative Molecular Imaging Combined With Positron Emission Tomography Improves Surgical Management of Peripheral Malignant Pulmonary Nodules.* Ann Surg, 2017. **266**(3): p. 479-488.
47. Predina, J.D., et al., *Identification of a Folate Receptor-Targeted Near-Infrared Molecular Contrast Agent to Localize Pulmonary Adenocarcinomas.* Mol Ther, 2018. **26**(2): p. 390-403.
48. Predina, J.D., et al., *A clinical trial of intraoperative near-infrared imaging to assess tumor extent and identify residual disease during anterior mediastinal tumor resection.* Cancer, 2019. **125**(5): p. 807-817.
49. van Dam, G.M., et al., *Intraoperative tumor-specific fluorescence imaging in ovarian cancer by folate receptor-alpha targeting: first in-human results.* Nat Med, 2011. **17**(10): p. 1315-9.
50. van Keulen, S., et al., *The Clinical Application of Fluorescence-Guided Surgery in Head and Neck Cancer.* J Nucl Med, 2019. **60**(6): p. 758-763.
51. Boogerd, L.S.F., et al., *Safety and effectiveness of SGM-101, a fluorescent antibody targeting carcinoembryonic antigen, for intraoperative detection of colorectal cancer: a dose-escalation pilot study.* Lancet Gastroenterol Hepatol, 2018. **3**(3): p. 181-191.
52. Shum, C.F., et al., *Novel Use of Folate-Targeted Intraoperative Fluorescence, OTL38, in Robot-Assisted Laparoscopic Partial Nephrectomy: Report of the First Three Cases.* J Endourol Case Rep, 2016. **2**(1): p. 189-197.
53. Hoogstins, C.E., et al., *A Novel Tumor-Specific Agent for Intraoperative Near-Infrared Fluorescence Imaging: A Translational Study in Healthy Volunteers and Patients with Ovarian Cancer.* Clin Cancer Res, 2016. **22**(12): p. 2929-38.
54. Schaap, D.P., et al., *Carcinoembryonic antigen-specific, fluorescent image-guided cytoreductive surgery with hyperthermic intraperitoneal chemotherapy for metastatic colorectal cancer.* Br J Surg, 2020. **107**(4): p. 334-337.
55. Rosenthal, E.L., et al., *Successful Translation of Fluorescence Navigation During Oncologic Surgery: A Consensus Report.* J Nucl Med, 2016. **57**(1): p. 144-50.
56. Hadjipanayis, C.G., G. Widhalm, and W. Stummer, *What is the Surgical Benefit of Utilizing 5-Aminolevulinic Acid for Fluorescence-Guided Surgery of Malignant Gliomas?* Neurosurgery, 2015. **77**(5): p. 663-73.
57. Tummers, W.S., et al., *Recommendations for reporting on emerging optical imaging agents to promote clinical approval.* Theranostics, 2018. **8**(19): p. 5336-5347.

58. Tipirneni, K.E., et al., *Oncologic Procedures Amenable to Fluorescence-guided Surgery.* Ann Surg, 2017. **266**(1): p. 36-47.
59. Wei, L., et al., *Toward Quantitative Neurosurgical Guidance With High-Resolution Microscopy of 5-Aminolevulinic Acid-Induced Protoporphyrin IX.* Front Oncol, 2019. **9**: p. 592.
60. Harlaar, N.J., et al., *Molecular fluorescence-guided surgery of peritoneal carcinomatosis of colorectal origin: a single-centre feasibility study.* Lancet Gastroenterol Hepatol, 2016. **1**(4): p. 283-290.
61. de Valk, K.S., et al., *A zwitterionic near-infrared fluorophore for real-time ureter identification during laparoscopic abdominopelvic surgery.* Nat Commun, 2019. **10**(1): p. 3118.
62. Sadot, E., et al., *Resection margin and survival in 2368 patients undergoing hepatic resection for metastatic colorectal cancer: surgical technique or biologic surrogate?* Ann Surg, 2015. **262**(3): p. 476-85; discussion 483-5.
63. van Keulen, S., et al., *The Sentinel Margin: Intraoperative Ex Vivo Specimen Mapping Using Relative Fluorescence Intensity.* Clin Cancer Res, 2019. **25**(15): p. 4656-4662.
64. Sanai, N. and M.S. Berger, *Glioma extent of resection and its impact on patient outcome.* Neurosurgery, 2008. **62**(4): p. 753-64; discussion 264-6.
65. Tummers, Q.R., et al., *The Value of Intraoperative Near-Infrared Fluorescence Imaging Based on Enhanced Permeability and Retention of Indocyanine Green: Feasibility and False-Positives in Ovarian Cancer.* PLoS One, 2015. **10**(6): p. e0129766.
66. Newton, A.D., et al., *Intraoperative fluorescence imaging in thoracic surgery.* J Surg Oncol, 2018. **118**(2): p. 344-355.
67. Boogerd, L.S., et al., *Laparoscopic detection and resection of occult liver tumors of multiple cancer types using real-time near-infrared fluorescence guidance.* Surg Endosc, 2017. **31**(2): p. 952-961.
68. Nishio, N., et al., *Optical molecular imaging can differentiate metastatic from benign lymph nodes in head and neck cancer.* Nat Commun, 2019. **10**(1): p. 5044.
69. Kaibori, M., et al., *Intraoperative indocyanine green fluorescent imaging for prevention of bile leakage after hepatic resection.* Surgery, 2011. **150**(1): p. 91-8.
70. Walsh, E.M., et al., *Fluorescence Imaging of Nerves During Surgery.* Ann Surg, 2019. **270**(1): p. 69-76.
71. Varela, R., et al., *Outcomes of DIEP Flap and Fluorescent Angiography: A Randomized Controlled Clinical Trial.* Plast Reconstr Surg, 2020. **145**(1): p. 1-10.
72. Albers, K.I., et al., *Visualising improved peritoneal perfusion at lower intra-abdominal pressure by fluorescent imaging during laparoscopic surgery: A randomised controlled study.* Int J Surg, 2020. **77**: p. 8-13.
73. van den Hoven, P., et al., *A systematic review of the use of near-infrared fluorescence imaging in patients with peripheral artery disease.* J Vasc Surg, 2019. **70**(1): p. 286-297 e1.
74. Nakaseko, Y., T. Ishizawa, and A. Saiura, *Fluorescence-guided surgery for liver tumors.* J Surg Oncol, 2018. **118**(2): p. 324-331.
75. Motono, N., et al., *Low-dose indocyanine green fluorescence-navigated segmentectomy: prospective analysis of 20 cases and review of previous reports.* J Thorac Dis, 2019. **11**(3): p. 702-707.
76. Alekseev, M., et al., *A study investigating the perfusion of colorectal anastomoses using fluorescence angiography: results of the FLAG randomized trial.* Colorectal Dis, 2020.
77. Hoogstins, C., et al., *Setting Standards for Reporting and Quantification in Fluorescence-Guided Surgery.* Mol Imaging Biol, 2019. **21**(1): p. 11-18.
78. Gambhir, S.S., et al., *Proceedings: Pathways for Successful Translation of New Imaging Agents and Modalities-Phase III Studies.* J Nucl Med, 2019. **60**(6): p. 736-744.
79. Pogue, B.W., et al., *Perspective review of what is needed for molecular-specific fluorescence-guided surgery.* J Biomed Opt, 2018. **23**(10): p. 1-9.

80. DeLong, J.C., et al., *Indocyanine green (ICG) fluorescence-guided laparoscopic adrenalectomy.* J Surg Oncol, 2015. **112**(6): p. 650-3.
81. Esteves, S., et al., *A pilot cost-effectiveness analysis of treatments in newly diagnosed high-grade gliomas: the example of 5-aminolevulinic Acid compared with white-light surgery.* Neurosurgery, 2015. **76**(5): p. 552-62; discussion 562.
82. Prager, M., et al., *Costs and effects of intraoperative fluorescence molecular imaging - A model-based, early assessment.* PLoS One, 2018. **13**(6): p. e0198137.
83. Miyata, Y., et al., *Intraoperative imaging of hepatic cancers using gamma-glutamyltranspeptidase-specific fluorophore enabling real-time identification and estimation of recurrence.* Sci Rep, 2017. **7**(1): p. 3542.


5

Chapter 5

Author's reply to: Real-time fluorescence imaging for cancer surgery: a pathologist's perspective

Lorraine J Lauwerends, Pieter B A A van Driel, Senada Koljenović, Alexander L Vahrmeijer, Stijn Keereweer

Lancet Oncology. 2021 Jul;22(7):e283.

In their Correspondence, Sachin C Sarode and Gargi S Sarode suggest that the pathologist's perspective is underrepresented in our recently published Review [1]. Their recommendations pertain to technical difficulties associated with fluorescence-guided surgery, which might affect histopathological interpretation and correlation.

In our Review, we clarify the need for an outcome measurement that remains effective and objective when evaluating a technique in which numerous factors influence detection of the fluorescence signal [2]. The effect of fluorescence findings on intraoperative, real-time decision making is ultimately the best measure of how fluorescence-guided surgery affects patient care. As such, we provide recommendations on how to comprehensively evaluate changes in intraoperative decision making as a result of fluorescence-guided surgery. Sarode and Sarode do not recommend amendments to reporting such changes, but instead highlight several well known factors that can influence the analysis of fluorescence signals.

Fluorescence-guided surgery is a complex procedure and its efficacy is influenced by many (often unquantifiable) factors, such as autofluorescence, optical tissue properties, patient and tumour characteristics, pharmacokinetics, targeting selectivity, and imaging systems [2]. Stromal desmoplasia might indeed play a role in targeting selectivity, and the pattern of invasion can influence signal detectability. These concerns are, therefore, compelling arguments in favour of our core message.

Variation in shrinkage of excised tissue is one of the reasons for which a wide tumour-free margin is required during standard surgical care. This tumour-free margin can be established more precisely with fluorescence-guided surgery. Subsequent correlation with histopathology will inform on clinical benefit. Ex-vivo fluorescence imaging of histopathology slides can assess targeting specificity, but does not inform on clinical outcome [3].

In a research setting, ethical medical regulations ensure that pathologists carry out comprehensive standard-procedure analyses. Additional analysis of fluorescent lesions is never blinded, similarly to what happens with fresh-frozen sectioning. Finally, the applicability of fluorescence-guided surgery is not limited to a tumour depth of 8 mm because fluorescence-guided surgery is used to scan the wound bed and specimen surface after resection [4].

REFERENCES

1. Lauwerends, L.J., et al., *Real-time fluorescence imaging in intraoperative decision making for cancer surgery.* Lancet Oncol, 2021. **22**(5): p. e186-e195.
2. Keereweer, S., et al., *Optical image-guided cancer surgery: challenges and limitations.* Clin Cancer Res, 2013. **19**(14): p. 3745-54.
3. Hernot, S., et al., *Latest developments in molecular tracers for fluorescence image-guided cancer surgery.* The Lancet Oncology, 2019. **20**(7): p. e354-e367.
4. van Keulen, S., et al., *The Sentinel Margin: Intraoperative Ex Vivo Specimen Mapping Using Relative Fluorescence Intensity.* Clin Cancer Res, 2019. **25**(15): p. 4656-4662.

Part III

Advances in Fluorescence Imaging for Head and Neck Cancer


6

Chapter 6

Tumour marker expression in head and neck malignancies to identify potential targets for intraoperative molecular near-infrared imaging

Lorraine J. Lauwerends, Bo E. Zweedijk, Hidde A. Galema, Lisanne K.A. Neijenhuis, Neeltje G. Dekker-Ensink, Robert J. Baatenburg de Jong, Cornelis Verhoef, Shadhvi S. Bhairosingh, Peter J.K. Kuppen, Alexander L. Vahrmeijer, Tessa M. van Ginhoven, Senada Koljenović, Sjors A. Koppes, Denise E. Hilling, Stijn Keereweer

Molecular Diagnosis & Therapy. 2024 Nov;28(6):811-820.

ABSTRACT

Introduction

Oral and laryngeal squamous cell carcinoma (OSCC and LSCC) and papillary thyroid carcinoma (PTC) are common head and neck cancers (HNCs) typically treated surgically. Challenges in tumour delineation often lead to inadequate resection margins in OSCC and LSCC, and missed multifocality in PTC. Fluorescence imaging (FI) using near-infrared tumour-targeting tracers may improve intraoperative identification of malignancy, facilitating precise excision. This study evaluates six potential FI targets in OSCC, LSCC and PTC.

Materials and methods

Immunohistochemical staining was performed on OSCC (n=20), LSCC (n=10) and PTC (n=10), assessing CEA, c-Met, EpCAM, EGFR, integrin αvβ6 and VEGF-α. Expression was scored (0-12) using the total immunostaining score (TIS) system, and categorized into absent (TIS 0), low (TIS 1-5), moderate (TIS 6-8), or high (TIS 9-12).

Results

Integrin αvβ6 showed significant overexpression in OSCC (TIS: 12; $p < 0.001$) and LSCC (TIS: 8; $p = 0.002$), with 80% of OSCC and 90% of LSCC exhibiting moderate-high expression. Similarly, EGFR expression was moderate-high in most OSCC (87.5%; TIS: 8) and universally high in LSCC (100%; TIS: 12). In PTC, EGFR and VEGF-α expressions were low-moderate, but significantly higher than in healthy tissue (TIS: 6; $p < 0.006$).

Conclusion

This study highlights integrin αvβ6 and EGFR as viable FI targets in OSCC and LSCC, especially integrin αvβ6 for tumour margin delineation. In PTC, despite lower expressions, the significant overexpression of VEGF-α, c-MET, and EGFR suggests their potential as FI targets. Our findings support the development of tumour-targeted FI tracers to improve surgical precision in HNC.

INTRODUCTION

Oral and laryngeal squamous cell carcinoma (OSSC and LSSC, respectively) and papillary thyroid carcinoma (PTC) are prevalent head and neck cancers (HNCs). Surgical resection is their cornerstone treatment, yet the management of HNC remains challenging due to their intricate anatomy, proximity to vital structures, and the potential functional impairments following surgery. Precise excision of tumours is crucial in these cases to optimize patient outcomes. Inadequate resection margins (i.e. close (1-5 mm) and positive (≤1 mm) resection margins together) are a major negative prognostic factor for overall survival across these cancers [1-3], and are nonetheless common in HNCs with reports in up to 19%, 26%, and 85% of cases for PTC, LSSC, and OSSC respectively [2-9]. Enhanced intraoperative detection, including the ability to identify multifocality in PTC patients, is vital for guiding the extent of surgery, where it may significantly influence surgical decisions. In contrast to OSCC and LSSC, where the primary surgical goal is to achieve clear margins due to their aggressive nature and poorer prognosis, PTC generally has a better survival outcome. Therefore, the balance between complete tumour resection and maintaining quality of life post-surgery is particularly critical in PTC. FI can aid in achieving this balance by precisely delineating tumour margins, potentially reducing the extent of unnecessary tissue removal and preserving function. Furthermore, FI could identify patients who were mistakenly preoperatively selected for a hemithyroidectomy. If FI reveals large extrathyroidal extension, a contralateral malignancy or lymph node involvement, one could directly perform a total thyroidectomy to enable treatment with radioactive iodine if deemed appropriate. This highlights the urgent clinical need for advanced intraoperative tools to facilitate precise tumour resection.

Fluorescence imaging (FI) of tumours in the near-infrared (NIR) region has shown significant potential and has been increasingly recognized as an effective approach for improving the precision of tumour excision during surgery [10, 11]. This technique involves the administration of a tumour-targeting fluorescent tracer before surgery, which binds to overexpressed molecular targets on cancer cells. One of various targeting strategies, such as using antibodies, small peptides, or activatable fluorophores, is employed to ensure precise tumour localization [12-14]. Dedicated camera systems are used to intraoperatively detect the fluorescent signal, facilitating real-time imaging of cancer tissue. Fluorophores emitting in the NIR range (700–900 nm) —a spectrum invisible to the naked eye— are used to avoid interference in the surgeon's field of view, optimize tissue penetration and minimize autofluorescence from surrounding tissues [15, 16].

Currently, there are no NIR imaging tracers available for HNCs that have been approved for clinical use [17]. Identifying targets that are overexpressed in HNC cells is crucial for developing effective tumour-targeting tracers. Moreover, these targets ideally should not be expressed in healthy tissues, to minimize background signal and improve specificity. With a focus on potential rapid translation towards clinical applications, this study evaluated six

targets with (pre-)clinically available NIR fluorescent tracers that are currently being investigated in various cancers: carcinoembryonic antigen (CEA) [18-22], epidermal growth factor receptor (EGFR)[11, 17, 23-26], epithelial cell adhesion molecule (EpCAM) [17, 23-25], vascular endothelial growth factor α (VEGF-α) [11, 26-32], c-mesenchymal-epithelial transition factor (c-MET) [33-38], and integrin αvβ6 [17, 25, 39, 40]. While these targets have shown potential for tumour imaging, the literature regarding their overexpression in OSCC is incomplete, and nearly absent in LSCC and PTC [11, 17-44].

Consequently, our study aimed to assess the suitability of these six targets for future clinical trials on FI-based tumour imaging in HNC. We examined their expression in OSCC, LSCC and PTC using immunohistochemical (IHC) staining, with an emphasis on their presence at the invasive front. These findings may expedite the initiation of FI clinical trials in HNC, contributing to the development of targeted imaging tracers.

MATERIALS AND METHODS

Tissue and Tumour Marker Selection

Formalin-fixed paraffin-embedded (FFPE) tissue specimens of patients with OSCC (n=20), LSSC (n=10), and PTC (n=10) were obtained from the Erasmus Medical Centre Tissue Bank. These samples, collected from patients that were surgically treated between 2014 and 2023, were reviewed for selection by dedicated pathologists (SKol and FvK). Only specimens containing both tumour and (adjacent) healthy epithelium and muscle tissue were selected for OSCC and LSCC. For thyroid tissue, two specimens per patient were selected: one consisting of PTC tissue, and one consisting of healthy thyroid tissue. Seven out of ten LSCC patients had received radiotherapy, and one out of ten PTC patients had received chemotherapy. None of the OSCC patients had received pre-operative adjuvant therapy. The tissues were sectioned (4 μm thickness) and immunohistochemically stained for expression of the six tumour markers: CEA, EpCAM, integrin αvβ6, VEGF-α, EGFR and c-MET (see Supplementary Table 1).

Immunohistochemical (IHC) Staining Protocol

The tissue slides were deparaffinized using xylene, followed by rehydration. After rinsing with demineralized water, slides were treated with 0.3% hydrogen peroxide (Merck Millipore, Darmstadt, Germany) for 20 minutes at room temperature to prevent endogenous peroxidase activity. Antigen retrieval methods varied based on antibody protocols (see Supplementary Table 1). For CEA and EpCAM, heat induction at 95 °C for 10 minutes using Envision FLEX target retrieval solution with low-pH (pH 6.0, DAKO) was performed. For c-MET and EGFR, Envision FLEX target retrieval solution with high-pH (pH 9.0, DAKO) was utilized. For αvβ6, antigen retrieval was carried out with 0.4% pepsin at 37 °C using a water bath for 20 minutes. No antigen retrieval was used for VEGF-α. Primary anti-

body incubation was done overnight at room temperature, diluted in 1% w/v Bovine Serum Albumin/Phosphate-Buffered Saline (BSA/PBS). Negative control samples were incubated with 1% w/v BSA/PBS. Tissue sections that were known to express the specific marker(s) served as positive controls. The next day, the slides were washed with PBS and incubated with HRP-labeled secondary antibodies (Envision+ System anti-mouse or anti-rabbit, both from DAKO) for 30 minutes at room temperature. A liquid 3,3'-diaminobenzidine (DAB+) Substrate Chromogen System (DAKO) was applied for 10 minutes for staining, followed by a 15-second application of hematoxylin (VWR international, Amsterdam, the Netherlands) for counterstaining. Lastly, the tissue sections were dehydrated for 60 minutes at 37 °C and mounted in Pertex (Histolab, Askim, Sweden).

Scoring Methods

A specialized head and neck pathologist (SKop) evaluated all samples using the total immunostaining score (TIS) system, comprising intensity score (IS) and proportion score (PS), as has been previously described [17, 25, 45]. The IS reflects the intensity of staining in cells, ranging from 0 to 3 (0: none; 1: weak; 2: moderate; 3: strong). The PS represents the percentage of cells that exhibited staining, ranging from 0 to 4 (0: no staining; 1: 1-10%; 2: 11-50%; 3; 51-80%; 4: 81-100%). The staining of background tissues, specifically healthy epithelium, muscle and thyroid tissue, was evaluated using the same scoring method. The TIS, a product of IS and PS, categorized marker expression into absent (TIS 0), low (TIS 1-5), moderate (TIS 6-8), or high (TIS 9-12). The expression rate was thus determined by calculating the proportion of markers exhibiting high, moderate and low expression. Furthermore, while this scoring system is commonly used in IHC evaluations for therapeutic targets, its application in this study is aimed at assessing the potential of these markers for FI. The emphasis on contrast and precise delineation at the tumour's invasive front is particularly relevant for imaging purposes. The expression pattern at the tumour's invasive front was therefore assessed separately in each sample. Markers with strong localized staining there, despite a lower overall PS, can still be useful for FI. This approach ensured that even markers with limited overall expression were evaluated for their potential to enhance tumour delineation in FI.

Statistics

Statistical analysis was performed using the R-studio software (version 4.1.0, R Foundation for Statistical Computing, Vienna, Austria). Patient characteristics were reported using descriptive statistics. The Mann-Whitney U test compared marker expression between tumour and healthy tissues, considering a p-value < 0.05 as significant.

RESULTS

Tissue samples (n=40) of patients with OSCC (n=20), LSCC (n=10) and PTC (n=10) were included in this study. Patient and tumour characteristics are presented in Table 1.

Table 1: Patient and tumour baseline characteristics

			Tumour type (n (%))		
		n (%)	**OSCC**	**LSCC**	**PTC**
Patients		40 (100)	20 (50)	10 (25)	10 (25)
Age, years (median [q1, q3])		63.50 [49.75, 68.25]	65.50 [53.5, 70.25]	64.50 [63.25, 68]	48.50 [46.25, 58.25]
Gender	Male	27 (67.5)	15 (75)	10 (100)	2 (20)
	Female	13 (32.5)	5 (25)	0 (0)	8 (80)
Differentiation grade	Good	3 (10)	2 (10)	1 (10)	n/a
	Good - moderate	1 (3.3)	1 (5)	-	
	Moderate	21 (70)	15 (75)	6 (60)	
	Moderate - poor	3 (10)	1 (5)	2 (20)	
	Poor	2 (6.7)	1 (5)	1 (10)	
Histological subtype	Classic type	10 (100)	n/a	n/a	10 (100)
pT-stage	pT-1	7 (17.5)	2 (10)	-	5 (50)
	pT-2	11 (27.5)	10 (50)	1 (10)	-
	pT-3	11 (27.5)	4 (20)	2 (20)	5 (50)
	pT-4	11 (27.5)	4 (20)	7 (70)	-

Abbreviations:

n/a = not applicable;

OSCC = *oral squamous cell carcinoma*;

LSCC = *laryngeal squamous cell carcinoma*;

PTC = *papillary thyroid carcinoma*

Target Expression in Oral Tissues

In OSCC, integrin αvβ6 expression was significantly higher than in healthy epithelium ($p < 0.001$) and muscle tissue ($p < 0.001$). Moderate to high expression was observed in 80% of tumour samples (median TIS: 12), whereas expression in epithelium and muscle tissue was low to absent (median TIS: 2.5 and 2, respectively). EGFR expression was moderate to high in 87.5% of the tumour samples (median TIS: 8), significantly surpassing that in epithelial and muscle tissue (median TIS: 5 and 0, $p = 0.028$ and $p < 0.001$ respectively). VEGF-α expression was moderate to high in 87.5% of both tumour and muscle tissue samples (median TIS: 8 vs. 8, $p = 0.701$). Expressions of c-MET, CEA and EpCAM were negligible in all tumour samples (median TIS: 0.5, 1.5, and 0, respectively). Marker expression in representative OSCC is shown in Fig. 1 and Supplementary Fig. 1a. Comparisons of TIS between OSCC,

epithelium and muscle tissue for all six tumour markers are presented in Fig. 2 and Table 2a. Expression rates (%) are presented in Supplementary Table 2a and Supplementary Fig. 2.

Target expression in laryngeal tissues

In laryngeal tissues, integrin αvβ6 expression was moderate to high in 90% of tumour samples (median TIS: 8), low to moderate in epithelium (median TIS: 6) and predominantly absent in muscle tissue (median TIS: 0). TIS was significantly higher in tumour than in muscle tissue (p = 0.002). EGFR expression was moderate to high in all tumour samples (100%; median TIS: 12), significantly exceeding that in epithelial and muscle tissue (median TIS: 7 and 0; p = 0.007 and p = 0.001, respectively). VEGF-α expression was moderate to high in both tumour and muscle tissue (median TIS: 10 vs. 8, p = 0.118). While absent in the majority of samples, there was moderate to high expression of EpCAM in 30% of tumours (median TIS: 0). Expressions of c-MET and CEA were (near-)absent in all tumour samples (median TIS: 0 and 0.5, respectively). See Fig. 1, Supplementary Fig. 1b, Fig. 2, Table 2b, Supplementary Table 2b and Supplementary Fig. 2.

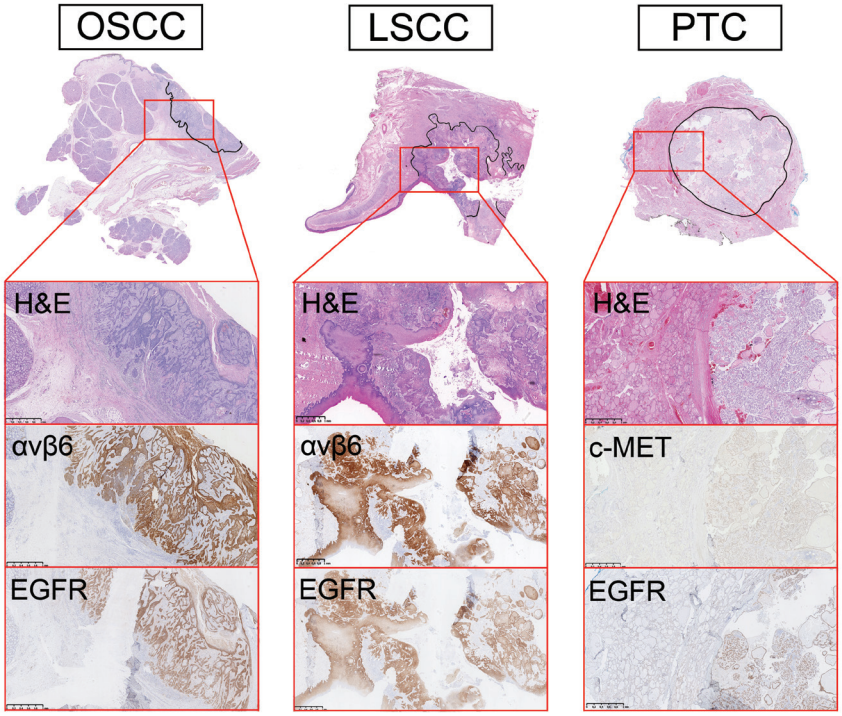

Figure 1: A representative tissue slide of an oral squamous cell carcinoma (OSCC), laryngeal squamous cell carcinoma (LSCC) and papillary thyroid carcinoma (PTC) with the hematoxylin and eosin (H&E) slide and two positive markers: integrin αvβ6 and EGFR in OSCC and LSCC, and c-MET and EGFR in PTC. Tumours are outlined in black. *c-MET = c-mesenchymal-epithelial transition factor; EGFR = epidermal growth factor receptor;*

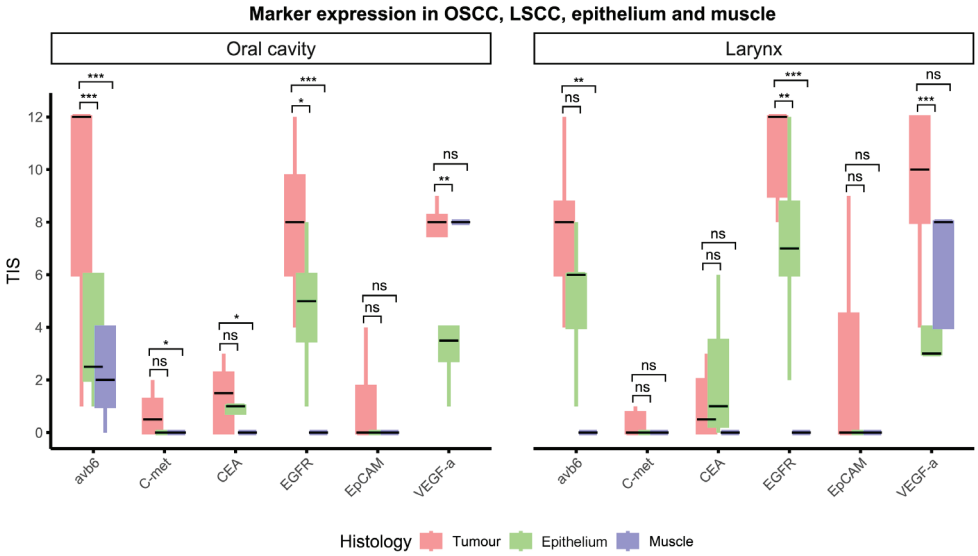

Figure 2: Total immunostaining score (TIS) for the six markers in oral (left) and laryngeal (right) cancer (red), as well as in surrounding epithelium (green) and muscle (blue), showing the difference in expression levels between tumour and healthy tissues. *ns = not significant; * = p < 0.05; ** = p < 0.01; *** = p < 0.001; OSCC = oral squamous cell carcinoma; LSCC = laryngeal squamous cell carcinoma; αvβ6 = integrin αvβ6; c-MET = c-mesenchymal-epithelial transition factor; CEA = carcinoembryonic antigen; EGFR = epidermal growth factor receptor; EpCAM = epithelial cell adhesion molecule; VEGF-α = vascular endothelial growth factor α*

Target expression in thyroid tissues

In thyroid tissues, EpCAM was moderately to highly expressed in 90% of PTC samples, but this was not significantly higher than in healthy thyroid tissue (median TIS 12 vs. 8, p = 0.057). EGFR and VEGF-α expressions were low to moderate in all tumour samples (100%; median TIS: 6 and 6, respectively), and significantly higher than in healthy thyroid (median TIS: 2 and 1, p = 0.006 and p < 0.001 respectively). Integrin αvβ6, c-MET and CEA expressions ranged from absent to low in the majority of tumour samples (90%, 80%, and 100%, respectively). However, despite being predominantly low, integrin αvβ6 and c-MET expression in PTC were significantly higher than in healthy thyroid tissue (median TIS 3.5 vs. 0, p = 0.002 and median TIS 2 vs. 0, p = 0.002, respectively). See Fig. 1, Supplementary Fig. 1c, Fig. 3, Table 2c, Supplementary Table 2c, Supplementary Fig. 2.

Expression pattern in tumour tissue

For all markers, no notable staining patterns were observed. More specifically, none of the targets were solely overexpressed at the invasive front.

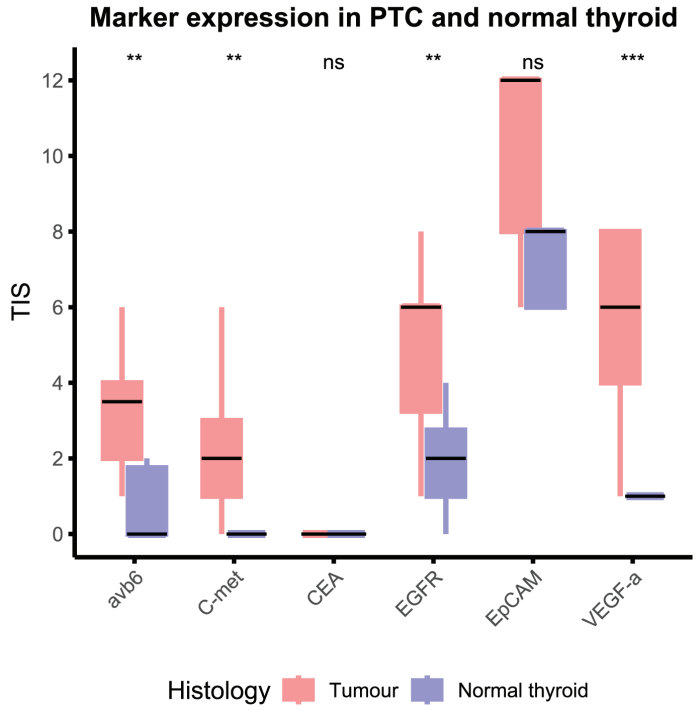

Figure 3: Total immunostaining score (TIS) for the six markers in cancerous (red) and normal (blue) thyroid tissue samples, showing the difference in expression levels between tumour and healthy tissues. *ns = not significant; * = p < 0.05; ** = p < 0.01; *** = p < 0.001; PTC = papillary thyroid carcinoma; αvβ6 = integrin αvβ6; c-MET = c-mesenchymal-epithelial transition factor; CEA = carcinoembryonic antigen; EGFR = epidermal growth factor receptor; EpCAM = epithelial cell adhesion molecule; VEGF-α = vascular endothelial growth factor α*

Table 2: Median total immunostaining scores (TIS) for oral (a) and laryngeal (b) squamous cell carcinoma, epithelium, and muscle, and for papillary thyroid carcinoma (c) and healthy thyroid

OSCC (a)					
	TIS; median [q1, q3]				
Staining	**tumour**	**epithelium**	**muscle**	**p-value tumour/ epithelium**	**p-value tumour/ muscle**
avb6	12 [6 - 12]	2.5 [2 - 6]	2 [1 - 4]	**< 0.001**	**< 0.001**
C-met	0.5 [0 - 1.2]	0 [0 - 0]	0 [0 - 0]	0.109	**0.032**
CEA	1.5 [0 - 2.2]	1 [0.8 - 1]	0 [0 - 0]	0.403	**0.013**
EGFR	8 [6 - 9.8]	5 [3.5 - 6]	0 [0 - 0]	**0.028**	**< 0.001**
EpCAM	0 [0 - 1.8]	0 [0 - 0]	0 [0 - 0]	0.076	0.076
VEGF-a	8 [7.5 - 8.2]	3.5 [2.8 - 4]	8 [8 - 8]	**0.002**	0.701

Table 2: Median total immunostaining scores (TIS) for oral (a) and laryngeal (b) squamous cell carcinoma, epithelium, and muscle, and for papillary thyroid carcinoma (c) and healthy thyroid (*continued*)

LSCC (b)					
	TIS; median [q1, q3]				
Staining	**tumour**	**epithelium**	**muscle**	**p-value tumour/ epithelium**	**p-value tumour/ muscle**
avb6	8 [6 - 8.8]	6 [4 - 6]	0 [0 - 0]	0.062	**0.002**
C-met	0 [0 - 0.8]	0 [0 - 0]	0 [0 - 0]	0.256	0.220
CEA	0.5 [0 - 2]	1 [0.2 - 3.5]	0 [0 - 0]	0.386	0.079
EGFR	12 [9 - 12]	7 [6 - 8.8]	0 [0 - 0]	**0.007**	**0.001**
EpCAM	0 [0 - 4.5]	0 [0 - 0]	0 [0 - 0]	0.456	0.220
VEGF-a	10 [8 - 12]	3 [3 - 4]	8 [4 - 8]	**0.001**	0.118
PTC (c)					
	TIS; median [q1, q3]				
Staining	**tumour**	**healthy thyroid**		**p-value**	
avb6	3.5 [2 - 4]	0 [0 - 1.8]		**0.002**	
C-met	2 [1 - 3]	0 [0 - 0]		**0.002**	
CEA	0 [0 - 0]	0 [0 - 0]		0.368	
EGFR	6 [3.2 - 6]	2 [1 - 2.8]		**0.006**	
EpCAM	12 [8 - 12]	8 [6 - 8]		0.057	
VEGF-a	6 [4 - 8]	1 [1 - 1]		**< 0.001**	

DISCUSSION

Our study investigated six potential imaging targets for various head and neck tumours. For oral and laryngeal cancer, integrin αvβ6 emerged as a key marker, exhibiting moderate to high overexpression in 80% and 90% of cases, respectively, as corroborated by previous research [17, 25]. Its absence in muscle and low expression in epithelium results in strong contrast for imaging of both superficial and deep tumour margins, further supported by its successful targeting in colorectal cancer with cRGD-ZW800-1, a zwitterionic, integrin-targeted NIR tracer, currently under investigation in OSCC (NCT 04191460) [40]. Although EGFR shows promise as an imaging target due to its negligible expression in muscle tissue, its inconsistent expression in oral and laryngeal epithelium limits its effectiveness in tumour detection and epithelial delineation [25]. Indeed, while antibody-dye conjugates cetuximab-IRDye800CW and panitumumab-IRDye800CW have shown promise in OSCC, their ability to provide clear contrast is compromised by the sequestration of labelled antibodies by off-target, normal tissues [10, 11, 41, 46, 47]. Consequently, pre-dosing with the unlabelled antibody has been proposed to enhance the tumour-specificity of these tracers [11, 41, 46]. Next, although FI with VEGF-α targeted tracer bevacizumab-800CW has shown promise in other tumour types, such as breast and pancreatic cancer [27-32], the widespread presence of VEGF-α in the surrounding muscle tissues of oral and laryngeal cancer undermines its

utility in detecting deep surface resection margins. This limitation is particularly relevant considering that inadequate surgical margins often occur at the deeper, muscle-adjacent planes. Furthermore, the requirement for early administration of antibody-based fluorescent tracers targeting EGFR and VEGF-α—necessitating an additional hospital visit—highlights the need for more logistically feasible fluorescent tracers in HNC and beyond, to alleviate patient inconvenience and improve clinical workflow. Finally, our findings indicate negligible expressions of c-MET, CEA, and EpCAM in tumour samples, suggesting they are unsuitable as FI targets in OSCC and LSCC. Indeed, while CEA expression has not been studied in HNC before, CEA-targeted fluorescent tracer SGM-101 is being evaluated in two phase III trials of FI in colorectal cancer, indicating the utility of targeting CEA in other cancers [21, 22]. Contrarily, preliminary and preclinical studies challenge our findings on c-MET and EpCAM in OSCC [23, 34, 48]. Notably, c-MET-targeted FI, demonstrated with EMI-137 and cMBP-ICG, alongside immunohistochemical confirmation of c-MET overexpression in OSCC, showed high sensitivity and specificity in oral cancer specimens [34, 48]. Similarly, an anti-EpCAM tracer conjugated with IRDye800CW efficiently delineated tumours in HNC models [23]. These findings underscore an opportunity for re-evaluating c-MET and EpCAM as feasible FI targets in OSCC and potentially other HNCs.

For thyroid cancer, EGFR and VEGF-α are moderately expressed in PTCs and significantly overexpressed when compared to healthy tissue, making them viable candidates for NIR FI targeting. Similarly, c-MET, though expressed at lower levels in PTC, exhibited significant overexpression compared to healthy tissue. This aligns with recent studies on the effectiveness of FI using MET-receptor targeted EMI-137 in enhancing the detection of multifocal PTC [33, 49]. Conversely, the high expression of EpCAM was noteworthy, but not significantly higher than normal thyroid tissue, limiting its utility for tumour detection and delineation. Although expression of integrin αvβ6 was significantly higher in PTC than in healthy thyroid tissue, TIS scores were absent to low, yielding no practical benefits. Expression of CEA was negligible in most PTC tissues. Research on NIR FI for the thyroid has mainly focused on using ICG or autofluorescence for parathyroid gland identification, aiming to minimize postoperative hypoparathyroidism risks [50]. The necessity for clear surgical margins in PTC is less critical due to the ability of PTC cells to absorb iodine, allowing for post-surgery radioactive iodine (RAI) ablation to target residual disease [51]. Yet, with half of metastatic thyroid cancers becoming RAI-refractory, there's an emerging need for novel, iodine-independent targeting methods to ensure complete removal of malignant tissue. In PTC, the goal is to achieve optimal tumour resection while preserving vital structures and function to maintain quality of life, given the generally favourable prognosis. FI can aid in this balance by providing precise tumour delineation, thus helping to avoid unnecessary tissue removal and associated complications. Although exploring NIR FI for PTC surgery margin assessment is in its infancy, its proven effectiveness in preserving parathyroid glands suggests wider applicability [52]. This underscores the need for further investigation into PTC-specific FI targets to improve tumour delineation.

It is important to note that IHC is typically used to assess overall tumour expression for therapeutic potential—such as using cetuximab in chemotherapy—rather than imaging utility. For delineating resection margins through FI, however, the presence of the target at the invasive front of the tumour is key. In theory, a target that might have relatively lower overall expression of the tumour with high expression at the invasive front could be less suited for therapeutic applications, yet could still be very valuable for intraoperative FI. Although no distinct tumour-staining patterns were observed for the markers in our study, future assessments or marker suitability for FI should continue to include this aspect in their evaluations. Additionally, our scoring method, which is based on the total staining pattern, includes both intracellular and membranous staining. This could lead to an over-representation of the portion of membranous receptors available for binding, affecting the suitability of certain markers for receptor-targeted imaging. Future studies should consider distinguishing between membranous and intracellular receptor expression to better evaluate each marker's potential for FI. Moreover, the major limitation of our study is the size of the patient cohort, with 20 OSCC, 10 LSCC, and 10 PTC cases included. This relatively small cohort size, primarily constrained by sample availability, limits the generalizability of our findings and the precision of biomarker expression estimates.

Our selection of OSCC, LSCC and PTC was driven by their prevalence and the clinical challenges they present in achieving clear surgical margins due to their anatomical complexity and proximity to vital structures. These specific tumour types also represent a range of tissue types (squamous cell and glandular), providing broader insights into the applicability of FI across different HNCs. Our study differs from existing clinical studies by including this diverse selection of tumour types, evaluating some of the same markers in different and additional tumour types, and exploring markers that have been limitedly tested or not tested at all in HNCs. This comprehensive approach provides a deeper understanding of the potential and applicability of these markers across various HNCs.

Furthermore, it should be noted that 7 out of 10 LSCC patients had received radiotherapy, and 1 out of 10 PTC patients had received chemotherapy. None of the OSCC patients had received pre-operative adjuvant therapy. Although we did not specifically analyze the impact of these treatments on target expression, our initial observations did not indicate any apparent effect. Future studies should consider these variables to comprehensively assess their potential impact on biomarker expression.

Based on our findings, integrin αvβ6, EGFR, c-MET and VEGF-α hold promise for clinical studies with tumour-specific FI tracers in HNC, depending on the specific tumour type. While the ideal scenario would be to identify a universal marker suitable for a wide variety of tumours in general, our findings suggest a present necessity to utilize a range of different targets for FI, given that a singular, universal target remains elusive. The efficacy of tracer binding to these markers is influenced by factors such as pharmacokinetics, target expression

in non-tumour tissues, tracer size, dose and timing [53]. Additionally, clinical fluorescent tracers may bind to different epitopes than those stained in our study, underscoring the need for clinical evaluation of tracer binding under varied conditions. Our study underscores the potential of NIR FI in HNC surgery, particularly highlighting integrin αvβ6 and EGFR as notable targets for OSCC and LSCC, and EGFR, c-MET and VEGF-α for PTC, paving the way for further research into molecular imaging tracers to enhance surgical outcomes.

CONCLUSION

Our results identify integrin αvβ6 and EGFR as key overexpressed markers in OSCC and LSCC, suggesting their suitability as targets for FI to improve tumour resection precision. Integrin αvβ6, in particular, offers a strong contrast for tumour margin delineation in OSCC and LSCC. In PTC, EGFR, c-MET, and VEGF-α showed notable overexpression compared to normal tissue, making them viable candidates for FI targets. These findings are instrumental for guiding future clinical trials in the development of tumour-specific FI tracers, aiming to enhance surgical precision and outcomes in HNC.

REFERENCES

1. Wu, S.S., et al., *Risk Factors Associated With Recurrence and Death in Patients With Tall Cell Papillary Thyroid Cancer: A Single-Institution Cohort Study With Predictive Nomogram.* JAMA Otolaryngol Head Neck Surg, 2023. **149**(1): p. 79-86.
2. Smits, R.W., et al., *Resection margins in oral cancer surgery: Room for improvement.* Head Neck, 2016. **38 Suppl 1**: p. E2197-203.
3. Tassone, P., et al., *Association of Positive Initial Margins With Survival Among Patients With Squamous Cell Carcinoma Treated With Total Laryngectomy.* JAMA Otolaryngol Head Neck Surg, 2018. **144**(11): p. 1030-1036.
4. Gallo, A., et al., *Prognostic value of resection margins in supracricoid laryngectomy.* Laryngoscope, 2004. **114**(4): p. 616-21.
5. Woolgar, J.A. and A. Triantafyllou, *A histopathological appraisal of surgical margins in oral and oropharyngeal cancer resection specimens.* Oral Oncol, 2005. **41**(10): p. 1034-43.
6. Nakayama, M., et al., *Clinical significance of intraoperative surgical margin study in supracricoid laryngectomy.* Auris Nasus Larynx, 2011. **38**(2): p. 261-5.
7. Orosco, R.K., et al., *Positive Surgical Margins in the 10 Most Common Solid Cancers.* Sci Rep, 2018. **8**(1): p. 5686.
8. Saraniti, C., et al., *Prognostic role of resection margin in open oncologic laryngeal surgery: survival analysis of a cohort of 139 patients affected by squamous cell carcinoma.* Braz J Otorhinolaryngol, 2019. **85**(5): p. 603-610.
9. Aryanpour, Z., et al., *A single institution experience with papillary thyroid cancer: Are outcomes better at comprehensive cancer centers?* Am J Surg, 2021. **222**(4): p. 802-805.
10. Krishnan, G., et al., *Fluorescent Molecular Imaging Can Improve Intraoperative Sentinel Margin Detection in Oral Squamous Cell Carcinoma.* J Nucl Med, 2022. **63**(8): p. 1162-1168.
11. Voskuil, F.J., et al., *Fluorescence-guided imaging for resection margin evaluation in head and neck cancer patients using cetuximab-800CW: A quantitative dose-escalation study.* Theranostics, 2020. **10**(9): p. 3994-4005.
12. Keereweer, S., et al., *Optical image-guided surgery--where do we stand?* Mol Imaging Biol, 2011. **13**(2): p. 199-207.
13. Zhang, R.R., et al., *Beyond the margins: real-time detection of cancer using targeted fluorophores.* Nat Rev Clin Oncol, 2017. **14**(6): p. 347-364.
14. Mieog, J.S.D., et al., *Fundamentals and developments in fluorescence-guided cancer surgery.* Nat Rev Clin Oncol, 2022. **19**(1): p. 9-22.
15. Frangioni, J.V., *New technologies for human cancer imaging.* J Clin Oncol, 2008. **26**(24): p. 4012-21.
16. Frangioni, J.V., *In vivo near-infrared fluorescence imaging.* Curr Opin Chem Biol, 2003. **7**(5): p. 626-34.
17. Lawaetz, M., et al., *Potential of uPAR, alphavbeta6 Integrin, and Tissue Factor as Targets for Molecular Imaging of Oral Squamous Cell Carcinoma: Evaluation of Nine Targets in Primary Tumors and Metastases by Immunohistochemistry.* Int J Mol Sci, 2023. **24**(4).
18. Framery, B., et al., *Toxicity and pharmacokinetic profile of SGM-101, a fluorescent anti-CEA chimeric antibody for fluorescence imaging of tumors in patients.* Toxicol Rep, 2019. **6**: p. 409-415.
19. Boonstra, M.C., et al., *Selecting Targets for Tumor Imaging: An Overview of Cancer-Associated Membrane Proteins.* Biomark Cancer, 2016. **8**: p. 119-133.
20. Tiernan, J.P., et al., *Carcinoembryonic antigen is the preferred biomarker for in vivo colorectal cancer targeting.* Br J Cancer, 2013. **108**(3): p. 662-7.
21. Gutowski, M., et al., *SGM-101: An innovative near-infrared dye-antibody conjugate that targets CEA for fluorescence-guided*

surgery. Surg Oncol, 2017. **26**(2): p. 153-162.
22. Galema, H.A., et al., *Fluorescence-guided surgery in colorectal cancer; A review on clinical results and future perspectives.* Eur J Surg Oncol, 2022. **48**(4): p. 810-821.
23. van Driel, P.B., et al., *EpCAM as multi-tumour target for near-infrared fluorescence guided surgery.* BMC Cancer, 2016. **16**(1): p. 884.
24. Boogerd, L.S.F., et al., *Fluorescence-guided tumor detection with a novel anti-EpCAM targeted antibody fragment: Preclinical validation.* Surg Oncol, 2019. **28**: p. 1-8.
25. Baart, V.M., et al., *EGFR and alphavbeta6 as Promising Targets for Molecular Imaging of Cutaneous and Mucosal Squamous Cell Carcinoma of the Head and Neck Region.* Cancers (Basel), 2020. **12**(6).
26. Hicklin, D.J. and L.M. Ellis, *Role of the vascular endothelial growth factor pathway in tumor growth and angiogenesis.* J Clin Oncol, 2005. **23**(5): p. 1011-27.
27. Lamberts, L.E., et al., *Tumor-Specific Uptake of Fluorescent Bevacizumab-IRDye800CW Microdosing in Patients with Primary Breast Cancer: A Phase I Feasibility Study.* Clin Cancer Res, 2017. **23**(11): p. 2730-2741.
28. Mulder, B.G.S., et al., *Intraoperative Molecular Fluorescence Imaging of Pancreatic Cancer by Targeting Vascular Endothelial Growth Factor: A Multicenter Feasibility Dose-Escalation Study.* J Nucl Med, 2023. **64**(1): p. 82-89.
29. Steinkamp, P.J., et al., *Fluorescence-Guided Visualization of Soft-Tissue Sarcomas by Targeting Vascular Endothelial Growth Factor A: A Phase 1 Single-Center Clinical Trial.* J Nucl Med, 2021. **62**(3): p. 342-347.
30. Ter Weele, E.J., et al., *Development, preclinical safety, formulation, and stability of clinical grade bevacizumab-800CW, a new near infrared fluorescent imaging agent for first in human use.* Eur J Pharm Biopharm, 2016. **104**: p. 226-34.
31. Terwisscha van Scheltinga, A.G., et al., *Intraoperative near-infrared fluorescence tumor imaging with vascular endothelial growth factor and human epidermal growth factor receptor 2 targeting antibodies.* J Nucl Med, 2011. **52**(11): p. 1778-85.
32. Vergeer, R.A., et al., *Detection by fluorescence of pituitary neuroendocrine tumour (PitNET) tissue during endoscopic transsphenoidal surgery using bevacizumab-800CW (DEPARTURE trial): study protocol for a non-randomised, non-blinded, single centre, feasibility and dose-finding trial.* BMJ Open, 2021. **11**(10): p. e049109.
33. Jonker, P.K.C., et al., *Intraoperative MET-receptor targeted fluorescent imaging and spectroscopy for lymph node detection in papillary thyroid cancer: novel diagnostic tools for more selective central lymph node compartment dissection.* Eur J Nucl Med Mol Imaging, 2022. **49**(10): p. 3557-3570.
34. Buckle, T., et al., *Translation of c-Met Targeted Image-Guided Surgery Solutions in Oral Cavity Cancer-Initial Proof of Concept Data.* Cancers (Basel), 2021. **13**(11).
35. de Jongh, S.J., et al., *The Optimal Imaging Window for Dysplastic Colorectal Polyp Detection Using c-Met-Targeted Fluorescence Molecular Endoscopy.* J Nucl Med, 2020. **61**(10): p. 1435-1441.
36. de Jongh, S.J., et al., *C-Met targeted fluorescence molecular endoscopy in Barrett's esophagus patients and identification of outcome parameters for phase-I studies.* Theranostics, 2020. **10**(12): p. 5357-5367.
37. Armstrong, G.R., et al., *A novel fluorescent c-met targeted imaging agent for intraoperative colonic tumour mapping: Translation from the laboratory into a clinical trial.* Surg Oncol, 2022. **40**: p. 101679.
38. Vries, H.M., et al., *c-MET Receptor-Targeted Fluorescence on the Road to Image-Guided Surgery in Penile Squamous Cell Carcinoma Patients.* J Nucl Med, 2022. **63**(1): p. 51-56.
39. Keereweer, S., et al., *Targeting integrins and enhanced permeability and retention (EPR)*

effect for optical imaging of oral cancer. J Surg Oncol, 2012. **105**(7): p. 714-8.

40. de Valk, K.S., et al., *First-in-Human Assessment of cRGD-ZW800-1, a Zwitterionic, Integrin-Targeted, Near-Infrared Fluorescent Peptide in Colon Carcinoma.* Clin Cancer Res, 2020. **26**(15): p. 3990-3998.
41. Nishio, N., et al., *Optimal Dosing Strategy for Fluorescence-Guided Surgery with Panitumumab-IRDye800CW in Head and Neck Cancer.* Mol Imaging Biol, 2020. **22**(1): p. 156-164.
42. Gao, R.W., et al., *Safety of panitumumab-IRDye800CW and cetuximab-IRDye800CW for fluorescence-guided surgical navigation in head and neck cancers.* Theranostics, 2018. **8**(9): p. 2488-2495.
43. Rosenthal, E.L., et al., *Safety and Tumor Specificity of Cetuximab-IRDye800 for Surgical Navigation in Head and Neck Cancer.* Clin Cancer Res, 2015. **21**(16): p. 3658-66.
44. Fakurnejad, S., et al., *Intraoperative Molecular Imaging for ex vivo Assessment of Peripheral Margins in Oral Squamous Cell Carcinoma.* Front Oncol, 2019. **9**: p. 1476.
45. Linders, D., et al., *CEA, EpCAM, alphavbeta6 and uPAR Expression in Rectal Cancer Patients with a Pathological Complete Response after Neoadjuvant Therapy.* Diagnostics (Basel), 2021. **11**(3).
46. Moore, L.S., et al., *Effects of an Unlabeled Loading Dose on Tumor–Specific Uptake of a Fluorescently Labeled Antibody for Optical Surgical Navigation.* Mol Imaging Biol, 2017. **19**(4): p. 610-616.
47. de Wit, J.G., et al., *EGFR-targeted fluorescence molecular imaging for intraoperative margin assessment in oral cancer patients: a phase II trial.* Nat Commun, 2023. **14**(1): p. 4952.
48. Wang, J., et al., *A c-MET-Targeted Topical Fluorescent Probe cMBP-ICG Improves Oral Squamous Cell Carcinoma Detection in Humans.* Ann Surg Oncol, 2023. **30**(1): p. 641-651.
49. Metman, M.J.H., et al., *MET-receptor targeted fluorescent imaging and spectroscopy to detect multifocal papillary thyroid cancer.* Eur J Nucl Med Mol Imaging, 2023.
50. Kuczma, P., et al., *Central node dissection in papillary thyroid carcinoma in the era of near-infrared fluorescence.* Front Endocrinol (Lausanne), 2023. **14**: p. 1110489.
51. Orosco, R.K., et al., *Molecular targeting of papillary thyroid carcinoma with fluorescently labeled ratiometric activatable cell penetrating peptides in a transgenic murine model.* J Surg Oncol, 2016. **113**(2): p. 138-43.
52. Rudin, A.V. and E. Berber, *Impact of fluorescence and autofluorescence on surgical strategy in benign and malignant neck endocrine diseases.* Best Pract Res Clin Endocrinol Metab, 2019. **33**(4): p. 101311.
53. Keereweer, S., et al., *Optical image-guided cancer surgery: challenges and limitations.* Clin Cancer Res, 2013. **19**(14): p. 3745-54.

SUPPLEMENTARY MATERIALS

Supplementary Table 1: Overview of the immunohistochemistry methods

Protein abbreviation	Antibody	Company	Antigen retrieval	Secondary antibody	Stock concentration
Integrin αvβ6	αvβ6 6.2.A1	Biogen Idec.	0,4% Pepsin	Anti-mouse	0.05 mg/ml
CEA	CI-P83-1	Santa Cruz	Dako PT link Target Retrieval Solution, pH 6.0	Anti-mouse	0.2 mg/ml
c-MET	EP1454Y	Bio SB	Dako PT link Target Retrieval Solution, pH 9.0	Anti-rabbit	0.479 mg/ml
EGFR	D38B1XP	Cell signaling technology	Dako PT link Target Retrieval Solution, pH 9.0	Anti-rabbit	0.1 mg/ml
EpCAM	MOC31	Acris antibodies	Dako PT link Target Retrieval Solution, pH 6.0	Anti-mouse	0.64 mg/ml
VEGF-α	G153-694	BD Pharmingen	No antigen retrieval	Anti-mouse	0.5 mg/ml

Supplementary Table 2: Percentages of samples exhibiting absent, low, moderate and high expression of all six markers in oral (A) and laryngeal (B) squamous cell carcinoma, epithelium, and muscle, and in papillary thyroid carcinoma (C) and healthy thyroid tissue.

A. OSCC																		
Staining		**avb6**			**C-met**			**CEA**			**EGFR**			**EpCAM**			**VEGF-a**	
Histology	**T**	**E**	**M**	**T**	**E**	**M**	**T**	**E**	**M**	**T**	**E**	**M**	**T**	**E**	**M**	**T**	**E**	**M**
Absent	-	-	17.6	50	87.5	100	37.5	25	100	-	-	100	62.5	100	100	-	-	-
Low	20	66.7	82.4	50	12.5	-	62.5	75	-	12.5	50	-	25	-	-	12.5	87.5	12.5
Moderate	15	33.3	-	-	-	-	-	-	-	50	50	-	-	-	-	62.5	12.5	87.5
High	65	-	-	-	-	-	-	-	-	37.5	-	-	12.5	-	-	25	-	-
B. LSCC																		
Staining		**avb6**			**C-met**			**CEA**			**EGFR**			**EpCAM**			**VEGF-a**	
Histology	**T**	**E**	**M**	**T**	**E**	**M**	**T**	**E**	**M**	**T**	**E**	**M**	**T**	**E**	**M**	**T**	**E**	**M**
Absent	-	-	80	70	90	100	50	30	100	-	-	100	70	80	100	-	-	-
Low	10	40	20	30	10	-	50	60	-	-	20	-	-	20	-	20	90	40
Moderate	60	50	-	-	-	-	-	10	-	30	50	-	10	-	-	30	10	60
High	30	10	-	-	-	-	-	-	-	70	30	-	20	-	-	50	-	-
C. PTC																		
Staining		**avb6**			**C-met**			**CEA**			**EGFR**			**EpCAM**			**VEGF-a**	
Histology	**T**		**N**		**T**	**N**	**T**		**N**	**T**		**N**	**T**		**N**	**T**		**N**
Absent	-		60		20	90	100		90	-		20	10		-	-		-
Low	90		40		60	10	-		10	40		80	-		-	50		100
Moderate	10		-		20	-	-		-	60		-	30		100	50		-
High	-		-		-	-	-		-	-		-	60		-	-		-

T: tumour, E: epithelium, M: muscle, N: normal (thyroid)

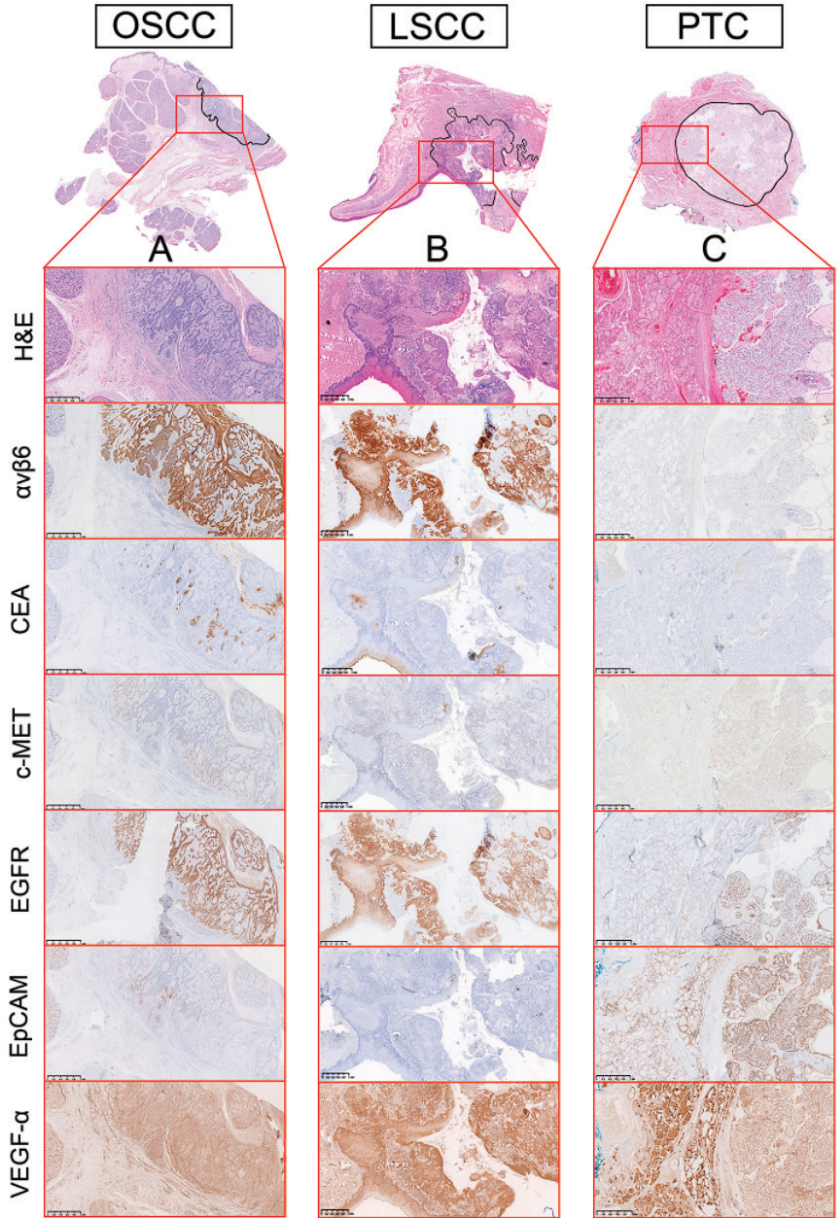

Supplementary Figure 1. Marker expression in representative oral squamous cell carcinoma (OSCC) (A), laryngeal squamous cell carcinoma (LSCC)(B) and papillary thyroid carcinoma (PTC)(C). Tumours are outlined in black.

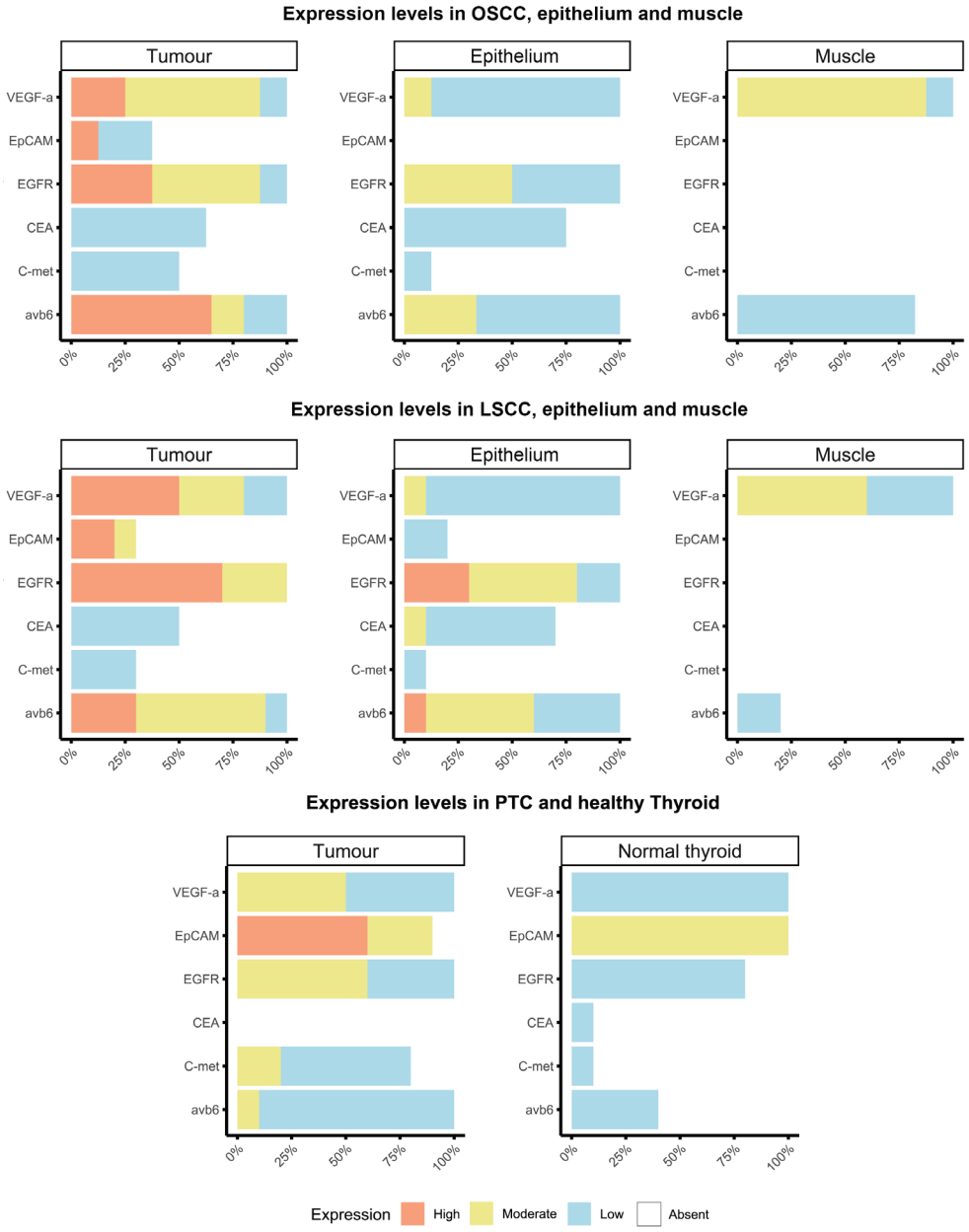

Supplementary Figure 2. Percentages of samples exhibiting absent, low, moderate and high expression of all six markers in oral and laryngeal squamous cell carcinoma, epithelium, and muscle, and in papillary thyroid carcinoma and normal thyroid tissue.


7

Chapter 7

Near-infrared fluorescence imaging-guided surgery using cRGD-ZW800 to improve surgical resection margins in oral cancer: a phase I/II feasibility trial

L.J. Lauwerends[†]& B.E. Zweedijk[†], H.A. Galema, D.J. Robinson, H.S. de Bruijn, H. Abbasi, T.L. March, A.R.P.M. Valentijn, M. Pool, H. Mast, B.P. Jonker, J.A.U. Hardillo, D. Monserez, A. Sewnaik, S. Koljenovic, C. Verhoef, R.J. Baatenburg de Jong, J.V. Frangioni, S.A. Koppes, D.E. Hilling, A.L. Vahrmeijer, S. Keereweer

Nature Communications (2026). doi:10.1038/s41467-026-73554-7

ABSTRACT

In oral squamous cell carcinoma (OSCC) surgery, inadequate tumor margins are reported in up to 85% of cases, adversely affecting outcomes. In this prospective, single-center study (n=31; NCT04191460), we evaluated the safety and imaging feasibility of cRGD-ZW800-1, a near-infrared fluorescent integrin-targeted tracer. The secondary objective was to determine whether intraoperative fluorescence imaging could identify inadequate resection margins and inform surgical decision-making. Patients received 0.01, 0.025, or 0.05 mg/kg cRGD-ZW800-1, and tracer uptake was quantified using in vivo multi-diameter single-fiber reflectance and single-fiber fluorescence spectroscopy to optimize dosing and timing. All doses were well tolerated, achieving tumor-to-background ratios exceeding 4.5, with optimal performance at 0.025 mg/kg. Fluorescence imaging detected all 23 inadequate margins, including nine undetected by conventional assessment (sensitivity 100% versus 70%), altered surgical plans in five cases, and avoided adjuvant radiotherapy in three cases. These findings demonstrate that cRGD-ZW800-1 is safe, tumor-specific, and facilitates intraoperative margin assessment in OSCC.

INTRODUCTION

Achieving complete tumor removal in oral cancer surgery remains a significant clinical challenge. Although preoperative imaging improves surgical planning, intraoperative margin assessment still relies on the surgeon's visual and tactile judgment. As distinguishing tumor from healthy tissue can be very difficult, inadequate margins, defined as tumor-positive (<1 mm) or close (≤5 mm), are reported in 67–85% of cases, with up to 40% being tumor-positive[1-4]. These margins are strongly associated with local recurrence, the need for adjuvant therapy, and poor survival outcomes[2, 5-9]. Selective frozen section analysis is currently the gold standard to assess surgical margins intraoperatively. However, this technique is time-consuming, can only examine a small part of the specimen, and is subject to sampling errors, thus frequently resulting in a high false-negative rate[10]. Therefore, there is a clear need for more accurate, objective, real-time, intraoperative techniques for tumor margin identification.

Fluorescence imaging (FI), using tumor-specific near-infrared (NIR) fluorescent agents, can be of additional value to guide the surgeon in the complete resection of tumors[11]. Several clinical studies have recently shown promising results regarding targeting specificity, imaging contrast, and intraoperative usability[11-19]. While FI has achieved high detection rates for tumor-positive margins in oral cancer (up to 100%), sensitivity for close margins remains limited (43-67%)[19]. As previously mentioned, close margins significantly increase recurrence and lower survival[8, 9], making the exploration of alternative fluorescent agents to mitigate close margins imperative. Additionally, NIR FI offers significant advantages over label-free techniques (e.g. autofluorescence), including enhanced tissue penetration and minimized interference from blood, making it particularly effective for imaging deep tumor tissue. These advantages have been confirmed in recent studies, underscoring the potential of NIR FI to improve the accuracy of tumor detection during surgery[20, 21].

cRGD-ZW800-1 is a zwitterionic, integrin-targeted fluorescent agent consisting of a cyclic pentapeptide (cRGD) conjugated to an 800nm fluorophore ZW800-1[22, 23]. Because of their low non-specific uptake in normal tissue, zwitterionic targeting ligands tend to exhibit higher tumor-to-background ratios (TBRs). cRGD, a clinically well-known peptide, binds to a wide range of integrins that are associated with neoangiogenesis. The αvβ6 integrin is also well-suited as a target for tumor imaging, as it is highly overexpressed in most invasive epithelial cancer types, including oral cancer, whereas its expression in normal tissue is limited[24, 25]. cRGD-ZW800-1 has shown tumor-specific imaging without toxicity in healthy participants and colon cancer patients[14]. Integrin expression levels are variable among different tumor types and different anatomical sites involve distinct tissue optical properties (e.g., scattering and light absorption) that affect the fluorescent signal in unpredictable ways. Therefore, a feasibility study in oral cancer is required, including correction of the fluorescent signal intensity to tissue optical properties[10, 16].

Multi-diameter single-fiber reflectance and single-fiber fluorescence (MDSFR/SFF) spectroscopy corrects for tissue optical properties to quantify intrinsic fluorescence, enabling objective comparison between tumor and healthy tissue. While previously used in clinical fluorescence imaging trials[15, 24, 25], true in vivo quantification of intrinsic fluorescence over time has never been achieved, primarily due to technical limitations. In this study, we applied MDSFR/SFF spectroscopy to measure cRGD-ZW800-1 concentrations in tumor and healthy tissue at multiple time points, providing valuable pharmacodynamic data. The oral cavity's accessibility allowed direct contact measurements, offering unique insights into the tracer's temporal behavior in vivo.

The aim of this study is to evaluate the safety and feasibility of cRGD-ZW800-1 in patients with oral squamous cell carcinoma (OSCC), and to identify the optimal timing interval and dose for intraoperative detection and margin assessment. Building on these findings, we further examine the potential of FI with cRGD-ZW800-1 in detecting inadequate resection margins and assess its impact on surgical decision-making.

METHODS

Clinical trial design

This prospective single-center, single arm Phase I/II study was performed in 31 patients diagnosed with OSCC at the Erasmus Medical Center (Rotterdam, The Netherlands) from July 2022 until April 2025. The study protocol (available in the Supplementary Information file) was approved by the local Ethics Review Committee (METC Erasmus MC) and conducted in full compliance with the principles of the Declaration of Helsinki of 1975, the ICH GCP guidelines, and the laws and regulations of the Netherlands. As this study involved the use of an Investigational Medicinal Product (IMP), authorization was granted by the Central Committee on Research Involving Human Subjects (CCMO, the Netherlands), which serves as the national competent authority of clinical trials with IMPs. The study is registered in the European Clinical Trials Database (EudraCT 2019-003416-30) in December 2019, and ClinicalTrials.gov (NCT04191460) in December 2020.

Eligible patients were 18 years or older, and able to provide written informed consent. Patients with biopsy-proven active malignancies other than OSCC were excluded, as were those with a history of surgery, chemo- or radiotherapy involving the oral cavity. Pregnant or breastfeeding patients were also excluded, as were patients with significant clinically abnormal hematological status, kidney and liver function. To minimize selection bias, all eligible patients were consecutively recruited after screening at a multidisciplinary meeting, ensuring all were considered for inclusion.

The primary outcome measures of this study were the safety and imaging feasibility of cRGD-ZW800-1, assessed through TBR, mean fluorescence intensity (MFI), and determination of the optimal dose and injection-to-imaging interval. Based on encouraging results from a prior investigation of cRGD-ZW800-1 in colorectal cancer[14], three dose levels (0.01, 0.025, and 0.05 mg/kg) were evaluated. The overarching goal was to assess whether intraoperative FI with cRGD-ZW800-1 can reliably detect all inadequate resection margins during oral cancer surgery and influence intraoperative decision-making.

Per the standard of care, patients are admitted to the hospital the day before surgery. The agent was administered via a venous access line via a slow infusion for 5-10 minutes, approximately 18 hours before surgery. Safety measurements entailed close patient monitoring before and after administration, consisting of repeated physical examinations, vital signs measurements, standard 12-lead-electrocardiograms (ECGs), and laboratory tests. Adverse events were monitored continuously by three independent researchers. When a complication was identified, it was classified according to the Common Terminology Criteria for Adverse Events (CTCAE), the required treatment was documented, and its progression or resolution was monitored.

After administration, MDSFR/SFF spectroscopy was performed in triplicate in the center of the tumor, on the edge of the tumor, and on normal tissue on the contralateral side of the oral cavity. This step consisted of direct contact fiber probe measurements at three time points after administration (0.5, 2 and 4 hours) and once more before the start of surgery (18 hours) to quantify the concentration of cRGD-ZW800-1 in and around the tumor over time.

Investigational agent

The fluorescent contrast agent used in this study is cRGD-ZW800-1, a cyclic 5-amino acid sequence (cRGDyK) conjugated to the 800 nm NIR fluorophore ZW800-1, which binds specifically to integrins (αvβ1, αVβ3, αvβ5, αvβ6, αvβ8, α5β1, α8β1 and αIIbβ3)[22]. The drug substance and drug product were manufactured at the Interdivisional GMP Facility LUMC (IGFL), part of the department of Clinical Pharmacy and Toxicology, Leiden University Medical Center under Good Manufacturing Practice (GMP) conditions, in accordance with Directive 2001/20/EC.

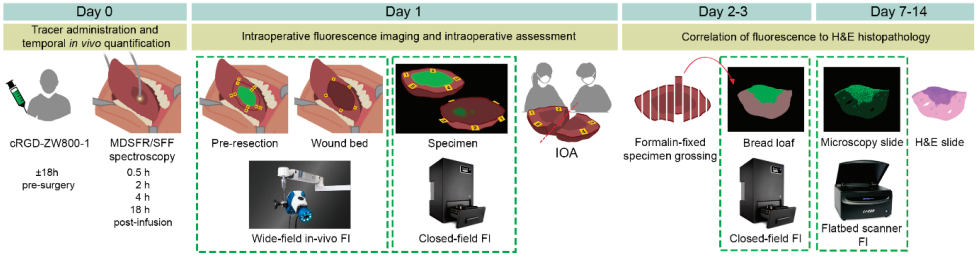

Figure 1. Clinical trial design. cRGD-ZW800-1 was administered intravenously approximately 18 hours before surgery. This was followed by in vivo quantification of the tracer with MDSFR/SFF spectroscopy, consisting of probe point measurements on both tumor and healthy tissue (contralateral) at 4 different time points (including right before surgery). On the day of surgery, wide-field FI was performed in vivo before (i.e., after delineation and parallel tag placement) and after resection, followed by closed-field FI of the specimen from different angles. Routine IOA of the resection margins was performed by the surgeon and a pathologist. After grossing, closed-field FI of the formalin-fixed bread loaves was performed. Finally, deparaffinized 4µm-thick microscopy slides were imaged in a flatbed FI scanner. Fluorescence in the bread loaves and microscopy slides was correlated with H&E histopathology.

H&E: Hematoxylin and Eosin; MDSFR/SFF: multi-diameter single-fiber reflectance and single-fiber fluorescence; FI: fluorescence imaging; IOA: intraoperative assessment. Illustrations were created using Procreate, and the figure was assembled and annotated in Adobe Photoshop (version 26.8.1).

Surgical procedure and intraoperative fluorescence imaging

Surgeries were performed by six board-certified Head and Neck Surgeons, with surgical experience varying from 4 to 25 years. Open surgical-field intraoperative FI was performed using the CE-marked Quest Spectrum Platform (Quest Medical Imaging, Middenmeer, The Netherlands) by a team of experienced fluorescence imaging experts. This system utilizes excitation at 780 nm with a power density of 10 mW/cm^2, and emission is detected in the range of 800–900 nm. In our study, the gain was set to 22.5 (default), and we tested an exposure time of 38 ms (default). To standardize imaging conditions, we aimed to keep the camera distance between 20–30 cm and positioned it perpendicular to the sample, although slight variations occasionally occurred. During in vivo FI, the tumor was first delineated mucosally without the use of FI (Figure 1), aiming for a 10 mm mucosal margin. FI was then performed, and any changes to the surgical plan based on fluorescence were documented. After resection, the wound bed was inspected for residual fluorescence, and the specimen was imaged ex vivo from multiple angles using the Pearl Trilogy Small Animal Imaging System (LI-COR Biosciences Inc., Nebraska, USA), a closed-field imaging system. This camera system uses excitation with 785 nm light at 3 mW/cm^2 power density, and emission is captured in the range of 810-830 nm. The gain and exposure time (range of 500 ms to 60 s) are automatically set by the acquisition software (Image Studio^{TM}) to produce a high dynamic range image. We adjusted the working distance to achieve the best focus, which varied depending on the specimen's height. During ex vivo imaging, all surgical planes were systematically evaluated based on fluorescence images acquired with the closed-field imaging system and compared to definitive histopathological assessment.

After closed-field FI, specimen-driven intraoperative assessment (IOA) was performed. IOA is standard-of-care for intraoperative margin assessment in the Erasmus MC[26]: it is performed in close cooperation by the surgeon and pathologist, including gross and microscopic (fresh frozen sectioning) margin evaluation. If close or positive margins were identified, additional resections were guided by parallel tags placed during initial delineation[27]. To prevent bias, both surgeon and pathologist were blinded to ex vivo FI findings. Fluorescent signals at specimen margins were only disclosed after standard IOA was completed.

Postoperative tissue analysis and immunohistochemistry

After IOA and any additional resections, all surgical specimens were mapped, formalin fixed and processed into bread loaves, which were then cut into blocks to be placed in cassettes. These sections were then analyzed separately using the Pearl imaging system to measure ex vivo fluorescence, before paraffin embedding.

Following ex vivo closed-field FI, definitive histopathological assessment was performed according to standard pathology protocols, evaluating all surgical resection planes, including both deep and mucosal margins. In line with these protocols, the resection specimen is oriented as a six-sided cuboid, where five surfaces represent true surgical resection margins (a standard approach also used in IOA), while the original mucosal surface (the exposed tumor-bearing side) does not constitute a tissue-tissue resection interface and is therefore excluded. Mucosal margins were assessed on the surgically created lateral planes, consistent with routine practice. We applied this same systematic evaluation to FI assessment, ensuring direct comparability with pathology. This aligns with a prior report on FI in oral cancer patients[19]. All tissue blocks were subsequently examined on hematoxylin and eosin (H&E)-stained sections by a dedicated head and neck pathologist, with definitive margin status determined independently of intraoperative findings.

After final histopathologic analysis, fluorescence imaging of the tissue slides was performed using a flatbed scanner (Odyssey M or Odyssey CLx, LI-COR Biosciences Inc., Nebraska, USA) to determine location of the fluorescent targeting agent, and to correlate fluorescent signal with H&E histopathology.

Finally, immunohistochemical (IHC) staining with the αvβ6 integrin was performed on representative 4 μm FFPE microsections containing fluorescent tissue, which included primary tumor, (occult) second primary tumor, healthy gingiva, healthy and inflamed salivary gland tissue, and atrophic bone (marrow) to verify αvβ6 expression. These microsections were also imaged using the Odyssey scanner.

In vivo MSDFR/SFF spectroscopy

MDSFR spectroscopy determines the scattering and absorption coefficients (from the reflectance spectra), while SFF spectroscopy measures tissue fluorescence[16, 28, 29]. Quantitative intrinsic fluorescence ($Q.\mu^{f}_{a,x}$) is defined as the product of the quantum efficiency across the emission spectrum Q[-], where Q is the fluorescence quantum yield of ZW800-1, and μ_a^f [mm^{-1}] is the tracer absorption coefficient at the excitation wavelength. The intrinsic fluorescence ($Q.\mu^{f}_{a,x}$) of cRGD-ZW800-1 was calculated by correcting the raw fluorescence spectrum for the tissue optical properties. All measurements were repeated in triplicate and median values were calculated per measurement location. Details of the spectral correction, linear fitting procedure, and quantification limits are provided in Supplementary Figure 1.

Statistical analysis

For the MDSFR/SFF spectroscopy, 3 spectra were acquired consecutively at each measurement location. These were averaged (weighted by the confidence interval of the spectral fit to the data), to form a weighted average at each measurement location at each time point. The quotient of the median group means of the tumor and contralateral (healthy) tissue constituted the in vivo TBR.

Ex vivo TBR was calculated by drawing a region of interest (ROI) spanning the tumor, and another in adjacent (muscle) tissue using the Pearl's integrated software (ImageStudio; LI-COR Biosciences Inc., Nebraska, USA). The MFIs were obtained per ROI. The (weighted) quotient of the tumor and muscle region MFI constituted the ex vivo TBR. Given that most inadequate margins occur in the deep margin rather than the mucosa[30], ex vivo TBR was calculated on formalin-fixed bread loaves, as they contain the more relevant deep margin and adjacent muscle tissue. Similar to other studies, we observed that the fluorescence signal remained unaffected after formalin fixation[31], ensuring the accuracy of our ex vivo TBR calculations.

In order to determine the sample size for dose-finding and feasibility, a lower threshold to differentiate signal from background noise is set at a mean TBR of $\mu 0=2.0$. Based on previous preclinical studies using cRGD-ZW800-1, and on experience from clinical trials using similar tumor-specific fluorescent targeting agents[32, 33], the $\mu 1$ is set to a mean of 4.0 with a standard deviation σ of 1.5. We have chosen a wider standard deviation than that observed in similar studies conducted on other cancer types, to account for the possibility of encountering a greater variation in integrin expression levels in oral cancers. Considering an α of 0.05 and a power of 80%, the sample size (n) is 7 per group, based on the One-Sample 2-sided t-test.

All patients with a detectable fluorescence signal were included in the surgical margin evaluation, which ultimately comprised the entire cohort (n=31). Since signal detectability could not be guaranteed in advance, the required sample size was calculated solely for the optimal

dose cohort. The primary endpoint is the rate of adequate surgical resection margins, based on the postoperative margin status. This analysis tests the null hypothesis that the adequate surgical margins rate is at most 15% versus the alternating hypothesis that the adequate surgical margins rate is at least 40%. The significance level (i.e., the probability of rejecting H0 when it is true) is α=0.05 and the power (i.e., the probability of deciding the regimen is active) is 80%. Based on the A'Hern single stage Phase II design[34], the expected sample size is 21. The minimal number of successes to indicate that the treatment is effective is 7.

The efficacy of FI was assessed by calculating standard diagnostic performance metrics, including sensitivity, specificity, negative predictive value (NPV), positive predictive value (PPV), and overall accuracy. Corresponding 95% confidence intervals (CI) were determined using an ANOVA-type Wilson score estimation that considers intra-patient clustering. To comprehensively evaluate both the intrinsic diagnostic performance and the clinical impact of FI, two complementary analyses were performed. First, a diagnostic accuracy analysis was conducted, in which all histopathological findings, both tumor-positive and tumor-negative, were evaluated in relation to fluorescence, irrespective of their impact on margin status. Second, a patient-level analysis was performed to evaluate findings relevant in the intraoperative surgical context. In this analysis, tissue clearly distant from the tumor and deemed non-suspicious by both surgeon and pathologist (e.g., en bloc resected salivary gland tissue) was excluded.

In the diagnostic accuracy analysis, all diagnostic performance metrics were derived by comparing both ex vivo intraoperative fluorescence findings and standard IOA with definitive (postoperative) histopathological assessment of the entire resection plane. Fluorescent areas corresponding to either tumor localisation (including second primary lesions distant from the surgical cut) or a close margin were classified as true positives (TP), whereas non-fluorescent areas corresponding to healthy tissue (including clear margins) were classified as true negatives (TN). Furthermore, fluorescent areas corresponding to healthy tissue (including clear margins) were classified as false positives (FP), while non-fluorescent areas corresponding to either tumor localisation (including second primary lesions distant from the surgical cut) or a close margin were classified as false negatives (FN).

This analysis therefore included separate tumor-positive lesions within the specimen that were not located at the surgical margin and therefore would not have impacted surgical decision-making.

In the patient-level analysis, only margin-related findings that could potentially influence surgical management were included. This analysis focused exclusively on fluorescence findings at the surgically assessed resection planes and did not involve a combined evaluation with IOA. Fluorescent signals arising from areas clearly unrelated to the tumor margin, such as en bloc–resected salivary gland tissue outside the resection interface, were not considered

relevant for intraoperative decision-making and were therefore excluded. Within this framework, fluorescent areas corresponding to inadequate (positive or close) margins were classified as TP, and a complete non-fluorescent margin surface corresponding to adequate margins classified as TN. Conversely, non-fluorescent areas corresponding to inadequate margins were considered FN, while fluorescent areas corresponding to clear margins were classified as FP. In addition, subgroup analyses were conducted, in which positive and close margins were evaluated separately. Specifically, one analysis compared positive margins with clear margins only, and one analysis compared close margins with clear margins only. In each case, fluorescence was regarded as a positive test result exclusively for the margin category under evaluation, and the same TP, TN, FP, and FN classification framework described above was applied.

Patient demographics, safety parameters, MFIs and TBRs were expressed in descriptive statistics (n, mean, SD). To assess differences in the inadequate margin detection between standard IOA and FI, the exact binomial McNemar's test was used. Differences in MFI were analyzed using the Wilcoxon rank test, and differences in TBR were evaluated using the Mann-Whitney U test. A p-value of <0.05 was considered statistically significant. Adobe Photoshop (version 26.8.1) and R studio (version 4.3.2) were used for statistical analysis and graph design.

RESULTS

Thirty-one patients with biopsy-proven OSCC scheduled for standard-of-care surgery were included in this study. The patients consisted of eight women and twenty-three men, with an average age at inclusion of 66 years (range, 34-91). Patient and study characteristics are summarized in Table 1.

Table 1. Study characteristics and inadequate resection margin detection using FI with cRGD-ZW800-1.

Pt	Age	Sex	Dose (mg/kg)	Tumor site	T- stage[a]	Intraoperative margin status	Inadequate margin found with IOA?	Inadequate margin found with FI?	Extra resection performed?	Postoperative margin status
1	53	F	0.05	Lateral tongue	cT3	Close	Yes	Yes	Yes	Clear
2	34	M	0.05	Lateral tongue	cT1	Close	Yes	Yes	No	Close
3	37	M	0.05	Posterior tongue	cT2	Positive	Yes	Yes	Yes	Close
4	65	M	0.05	Retromolar trigone	cT2	Close	No	Yes	Yes	Close
5	76	M	0.05	Lateral tongue	cT2	Close	Yes	Yes	Yes	Clear
7	46	M	0.05	Lateral tongue	cT2	Close	Yes	Yes	No	Close
8	59	M	0.05	Lateral tongue	cT4a	Positive	Yes	Yes	Yes	Close
6	75	M	0.01	Floor of mouth	cT2	Clear	n/a	n/a	n/a	Clear
9	53	F	0.01	Lateral tongue	cT2	Close	No	Yes	Yes	Close
10	59	M	0.01	Floor of mouth	cT1	Close	-**	Yes	No	Close
11	77	F	0.025	Alveolar process mandibula	cT2	Clear	n/a	n/a	n/a	Clear
12	73	M	0.025	Retromolar trigone	cT2	Positive	Yes	Yes	Yes	Close
13	64	M	0.025	Alveolar process mandibula	cT2	Close	No	Yes	No	Close
14	68	M	0.025	Alveolar process maxilla	cT4b	Clear	n/a	n/a	n/a	Clear
15	68	M	0.025	Floor of mouth	cT1	Close*	Yes	Yes	Yes	Clear
16	77	M	0.025	Lateral tongue	cT2	Close*	Yes	Yes	Yes	Close
17	68	V	0.025	Floor of mouth	cT1	Positive	No	Yes	Yes	Close
18	63	V	0.025	Alveolar process	cT2	Close	Yes	Yes	Yes	Clear
19	91	M	0.025	Alveolar process	cT4	Positive	Yes	Yes	Yes	Close
20	47	M	0.025	Lateral tongue	cT2	Positive	Yes***	Yes	Yes	Clear
21	69	M	0.025	Lateral tongue	cT3	Clear	n/a	n/a	n/a	Clear
22	66	M	0.025	Ventral tongue/floor of mouth	cT2	Clear	n/a	n/a	n/a	Clear
23	70	M	0.025	Lateral tongue	cT2	Close	Yes	Yes	Yes	Close
24	75	F	0.025	Lateral tongue	cT2	Clear	n/a	n/a	n/a	Clear



Table 1. Study characteristics and inadequate resection margin detection using FI with cRGD-ZW800-1. (*continued*)

Pt	Age	Sex	Dose (mg/kg)	Tumor site	T- stage[a]	Intraoperative margin status	Inadequate margin found with IOA?	Inadequate margin found with FI?	Extra resection performed?	Postoperative margin status
25	81	F	0.025	Lateral tongue	cT3	Close	No	Yes	No	Close
26	79	M	0.025	Lateral tongue	cT3	Positive	No	Yes	Yes	Clear
27	77	F	0.025	Buccal mucosa	cT4a	Clear	n/a	n/a	n/a	Clear
28	75	M	0.025	Lateral tongue	cT2	Clear	n/a	n/a	n/a	Clear
29	67	M	0.025	Floor of mouth	cT2	Positive	No	Yes	No	Positive
30	63	M	0.025	Floor of mouth	cT3	Close	No	Yes	No	Close
31	69	M	0.025	Lateral tongue	cT1	Close	No	Yes	Yes	Clear

[a]TNM staging was based on American Joint Committee on Cancer (AJCC). Cancer Staging Manual, 8th edition (2017). Springer.

* Second primary lesion present

** No IOA performed

*** Partially, of the multiple inadequate margins only one was detected using IOA

IOA: intraoperative assessment; FI: fluorescence imaging; n/a: not applicable

Safety and tolerability

No signs of acute or chronic toxicity were observed following administration of cRGD-ZW800-1, and no hypersensitivity reactions occurred. Across the study cohort, twelve adverse events (AEs) and five serious adverse events (SAEs) were reported in eight patients (Supplementary Table 1). All reported AEs and SAEs were unrelated to cRGD-ZW800-1 and were attributed to the expected postoperative course. Importantly, no AEs occurred between tracer administration and surgery. Furthermore, the use of FI did not contribute to further morbidity. Additional resections were performed only when histopathologically justified and involved only a few millimeters of extra tissue, which did not necessitate unplanned reconstructions and therefore did not prolong hospital stay.

Vital signs and ECGs remained stable following tracer injection, with no clinically significant changes observed. A decrease in hemoglobin (Hb) levels was noted in three patients, likely resulting from pre-existing malnutrition and dehydration frequently associated with oral cavity cancer due to pain and impaired oral intake. Given that all patients received intravenous fluids prior to tracer administration, the Hb decrease is attributed to hemodilution rather than any tracer-related effect, consistent with prior reports[35, 36]. All administered doses (0.01, 0.025, and 0.05 mg/kg) were well tolerated.

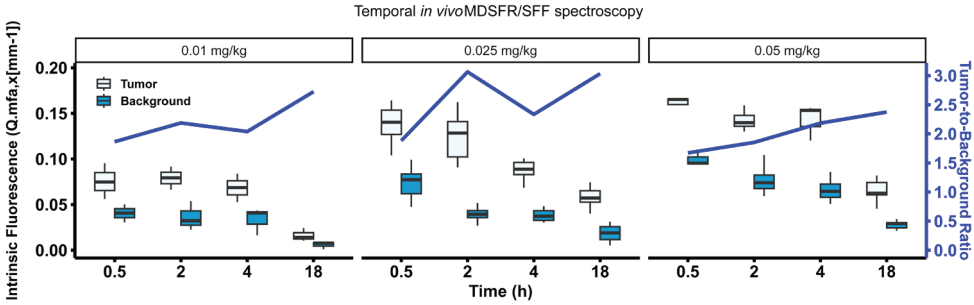

Figure 2. Temporal quantification of intrinsic fluorescence with MDSFR/SFF spectroscopy at 0.5, 2, 4 and 18 hours post-administration for dose groups 0.01 (n=3), 0.025 (n=21) and 0.05 mg/kg (n=7) (left to right), where "n" denotes the number of patients allocated to each dose group. Measurements were performed in triplicate in the center of the tumor and on the contralateral side of the oral cavity. This step consisted of direct contact fiber probe measurements at three time points after administration (0.5, 2, 4 and 18 hours). $Q.\mu^{f}_{a,x}$ was significantly higher in the tumor compared to healthy tissue for all time points in dose groups 0.025 and 0.05 mg/kg ($p < 0.001$). Blue lines represent the mean in vivo tumor-to-background ratios (weighted quotient of the tumor and background region $Q.\mu^{f}_{a,x}$), that increase over time in dose groups 0.025 and 0.05 mg/kg. The horizontal dashed line represents the TBR threshold of 2. Box plots show the median (centre line), the interquartile range (box bounds; 25th–75th percentiles), and whiskers extending to the most extreme data points within 1.5× the interquartile range from the quartiles. *MDSFR/SFF: multi-diameter single-fiber reflectance and single-fiber fluorescence. The source data is available as a Source Data File.*

In vivo quantification of cRGD-ZW800-1

Temporal quantification of the intrinsic fluorescence ($Q.\mu^{f}_{a,x}$) values with MDSFR/SFF spectroscopy revealed TBRs of 2.72 ± 2.27 (n=3), 3.03 ± 1.36 (n=21) and 2.37 ± 0.59 (n=7) for dose cohorts 0.01, 0.025 and 0.05 mg/kg, respectively, measured 18 hours post-administration. Although TBR (i.e., imaging contrast) after 18 hours was relatively high for the group that received 0.01 mg/kg, the $Q.\mu^{f}_{a,x}$ of tumor tissue was very low (0.02 ± 0.01), and not significantly greater than the intrinsic background fluorescence (p=0.114). Importantly, Figure 2 demonstrates sufficient contrast (TBR ≥ 2.0) after only two hours for the group that received 0.025 mg/kg, suggesting that administration on the day of surgery is feasible, making it logistically more favorable.

Dose finding and injection time window

The first dose group (n=7) received 0.05 mg/kg cRGD-ZW800-1. Excellent intraoperative contrast and tumor-specificity were found in all cases *(*Figure 2*)*. These results allowed for dose de-escalation for the second dose cohort, which was set to receive 0.01 mg/kg. After inclusion of three patients, interim analysis clearly showed adequate TBRs, further increasing over time (Figure 2). However, absolute in vivo fluorescence intensity was consistently relatively low, indicating less optimal intraoperative usability. It was therefore decided to include a third dose cohort (n=7) that received an intermediate dose of 0.025 mg/kg.

In vivo FI before resection

Intraoperative FI did not interfere with the standard procedure, and the total incremental operation time related to in vivo FI never exceeded 10 minutes (mean 5.52 minutes, range: 4-10 min). Strong mucosal fluorescence was observed in all tumors before resection in all patients (Figure 3C). Referencing the initial mucosal outline defined by the surgeon prior to imaging, the fluorescent areas never suggested inadequate margins, supporting the surgeon's accurate assessment, subsequently confirmed by histopathology. This indicates that mucosal delineation can be achieved with well-defined boundaries and high contrast using FI, resulting in adequate identification of all mucosal margins. Although a consistent fluorescence signal was observed in healthy gingiva (Supplementary Fig. 2), ex vivo FI revealed sufficient mucosal contrast with a mean TBR of 2.04 (SD 0.79) in gingival tumor specimens. Furthermore, in vivo spectroscopy measurements confirmed that all individual patients with gingival tumors achieved adequate TBRs, with the lowest measured TBR being 2.1, indicating that physiological fluorescence in healthy gingival did not impose an issue for mucosal tumor delineation. In one patient, a second primary lesion with a diameter of 5 mm was found by the surgeon during inspection, also showing a clear fluorescent signal.

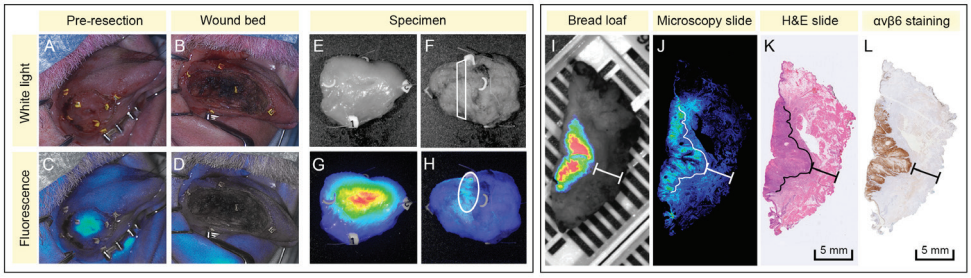

Figure 3. Intra- and postoperative fluorescence imaging of an oral squamous cell carcinoma of the lateral tongue from a patient with a close surgical margin. In vivo fluorescence imaging of the outlined tumor before resection (A, C), and of the wound bed, after resection (B, D), by ex vivo fluorescence imaging of the resected specimen in a closed-field system (E-H). The specimen is imaged from different angles, e.g., mucosal (E, G) and the deep margin (F, H), where a fluorescence signal is visible in the close margin (solid oval). Finally, fluorescence in formalin-fixed bread loaves (I, outlined in F) and deparaffinized microscopy slide (J) are correlated with H&E histopathology (K) and αvβ6 immunohistochemistry (L). In (I, J, K, L) the tumor is delineated, and close margin indicated in white/black. Images (A-D) were obtained with the Quest Spectrum Platform, (E-I) were obtained with the Pearl Trilogy, J was obtained with the Odyssey CLx Imaging System, K and L were digitally scanned with a virtual microscope (Nanozoomer 2.0 HT, Hamamatsu Photonics, Shizuoka, Japan), and the scale bar was determined using NDP.view2 Viewing software (Hamamatsu Photonics, Shizuoka, Japan). *H&E: Hematoxylin and Eosin.*

In vivo FI of the wound bed

Residual fluorescence in the wound bed was observed in 4 of 31 cases (13%). In one patient with a tumor located in the alveolar process, the surgeon suspected residual malignancy immediately post-resection. Intraoperative FI corroborated this suspicion by revealing a localized fluorescent signal in the wound bed. Following pathological confirmation by IOA, a limited additional resection was performed at the corresponding site. In the remaining three cases, fluorescence was detected in non-suspicious anatomical structures: the mandibular bone marrow at the resection plane (n=2) and lingual salivary gland tissue (n=1). None of these areas were deemed clinically suspicious, and the corresponding margins on the tumor specimen were histologically tumor-negative.

Intraoperative ex vivo closed-field imaging of the specimen

Consistent with pre-resection FI, a well-demarcated fluorescent signal was seen in the tumor on the mucosal side of the freshly resected specimen in all imaged (n=31) cases. Intraoperative closed-field resection specimen FI could not be performed for one case, due to a malfunction of the imaging device. Fluorescent areas were also observed on the deep surface (i.e., the non-mucosal margin of the specimen which is exposed after resection) of all imaged specimens. The vast majority of these visible fluorescent spots were integrin-specific, indicating the presence of either salivary glands (n=14) or inadequate margins (n=23). While fluorescent, salivary gland tissue was macroscopically easily distinguishable by the surgeon and pathologist, posing no clinically relevant challenges. In the two cases of partial man-

dibulectomy mentioned above, the corresponding surgical cut on the specimen showed fluorescent signal too, but there was no inadequate bony margin.

The regions of highest fluorescence on the deep margin were identified and correlated with final histopathology (i.e., the sentinel margin approach[37, 38]). All close (1-5 mm) and positive (<1 mm) resection margins exhibited fluorescence intensity-peaks (example shown in Figure 3H). In the full cohort (n=31), 15 close and 8 positive margins were all successfully detected using FI, whereas nine inadequate margins were missed by standard IOA by surgeon and pathologist (three positive and six close margins). Resulting in a detection rate of 100% for FI (23/23), compared with 61% for IOA (14/23). The case in which closed-field inspection could not be performed due to malfunction of the device had a close margin (1-5 mm, n=1), which exhibited a clear fluorescence signal during postoperative FI. Focusing on the optimal-dose cohort (n = 21), all 14 inadequate margins (6 positive and 8 close margins) were again detected by FI, while IOA missed seven cases (three positive, four close). This corresponded to a detection rate of 100% for FI (14/14), compared with 50% for IOA (7/14). Consequently, FI demonstrated a significant higher inadequate margin detection rate compared to standard IOA for both the full cohort (100% vs. 61%, Exact binomial McNemar's test, p = 0.004) and the optimal-dose cohort (100% vs. 50%, Exact binomial McNemar's test, p = 0.008).

Diagnostic performance of FI

To assess diagnostic accuracy, all surgical resection planes were included, together with any separate tumor lesions identified within the specimen. In total, 155 surgical resection planes were assessed in 31 patients (5 resection planes for each patient). Of these resection planes, 56 exhibited fluorescence, yielding a total of 63 distinct fluorescent spots. In 47 (74.6%) of these spots, an inadequate margin was confirmed on definitive histopathological assessment. The remaining 16 (25.4%) fluorescent spots corresponded to histopathologically adequate resection margins and originated from non-tumor tissue, specifically salivary gland tissue (n = 14) or bone marrow (n = 2). Ninety-nine resection planes were histopathologically adequate and showed no fluorescent signal. In addition, one second primary lesion (5 mm in diameter) demonstrated clear fluorescence both in vivo and ex vivo. In another case, a second primary lesion measuring 1.4 mm exhibited a distinct fluorescent signal ex vivo using closed-field flatbed imaging (Supplementary Fig. 3, top row), whereas no fluorescence was detected in vivo. Furthermore, one patient presented with multiple microsatellite lesions within the specimen, at a distance of >5mm from the surgical margin, consisting of several tumor foci with diameters ranging from 50 to 300 μm (total area < 0.8 mm), none of which showed fluorescence (Supplementary Fig. 3, bottom row). Overall, these findings resulted in a sensitivity of 98.0% (95% CI, 90.2-99.6%) and NPV of 99.0% (95% CI 94.5-99.9%) for FI. Additional diagnostic performance metrics included a specificity of 86.1% (95% CI 79.1-91.1%), a PPV of 75.4% (95% CI, 63.7-84.6%), and an overall accuracy of 89.7% (95% CI 84.9-94.5%). These results demonstrate robust performance of FI, even

when including areas that would not have impacted surgical decision-making. The reduced specificity was largely attributable to fluorescence originating from salivary gland tissue (n=14), which can be readily distinguished from tumor tissue during surgery.

For standard IOA, each surgical specimen was systematically evaluated across the same five tissue-tissue resection planes, yielding a total of 155 assessed planes. As noted above, definitive histopathology confirmed that 47 of these margins were inadequate. IOA correctly identified 34 of these inadequate planes (72.3%), while 13 (27.7%) were missed. The remaining 108 planes were histopathologically adequate and were all classified as adequate during IOA. Notably, standard IOA detected the previously described larger second primary tumor (5.0 mm in diameter) but failed to identify both the microsatellite lesions and the small second primary tumor (1.4 mm in diameter). Consequently, IOA demonstrated a sensitivity of 70.0% (95% CI 57.2-80.5%), while maintaining a specificity of 100% (95% CI, 96.6-100%). This performance reflects a substantially higher false-negative rate compared with FI, highlighting that, despite similar overall accuracy, IOA misses a significantly greater number of tumor foci (Exact binomial McNemar's test, $p < 0.001$). Importantly, minimizing false negatives is clinically more critical than minimizing false positives, as undetected tumor tissue poses a direct risk to patient outcomes[2, 5-9], whereas false-positive findings primarily result in additional tissue sampling without compromising patient safety. Further details on the diagnostic performance of both IOA and FI are provided in Table 2.

Table 2. Diagnostic performance of FI with cRGD-ZW800-1 compared to standard-of-care IOA across all histopathological findings, using definitive histopathological assessment as reference standard. 95% CIs were calculated using the ANOVA-type Wilson score.

	FI	**IOA**
True positive (TP)	49[a]	35[d]
False positive (FP)	16[b]	0
False negative (FN)	1[c]	15[e]
True negative (TN)	99	108
Sensitivity (95% CI)	98.0% (49/50) (90.2-99.6%)	70.0% (35/50) (57.2-80.5%)
Specificity (95% CI)	86.1% (99/115) (79.1-91.1%)	100% (108/108) (96.6-100%)
Accuracy (95% CI)	89.7% (148/165) (84.9-94.5%)	90.5% (143/158) (85.5-94.1%)
Positive predictive value (PPV) (95% CI)	75.4% (49/65) (63.7-84.6%)	100% (35/35) (90.0-100%)
Negative predictive value (NPV) (95% CI)	99.0% (99/100) (94.5-99.9%)	87.8% (108/123) (81.4-92.2%)

FI: fluorescence imaging; IOA: intraoperative assessment; CI: confidence interval

[a] true positive fluorescent signal originating from inadequate (i.e. positive (<1mm) and close (1-5mm)) resection margins (n=47), and second primary tumors (n=2)

[b] false positive fluorescent signal originating from bone (marrow) (n=2) and salivary gland (n=14)

[c] false negative finding caused by a small tumor focus (total area < 0.8 mm) consisting of multiple microsatellite lesions with diameters ranging from 50 to 300 μm (n=1)

[d] true positive referring to inadequate (i.e. positive (<1mm) and close (1-5mm)) resection margins (n = 34) and second primary tumors (n = 1) correctly identified by IOA.

[e] false negative findings caused by inadequate (i.e. positive (<1mm) and close (1-5mm)) resection margins (n=13), second primary (n=1), and the aforementioned small tumor focus containing multiple microsatellite lesions (n=1)

Clinical performance of FI

When evaluating the potential clinical impact of the FI performance, we found that all inadequate margins were consistently detected, yielding a patient-level sensitivity of 100% (95% CI 85.7–100%) and a NPV of 100% (95% CI 61.6–100%). In addition, the specificity was 75.0% (95% CI 40.9–93.6%), the PPV was 92.0% (95% CI 75.2–98.3%), and an overall accuracy was 93.5% (95% CI 80.5-98.5%). The observed specificity of 75.0% was entirely attributable to two instances of a false-positive fluorescent signal in bone marrow, which were clinically non-suspicious but fell within the resection plane of the primary tumor and were therefore included in the analysis. In the subgroup analysis, which assessed the detection of both positive and of close margins separately, FI achieved a sensitivity of 100% and specificity of 75.0% in both analyses. When compared with standard IOA, overall accuracy for FI and IOA was broadly similar; however, patient-level sensitivity was markedly higher for FI compared to IOA (100% vs. 70.0%, respectively), reflecting that, in our study population, FI prevented false-negative findings altogether. Further details on the clinical evaluation of FI are provided in Table 3.

Table 3. Patient-level evaluation of FI with cRGD-ZW800-1 for the detection of inadequate surgical margins, using definitive histopathological assessment as reference standard. 95% CIs were calculated using the ANOVA-type Wilson score.

	FI Close and positive (<1-5mm) vs. *clear* margins	**FI** Close (1-5mm) vs. *clear* margins	**FI** Positive (<1mm) vs. *clear* margins
True positive (TP)	23[a]	15[c]	8[d]
False positive (FP)	2[b]	2[b]	2[b]
False negative (FN)	0	0	0
True negative (TN)	6	6	6
Sensitivity (95% CI)	100% (23/23) (85.7-100%)	100% (15/15) (81.7-100%)	100% (8/8) (67.7-100%)
Specificity (95% CI)	75.0% (6/8) (40.9-93.6%)	75.0% (6/8) (40.9-93.6%)	75.0% (6/8) (40.9-93.6%)

Table 3. Patient-level evaluation of FI with cRGD-ZW800-1 for the detection of inadequate surgical margins, using definitive histopathological assessment as reference standard. 95% CIs were calculated using the ANOVA-type Wilson score. (*continued*)

	FI Close and positive (<1-5mm) vs. *clear* margins	**FI** Close (1-5mm) vs. *clear* margins	**FI** Positive (<1mm) vs. *clear* margins
Accuracy (95% CI)	93.5% (29/31) (80.5-98.5%)	91.3% (21/23) (74.5-97.8%)	87.5% (14/16) (62.7-97.4%)
Positive predictive value (PPV) (95% CI)	92.0% (23/25) (75.2-98.3%)	88.2% (15/17) (66.8-96.9%)	80.0% (8/10) (51.8-94.6%)
Negative predictive value (NPV) (95% CI)	100% (6/6) (61.6-100%)	100% (6/6) (61.6-100%)	100% (6/6) (61.7-100%)

FI: fluorescence imaging; CI: confidence interval

[a] true positive fluorescent signal originating from inadequate (i.e. positive (<1mm) and close (1-5mm)) resection margins (n=23)

[b] false positive fluorescent signal originating from bone (marrow) at the resection margin (n=2).

[c] true positive fluorescent signal originating from close resection margins (n=15)

[d] true positive fluorescent signal originating from positive resection margins (n=8)

Effect of FI on intraoperative decision making

As all dose cohorts showed a detectable fluorescence signal using both in vivo and ex vivo FI, all patients (n=31) were included in margin assessment. As previously reported, FI combined with standard IOA revealed inadequate margins in 23 patients (74%, 23/31), including eight patients with positive margins and 15 with close margins (Table 1). Additional resections were performed in 70% of the patients with inadequate margins (16/23), comprising seven positive margins and nine close margins. Notably, 31% (5/16) of these resections were based exclusively on FI findings, which had been overlooked during the initial IOA. In contrast, no further resections were undertaken in 30% (7/23) of patients with inadequate margins, which included one with a positive margin and six with close margins. In one patient with a close margin, an additional resection was not feasible due to tumor proximity to critical anatomical structures. Furthermore, in one patient no IOA was performed; in this case, a pre-emptive additional resection had already been carried out during surgery and was deemed sufficient at the time. However, definitive pathology later revealed a close margin elsewhere, which, in retrospect, was apparent on FI. Importantly, in four patients, the tissue samples for assessment were mistakenly taken from areas immediately adjacent to, rather than directly from, the fluorescent spots identified by FI. This sampling error resulted in seemingly clear margins during standard IOA. To ensure a thorough and accurate evaluation, these cases were carefully reviewed in collaboration with the dedicated head and neck pathologist. Each corresponding histological section was examined individually, and the spatial relationship between the fluorescent signal and the inadequate margin was precisely mapped. This detailed review confirmed that the fluorescence signal had accurately indicated the location of the inadequate margin in all four cases. Accordingly, these cases were classified as true

positives with respect to FI. These cases highlight an important limitation of relying solely on frozen section analysis. If fluorescence findings had been acted upon without the mandatory frozen section confirmation required by the study protocol, the inadequate margins would have been identified and addressed intraoperatively. Lastly, in one patient, additional resection was not performed because achieving clear margins would have required a marginal mandibular resection, and the periosteum was clinically intact. In accordance with our standard practice, the surgeon deliberately opted against further resection.

Fluorescent signals detected on the deep margins of the specimens, areas not deemed clinically suspicious during IOA, prompted further examination with frozen sections. This identified nine inadequate margins that had been missed by IOA (three positive, six close). In two positive and three close margins, this resulted in additional resections. Final histopathological analysis confirmed that these extra resections were free of malignant tissue, thereby ensuring that all five patients ultimately achieved wider surgical margins. Notably, in three of these cases, the FI-guided additional resections allowed for the avoidance of adjuvant radiotherapy. In the remaining four cases, no additional resections were performed due to wrong tissue sampling (n=3) and tumor proximity to critical structures (n=1), as previously explained.

With a p-value of less than 0.001, the null hypothesis, that the adequate margin rate is 15% or less, was strongly rejected. This provides robust statistical evidence that the proportion of adequate surgical margins following the implementation of FI is significantly higher. The pre-specified A'Hern single-stage Phase II design was based solely on the optimal dose group (n=21), calculated under the assumption that only the optimal dose group would be eligible for analysis, given the initial uncertainty regarding fluorescent signal in other dose cohorts. Within the optimal dose group, 14 patients had in inadequate surgical margin, of which only 7 (50%) were identified using IOA. In contrast, FI identified all inadequate margins (100%). As previously mentioned, additional resections could not be performed in all cases due to various reasons. Had these additional resections been feasible, the percentage of adequate margins following the implementation of this technique would have been even higher, further strengthening the statistical significance of the findings.

Postoperative closed-field imaging of bread loaves

Absolute fluorescence intensities increased for both tumor and background tissue with increasing dose (Supplementary Fig. 4*).* The MFI was significantly higher in tumor than in background tissue for all doses ($p<0.05$). The mean ex vivo TBRs were adequate for all cases at 4.52 ± 1.60 (n=3), 5.73 ± 2.75(n=21) and 5.76 ± 2.03 (n=7) for dose cohorts 0.01, 0.025 and 0.05 mg/kg, respectively (Figure 4).

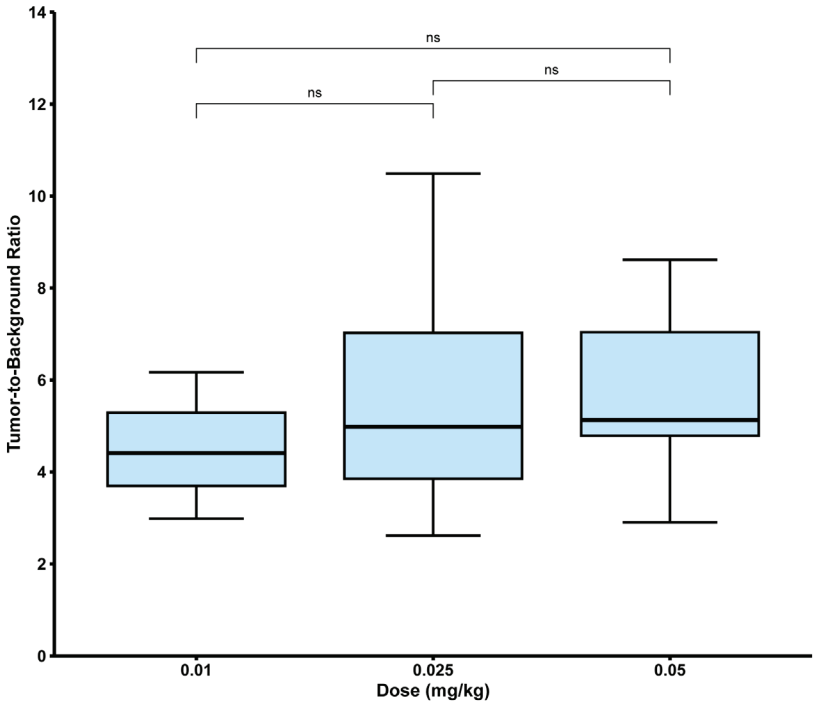

Figure 4. Ex vivo Tumor-to-Background Ratios (TBR) in bread loaves, for doses 0.01 mg/kg (n=3), 0.025 mg/kg (n= 21) and 0.05 mg/kg (n=7), where "n" denotes the number of patients allocated to each dose group. For all dose groups TBRs were adequate. Box plots show the median (centre line), the interquartile range (box bounds; 25th–75th percentiles), and whiskers extending to the most extreme data points within 1.5× the interquartile range from the quartiles. *The source data is available as a Source Data File. ns: non-significant (two-sided Mann-Whitney U-test)*

Correlation between final histopathology and FI

Final histopathological analysis revealed 15 cases with close margins and 1 case with a positive margin. This specific positive margin was detected using FI, but no additional resection could be performed as the frozen section was taken adjacent to the fluorescent area. Had we relied solely on FI, even this single positive margin could have been addressed, resulting in zero positive margins postoperatively. Without the use of FI, final histopathology would have revealed three positive margins, as two positive margins were missed during standard IOA. All inadequate margins were located at the deep resection plane, and all were successfully visualized intraoperatively using FI. IHC staining showed a high correlation between tumor localization, αvβ6 expression and fluorescence signal (Figure 3, image J-L), emphasizing the specificity of cRGD-ZW800-1. Some mild fluorescence was also observed outside the tumor boundaries (Figure 3, image J), originating from a desmoplastic reaction at the tumor border. This region exhibited αvβ6 expression, although at substantially lower levels compared to tumor. Importantly, this low-level signal was not detectable during imaging of the fresh specimen or bread loaves and did not interfere with intraoperative margin assessment.

Additionally, the previously mentioned second primary tumor that demonstrated fluorescence both in vivo and ex vivo, was confirmed to be malignant. The second primary tumor that only exhibited a fluorescent signal ex vivo showed colocalized αvβ6 expression during IHC staining (Supplementary Fig. 3, top row). Furthermore, despite the absence of detectable fluorescence both in vivo and ex vivo on the patient with multiple micro-satellite lesions, IHC staining revealed elevated αvβ6 expression (Supplementary Fig. 3, bottom row).

cRGD-ZW800-1 uptake in non-tumor tissues

Fluorescent gingival tissue exhibited αvβ6 expression at the junctional epithelium (Supplementary Fig. 2). Salivary gland tissue was, regardless of presence of inflammation, consistently strongly fluorescent, with IHC staining revealing αvβ6 expression in the ductal cells (Supplementary Fig. 5). Ex vivo images revealed increased fluorescence in bone (marrow). Here, IHC staining showed no αvβ6 expression (Supplementary Fig. 6).

DISCUSSION

This study demonstrated that cRGD-ZW800-1 was safe, well-tolerated, tumor-specific, and effectively detected inadequate margins during FI of oral cancer. Most importantly, FI altered surgical decision-making in five cases (16%, 5/31) by identifying inadequate margins that were overlooked during routine IOA, underscoring the clinical value of intraoperative FI. Tumors fluoresced intensely both in vivo and ex vivo, and visible fluorescence (excluding salivary glands) in the deep margin was in all cases congruent with margin inadequacy. Study proceedings did not meaningfully interfere with the standard of care, nor resulted in significantly prolonged surgery time. Given the use of FI in this study (pre-resection, wound bed and on the resected specimen), this is a type E study when considering the effect of FI on intraoperative decision-making[10].

To comprehensively evaluate the performance of FI, we conducted two complementary analyses within this study. First, a diagnostic accuracy analysis evaluated all histopathological findings, both tumor-positive and tumor-negative, in relation to fluorescence, irrespective of their impact on margin status. Second, a patient-level analysis focused exclusively on clinically relevant margins to explore the potential implications of fluorescence for intraoperative decision-making. While specificity was higher in the diagnostic accuracy analysis compared with the patient-level analysis (86.1 vs. 75.0%, respectively), sensitivity remained consistently high in both analyses (98.0% vs. 100%, respectively). The lower specificity in the patient-level analysis resulted from the more stringent definition of true negatives, as only patients with completely adequate margins across all five surgically assessed resection planes were classified as true negatives, whereas any inadequacy in a single plane excluded the case from the true negative count. Within the study population, only one tumor focus was not detected (microsatellite lesions, total diameter < 0.8 mm); however, this focus had

no clinical impact on surgical management, as it was located at the specimen at a distance of >5mm from the resection plane and therefore did not affect margin status. In comparison, IOA demonstrated substantially lower sensitivity (70%, 95% CI 57.2-80.5%). When comparing the diagnostic accuracy and patient-level analyses, the patient-level approach is particularly informative for surgical practice, as it captures the added value of FI in detecting clinically relevant inadequate margins and guiding intraoperative decisions. The consistently high patient-level sensitivity of FI is clinically significant, since missing inadequate margins is closely linked to local recurrence, the need for adjuvant therapy, and poorer survival outcomes[2, 5-9]. Despite comparable overall accuracy between FI and IOA (93.5% vs. 90.5%, respectively), FI demonstrated markedly higher patient-level sensitivity (100% vs. 70.0%), underscoring its ability to substantially reduce false negatives and enhance detection of inadequate margins.

Building on these findings, it is noteworthy that, in addition to the high patient-level sensitivity for detecting all clinically relevant inadequate margins, FI also achieved 100% sensitivity in detecting both close and positive margins separately. These findings underscore the ability of FI to reliably detect clinically relevant inadequate margins that might otherwise have been missed. Although IOA is regarded as the gold standard for intraoperative margin assessment at our institution, it is resource-intensive and routinely available only in selected centres[2, 7]. Consequently, the present comparison may underestimate the true added value of FI, as in typical clinical practice its benefit would likely be even greater, reflected by the high rate of close or positive margins after initial resection prior to IOA (23/31, 74%). Collectively, our findings highlight a distinct performance profile compared to earlier reports. For instance, de Wit et al. [19] reported a patient-level sensitivity of 100% for tumor-positive margins but only 67.4% for close margins using EGFR-targeted FI with cetuximab-800CW, with a combined specificity of 41.7%. Furthermore, van Keulen et al. [39] evaluated fluorescently labelled panitumumab-IRDye800 in oral cancer, achieving 95% sensitivity and 89% specificity for detecting inadequate margins (<5 mm). Compared with these studies, our approach achieved a sensitivity of 100% and a specificity of 75%, reflecting robust detection of both positive and close margins while maintaining acceptable specificity.

The observed variability in specificity, both within the present study and relative to previously reported values, is partly attributable to the inherent challenges of defining and enumerating true negative findings in fluorescence-guided surgery. In this study, we defined true negatives as non-fluorescent surgical resection planes histopathologically confirmed as adequate, providing a practical yet approximate framework. Alternative specimen partitioning or negative area counting could alter these metrics, underscoring their limitations. Consistent with prior literature, this emphasizes interpreting FI by its clinical impact and intraoperative guidance value, rather than formal diagnostic accuracy reliant on an ill-defined denominator[10]. Still, our results show it reliably identified all clinically relevant inadequate margins,

achieving 100% sensitivity and 75.0% specificity in the patient-level analysis, thereby accurately highlighting critical margins for surgical decision-making.

In this study, intraoperative FI was substantiated through objective in vivo assessment of tracer pharmacokinetics using MDSFR/SFF spectroscopy. By correcting for patient-specific optical tissue properties, known to be influenced by a wide range of often unquantifiable biological and anatomical factors[40], this method enabled accurate assessment of tracer kinetics in vivo and guided optimization of dose and timing. This study uniquely combines qualitative FI with quantitative spectroscopy, offering a robust framework for future clinical translation of targeted fluorescent tracers.

Although the 0.01 mg/kg dose group showed relatively high TBRs, the absolute tumor fluorescence was too dim for reliable intraoperative visualization. This underscores a critical distinction: TBR is a post-processed metric that does not always correlate with the subjective visual contrast perceived during surgery. Both the 0.025 and 0.05 mg/kg groups demonstrated sufficient intensity and TBRs >2 starting 2 hours post-injection, and remaining consistently above this threshold for at least 18 hours in the 0.025 mg/kg cohort. Therefore, 0.025 mg/kg was identified as the "near-optimal" dose (per regulatory definitions) since it achieved equivalent imaging performance to the 0.05 mg/kg dose with half the amount of tracer. As a zwitterionic small molecule, cRGD-ZW800-1 demonstrated high TBRs and favorable pharmacokinetics, characterized by rapid tumor accumulation and efficient clearance from non-target tissues, advantages over conventional, antibody-based fluorescent tracers[22, 41, 42].

Importantly, adequate TBRs were achieved as early as 2 hours post-injection, highlighting a practical window of 2 to 18 hours for imaging. This flexibility enables same-day administration, offering a logistical advantage over full-length antibody-based tracers such as panitumumab-IRDye800CW and cetuximab-IRDye800CW, which require administration several days prior to surgery, often necessitating additional hospital visits and pre-dosing with unlabeled antibody to improve contrast[15, 16, 19, 38, 43]. Furthermore, infusion reactions have been reported with cetuximab, even in the unlabeled form[16, 44, 45]. No adverse events were associated with cRGD-ZW800-1 in this study. In addition, cRGD-ZW800-1 targets integrin αvβ6, a biomarker overexpressed in OSCC and concentrated at invasive tumor fronts, with limited expression in normal epithelium[46, 47]. While the FDA-approved fluorophore indocyanine green (ICG) has been widely studied for intraoperative detection of oral cancers. Its non-specific accumulation in surrounding tissues often leads to a decrease in tumor contrast, limiting tumor delineation. In contrast, cRGD-ZW800-1 provides receptor-mediated tumor targeting and lower background fluorescence, resulting in higher tumor-to-background ratios under intraoperative conditions[20, 48]. This target specificity enables precise discrimination at the deep margin, resulting in a 100% detection rate of inadequate surgical margins (Table 1).

In all subjects and dose groups, fluorescence was observed in uninvolved gingiva, consistent with αvβ6 expression in healthy junctional epithelium[49, 50]. As none of the cases presented with an inadequate mucosal margin, this fluorescent signal did not impose any clinically relevant difficulties. In general, the deep margin is rightly considered more important than the mucosal margin, as 87% of inadequate margins involve the deep margin, and no significant difference in recurrence rate was found between close and clear mucosal margins[30]. As mentioned before, salivary gland tissue also showed an αvβ6-specific fluorescence signal, which could be accounted for with relative ease, as salivary gland tissue was easily distinguishable by both surgeon and pathologist. Prior studies on oral cancer imaging using cetuximab-800CW observed similar fluorescent signals originating from salivary gland tissue (29-47% of false positives)[16, 19]. Lastly, a false-positive fluorescence signal was observed in the mandibular bone marrow. Importantly, all of the aforementioned false-positive signals, including those detected in uninvolved gingiva and salivary gland tissue, were clinically not suspicious for malignancy. Each fluorescent area underwent careful histopathological evaluation, thereby confirming the absence of malignant tissue. As a result, these signals did not influence intraoperative decision-making, lead to unnecessary resections, or compromise patient safety. This observation underscores that, although such false-positive signals may occur, their presence can be effectively managed through standard pathological confirmation without impacting the clinical utility of fluorescence-guided surgery.

In one case, multiple micro-satellite lesions (diameters varying from 50 to 300 μm) did not exhibit fluorescence in vivo or ex vivo. While IHC demonstrated expression of the integrin (Supplementary Fig. 3, Image F), tumor fields were sparse and widely spaced, spanning a maximum diameter of < 0.8 mm. The lack of fluorescence is likely due to the fact that, although integrin expression indicates early neovascularization processes, functional blood vessels had not yet formed or connected to these lesions. As a result, the fluorescent tracer was unable to reach the tumor areas, leading to the absence of fluorescence signal. In another case, a second primary tumor (maximum diameter of 1.4 mm) was not fluorescent during in vivo FI, but was detectable during ex vivo FI (Supplementary Fig. 3, top row). Although such small secondary lesions are uncommon, these findings highlight a potential limitation for identifying subclinical tumor deposits using the current intraoperative camera systems. In this case, the missed second primary tumor had no impact on margin status, as they were located within the original planned resection area.

Within head and neck pathology, the definition of an inadequate surgical margin remains a topic of debate. Literature suggests that thresholds for close or positive margins may vary depending on tumor subsite, biological characteristics, and factors such as the worst pattern of invasion (WPOI)[51, 52]. In this study, we applied a 5 mm cutoff in line with our institute's protocol and consistent with the Royal College of Pathologists and National Comprehensive Cancer Network (NCCN) guidelines[53, 54]. Importantly, the exact cutoff is less critical for the purpose of evaluating FI, as the primary goal was to assess whether this technique could

reliably identify margins that are narrower than the defined threshold. While this approach allows for standardized assessment within our cohort, it is important to acknowledge that other institutions or clinical settings may adopt different margin definitions based on local practice. Nevertheless, despite these variations, our results demonstrate that fluorescence imaging has the potential to enhance intraoperative margin detection, independent of the specific numerical cutoff applied.

In four cases, accurately targeting fluorescent signals for intraoperative frozen section sampling proved challenging, limiting immediate resection. Importantly, this did not reflect failure of FI itself, as these cases were carefully reviewed in collaboration with the head and neck pathologist, confirming that the fluorescent signal accurately corresponded to the inadequate margins in all cases. These observations underscore the potential of FI to reliably identify inadequate margins, while also illustrating the technical learning curve in integrating FI into clinical practice and highlight the need for standardized protocols and training to ensure accurate localization and sampling. Implementation of FI in standard surgical practice could improve intraoperative decision-making, provided that its use is optimized through appropriate training.

cRGD-ZW800-1 demonstrated favorable safety profile and strong tumor specificity; however, long-term oncologic outcomes remain to be established. To robustly determine the clinical utility of FI in OSCC surgery, prospective trials are needed to assess its effect on long-term outcomes, including recurrence rate, survival and quality of life. A multicenter randomized controlled trial will be critical to determine whether FI significantly reduces the incidence of positive margins compared to standard surgical care. Defining this effect will be essential to confirm FI's potential to improve oncologic outcomes and to support its broader integration into standard surgical practice.

Building on the encouraging results from this Phase I/II study, the next steps involve the development of a multicenter randomized controlled trial to provide data that could inform potential changes in national clinical guidelines. By demonstrating the clinical benefits of FI in real-world settings, it is hypothesized that FI can be established as a standard tool in oral cancer surgery, ultimately improving surgical precision and patient outcomes. Preparations for this multicentre trial are currently ongoing.

CONCLUSION

In conclusion, this study establishes cRGD-ZW800-1 as a safe, effective, and tumor-specific fluorescent tracer for oral cancer surgery. Uniquely, it combines qualitative intraoperative FI with objective, quantitative in vivo spectroscopy to validate tracer performance and inform optimal dosing and timing strategies. The integration of temporal pharmacokinetic insights, enabled by MDSFR/SFF spectroscopy, allowed for data-driven optimization of the imaging protocol.

Importantly, FI guided the identification of all inadequate resection margins, including those missed during routine intraoperative assessment, directly influencing surgical decision-making in real time and preventing adjuvant radiotherapy in selected cases. These findings highlight the substantial oncological value of fluorescence-guided surgery in improving margin assessment and surgical precision. Together, the clinical feasibility, safety profile, and diagnostic performance of cRGD-ZW800-1 support its further development and integration into surgical workflows aimed at improving outcomes in patients with oral cavity cancer.

REFERENCES

1. Woolgar, J.A. and A. Triantafyllou, *A histopathological appraisal of surgical margins in oral and oropharyngeal cancer resection specimens.* Oral Oncol, 2005. **41**(10): p. 1034-43.
2. Smits, R.W., et al., *Resection margins in oral cancer surgery: Room for improvement.* Head Neck, 2016. **38 Suppl 1**: p. E2197-203.
3. Orosco, R.K., et al., *Positive Surgical Margins in the 10 Most Common Solid Cancers.* Sci Rep, 2018. **8**(1): p. 5686.
4. Lauwerends, L.J., et al., *The complementary value of intraoperative fluorescence imaging and Raman spectroscopy for cancer surgery: combining the incompatibles.* Eur J Nucl Med Mol Imaging, 2022. **49**(7): p. 2364-2376.
5. Dik, E.A., et al., *Resection of early oral squamous cell carcinoma with positive or close margins: relevance of adjuvant treatment in relation to local recurrence: margins of 3 mm as safe as 5 mm.* Oral Oncol, 2014. **50**(6): p. 611-5.
6. Varvares, M.A., et al., *Surgical margins and primary site resection in achieving local control in oral cancer resections.* Laryngoscope, 2015. **125**(10): p. 2298-307.
7. Barroso, E.M., et al., *Performance of Intraoperative Assessment of Resection Margins in Oral Cancer Surgery: A Review of Literature.* Front Oncol, 2021. **11**: p. 628297.
8. Smits, R.W.H., et al., *Intraoperative Assessment of the Resection Specimen Facilitates Achievement of Adequate Margins in Oral Carcinoma.* Front Oncol, 2020. **10**: p. 614593.
9. Hamman, J., et al., *Impact of Close Margins in Head and Neck Mucosal Squamous Cell Carcinoma: A Systematic Review.* Laryngoscope, 2022. **132**(2): p. 307-321.
10. Lauwerends, L.J., et al., *Real-time fluorescence imaging in intraoperative decision making for cancer surgery.* Lancet Oncol, 2021. **22**(5): p. e186-e195.
11. Vahrmeijer, A.L., et al., *Image-guided cancer surgery using near-infrared fluorescence.* Nat Rev Clin Oncol, 2013. **10**(9): p. 507-18.
12. van Dam, G.M., et al., *Intraoperative tumor-specific fluorescence imaging in ovarian cancer by folate receptor-alpha targeting: first in-human results.* Nat Med, 2011. **17**(10): p. 1315-9.
13. van Keulen, S., et al., *The clinical application of fluorescence-guided surgery in head and neck cancer.* J Nucl Med, 2019. **60**(6): p. 758-763.
14. de Valk, K.S., et al., *First-in-Human Assessment of cRGD-ZW800-1, a Zwitterionic, Integrin-Targeted, Near-Infrared Fluorescent Peptide in Colon Carcinoma.* Clin Cancer Res, 2020. **26**(15): p. 3990-3998.
15. Nishio, N., et al., *Optimal Dosing Strategy for Fluorescence-Guided Surgery with Panitumumab-IRDye800CW in Head and Neck Cancer.* Mol Imaging Biol, 2020. **22**(1): p. 156-164.
16. Voskuil, F.J., et al., *Fluorescence-guided imaging for resection margin evaluation in head and neck cancer patients using cetuximab-800CW: A quantitative dose-escalation study.* Theranostics, 2020. **10**(9): p. 3994-4005.
17. Voskuil, F.J., et al., *Exploiting metabolic acidosis in solid cancers using a tumor-agnostic pH-activatable nanoprobe for fluorescence-guided surgery.* Nat Commun, 2020. **11**(1): p. 3257.
18. Stibbe, J.A., et al., *Highlighting the Undetectable - Fluorescence Molecular Imaging in Gastrointestinal Endoscopy.* Mol Imaging Biol, 2023. **25**(1): p. 18-35.
19. de Wit, J.G., et al., *EGFR-targeted fluorescence molecular imaging for intraoperative margin assessment in oral cancer patients: a phase II trial.* Nat Commun, 2023. **14**(1): p. 4952.
20. Wu, Z., et al., *Clinical application of indocyanine green fluorescence navigation*

technology to determine the safe margin of advanced oral squamous cell carcinoma. Gland Surg, 2022. **11**(2): p. 352-357.
21. Yang, Y., et al., *Fluorescence-amplified nanocrystals in the second near-infrared window for in vivo real-time dynamic multiplexed imaging.* Nat Nanotechnol, 2023. **18**(10): p. 1195-1204.
22. Choi, H.S., et al., *Synthesis and in vivo fate of zwitterionic near-infrared fluorophores.* Angew Chem Int Ed Engl, 2011. **50**(28): p. 6258-63.
23. de Valk, K.S., et al., *A zwitterionic near-infrared fluorophore for real-time ureter identification during laparoscopic abdominopelvic surgery.* Nat Commun, 2019. **10**(1): p. 3118.
24. Keereweer, S., et al., *Targeting integrins and enhanced permeability and retention (EPR) effect for optical imaging of oral cancer.* J Surg Oncol, 2012. **105**(7): p. 714-8.
25. Lauwerends, L.J., et al., *Tumour Marker Expression in Head and Neck Malignancies to Identify Potential Targets for Intraoperative Molecular Near-Infrared Imaging.* Mol Diagn Ther, 2024. **28**(6): p. 811-820.
26. Aaboubout, Y., et al., *Specimen-driven intraoperative assessment of resection margins should be standard of care for oral cancer patients.* Oral Dis, 2021. **27**(1): p. 111-116.
27. van Lanschot, C.G.F., et al., *Relocation of inadequate resection margins in the wound bed during oral cavity oncological surgery: A feasibility study.* Head Neck, 2019. **41**(7): p. 2159-2166.
28. Koller, M., et al., *Implementation and benchmarking of a novel analytical framework to clinically evaluate tumor-specific fluorescent tracers.* Nat Commun, 2018. **9**(1): p. 3739.
29. de Jongh, S.J., et al., *C-Met targeted fluorescence molecular endoscopy in Barrett's esophagus patients and identification of outcome parameters for phase-I studies.* Theranostics, 2020. **10**(12): p. 5357-5367.
30. Brouwer de Koning, S.G., et al., *Assessment of the deep resection margin during oral cancer surgery: A systematic review.* Eur J Surg Oncol, 2021. **47**(9): p. 2220-2232.
31. Kapoor, S., et al., *Effect of Formalin Fixation for Near-Infrared Fluorescence Imaging with an Antibody-Dye Conjugate in Head and Neck Cancer Patients.* Mol Imaging Biol, 2021. **23**(2): p. 270-276.
32. Keereweer, S., et al., *Optical imaging of oral squamous cell carcinoma and cervical lymph node metastasis.* Head Neck, 2012. **34**(7): p. 1002-8.
33. Keereweer, S., et al., *Dual wavelength tumor targeting for detection of hypopharyngeal cancer using near-infrared optical imaging in an animal model.* Int J Cancer, 2012. **131**(7): p. 1633-40.
34. A'Hern, R.P., *Sample size tables for exact single-stage phase II designs.* Stat Med, 2001. **20**(6): p. 859-66.
35. Maiden, M.J., et al., *Haemoglobin concentration and volume of intravenous fluids in septic shock in the ARISE trial.* Crit Care, 2018. **22**(1): p. 118.
36. Perel, A., *The relationship between the decrease in haemoglobin concentration and the volume of fluids administered during resuscitation from septic shock may not be so "weak".* Crit Care, 2018. **22**(1): p. 234.
37. van Keulen, S., et al., *The Sentinel Margin: Intraoperative Ex Vivo Specimen Mapping Using Relative Fluorescence Intensity.* Clin Cancer Res, 2019. **25**(15): p. 4656-4662.
38. Krishnan, G., et al., *Fluorescent Molecular Imaging Can Improve Intraoperative Sentinel Margin Detection in Oral Squamous Cell Carcinoma.* J Nucl Med, 2022. **63**(8): p. 1162-1168.
39. van Keulen, S., et al., *Rapid, non-invasive fluorescence margin assessment: Optical specimen mapping in oral squamous cell carcinoma.* Oral Oncol, 2019. **88**: p. 58-65.
40. Keereweer, S., et al., *Optical image-guided cancer surgery: challenges and limitations.* Clin Cancer Res, 2013. **19**(14): p. 3745-54.
41. Choi, H.S., et al., *Renal clearance of quantum dots.* Nat Biotechnol, 2007. **25**(10): p. 1165-70.

42. Choi, H.S., et al., *Targeted zwitterionic near-infrared fluorophores for improved optical imaging.* Nat Biotechnol, 2013. **31**(2): p. 148-53.
43. Moore, L.S., et al., *Effects of an Unlabeled Loading Dose on Tumor-Specific Uptake of a Fluorescently Labeled Antibody for Optical Surgical Navigation.* Mol Imaging Biol, 2017. **19**(4): p. 610-616.
44. Gao, R.W., et al., *Safety of panitumumab-IRDye800CW and cetuximab-IRDye800CW for fluorescence-guided surgical navigation in head and neck cancers.* Theranostics, 2018. **8**(9): p. 2488-2495.
45. Rosenthal, E.L., et al., *Safety and Tumor Specificity of Cetuximab-IRDye800 for Surgical Navigation in Head and Neck Cancer.* Clin Cancer Res, 2015. **21**(16): p. 3658-66.
46. Baart, V.M., et al., *EGFR and alphavbeta6 as Promising Targets for Molecular Imaging of Cutaneous and Mucosal Squamous Cell Carcinoma of the Head and Neck Region.* Cancers (Basel), 2020. **12**(6).
47. Lawaetz, M., et al., *Potential of uPAR, alphavbeta6 Integrin, and Tissue Factor as Targets for Molecular Imaging of Oral Squamous Cell Carcinoma: Evaluation of Nine Targets in Primary Tumors and Metastases by Immunohistochemistry.* Int J Mol Sci, 2023. **24**(4).
48. Pan, J., et al., *Real-time surveillance of surgical margins via ICG-based near-infrared fluorescence imaging in patients with OSCC.* World J Surg Oncol, 2020. **18**(1): p. 96.
49. Csiszar, A., et al., *Distinctive molecular composition of human gingival interdental papilla.* J Periodontol, 2007. **78**(2): p. 304-14.
50. Ghannad, F., et al., *Absence of alphavbeta6 integrin is linked to initiation and progression of periodontal disease.* Am J Pathol, 2008. **172**(5): p. 1271-86.
51. Tasche, K.K., et al., *Definition of "Close Margin" in Oral Cancer Surgery and Association of Margin Distance With Local Recurrence Rate.* JAMA Otolaryngol Head Neck Surg, 2017. **143**(12): p. 1166-1172.
52. Kohler, H.F., et al., *The impact of worst pattern of invasion on the extension of surgical margins in oral squamous cell carcinoma.* Head Neck, 2022. **44**(3): p. 691-697.
53. Pathologists, T.R.C.o., *Tissue pathways for oral and head and neck pathology (G077)*. 2023: London.
54. Network, N.C.C., *NCCN Clinical Practice Guidelines in Oncology: Head & Neck Cancers, Version 5.2025*. 2025: Plymouth Meeting (PA).

SUPPLEMENTARY MATERIALS

Supplementary Table 1. Overview of Adverse Events

Dose cohort (mg/kg)	Patient ID	System organ class / preferred term	Symptom	Severity	Serious adverse event	Relationship to ZW800-1	Occurrence
0.05	1	Infections and infestations	Soft tissue infection: neck abscess	2	No	unrelated	Single occasion
0.05	3	Bleeding	Bleeding from free forearm flap at tongue base	3	Yes	unrelated	Single occasion
0.05	3	Respiratory, thoracic and mediastinal disorders	Pneumonia	2	No	unrelated	Single occasion
0.025	12	Infections and infestations	Wound infection	2	No	unrelated	Single occasion
0.025	13	Respiratory, thoracic and mediastinal disorders	Pneumonia	2	No	unrelated	Single occasion
0.025	13	Infections and infestations	Wound infection	3	No	unrelated	Single occasion
0.025	15	Infections and infestations	Infection of element 13- 21 (mouth)	3	No	unrelated	Single occasion
0.025	16	Infections and infestations	Wound infection	2	No	unrelated	Single occasion
0.025	19	Infection and infestations	Wound infection	2	No	unrelated	Single occasion
0.025	20	Other, specify	Trauma capitis	2	No	unrelated	Single occasion
0.025	23	Bleeding	Bleeding from free forearm flap	3	Yes	unrelated	Single occasion
0.025	23	Renal and urinary disorders	Prerenal kidney dysfunction*	2	Yes	unrelated	Single occasion
0.025	24	Bleeding	Bleeding from lateral tongue	1	Yes	unrelated	Single occasion
0.025	28	Bleeding	Bleeding from free forearm flap	2	No	unrelated	Single occasion
0.025	28	Renal and urinary disorders	Urinary tract infection	2	No	unrelated	Single occasion

Supplementary Table 1. Overview of Adverse Events (*continued*)

Dose cohort (mg/kg)	Patient ID	System organ class / preferred term	Symptom	Severity	Serious adverse event	Relationship to ZW800-1	Occurrence
0.025	28	Infections and infestations	Wound infection	2	No	unrelated	Single occasion
0.025	29	Bleeding	Bleeding from tongue	2	Yes	Unrelated	Single occasion

*The renal insufficiency was attributed to a prerenal cause due to fluid depletion and insufficient intake in this patient, with renal function recovering within 4 days following fluid resuscitation.

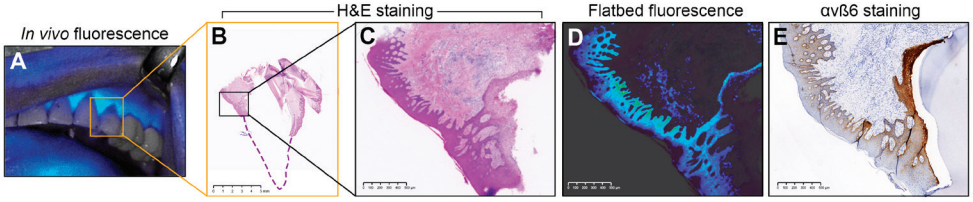

Supplementary Figure 1. Fluorescence in the gingiva**.** The gingiva were consistently a source of *in vivo* fluorescence (A). Indeed, flatbed scanning fluorescence imaging confirmed localized fluorescent signal at the epithelial junction (D), which was confirmed with immunohistopathology to strongly express αvβ6 (E).

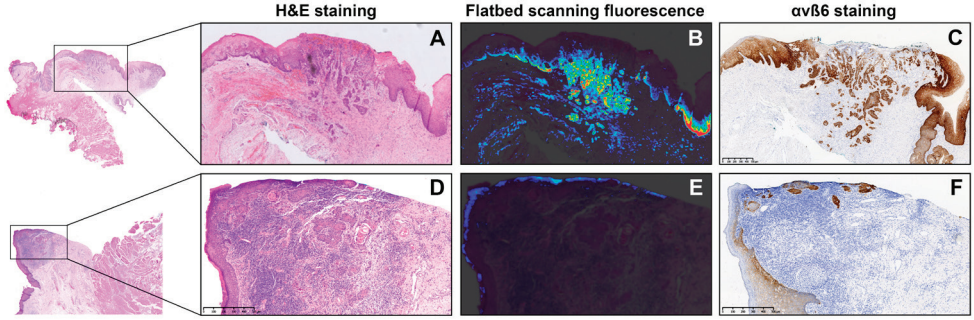

Supplementary Figure 2. Additional lesions. Top row: H&E stained (A) second primary lesion which was not fluorescent *in vivo*, but was clearly fluorescent on flatbed scanning fluorescence images (B). Dense area of tumor fields exhibiting strong αvβ6 expression (C). Bottom row: H&E stained (D) multiple microscopic tumor fields (<0.4mm) which were not fluorescent *in* or *ex vivo* (E). Tumor fields exhibited strong αvβ6 expression (F), but due to their sparsity do not generate a detectable signal.

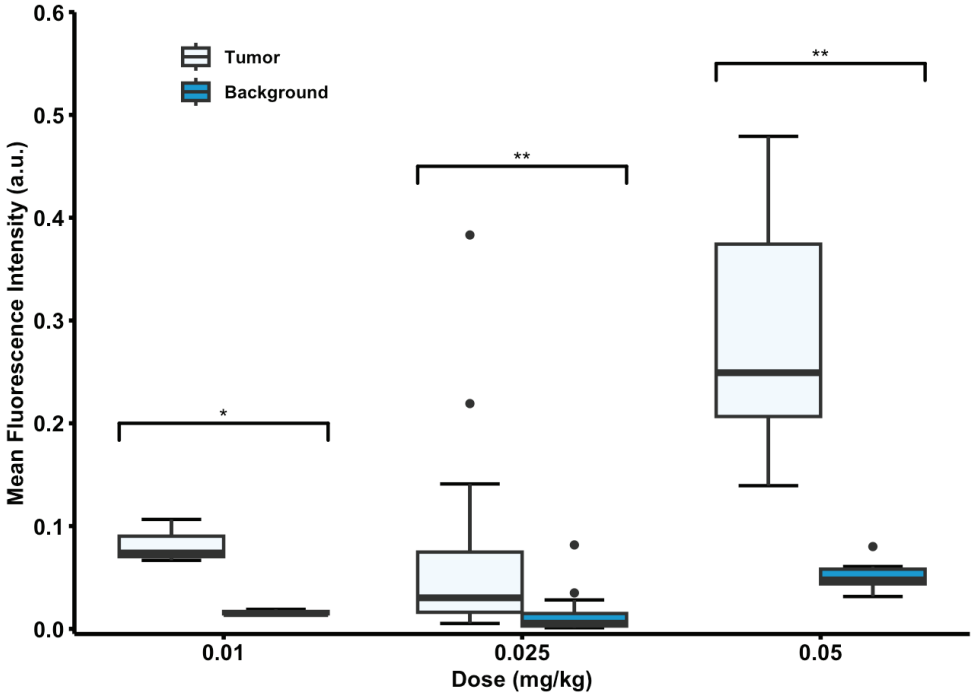

Supplementary Figure 3. Mean fluorescence intensities (MFI) in bread loaves, for doses 0.01 mg/kg (n=3), 0.025 mg/kg (n=21) and 0.05 mg/kg (n=7), where "n" denotes the number of patients allocated to each dose group. For all dose groups, mean fluorescence intensities were significantly higher in tumor than in background tissue ($p<0.05$). Box plots show the median (centre line), the interquartile range (box bounds; 25th–75th percentiles), and whiskers extending to the most extreme data points within 1.5× the interquartile range from the quartiles, and dots indicate outliers. *The source data is available as a Source Data File. *: $p < 0.005$; **: two-sided $p < 0.05$ (Wilcoxon Rank-test).*

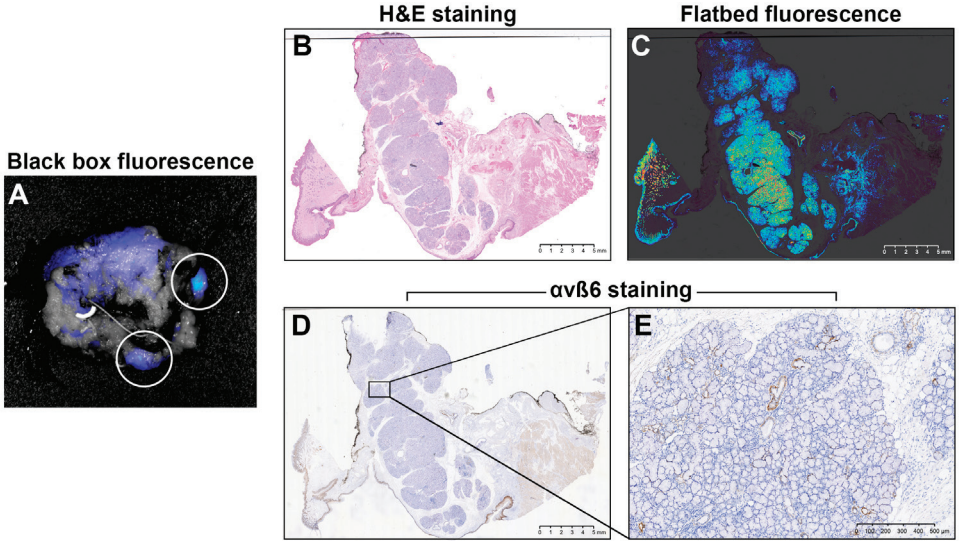

Supplementary Figure 4. Fluorescence in salivary gland tissue. Circled fluorescent spots in deep margin of specimen indicate salivary gland tissue (A). H&E staining of salivary gland (B), strong signal in flatbed scanning fluorescence imaging of microscopy slide (C), immunohistochemistry indicates expression of integrin αvβ6 in the ductal cells of salivary gland tissue (D).

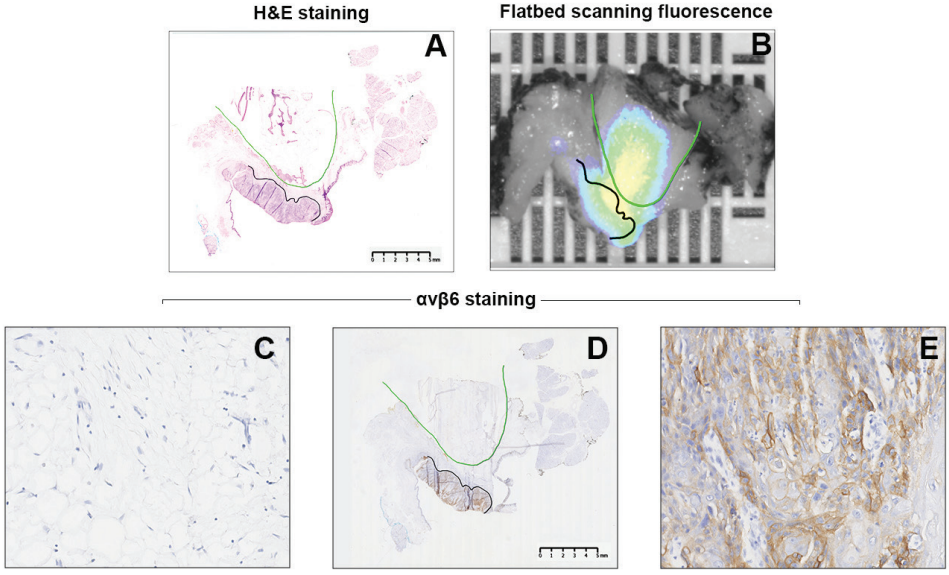

Supplementary Figure 5. Fluorescence in bone. H&E staining of a slide containing tumor (black delineated), and bone (marrow) (green delineated). Moderate signal in bone marrow using closed-field fluorescence imaging of bread loaf (B). Strong expression of αvβ6 in tumor (D, E), whereas fluorescent bone (marrow) displayed none (C, D).

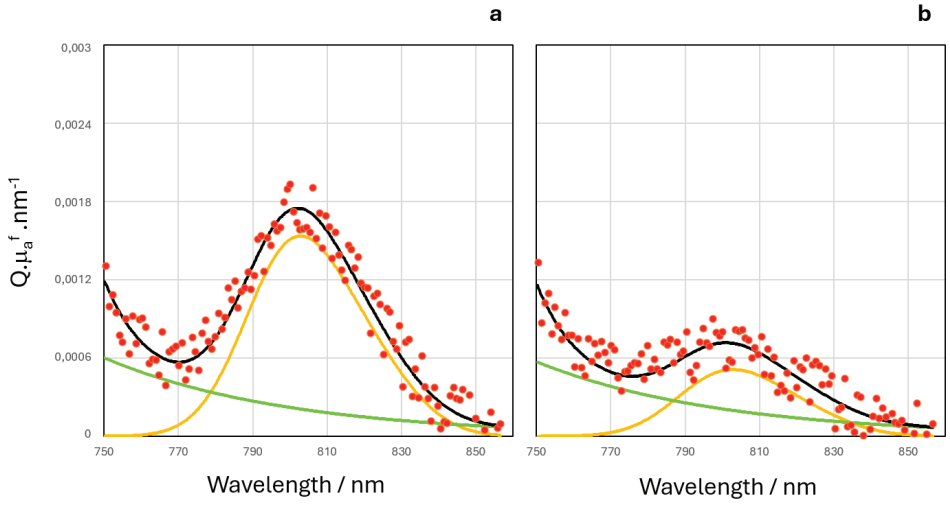

Supplementary Figure 6. An example of a SFF emission spectrum collected from (a) the centre of tumor and (b) contralateral normal tissue 18h after tracer administration, that has been corrected for the tissue optical properties (m_a and m'_s) at the excitation wavelength and in the within the emission band of the fluorophore. Where the corrected data (red circles) is the fitted with a linear combination of in-vivo basis spectrum for c-RGD-800ZW-1 (orange dashed line, fitted as a skewed gaussian) determined from a large group of measurements with the tracer present, and the basis spectrum for background autofluorescence, (green line) which is a combination of tissue autofluorescence and background fluorescence in the spectroscopy system.

Supplementary Movie 1. In vivo fluorescence imaging. Representative video (2x speed) of real-time in vivo near-infrared fluorescence imaging before and during resection in a patient with a tumor in the lateral tongue.

https://static-content.springer.com/esm/art%3A10.1038%2Fs41467-026-73554-7/MediaObjects/41467_2026_73554_MOESM3_ESM.mov

Part IV

Integrating Fluorescence Imaging with Raman Spectroscopy


8

Chapter 8

The complementary value of intraoperative fluorescence imaging and Raman spectroscopy for cancer surgery: combining the incompatibles

L.J. Lauwerends* & H. Abbasi*, T.C. Bakker Schut, P.B.A.A. Van Driel, J.A.U. Hardillo, I.P. Santos, E.M. Barroso, S. Koljenović, A.L. Vahrmeijer, R.J. Baatenburg de Jong, G.J. Puppels, S. Keereweer

European Journal of Nuclear Medicine and Molecular Imaging. 2022 Jun;49(7):2364-2376.

ABSTRACT

A clear margin is an important prognostic factor for most solid tumours treated by surgery. Intraoperative fluorescence imaging using exogenous tumour-specific fluorescent agents has shown particular benefit in improving complete resection of tumour tissue. However, signal processing for fluorescence imaging is complex, and fluorescence signal intensity does not always perfectly correlate with tumour location. Raman spectroscopy has the capacity to accurately differentiate between malignant and healthy tissue based on their molecular composition. In Raman spectroscopy, specificity is uniquely high, but signal intensity is weak and Raman measurements are mainly performed in a point-wise manner on microscopic tissue volumes, making whole-field assessment temporally unfeasible. In this review, we describe the state-of-the-art of both optical techniques, paying special attention to the combined intraoperative application of fluorescence imaging and Raman spectroscopy in current clinical research. We demonstrate how these techniques are complementary and address the technical challenges that have traditionally led them to be considered mutually exclusive for clinical implementation. Finally, we present a novel strategy that exploits the optimal characteristics of both modalities to facilitate resection with clear surgical margins.

INTRODUCTION

Cancer is the leading cause of premature death in Europe and the United States and one of the most important public health issues worldwide [1, 2]. Depending on the tumour type and stage, different treatment options are available. Surgery is the main treatment modality for most solid tumours, often integrated in a more extensive (neo-)adjuvant treatment strategy. Surgical resection is generally aimed at complete macroscopic and microscopic removal of the cancer. However, inadequate resection of the tumour (i.e., presence of cancer cells at the margin or <5mm from the resection surface) frequently occurs. The worldwide extent of this problem is illustrated in Table 1, showing the percentage of positive surgical margins for the most common cancer types. Although a clear surgical margin may not be pivotal in all cancer types (e.g., during debulking procedures for brain tumours [3]), it is the main prognostic factor for survival in most types of cancer. Moreover, inadequate surgical tumour resection most often warrants adjuvant treatment, which is associated with increased morbidity and costs. During the operation, an oncologic surgeon takes into account all relevant clinical information that is available, including cancer type, tumour differentiation, and preoperative imaging reports. However, the actual surgical cut is based on subjective tactile and visual assessment of the tissue to determine which tissue needs to be excised. Although the primary aim is to completely excise the tumour, precise margin delineation is imperative in many delicate areas where wider resections inevitably lead to increased morbidity and loss of functionality.

Table 1. Percentage of positive surgical margins for the most common cancer types (estimated new cases worldwide, 2020). *Males and females combined.

Cancer type (solid tumours only)	Estimated new cases[30]*	Incidence[30]*	Positive margins
Breast	2,261,419	12%	20-70% [31-34]
Trachea, lung & bronchus	2,206,771	11%	5-17% [35-38]
Prostate	1,414,259	7%	7-75% [39-42]
Colorectal	1,931,590	10%	12-58% [43-45]
Urinary bladder	573,278	3%	0-25% [46-48]
Kidney & renal pelvis	431,288	2%	7-11% [49-52]
Uterine corpus	417,367	2%	4-17% [34, 53]
Pancreas	495,773	3%	18-85% [54-57]
Thyroid	586,202	3%	10-11% [34, 58, 59]
Lip, oral cavity	377,713	2%	5-43% [60, 61]

Over the past two decades, important advances have been made to improve assessment of surgical margins by the introduction of intraoperative imaging techniques. Besides frozen section analysis, several optical methods have been studied to perform intraoperative margin assessment in surgical oncology, including optical coherence tomography (OCT) [4], photoacoustic tomography, terahertz imaging, second harmonic generation, confocal

microscopy, fluorescence (lifetime) imaging, autofluorescence imaging (AFI), narrow-band imaging, hyper-spectral imaging, diffuse reflectance spectroscopy, Fourier transform infrared spectroscopy, and Raman spectroscopy (RS) [5-10]. Among them, intraoperative fluorescence imaging (FI) using exogenous tumour-specific fluorescent agents has shown to be particularly beneficial for surgical margin assessment in clinical trials [11-22], and it has been shown that RS can objectively discriminate between normal and malignant tissue [23-27]. Intraoperative FI provides a wide-field real-time tumour-specific image to guide the surgical resection. However, detection and interpretation of the fluorescent signal are complex, and are influenced by optical tissue properties, targeting-specificity of fluorescent agents and accuracy of the imaging system. Each of these factors has an effect on image resolution, sensitivity and/or specificity of the technique [28]. RS on the other hand provides detailed identification of malignant tissues with high sensitivity and specificity [29]. It does not provide the surgeon with a wide-field image because it generally requires 'point' (i.e., of small tissue volumes) measurements of the tissue. This compromises the possibility of scanning the complete resection surface.

In this review, we describe the state-of-the-art of FI and RS and include an overview of the advantages and limitations for their use in image-guided cancer surgery. Next, we demonstrate how these two techniques are complementary and how they can overcome each other's disadvantages and limitations. Finally, we highlight the technical challenges that need to be addressed to implement this novel approach into clinical practice.

IMAGE-GUIDED CANCER SURGERY USING FLUORESCENCE IMAGING

Intraoperative FI of tumour tissue requires the systemic administration of a cancer-specific exogenous fluorescent agent that can identify the tumour using a spectrum of targeting strategies, including antibodies, small peptides and activatable fluorophores [62-64]. The use of fluorophores that emit light in the first near-infrared (NIR-I) range (650–900 nm) results in deeper tissue penetration of the photons and lower autofluorescence from surrounding tissues [65-67]. Because the human eye is insensitive to light in this spectrum, dedicated intraoperative camera systems are required to detect the fluorescent signal [13, 68-71]. Figure 1 shows the clinical status of targeted fluorescent agents in the visible channel, NIR-I-700-nm-channel, and NIR-I-800-nm-channel together with their excitation and emission wavelengths.

FI exhibits several favourable characteristics for clinical translation. Preclinical studies have demonstrated low toxicity with high sensitivity and specificity for tumour detection using targeted fluorescent agents [62, 63, 72, 73]. Besides the minimal risks associated with the use of lasers in the imaging system, there are no safety issues for the clinicians because no ionising radiation is used, and the technique is capable of real-time detection without interfering with the surgical field. Importantly, the whole-field imaging facilitates analysis of the complete surgical margin and remaining wound bed.

The simultaneous development of clinically available fluorescent agents and intraoperative camera systems over the past decade has now positioned intraoperative FI as a promising real-time detection modality for surgeons in oncology. Since the first clinical trial of FI with tumour-specific NIR fluorescent agents [13], ground-breaking results have been reported in patients with various cancer types, consistently showing excellent safety records [11-22, 74]. Indocyanine green (ICG), a nonspecific and US Food and Drug Administration approved compound, has commonly been used for FI in various settings [75, 76]. Methylene blue (MB) was approved as the second NIR fluorescent agent for fluorescence-based intraoperative imaging [77]. Fluorescein sodium, 5-ALA, and Cytalux/Pafolacianine are three other clinically approved fluorescent agents. To date, fluorescent agents [78, 79] have been developed for detection of cancer cells [80-83], sentinel lymph nodes [11, 71, 84, 85], atherosclerosis [86, 87], arthritis [88-90], ureters [91-93], bile ducts [94], and nerves [95, 96]. For visualisation of these fluorescent agents, specialized intraoperative imaging systems have been developed for open surgery [13, 14, 63, 68-70, 97, 98], endoscopy [99], laparoscopy [100], thoracoscopy [101] and robotic surgery [102, 103]. Figure 2 shows the intraoperative impact of using fluorescence-guided surgeries.

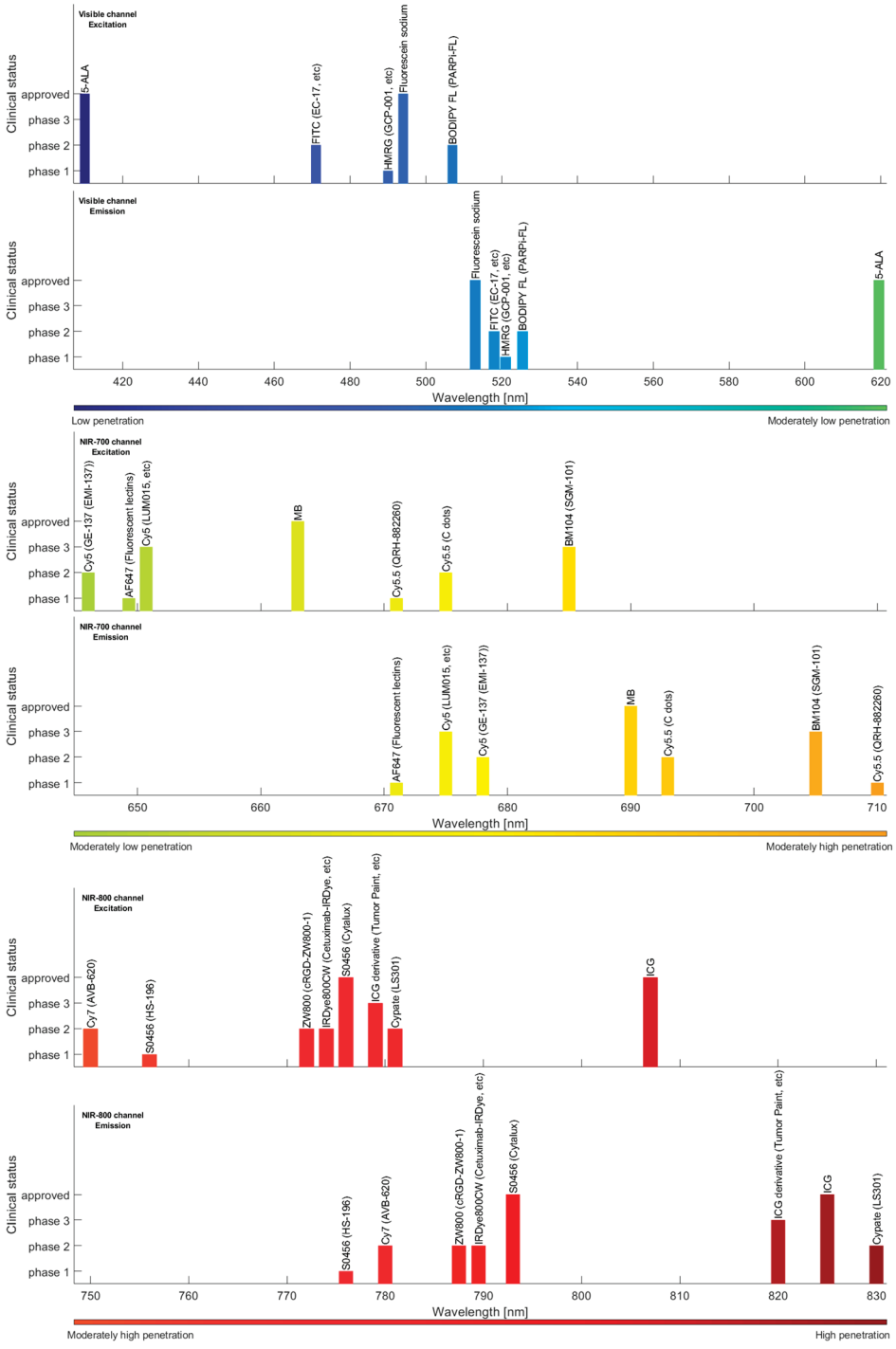

Figure 1. Excitation and emission wavelengths of approved and clinical fluorescent agents in the visible channel, NIR-700-nm-channel, and NIR-800-nm-channel (data collected from [108-112]).

Despite a strong driving force coming from the auspicious results of these trials, there is still a fundamental controversy in the scientific field on how to cope with the complex process of optical imaging. Optical properties of the tissue can attenuate fluorescence signals; light scattering for example may cause blurred images. In addition, tumour-to-background ratios are influenced by nonspecific autofluorescence of the surrounding healthy tissues, although this disturbance is lower in the NIR region. Further, fluorescence intensity is further dependent on many factors, such as the concentration and fluorescence quantum yield of the fluorescent agent, the affinity of the fluorescent agent, the abundance of target receptors or epitopes, and the imaging system [28]. Innovative calculation methods have been developed that can partly correct for the perturbation caused by tissue optical properties, but a millimetre-scale sharp delineation of the tumour remains challenging in many cases [98, 104-107]. Considering all these factors, sufficient understanding of these processes by the surgeon is essential to adequately interpret the intraoperative fluorescence image at hand.

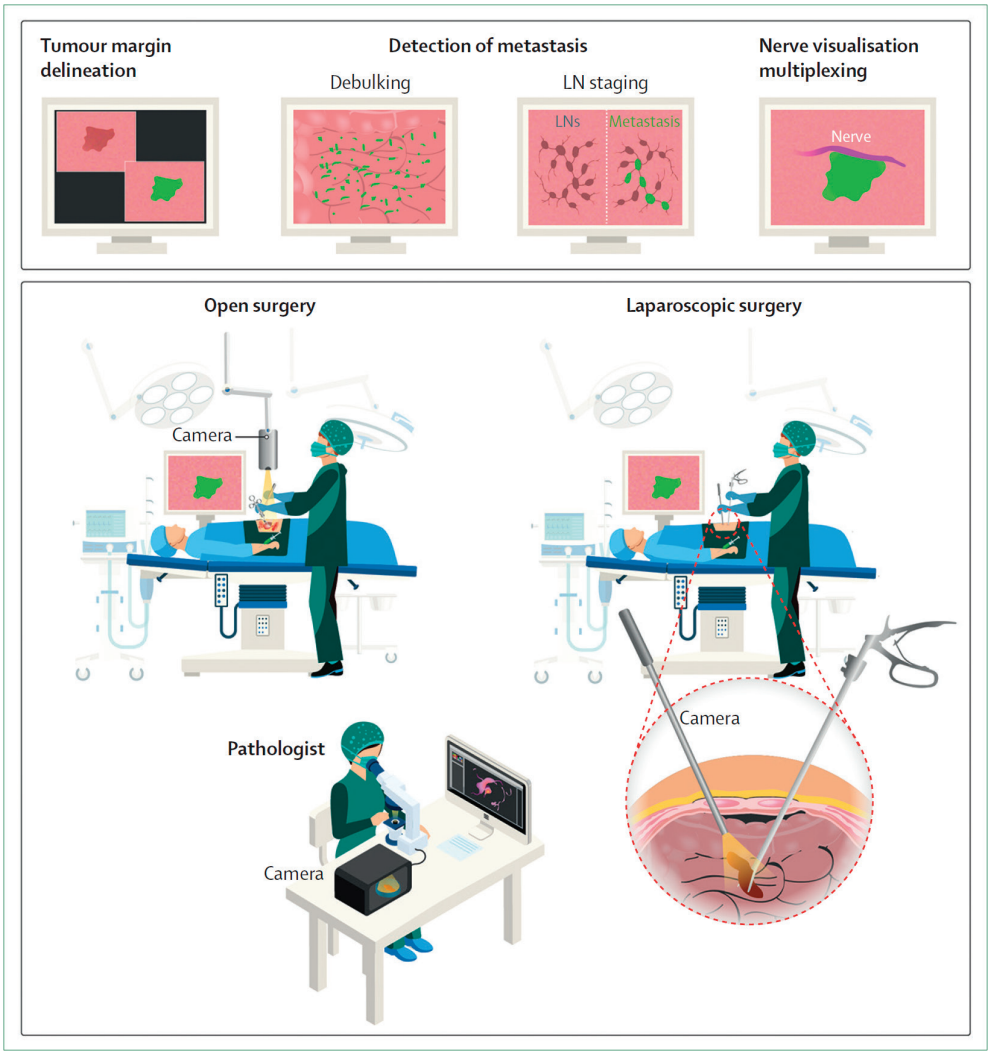

Figure 2. (Top) Schematic illustration of the intraoperative impact of using fluorescence-guided surgeries. (Bottom) Implementation of fluorescence guidance. Following the administration of the fluorescent agent, the tissues of interest can be visualised with a dedicated NIR camera in real-time during open or laparoscopic surgery. In addition to guiding the surgeon during the resection, rapid feedback on the presence of fluorescence can be provided by imaging the resected tissue on a back table with a NIR camera and microscope in the operating room (taken from [79] with permission).

INTRAOPERATIVE USE OF RAMAN SPECTROSCOPY

Raman spectroscopy is an optical technique that can be used for real-time characterisation of biological tissue *in* and *ex vivo*. A Raman spectrum of tissue is a representation of the molecular composition of that tissue. As cancer alters the molecular composition of tissue, RS can be used for discrimination between tumour and healthy tissue. Contrary to FI, the technique does not require preparation or staining of the tissue to be analysed, which facilitates clinical application. With the use of optical fibres, many body locations can be assessed *in vivo* using hand-held RS probes [113]. RS has a high diagnostic accuracy for cancer detection, with reported overall diagnostic sensitivities and specificities between 73% - 100% and 66% - 100%, respectively [114]. Its intraoperative application has recently been explored in brain tumour biopsies [115] and brain tumour surgery [116, 117], as well as in debulking procedures of ovarian cancer [118]. RS can further be used for peripheral nerve visualisation and identification and sparing of vital structures during oncological surgery [119, 120].

The two regions of the Raman spectrum that are relevant to cancer diagnostics are the fingerprint and the high wavenumber (HWVN) regions (Figure 3 |d, e). Most biomedical research on RS studies the fingerprint region (~400-2000 cm^{-1}). This region is rich in spectral features, including the biochemical signatures associated with lipids, proteins, nucleic acids (DNA) and blood [121]. However, processing times in this region are long; signal intensity is relatively low, and molecular discrimination is generally based on minute spectral differences, necessitating complex and robust machine-learning algorithms [29, 122]. Furthermore, *in vivo* applications for RS require fibre-optic probes. These fibres, made of fused silica, generate intense background emission requiring complex optical filtering [123]. Contrary to the fingerprint region, no Raman signal is generated in fused silica in the HWVN region, which ranges from ~2400-3800 cm^{-1}. In addition to its amenability for use with optical fibres, the signal in the HWVN region is much more intense than in the fingerprint region. While it contains less detailed spectral information, the HWVN region can be utilised to distinguish malignant from healthy tissue with a more straightforward approach. An additional benefit of performing RS in the HWVN over the fingerprint region is the greater spectral distance from fluorescence emission, when excited with a red or NIR laser. As a result, the Raman signal in the HWVN region experiences less interference with that of fluorescence as compared to the fingerprint region.

In oral cancer, it has been demonstrated that HWVN Raman spectra can identify cancer *ex vivo* based on the water concentration in freshly excised specimens [23]. This water concentration differs consistently across the border between tumour and healthy surrounding tissue over a distance of about 5 mm [124]. The water concentration averages from 76% in the tumour to about 54% in the surrounding healthy tissue. The variation in water concentration inside tumour tissue appeared to be much lower (8%) than that in the healthy tissue (24%)

[124]. Acquisition of HWVN Raman spectra occurred in a point-based manner, i.e., grid-wise measurements of microscopic tissue volumes with instant signal processing (<0.1 s).

Based on these findings, the development of an automated fibre-optic needle probe for determination of the water concentration profile across the margins of a resection specimen has been initiated. The needle probe is placed on the resection surface and then driven into the tissue while recording spectra at regular distance intervals along its path. The goal is to measure the distance between resection surface and tumour border in this way, to enable rapid and objective margin assessment without the need for specimen grossing [125-127, *manuscript in preparation Aaboubout et al.*].

The combination of other imaging modalities with selective sampling of suspicious areas by RS as a powerful label-free analytical technique has also been explored [128, 129]. Such approaches include MRI, second harmonic generation, OCT, AFI, total internal reflection fluorescence, or quantitative phase microscopy [130-138]. In general, the basic concept behind these multimodal approaches is to combine the high sensitivity of an imaging modality (i.e. rapid identification of areas that need further inspection) with the high selectivity of RS tissue analysis.

THE POTENTIAL COMPLEMENTARY VALUE OF COMBINED FLUORESCENCE IMAGING AND RAMAN SPECTROSCOPY

In FI, the signal originates from the interaction of light with the administrated fluorescent agent binding in the tumour. In RS, however, the signal originates from the interaction of light with the tissue itself, regardless of the specificity of fluorescent agent binding. Owing to the distinctly different physical signal origins of FI and RS, the provided information is complementary.

FI allows for real-time whole-field imaging of the surgical field, with high signal intensity. However, fluorescence signal intensity is limited by intrinsic optical tissue properties as well as the concentration and fluorescent quantum yield of the fluorescent agent [28]. On the other hand, RS can detect tumour with uniquely high specificity, but the signal intensity is very weak and can be hindered by photon shot noise originating from light interaction with components of the specimen present in the cross-section of the illumination and detection paths [139]. Additionally, its limitation to point measurements does not allow for real-time, whole-field tissue analysis. Therefore, a combination of FI that has high sensitivity at the expense of a somewhat lower specificity, with RS that provides high specificity would be very advantageous. FI would be employed *in vivo* for real-time identification of fluorescence, fol-

lowed by objective verification of malignancy with RS to yield superior diagnostic accuracy over either modality used in isolation.

Other than helping to distinguish malignant from healthy tissue (i.e., during excision with tumour-free margins and debulking procedures), FI has additional advantages for surgical oncology. Due to its ability to scan large surfaces, FI is a useful tool for identifying additional occult lesions as well as relevant vital structures that require preservation during cancer surgery [140]. FI has been employed to identify separately located clinically occult tumours in a variety of contexts, including peritoneal metastases [141], sentinel lymph nodes [142], pulmonary [143], and abdominal [144] lesions. Such findings have been described to result in improved survival rates, changes in personalised treatment, and reduced morbidity associated with damage to healthy surrounding structures.

Besides securing adequate margins and achieving conservative resection during cancer surgery, RS can complement FI in several other ways. When fluorescent areas are detected in the wound bed or elsewhere in the scanned surface (e.g., abdomen), RS could be the ideal tool to instantly assess this suspect region, thereby confirming or ruling out the presence of occult lesions. For unanticipated intraoperative findings such as the detection of clinically occult peritoneal metastases during colorectal cancer surgery [141], subsequent *in vivo* RS could be used to confirm malignancy without the need for time-consuming fresh frozen sectioning. Even in case of a clinically suspicious non-fluorescent lesion, RS can provide timely analysis. Similarly, RS has potential for use as an additional confirmation of fluorescent findings during debulking procedures and in the identification of vital structures.

However, laser-induced fluorescence itself can be a limiting factor for Raman measurements. Because fluorescent signals are generally orders of magnitude stronger, obscuring the Raman signal, these techniques were traditionally considered mutually exclusive. Figure 3 shows this interference in preliminary tests where RS was performed utilising the standard excitation wavelength of 671 nm on freshly excised tissue of a patient after injection of a fluorescent agent in the NIR-800-nm-channel. The interface can be eliminated by shifting the excitation wavelength to 976 nm.

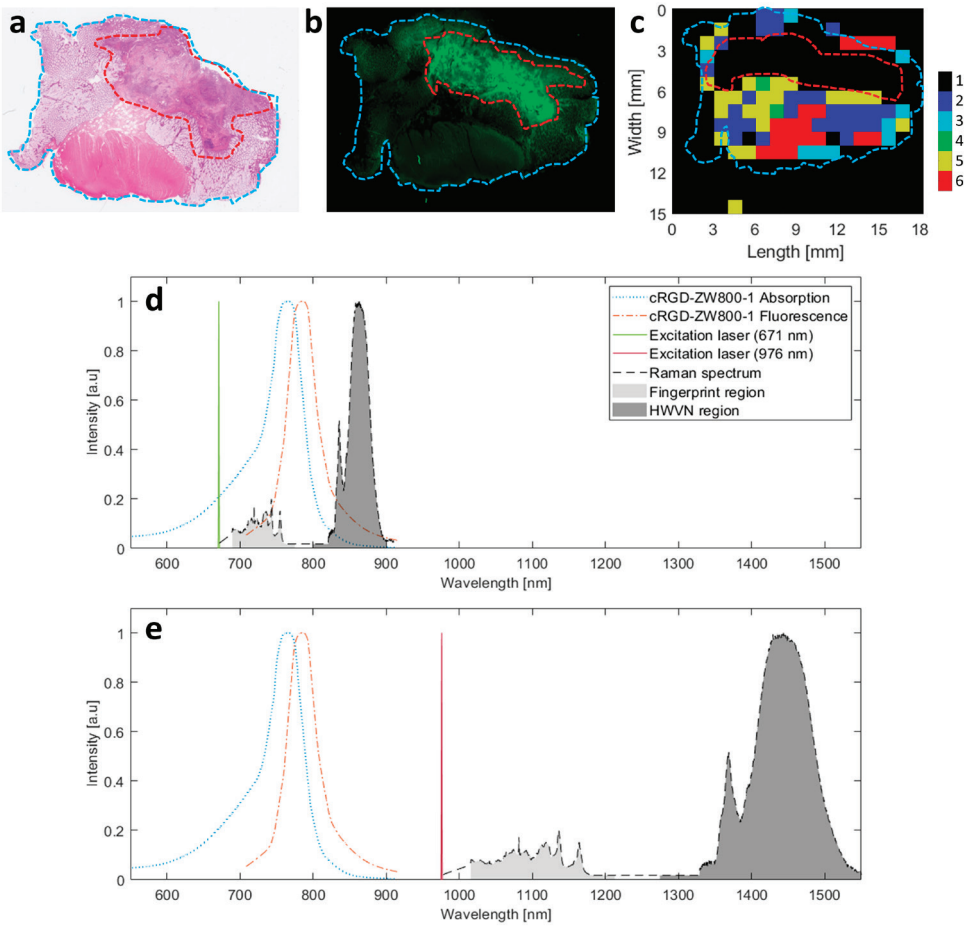

Figure 3. FI and RS image of tissue section of colorectal cancer containing cRGD-ZW800-1 and surrounding healthy tissue. Ethical approval for collection of this tissue falls under the METC LUMC, as part of studies registered in the European Trials Database under numbers 2016-000397-38 and 2017-002772-60 [73]. Tumour is delineated by the red dotted line, tissue is delineated by blue dotted line (a, b, and c). a) Haematoxylin and eosin stained slide. b) Fluorescent image showing colocalisation of signal with tumour. c) Cluster analysis of the Raman image illustrating that the tumour area cannot be characterised by RS because the fluorescence signal is too strong. d) fluorescence spectrum of cRGD-ZW800-1 showing overlap with the acquired Raman signal at an excitation wavelength of 671 nm. HWVN region provides stronger Raman signal intensity than other Raman regions and overlaps with the tail of fluorescence emission. e | space between fluorescence spectrum of cRGD-ZW800-1 and the acquired Raman signal at an excitation wavelength of 976 nm.

Combining FI with RS indeed requires careful matching of excitation and emission wavelengths of RS and the exogenous fluorescent agents; several groups have studied various approaches to deal with this issue. The excitation of fluorescent labels can be avoided by shifting the wavelength of the Raman laser to a longer wavelength [145].

In a study using phantoms and breast specimens stained with patent blue dye (BD), it was demonstrated that fluorescence induction from surgical pigments could be circumvented by combining a laser with a longer wavelength (785 nm vs. 685 nm) with an Indium Gallium Arsenide (InGaAs) camera capable of measuring the water/total area ratio of the HWVN spectrum[146]. Noting that haemoglobin and BD have no adverse effect on water content analysis, the Raman system was shown to accurately distinguish tumour from healthy tissue, as well as differentiate between normal and metastatic axillary lymph nodes in the presence of BD [147].

Another study combined fingerprint RS with wide-field AFI spectral imaging for intraoperative margin assessment in breast-conserving surgery [130]. AFI was employed to effectively 'screen out' the adipose tissue, enabling RS to more efficiently target the non-adipose tissue regions that are at a higher risk of malignancy, with superior diagnostic value as a result.

When it comes to the combination of FI and RS, 5-aminolevulinic acid (5-ALA) is the most frequently studied fluorescent agent. In 2006, *in vivo* fingerprint RS was studied on bladder cancer biopsies obtained under the guidance of 5-ALA induced protoporphyrin-IX (PPIX) FI [148]. Although a NIR laser emitting at 830 nm was used to reduce the interference of PPIX fluorescence emission in the visible area, additional fluorescence background was observed in the sample obtained from fluorescent areas, obscuring the RS signal and requiring algorithmic removal. Therefore, a new classification algorithm was trained based on biopsies with 5-ALA, which improved accuracy (from sensitivity and specificity of 43% and 71%, to 75% and 89%, respectively) [149]. Furthermore, it was demonstrated how the classification accuracy could be further improved by combining fluorescence and RS information on biopsies with 5-ALA (sensitivity and specificity of 100% and 81%, respectively).

More recently, *ex vivo* RS was performed to differentiate glioma from normal brain in the presence of 5-ALA [150]. It was shown that RS could identify glioma with an accuracy of 0.85-1.00 (along with a 95% confidence interval) using a 785-nm laser and collecting Raman spectra in the fingerprint region. In optical tissue phantoms, tumour margin could be delineated using this approach [151]. Additionally, fingerprint RS was studied on tissues containing verteporfin and temoporfin, two fluorescent agents (photosensitisers) with activation at ~690 and ~650 nm, respectively [152]. With fluorescence emission similar to PPIX (600- 800 nm), both agents were shown to be compatible with a 785 nm excitation Raman system. However, no clinical *in vivo* intraoperative studies have been reported yet.

To summarise, several studies showed successful Raman measurements in the presence of fluorescent agents with emission in the visible and NIR-700-nm-channel regions. However, to the best of our knowledge, there is no report on performing Raman measurements with the agents in the NIR-800-nm-channel (e.g., ICG). ICG is the most widely used fluorescent agent in clinical trials of fluorescence-guided surgery (FGS) [153, 154]. It has peak fluores-

cence emission in the NIR-I region and a long emission tail that extends into the NIR-II (1000-1700 nm) region [155], which is very challenging to combine with RS because of reduced Raman scattering at higher wavelengths, as well as the limited quantum efficiency of silicon-based CCD detectors, which declines to below 30% beyond 1000 nm.

A novel HWVN RS system was recently developed to characterise tumour in highly pigmented skin lesions (i.e., melanomas) [156-158]. These melanocytic lesions have absorption characteristics at long wavelengths, similar to NIR fluorophores. Tissue characterisation was still feasible after increasing the laser excitation wavelength to/beyond the NIR region (>900 nm), demonstrating that the combined and simultaneous use of FGS with NIR fluorophores and RS is technically feasible. Using this HWVN RS system, resection margins can be improved by utilising the optimal characteristics of FI in the NIR region with tumour-specific fluorescent agents, combined with the specificity of RS based on differences in water concentration in this region. A laser excitation wavelength of 976 nm in combination with a novel low-noise InGaAs detector showed perfect elimination of laser-induced fluorescence of pigmented tissues. Collection of Raman signal in the short-wave infrared (SWIR) region with a high quantum efficiency (>90%) up to 1570 nm showed minimal fluorescence contribution in the obtained spectra excited with 976 nm laser. RS with a low noise InGaAs multichannel detector in the SWIR region can open up possibilities of combining RS and FI in a clinical, intraoperative setting, even in the presence of fluorescent agents in the NIR-800-nm-channel.

Although RS is generally a label-free method, systemic injection of molecular imaging agents for Raman signal enhancement has recently been studied preclinically for margin assessment purposes. By selectively accumulating in the tumour tissue, multi-purpose nanoparticles could be used for FI while simultaneously enhancing the Raman signal, as well as providing the option of photothermal tumour ablation [159-161]. This promising approach still awaits clinical translation.

CONCLUSION AND FUTURE WORK

While combining FI with RS to achieve both whole-field imaging of the surgical field and objective margin verification would be very advantageous, these techniques have traditionally been considered mutually exclusive. Careful matching of RS excitation wavelengths and fluorophore emission wavelengths is required, presenting various technical hurdles. This issue could be solved by quantification of differences in water concentration in the HWVN region. After FI with tumour-specific fluorescent agents, HWVN RS may be used to assess margin adequacy. In addition, evidence for the utility of RS in the identification of occult lesions and vital structures underlines its potential as an adjunct to FGS in all its basic applications. It is worth mentioning that intraoperative imaging techniques can also be beneficial

for other applications, not limited to cancer surgery. These include delineation of targeted borders for precise surgical resections, evaluation of vascular perfusion, and identification of vital structures, such as nerves or ureters [140]. The synergistic effect of FI and RS could also be exploited for these applications.

REFERENCES

1. Siegel, R.L., K.D. Miller, and A. Jemal, *Cancer statistics, 2018.* CA Cancer J Clin, 2018. **68**(1): p. 7-30.
2. Bray, F. et al. *Global cancer statistics 2018: GLOBOCAN estimates of incidence and mortality worldwide for 36 cancers in 185 countries.* CA Cancer J Clin, 2018. **68**(6): p. 394-424.
3. Eyupoglu, I.Y., M. Buchfelder, and N.E. Savaskan, *Surgical resection of malignant gliomas-role in optimizing patient outcome.* Nat Rev Neurol, 2013. **9**(3): p. 141-51.
4. van Manen, L. et al. *The clinical usefulness of optical coherence tomography during cancer interventions.* J Cancer Res Clin Oncol, 2018. **144**(10): p. 1967-1990.
5. Brouwer de Koning, S.G. et al. *Assessment of the deep resection margin during oral cancer surgery: A systematic review.* European Journal of Surgical Oncology, 2021.
6. Balasundaram, G. et al. *Biophotonic technologies for assessment of breast tumor surgical margins—A review.* Journal of Biophotonics, 2021. **14**(1): p. e202000280.
7. Lauwerends, L.J. et al. *Current Intraoperative Imaging Techniques to Improve Surgical Resection of Laryngeal Cancer: A Systematic Review.* Cancers, 2021. **13**(8): p. 1895.
8. Shipp, D.W. et al. *Intra-operative spectroscopic assessment of surgical margins during breast conserving surgery.* Breast Cancer Research, 2018. **20**(1): p. 69.
9. Heidkamp, J. et al. *Novel imaging techniques for intraoperative margin assessment in surgical oncology: A systematic review.* International Journal of Cancer, 2021. **149**(3): p. 635-645.
10. Sachańbiński, T. and B. Radecka, *Review of methods of intraoperative margin assessment in breast conserving surgery.* Nowotwory. Journal of Oncology, 2021. **0**(0).
11. Schaafsma, B.E. et al. *The clinical use of indocyanine green as a near-infrared fluorescent contrast agent for image-guided oncologic surgery.* Journal of surgical oncology, 2011. **104**(3): p. 323-32.
12. Hutteman, M. et al. *Near-infrared fluorescence imaging in patients undergoing pancreaticoduodenectomy.* Eur Surg Res, 2011. **47**(2): p. 90-7.
13. van Dam, G.M. et al. *Intraoperative tumor-specific fluorescence imaging in ovarian cancer by folate receptor-alpha targeting: first in-human results.* Nature medicine, 2011. **17**(10): p. 1315-9.
14. Vahrmeijer, A.L. et al. *Image-guided cancer surgery using near-infrared fluorescence.* Nature reviews. Clinical oncology, 2013. **10**(9): p. 507-18.
15. van der Vorst, J.R. et al. *Near-infrared fluorescence-guided resection of colorectal liver metastases.* Cancer, 2013. **119**(18): p. 3411-8.
16. Handgraaf, H.J.M. et al. *Real-time near-infrared fluorescence imaging using cRGD-ZW800-1 for intraoperative visualization of multiple cancer types.* Oncotarget, 2017. **8**(13): p. 21054-21066.
17. Handgraaf, H.J.M. et al. *Long-term follow-up after near-infrared fluorescence-guided resection of colorectal liver metastases: A retrospective multicenter analysis.* Eur J Surg Oncol, 2017. **43**(8): p. 1463-1471.
18. Boogerd, L.S.F. et al. *Safety and effectiveness of SGM-101, a fluorescent antibody targeting carcinoembryonic antigen, for intraoperative detection of colorectal cancer: a dose-escalation pilot study.* Lancet Gastroenterol Hepatol, 2018. **3**(3): p. 181-191.
19. Hekman, M.C. et al. *Tumor-targeted Dual-modality Imaging to Improve Intraoperative Visualization of Clear Cell Renal Cell Carcinoma: A First in Man Study.* Theranostics, 2018. **8**(8): p. 2161-2170.
20. van Keulen, S. et al. *The Clinical Application of Fluorescence-Guided Surgery in Head and Neck Cancer.* J Nucl Med, 2019. **60**(6): p. 758-763.
21. Voskuil, F.J. et al. *Exploiting metabolic acidosis in solid cancers using a tumor-agnostic pH-activatable nanoprobe for fluorescence-*

guided surgery. Nat Commun, 2020. **11**(1): p. 3257.
22. Schaap, D.P. et al. *Carcinoembryonic antigen-specific, fluorescent image-guided cytoreductive surgery with hyperthermic intraperitoneal chemotherapy for metastatic colorectal cancer.* Br J Surg, 2020. **107**(4): p. 334-337.
23. Barroso, E.M. et al. *Discrimination between oral cancer and healthy tissue based on water content determined by Raman spectroscopy.* Anal Chem, 2015. **87**(4): p. 2419-26.
24. Liao, Z. et al. *Feasibility of integrated high-wavenumber Raman imaging and fingerprint Raman spectroscopy for fast margin assessment in breast cancer surgery.* Journal of Raman Spectroscopy, 2020. **51**(10): p. 1986-1995.
25. Pence, I.J. et al. *Discrimination of liver malignancies with 1064 nm dispersive Raman spectroscopy.* Biomed Opt Express, 2015. **6**(8): p. 2724-37.
26. Thomas, G. et al. *Evaluating feasibility of an automated 3-dimensional scanner using Raman spectroscopy for intraoperative breast margin assessment.* Sci Rep, 2017. **7**(1): p. 13548.
27. Haifler, M. et al. *Discrimination of malignant and normal kidney tissue with short wave infrared dispersive Raman spectroscopy.* J Biophotonics, 2018. **11**(6): p. e201700188.
28. Keereweer, S. et al. *Optical image-guided cancer surgery: challenges and limitations.* Clinical cancer research : an official journal of the American Association for Cancer Research, 2013. **19**(14): p. 3745-54.
29. Koljenovic, S. et al. *Tissue characterization using high wave number Raman spectroscopy.* J Biomed Opt, 2005. **10**(3): p. 031116.
30. Sung, H. et al. *Global Cancer Statistics 2020: GLOBOCAN Estimates of Incidence and Mortality Worldwide for 36 Cancers in 185 Countries.* CA Cancer J Clin, 2021. **71**(3): p. 209-249.
31. Jacobs, L., *Positive margins: the challenge continues for breast surgeons.* Ann Surg Oncol, 2008. **15**(5): p. 1271-2.
32. Miller, A.R. et al. *Positive margins following surgical resection of breast carcinoma: analysis of pathologic correlates.* J Surg Oncol, 2004. **86**(3): p. 134-40.
33. Pleijhuis, R.G. et al. *Obtaining adequate surgical margins in breast-conserving therapy for patients with early-stage breast cancer: current modalities and future directions.* Ann Surg Oncol, 2009. **16**(10): p. 2717-30.
34. Orosco, R.K. et al. *Positive Surgical Margins in the 10 Most Common Solid Cancers.* Sci Rep, 2018. **8**(1): p. 5686.
35. Magdeleinat, P. et al. *Surgical treatment of lung cancer invading the chest wall: results and prognostic factors.* Ann Thorac Surg, 2001. **71**(4): p. 1094-9.
36. Osarogiagbon, R.U. et al. *Prevalence, Prognostic Implications, and Survival Modulators of Incompletely Resected Non-Small Cell Lung Cancer in the U.S. National Cancer Data Base.* J Thorac Oncol, 2016. **11**(1): p. e5-16.
37. Tandberg, D.J. et al. *Patterns of Failure After Surgery for Non-Small-cell Lung Cancer Invading the Chest Wall.* Clin Lung Cancer, 2017. **18**(4): p. e259-e265.
38. Predina, J.D. et al. *Clinical implications of positive margins following non-small cell lung cancer surgery.* J Surg Oncol, 2016. **113**(3): p. 264-9.
39. Bellangino, M. et al. *Systematic Review of Studies Reporting Positive Surgical Margins After Bladder Neck Sparing Radical Prostatectomy.* Curr Urol Rep, 2017. **18**(12): p. 99.
40. Shipley, W.U. et al. *Radiation with or without Antiandrogen Therapy in Recurrent Prostate Cancer.* N Engl J Med, 2017. **376**(5): p. 417-428.
41. Srougi, V. et al. *Surgical method influences specimen margins and biochemical recurrence during radical prostatectomy for high-risk prostate cancer: a systematic review and meta-analysis.* World J Urol, 2017. **35**(10): p. 1481-1488.
42. Yossepowitch, O. et al. *Positive surgical margins after radical prostatectomy: a*

systematic review and contemporary update. Eur Urol, 2014. **65**(2): p. 303-13.

43. Nuyttens, J.J. et al. *High-dose-rate intraoperative radiotherapy for close or positive margins in patients with locally advanced or recurrent rectal cancer.* Int J Radiat Oncol Biol Phys, 2004. **58**(1): p. 106-12.
44. Alberda, W.J. et al. *The Importance of a Minimal Tumor-Free Resection Margin in Locally Recurrent Rectal Cancer.* Dis Colon Rectum, 2015. **58**(7): p. 677-85.
45. Alberda, W.J. et al. *Intraoperative radiation therapy reduces local recurrence rates in patients with microscopically involved circumferential resection margins after resection of locally advanced rectal cancer.* Int J Radiat Oncol Biol Phys, 2014. **88**(5): p. 1032-40.
46. DiLizia, E.M. and F. Sadeghi, *Surgical and pathological outcomes of robotic-assisted radical cystectomy for bladder cancer in the community setting.* J Robot Surg, 2017.
47. Yuh, B. et al. *Systematic review and cumulative analysis of oncologic and functional outcomes after robot-assisted radical cystectomy.* Eur Urol, 2015. **67**(3): p. 402-22.
48. Novara, G. et al. *Soft tissue surgical margin status is a powerful predictor of outcomes after radical cystectomy: a multicenter study of more than 4,400 patients.* J Urol, 2010. **183**(6): p. 2165-70.
49. Seisen, T. et al. *A Systematic Review and Meta-analysis of Clinicopathologic Factors Linked to Intravesical Recurrence After Radical Nephroureterectomy to Treat Upper Tract Urothelial Carcinoma.* Eur Urol, 2015. **67**(6): p. 1122-1133.
50. Kryvenko, O.N., *Positive Surgical Margins Increase Risk of Recurrence after Partial Nephrectomy for High Risk Renal Tumors. Shah PH, Moreira DM, Okhunov Z, Patel VR, Chopra S, Razmaria AA, Alom M, George AK, Yaskiv O, Schwartz MJ, Desai M, Vira MA, Richstone L, Landman J, Shalhav AL, Gill I, Kavoussi LR. J Urol. 2016 Aug;196(2):327-34.* Urol Oncol, 2017. **35**(6): p. 449-450.
51. Ani, I. et al. *Prevalence and impact on survival of positive surgical margins in partial nephrectomy for renal cell carcinoma: a population-based study.* BJU Int, 2013. **111**(8): p. E300-5.
52. Alemozaffar, M., C.P. Filson, and V.A. Master, *The importance of surgical margins in renal cell and urothelial carcinomas.* J Surg Oncol, 2016. **113**(3): p. 316-22.
53. Seagle, B.L. et al. *Survival after pelvic exenteration for uterine malignancy: A National Cancer Data Base study.* Gynecol Oncol, 2016. **143**(3): p. 472-478.
54. Handgraaf, H.J. et al. *Current and future intraoperative imaging strategies to increase radical resection rates in pancreatic cancer surgery.* Biomed Res Int, 2014. **2014**: p. 890230.
55. Menon, K.V. et al. *Impact of margin status on survival following pancreatoduodenectomy for cancer: the Leeds Pathology Protocol (LEEPP).* HPB (Oxford), 2009. **11**(1): p. 18-24.
56. Verbeke, C.S. and I.P. Gladhaug, *Resection margin involvement and tumour origin in pancreatic head cancer.* Br J Surg, 2012. **99**(8): p. 1036-49.
57. Esposito, I. et al. *Most pancreatic cancer resections are R1 resections.* Ann Surg Oncol, 2008. **15**(6): p. 1651-60.
58. Kluijfhout, W.P. et al. *Microscopic Positive Tumor Margin Does Not Increase the Risk of Recurrence in Patients with T1-T2 Well-Differentiated Thyroid Cancer.* Ann Surg Oncol, 2016. **23**(5): p. 1446-51.
59. Wang, L.Y. et al. *Microscopic Positive Margins in Differentiated Thyroid Cancer Is Not an Independent Predictor of Local Failure.* Thyroid, 2015. **25**(9): p. 993-8.
60. Smits, R.W. et al. *Resection margins in oral cancer surgery: Room for improvement.* Head Neck, 2016. **38 Suppl 1**: p. E2197-203.
61. McMahon, J. et al. *Influence of condition of surgical margins on local recurrence and disease-specific survival in oral and oropharyngeal cancer.* Br J Oral Maxillofac Surg, 2003. **41**(4): p. 224-31.
62. Keereweer, S. et al. *Optical image-guided surgery--where do we stand?* Mol Imaging Biol, 2011. **13**(2): p. 199-207.

63. Zhang, R.R. et al. *Beyond the margins: real-time detection of cancer using targeted fluorophores.* Nat Rev Clin Oncol, 2017. **14**(6): p. 347-364.
64. Mieog, J.S.D. et al. *Fundamentals and developments in fluorescence-guided cancer surgery.* Nat Rev Clin Oncol, 2021.
65. Frangioni, J.V., *In vivo near-infrared fluorescence imaging.* Curr Opin Chem Biol, 2003. **7**(5): p. 626-34.
66. Frangioni, J.V., *New technologies for human cancer imaging.* J Clin Oncol, 2008. **26**(24): p. 4012-21.
67. Weissleder, R. and V. Ntziachristos, *Shedding light onto live molecular targets.* Nat Med, 2003. **9**(1): p. 123-8.
68. Mieog, J.S. et al. *Novel intraoperative near-infrared fluorescence camera system for optical image-guided cancer surgery.* Mol Imaging. **9**(4): p. 223-31.
69. Troyan, S.L. et al. *The FLARE intraoperative near-infrared fluorescence imaging system: a first-in-human clinical trial in breast cancer sentinel lymph node mapping.* Annals of surgical oncology, 2009. **16**(10): p. 2943-52.
70. van Driel, P.B. et al. *Characterization and evaluation of the artemis camera for fluorescence-guided cancer surgery.* Mol Imaging Biol, 2015. **17**(3): p. 413-23.
71. Brouwer, O.R. et al. *Feasibility of sentinel node biopsy in head and neck melanoma using a hybrid radioactive and fluorescent tracer.* Ann Surg Oncol, 2012. **19**(6): p. 1988-94.
72. Marshall, M.V. et al. *Single-dose intravenous toxicity study of IRDye 800CW in Sprague-Dawley rats.* Mol Imaging Biol, 2010. **12**(6): p. 583-94.
73. de Valk, K.S. et al. *First-in-Human Assessment of cRGD-ZW800-1, a Zwitterionic, Integrin-Targeted, Near-Infrared Fluorescent Peptide in Colon Carcinoma.* Clin Cancer Res, 2020. **26**(15): p. 3990-3998.
74. Crane, L.M. et al. *Intraoperative near-infrared fluorescence imaging for sentinel lymph node detection in vulvar cancer: first clinical results.* Gynecol Oncol, 2011. **120**(2): p. 291-5.
75. Ishizawa, T. et al. *Real-time identification of liver cancers by using indocyanine green fluorescent imaging.* Cancer, 2009. **115**(11): p. 2491-504.
76. Purich, K. et al. *Intraoperative fluorescence imaging with indocyanine green in hepatic resection for malignancy: a systematic review and meta-analysis of diagnostic test accuracy studies.* Surg Endosc, 2020. **34**(7): p. 2891-2903.
77. Hong, G., A.L. Antaris, and H. Dai, *Near-infrared fluorophores for biomedical imaging.* Nature Biomedical Engineering, 2017. **1**(1): p. 0010.
78. Joshi, B.P. and T.D. Wang, *Targeted Optical Imaging Agents in Cancer: Focus on Clinical Applications.* Contrast Media Mol Imaging, 2018. **2018**: p. 2015237.
79. Hernot, S. et al. *Latest developments in molecular tracers for fluorescence image-guided cancer surgery.* Lancet Oncol, 2019. **20**(7): p. e354-e367.
80. Weissleder, R. et al. *In vivo imaging of tumors with protease-activated near-infrared fluorescent probes.* Nat Biotechnol, 1999. **17**(4): p. 375-8.
81. Choi, H.S. et al. *Targeted zwitterionic near-infrared fluorophores for improved optical imaging.* Nat Biotechnol, 2013. **31**(2): p. 148-53.
82. Lamberts, L.E. et al. *Tumor-Specific Uptake of Fluorescent Bevacizumab-IRDye800CW Microdosing in Patients with Primary Breast Cancer: A Phase I Feasibility Study.* Clin Cancer Res, 2017. **23**(11): p. 2730-2741.
83. Miller, S.E. et al. *First-in-human intraoperative near-infrared fluorescence imaging of glioblastoma using cetuximab-IRDye800.* J Neurooncol, 2018. **139**(1): p. 135-143.
84. van der Vorst, J.R. et al. *Randomized comparison of near-infrared fluorescence imaging using indocyanine green and 99(m) technetium with or without patent blue for the sentinel lymph node procedure in breast cancer patients.* Ann Surg Oncol, 2012. **19**(13): p. 4104-11.

85. Hutteman, M. et al. *Randomized, double-blind comparison of indocyanine green with or without albumin premixing for near-infrared fluorescence imaging of sentinel lymph nodes in breast cancer patients.* Breast Cancer Res Treat, 2011. **127**(1): p. 163-70.
86. Deguchi, J.O. et al. *Inflammation in atherosclerosis: visualizing matrix metalloproteinase action in macrophages in vivo.* Circulation, 2006. **114**(1): p. 55-62.
87. Osborn, E.A. et al. *Metabolic and Molecular Imaging of Atherosclerosis and Venous Thromboembolism.* J Nucl Med, 2017. **58**(6): p. 871-877.
88. Kelderhouse, L.E., S. Mahalingam, and P.S. Low, *Predicting Response to Therapy for Autoimmune and Inflammatory Diseases Using a Folate Receptor-Targeted Near-Infrared Fluorescent Imaging Agent.* Mol Imaging Biol, 2016. **18**(2): p. 201-8.
89. Wunder, A. et al. *In vivo imaging of protease activity in arthritis: a novel approach for monitoring treatment response.* Arthritis Rheum, 2004. **50**(8): p. 2459-65.
90. Slooter, M.D. et al. *Near infrared fluorescence imaging for early detection, monitoring and improved intervention of diseases involving the joint.* Connect Tissue Res, 2015. **56**(2): p. 153-60.
91. Verbeek, F.P. et al. *Near-infrared fluorescence imaging of both colorectal cancer and ureters using a low-dose integrin targeted probe.* Ann Surg Oncol, 2014. **21 Suppl 4**: p. S528-37.
92. Verbeek, F.P. et al. *Intraoperative near infrared fluorescence guided identification of the ureters using low dose methylene blue: a first in human experience.* J Urol, 2013. **190**(2): p. 574-9.
93. Mahalingam, S.M. et al. *Intraoperative Ureter Visualization Using a Novel Near-Infrared Fluorescent Dye.* Mol Pharm, 2018. **15**(8): p. 3442-3447.
94. Diana, M. et al. *Prospective Evaluation of Precision Multimodal Gallbladder Surgery Navigation: Virtual Reality, Near-infrared Fluorescence, and X-ray-based Intraoperative Cholangiography.* Ann Surg, 2017. **266**(5): p. 890-897.
95. Nguyen, Q.T. and R.Y. Tsien, *Fluorescence-guided surgery with live molecular navigation--a new cutting edge.* Nat Rev Cancer, 2013. **13**(9): p. 653-62.
96. Whitney, M.A. et al. *Fluorescent peptides highlight peripheral nerves during surgery in mice.* Nat Biotechnol, 2011. **29**(4): p. 352-6.
97. de Boer, E. et al. *Optical innovations in surgery.* Br J Surg, 2015. **102**(2): p. e56-72.
98. Themelis, G. et al. *Real-time intraoperative fluorescence imaging system using light-absorption correction.* J Biomed Opt, 2009. **14**(6): p. 064012.
99. Nagengast, W.B. et al. *Near-infrared fluorescence molecular endoscopy detects dysplastic oesophageal lesions using topical and systemic tracer of vascular endothelial growth factor A.* Gut, 2017.
100. van der Poel, H.G. et al. *Intraoperative laparoscopic fluorescence guidance to the sentinel lymph node in prostate cancer patients: clinical proof of concept of an integrated functional imaging approach using a multimodal tracer.* Eur Urol, 2011. **60**(4): p. 826-33.
101. Newton, A.D. et al. *Intraoperative fluorescence imaging in thoracic surgery.* J Surg Oncol, 2018.
102. KleinJan, G.H. et al. *Optimisation of fluorescence guidance during robot-assisted laparoscopic sentinel node biopsy for prostate cancer.* Eur Urol, 2014. **66**(6): p. 991-8.
103. Marano, A. et al. *Application of fluorescence in robotic general surgery: review of the literature and state of the art.* World J Surg, 2013. **37**(12): p. 2800-11.
104. Middelburg, T.A. et al. *Correction for tissue optical properties enables quantitative skin fluorescence measurements using multi-diameter single fiber reflectance spectroscopy.* J Dermatol Sci, 2015. **79**(1): p. 64-73.
105. Brooks, S. et al. *Sources of variability in the quantification of tissue optical properties by multidiameter single-fiber reflectance and fluorescence spectroscopy.* J Biomed Opt, 2015. **20**(5): p. 57002.

106. van Leeuwen-van Zaane, F. et al. *In vivo quantification of the scattering properties of tissue using multi-diameter single fiber reflectance spectroscopy.* Biomed Opt Express, 2013. **4**(5): p. 696-708.
107. Kruijt, B. et al. *In vivo quantification of chromophore concentration using fluorescence differential path length spectroscopy.* J Biomed Opt, 2009. **14**(3): p. 034022.
108. Liu, R. et al. *Current trends and key considerations in the clinical translation of targeted fluorescent probes for intraoperative navigation.* Aggregate, 2021. **2**(3): p. e23.
109. Yoon, K. et al. *A Multi-detection Fluorescence Dye with 5-ALA and ICG Using Modified Light Emitting Diodes.* Current Optics and Photonics, 2019. **3**(3): p. 256-262.
110. Zheng, Y. et al. *Fluorescence-guided surgery in cancer treatment: current status and future perspectives.* Annals of Translational Medicine, 2019: p. 6.
111. Nagaya, T. et al. *Fluorescence-Guided Surgery.* Frontiers in Oncology, 2017. **7**(314).
112. Pahang, F. et al. *Fluorescence properties of methylene blue molecules coupled with metal oxide nanoparticles.* OSA Continuum, 2020. **3**(3): p. 688-697.
113. Kallaway, C. et al. *Advances in the clinical application of Raman spectroscopy for cancer diagnostics.* Photodiagnosis Photodyn Ther, 2013. **10**(3): p. 207-19.
114. Wang, W. et al. *Real-time in vivo cancer diagnosis using Raman spectroscopy.* J Biophotonics, 2015. **8**(7): p. 527-45.
115. Ji, M. et al. *Detection of human brain tumor infiltration with quantitative stimulated Raman scattering microscopy.* Sci Transl Med, 2015. **7**(309): p. 309ra163.
116. Jermyn, M. et al. *Intraoperative brain cancer detection with Raman spectroscopy in humans.* Sci Transl Med, 2015. **7**(274): p. 274ra19.
117. Hollon, T.C. et al. *Rapid Intraoperative Diagnosis of Pediatric Brain Tumors Using Stimulated Raman Histology.* Cancer Res, 2018. **78**(1): p. 278-289.
118. Moradi, H. et al. *Raman micro-spectroscopy applied to treatment resistant and sensitive human ovarian cancer cells.* J Biophotonics, 2017. **10**(10): p. 1327-1334.
119. Minamikawa, T., Y. Harada, and T. Takamatsu, *Ex vivo peripheral nerve detection of rats by spontaneous Raman spectroscopy.* Sci Rep, 2015. **5**: p. 17165.
120. Kumamoto, Y. et al. *Rapid and accurate peripheral nerve imaging by multipoint Raman spectroscopy.* Sci Rep, 2017. **7**(1): p. 845.
121. Masson, L.E. et al. *Dual excitation wavelength system for combined fingerprint and high wavenumber Raman spectroscopy.* Analyst, 2018. **143**(24): p. 6049-6060.
122. Laing, S. et al. *Surface-enhanced Raman spectroscopy for in vivo biosensing.* Nature Reviews Chemistry, 2017. **1**(8).
123. Santos, L.F. et al. *Fiber-optic probes for in vivo Raman spectroscopy in the high-wavenumber region.* Anal Chem, 2005. **77**(20): p. 6747-52.
124. Barroso, E.M. et al. *Raman spectroscopy for assessment of bone resection margins in mandibulectomy for oral cavity squamous cell carcinoma.* Eur J Cancer, 2018. **92**: p. 77-87.
125. Aaboubout, Y. et al. *Specimen-driven intraoperative assessment of resection margins should be standard of care for oral cancer patients.* Oral Dis, 2021. **27**(1): p. 111-116.
126. Puppels, G.J. et al. *Tissue sample analysis*. 2017, International Publication Number WO 2017/126955 A1
127. Puppels, G.J. et al. *Optical Probe for Measuring a Tissue Sample*. 2017, International Publication Number WO 2017/111576 A1
128. Lizio, M.G., R. Boitor, and I. Notingher, *Selective-sampling Raman imaging techniques for ex vivo assessment of surgical margins in cancer surgery.* Analyst, 2021. **146**(12): p. 3799-3809.
129. Schie, I., C. Stiebing, and J. Popp, *Looking for a perfect match: multimodal combinations of Raman spectroscopy for biomedical applications.* J Biomed Opt, 2021. **26**(8).

130. Lizio, M.G. et al. *Combined total internal reflection AF spectral-imaging and Raman spectroscopy for fast assessment of surgical margins during breast cancer surgery.* Biomed Opt Express, 2021. **12**(2): p. 940-954.
131. Bendau, E. et al. *Distinguishing metastatic triple-negative breast cancer from nonmetastatic breast cancer using second harmonic generation imaging and resonance Raman spectroscopy.* Journal of Biophotonics, 2020. **13**(7): p. e202000005.
132. Bocklitz, T.W. et al. *Pseudo-HE images derived from CARS/TPEF/SHG multimodal imaging in combination with Raman-spectroscopy as a pathological screening tool.* BMC Cancer, 2016. **16**(1): p. 534.
133. Chowdhury, A.U. et al. *Second Harmonic Generation Guided Raman Spectroscopy for Sensitive Detection of Polymorph Transitions.* Analytical Chemistry, 2017. **89**(11): p. 5958-5965.
134. Kang, J.W. et al. *Combined confocal Raman and quantitative phase microscopy system for biomedical diagnosis.* Biomedical Optics Express, 2011. **2**(9): p. 2484-2492.
135. Kong, K. et al. *Diagnosis of tumors during tissue-conserving surgery with integrated autofluorescence and Raman scattering microscopy.* Proceedings of the National Academy of Sciences, 2013. **110**(38): p. 15189-15194.
136. Boitor, R. et al. *Clinical integration of fast Raman spectroscopy for Mohs micrographic surgery of basal cell carcinoma.* Biomedical Optics Express, 2021. **12**(4): p. 2015-2026.
137. Boitor, R. et al. *Automated multimodal spectral histopathology for quantitative diagnosis of residual tumour during basal cell carcinoma surgery.* Biomedical Optics Express, 2017. **8**(12): p. 5749-5766.
138. Schie, I.W. et al. *Morpho-molecular signal correlation between optical coherence tomography and Raman spectroscopy for superior image interpretation and clinical diagnosis.* Scientific Reports, 2021. **11**(1): p. 9951.
139. Mosca, S. et al. *Spatially offset Raman spectroscopy.* Nature Reviews Methods Primers, 2021. **1**(1): p. 21.
140. Lauwerends, L.J. et al. *Real-time fluorescence imaging in intraoperative decision making for cancer surgery.* Lancet Oncol, 2021. **22**(5): p. e186-e195.
141. Harlaar, N.J. et al. *Molecular fluorescence-guided surgery of peritoneal carcinomatosis of colorectal origin: a single-centre feasibility study.* Lancet Gastroenterol Hepatol, 2016. **1**(4): p. 283-290.
142. Nishio, N. et al. *Optical molecular imaging can differentiate metastatic from benign lymph nodes in head and neck cancer.* Nat Commun, 2019. **10**(1): p. 5044.
143. Newton, A.D. et al. *Intraoperative fluorescence imaging in thoracic surgery.* J Surg Oncol, 2018. **118**(2): p. 344-355.
144. Boogerd, L.S. et al. *Laparoscopic detection and resection of occult liver tumors of multiple cancer types using real-time near-infrared fluorescence guidance.* Surg Endosc, 2017. **31**(2): p. 952-961.
145. Puppels, G.J. et al. *Carotenoids located in human lymphocyte subpopulations and natural killer cells by Raman microspectroscopy.* Cytometry, 1993. **14**(3): p. 251-6.
146. Hubbard, T.J.E. et al. *Utilization of Raman spectroscopy to identify breast cancer from the water content in surgical samples containing blue dye.* Translational Biophotonics, 2021.
147. Horsnell, J. et al. *Raman Spectroscopy: A Promising Method of Assessing Axillary Lymph Nodes Even in the Presence of Blue Dye.* European Journal of Surgical Oncology, 2010. **36**(11): p. 1111.
148. Grimbergen, M. et al. *Feasibility of Raman spectroscopy in vitro after 5-ALA-based fluorescence diagnosis in the bladder*. SPIE BiOS. Vol. 6078. 2006: SPIE.
149. Grimbergen, M.C.M. et al. *Raman spectroscopy of bladder tissue in the presence of 5-aminolevulinic acid.* Journal of Photochemistry and Photobiology B: Biology, 2009. **95**(3): p. 170-176.

150. Livermore, L.J. et al. *Raman spectroscopy to differentiate between fresh tissue samples of glioma and normal brain: a comparison with 5-ALA–induced fluorescence-guided surgery.* Journal of Neurosurgery JNS, 2020: p. 1-11.
151. Horgan, C.C. et al. *Image-guided Raman spectroscopy probe-tracking for tumor margin delineation.* J Biomed Opt, 2021. **26**(3).
152. Horgan, C.C. et al. *Integrated photodynamic Raman theranostic system for cancer diagnosis, treatment, and post-treatment molecular monitoring.* Theranostics, 2021. **11**(4): p. 2006-2019.
153. Schaafsma, B.E. et al. *The clinical use of indocyanine green as a near-infrared fluorescent contrast agent for image-guided oncologic surgery.* J Surg Oncol, 2011. **104**(3): p. 323-32.
154. Egloff-Juras, C. et al. *NIR fluorescence-guided tumor surgery: new strategies for the use of indocyanine green.* Int J Nanomedicine, 2019. **14**: p. 7823-7838.
155. Carr, J.A. et al. *Shortwave infrared fluorescence imaging with the clinically approved near-infrared dye indocyanine green.* Proceedings of the National Academy of Sciences, 2018. **115**(17): p. 4465-4470.
156. Santos, I.P., et al., *Implementation of a novel low-noise InGaAs detector enabling rapid near-infrared multichannel Raman spectroscopy of pigmented biological samples.* Journal of Raman Spectroscopy, 2015. **46**(7): p. 652-660.
157. Santos, I.P., et al., *Raman Spectroscopic Characterization of Melanoma and Benign Melanocytic Lesions Suspected of Melanoma Using High-Wavenumber Raman Spectroscopy.* Anal Chem, 2016. **88**(15): p. 7683-8.
158. Santos, I.P., et al., *Improving clinical diagnosis of early-stage cutaneous melanoma based on Raman spectroscopy.* British Journal of Cancer, 2018. **119**(11): p. 1339-1346.
159. Pal, S., et al., *DNA-enabled rational design of fluorescence-Raman bimodal nanoprobes for cancer imaging and therapy.* Nature Communications, 2019. **10**(1): p. 1926.
160. Andreou, C., et al., *Imaging of Liver Tumors Using Surface-Enhanced Raman Scattering Nanoparticles.* ACS Nano, 2016. **10**(5): p. 5015-5026.
161. Wang, C., et al., *Advanced Nanotechnology Leading the Way to Multimodal Imaging-Guided Precision Surgical Therapy.* Advanced Materials, 2019. **31**(49): p. 1904329.


9

Chapter 9

Development of a near-infrared Raman spectroscopy setup compatible with fluorescence-guided surgery

Hamed Abbasi, Lorraine J. Lauwerends, Tom C. Bakker Schut, Inês P. Santos, Peter J. Caspers, Jose A.U. Hardillo, Senada Koljenović, Alexander L. Vahrmeijer, Robert J. Baatenburg de Jong, Stijn Keereweer, Gerwin J. Puppels

Analyst. 2023 Jun 12;148(12):2676-2682.

ABSTRACT

Near-infrared (NIR) fluorescence imaging using exogenous fluorescent agents provides whole-field images in real-time to assist the surgeon in the excision of a tumor. Although the method has high sensitivity, the specificity can sometimes be lower than expected. Raman spectroscopy can detect tumor with high specificity. Therefore, a combination of both techniques can be advantageous. A complication that must be addressed is that the NIR spectral region is favored by both techniques for (*in vivo*) tissue analysis. When fluorescence and Raman emissions spectrally overlap, it becomes challenging or impossible to detect the Raman signal. In this paper, by avoiding this overlap, we describe a Raman spectroscopy setup capable of recording high-quality Raman spectra from tissue containing NIR exogenous fluorescent agents. We identify an optimal wavelength interval (900 – 915 nm) for Raman excitation, which avoids both excitation of fluorescent dyes and Raman signal self-absorption by the tissue. In this way, Raman spectroscopy can be combined with the currently most-used NIR fluorescent dyes. This combined novel setup could pave the way for clinical trials benefiting from both fluorescence imaging and Raman spectroscopy to avoid positive margins in cancer surgery.

INTRODUCTION

Surgery with the aim to remove all tumor tissue is the main treatment modality for most solid cancers. Clear surgical margins are the main prognostic marker for survival in most cases, and inadequate resection generally necessitates adjuvant treatment, associated with increased morbidity, costs, and even mortality. Inadequate resection of the tumor frequently occurs, resulting in positive surgical margins [1]. Although preoperative imaging provides important information on tumor location, surgeons can only rely on visual inspection and palpation to determine the tumor border in the operating room (OR).

Intraoperative optical imaging can provide real-time feedback, aiding in tumor border identification. The combination of whole-field fluorescence-guided surgery (FGS) and Raman Spectroscopy (RS) can be ideal for this purpose [1-5]. FGS using exogenous tumor-specific fluorescent targeting agents has clinically demonstrated benefits for intraoperative margin assessment [6-12]. It facilitates real-time whole-field imaging of the complete surgical field at high sensitivity, but the signal interpretation is complex, and specificity is limited, especially for nonspecific agents. RS, on the other hand, can objectively differentiate between malignant and healthy tissues with high specificity at user-selected locations in the tissue [13-17]. Although these techniques can provide complementary information, they have traditionally been considered mutually exclusive because the low-intensity Raman signal can easily become undetectable in the presence of exogenous fluorophores.

To overcome the interference of intense fluorescence emission, several approaches have been developed, including photo-bleaching [18], confocal detection [19], surface-enhanced Raman spectroscopy (SERS) [20], shifted-excitation Raman difference spectroscopy (SERDS) [21-23], polarization-resolved signal detection [24], and time-resolved signal detection (time gating) [25-27]. However, if feasible, the most straightforward way is to avoid the overlap of the RS excitation wavelength and fluorophore absorption wavelengths [1]. This approach was used by Puppels et al. in 1993, where lymphocyte subpopulations were selected by means of fluorescence-activated cell sorting (FACS, 488 nm excitation), and Raman spectra were obtained with 660 nm laser excitation, thereby avoiding excitation of the fluorescent labels [28]. More recently, this approach was used to identify breast cancer from the water content in surgical samples containing patent blue dye. [29]. While RS using 680 nm laser excitation caused complete obscuration of the Raman signal by the fluorescence of the dye, 785 nm laser excitation allowed differentiation between tumor and healthy tissue in human breast tissue specimens.

Due to the low sensitivity of silicon-based CCD detectors for the wavelength range above 1000 nm, this approach remained mainly limited to the fluorescent materials that emit in the visible range (e.g., photosensitizers: PPIX, Verteporfin, and Temoporfin) [30-33]. In 2015, a novel low-noise InGaAs detector enabled the measurement of shot-noise limited Raman

spectra in the short-wave infrared (SWIR) region [34]. Excitation with a 976 nm laser allowed RS of otherwise highly fluorescent pigmented skin lesions suspected of melanoma [35]. However, this laser shifts Raman emission in the high wavenumber (HWN) spectral region to around 1.5 micron, where water has a significant absorption band, causing Raman signal absorption.

Tissue water content is an important discriminator between tumor and surrounding healthy tissue and therefore must be measured accurately [13, 36]. Therefore, an excitation wavelength long enough to avoid the absorption band of exogenous fluorescent agents whilst being short enough to avoid Raman signal absorption by the tissue is required, including the spectral region of the broad Raman water band between 3150 and 3800 cm^{-1}. This paper presents the implementation of a 909 nm HWN Raman setup which avoids the absorption band of the most used fluorescent agents and avoids significant tissue self-absorption of Raman signal, thus enabling high-quality Raman spectra measurements of highly fluorescent biological tissues. The performance of the developed setup was tested with phantoms and human tissues containing several exogenous fluorescent agents.

METHODS

RS systems

Three RS systems were used. The first system (hereafter referred to as 671 nm RS system) was a custom-built multichannel Raman module (RiverD International B.V., The Netherlands) equipped with a 671 nm laser (Crystalaser, CL671-150-SO). HWN Raman spectra were recorded in the interval from 2500 to 4000 cm^{-1} using a thermo-electrically cooled (–65 °C) back-illuminated deep depletion CCD (Andor iDus 401, DU401A BR-DD, Andor Technology Ltd., UK). The system was coupled to a fiber-optic needle probe (art photonics GmbH, Germany) described in [36].

The second system (hereafter referred to as 976 nm RS system) was an SWIR multichannel Raman instrument for measurements in the HWV spectral region, using 976 nm laser excitation [34].

In the third system (hereafter referred to as 909 nm RS system), the laser of the 976 nm RS system was replaced by a 909 nm laser (Model MDL-III-915L, CNI, China). The angle of the diffraction grating in the spectrometer (BaySpec Inc., San Jose, CA, USA) as well as the position of the detector (Cougar-640, Xenics, Leuven, Belgium) were adjusted to enable measurement of Raman spectra in the HWN spectral region excited by the 909 nm laser. Moreover, as compared to the setup described in [34], an optical fiber was added to the system. Figure 1 shows the schematic of the 909 nm RS system.

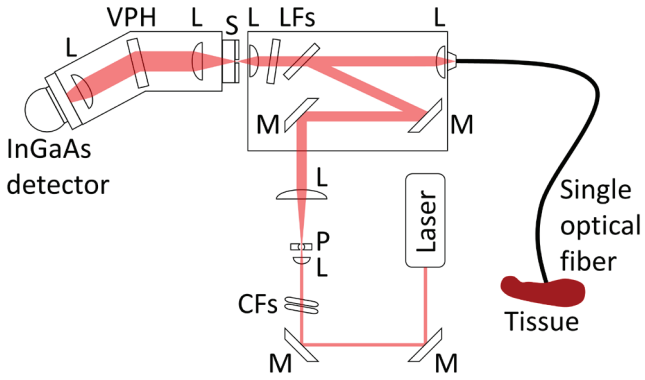

Figure 1. Schematic representation of the experimental setup (909 nm RS system). M: Mirror, CFs: Cleaning Filters, L: Lens, P: Pinhole, LFs: Longpass Filters, S: Slit, VPH: Volume Phase Holographic grating. Single optical fiber (multimode, fused silica, core: 100 µm) is used for guiding laser light to the tissue and scattered light back from the tissue. As compared to the 976 nm RS system, the spectral laser-cleaning filters and beam expander were changed to match the central wavelength and beam size of the new laser, respectively. A pinhole (diameter: 25 µm) was also added to the beam expander (Keplerian telescope) to spatially clean the laser beam. The slit was replaced with a wider slit (width: 100 µm) to avoid aliasing and also to increase the optical throughput of the system.

Fluorescence imaging systems

Three fluorescence imaging systems have been used in this study. The Quest Spectrum 2.0 (Quest Medical Imaging B.V.), hereafter referred to as the Quest camera, was used for intraoperative *in vivo* imaging in the OR during the resection. The Quest camera was also used for *ex vivo* imaging of resected tissues during residual tissue collection. The Pearl Trilogy (LI-COR Biosciences), hereafter referred to as the Pearl, and the Odyssey CLx Imager (LI-COR Biosciences), hereafter referred to as the Odyssey, were used for *ex vivo* imaging of collected tissues outside the OR.

Phantoms

An Intralipid 20% emulsion (Fresenius Kabi B.V., Netherlands) was used to compare 909 nm and 976 nm RS systems. Bovine serum albumin (BSA) phantoms with different water mass percentages containing exogenous fluorescent agents were prepared to examine the ability of the 909 nm RS system to determine the water mass percentages. These phantoms comprised of water, BSA (Sigma Chemical Co, USA), and one of three exogenous fluorescent agents, SGM-101, Methylene blue (MB), or Indocyanine green (ICG). MB and ICG are nonspecific fluorescent agent used in intraoperative fluorescence imaging. SGM-101 is a tumor-specific molecule that consists in a CEA-specific, chimeric monoclonal antibody conjugated to a NIR-emitting fluorochrome (BM104) [37, 38]. BSA mass percentages in the phantoms ranged between 2.5% and 25%, with 2.5% intervals. SGM-101, MB, and ICG were added to final concentrations of 1, 10, and 100 µg/ml to mimic the reported tissue concentrations of these agents in the tumor during trials of FGS [38-41]. Figure 2 shows the prepared phantoms.

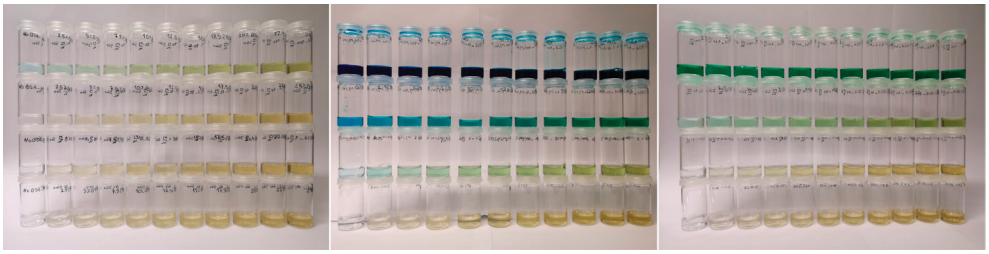

Figure 2. Prepared Phantoms: SGM-101 (left), MB (middle), and ICG (right). In each row of vials, from left to right, the water percentage is reduced from 100% to 75%, and the BSA percentage is increased from 0% to 25%. The bottom rows are blank solutions (no fluorescent agent). The bottom's second, third, and fourth rows have fluorescent agents' concentrations of 1 µg/mL, 10 µg/mL, and 100 µg/mL, respectively.

Specimen

Residual tissue (superfluous tissue after standard pathology procedures) was collected (without interfering with standard clinical procedures) from six patients with colorectal cancer who had undergone FGS. The study was approved by the local Ethics Review Committee (METC Erasmus MC: MEC-2019-0794), and conducted in full compliance with the laws and regulations of the Netherlands. All pieces of collected residual tissue were checked with the Quest camera for fluorescence signal. Raman measurements on fresh tissues were performed directly after the resection. Raman measurements on frozen tissues were performed after thawing.

RESULTS AND DISCUSSION

Amongst all currently clinically approved fluorescent agents and those under clinical development, ICG has the longest absorption wavelength [1]. The 976 nm RS system has an excitation wavelength that is more than 150 nm longer than the absorption peak of ICG. However, the 3150-3800 cm^{-1} spectral region of the Raman water band overlaps with the NIR water absorption peak between 1400 nm and 1500 nm. This leads to absorption of Raman signal in the tissue, which significantly affects the Raman spectrum. This is illustrated in Figure 3, which shows HWN Raman spectra of a phantom (intralipid 20%) collected with the 909 nm and 976 nm RS systems with comparable optical pathways through the sample. Both spectra were recorded using a single optical fiber with a sampling depth of about 250 µm [39]. It makes clear that in applications that aim to determine the water content of tissue, self-absorption of Raman signal must be taken into account and avoided to the extent possible by proper choice of laser excitation wavelength.

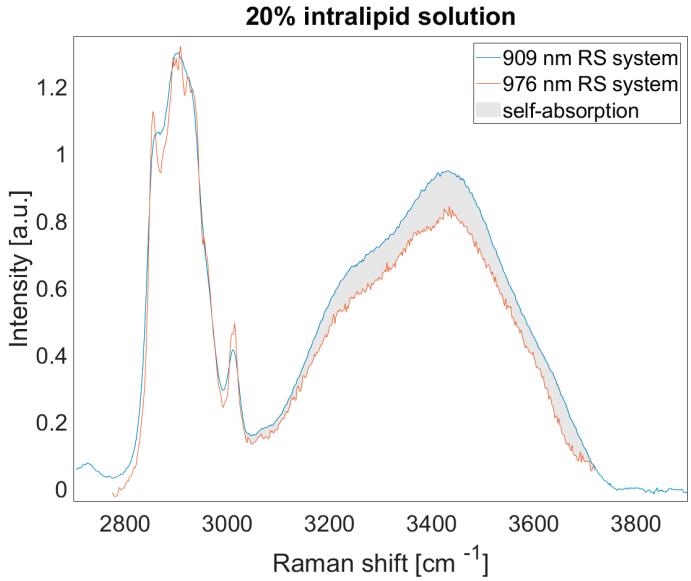

Figure 3. Intralipid 20% emulsion measured with 976 nm and 909 nm RS systems (normalized to the CH band). The difference between the observed intensities is mainly due to higher self-absorption of Raman photons excited by the 976 nm laser as compared to the 909 nm laser. The difference in the shape of the peak at the CH-stretching band is due to the wider slit used in the 909 nm RS system.

For the 909 nm RS system, the HWN Raman spectrum is below 1400 nm where water absorption is negligible. The ICG absorption peak is ca. 100 nm shorter than the laser wavelength of the 909 nm RS system; however, the tail of its absorption spectrum reaches the laser wavelength. Therefore, the amount of induced fluorescence in the 909 nm RS system is a function of agent concentration in the tissue. To assess if the induced fluorescence in the 909 nm RS system is negligible, the BSA phantom study was performed with various concentrations of SGM-101, MB, and ICG. Typically, a few milligrams of an agent are pre-operatively administered to the patient; however, a considerable amount of the administered dosage is cleared through the liver (excretion into bile and feces) and/or through the kidney (excretion into urine) [40]. Therefore, the absolute concentration of the agent in the target tissue is much lower than the administered dosage. For ICG and other agents (e.g., 5-ALA, and Cetuximab-800CW), absolute concentrations between 1 to 10 µg/mL are reported [41-44].

Figure 4 shows the result of the phantom study where the water concentration in mass percentage of the BSA phantoms was measured in the presence of SGM-101, MB, and ICG at different concentrations. The water concentration of the phantoms was calculated from the ratio of the OH and CH bands, as described by Caspers et al. [45]. The results of the phantom study showed that in the expected range for absolute concentration in the tissue, the 909 nm RS system can determine the water percentage with an absolute error below

1%. The absolute error was calculated as the difference between the calculated and actual percentages. Therefore, it can be concluded that the fluorescence interference in the 909 nm RS system is negligible.

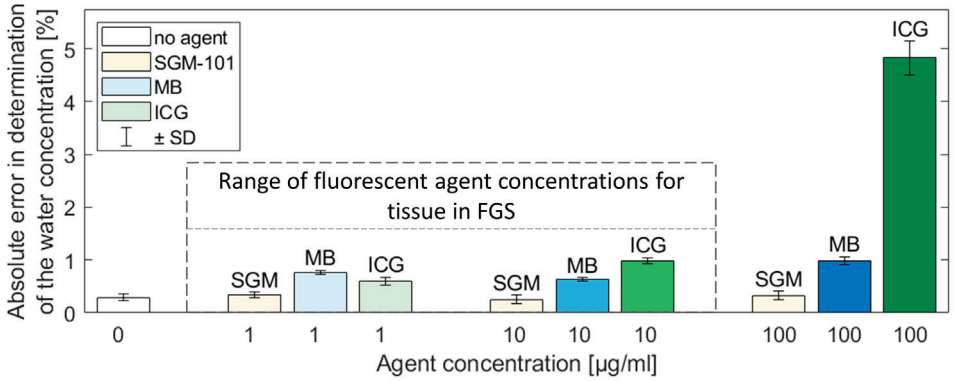

Figure 4. Absolute error in determining the water mass percentage in BSA-water phantoms containing different concentrations of SGM-101, MB, and ICG measured using 909 nm RS system. In the expected concentration of the fluorescent agent in the tissue during FGS, i.e., between 1 to 10 μg/ml, the 909 nm RS system can determine water mass percentage with an absolute error of less than 1% in all three examined fluorescent agents.

Table 1 presents the specification of the collected tissues from patients and the utilized experimental systems.

Table 1. specification of the collected tissues from patients and the utilized experimental systems.

Patient	Tissue type	Agent used in FGS	Fluorescence imaging channel	RS system (tissue condition)
1	colorectal	SGM-101	700 nm	909 nm (thawed)
2	colorectal	SGM-101	700 nm	909 nm (thawed)
3	omental flap (adipose)	ICG	800 nm	909 nm (fresh)
4	colorectal	cRGD-ZW800-1	800 nm	909 nm (thawed)
5	colorectal	ICG	800 nm	671 nm (fresh)
6	colorectal	cRGD-ZW800-1	800 nm	671 nm (fresh)

Figure 5 shows typical HWN Raman spectra measured with 909 nm RS system (top two rows) and 671 nm RS system (bottom row) of tissues resected from FGS containing different fluorescent agents. For each specimen, the measured spectrum including both Raman and fluorescence is shown in the left box, and the Raman spectrum after subtraction of the fluorescence background is shown in the right box. For tissues measured with the 671 nm RS system (Figure 5 g – i), the Raman signal to fluorescence ratio is very small. This makes proper fluorescence signal subtraction needed for interpretation of the Raman signal unreliable. The 671 nm RS system completely failed to present HWN Raman spectra from tissue containing ICG (g2). In h2 and i2 (cRGD-ZW800-1), the lipid/protein band is not well separated from the water band due to the intense fluorescence seen by the detector in the 671 nm RS system. For tissues measured with the 909 nm RS system (Figure 5 a – f) on the other hand, fluorescence signal background is virtually absent. For each spectrum, the ratio of Raman to fluorescence (R/F) in the CH-stretching band (2910 – 2966 cm^{-1}) is shown. In the spectra measured with the 909 nm RS system, R/F is a few thousand times greater than those measured with the 671 nm RS system.

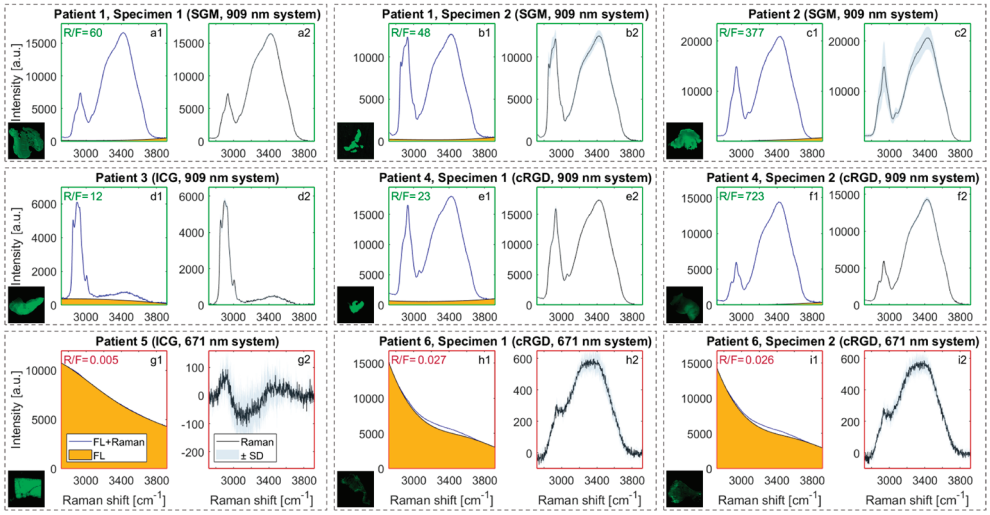

Figure 5. Raman spectra of resected tissues from patients treated with FGS using ICG, cRGD-ZW800-1, and SGM-101 measured with 909 nm RS system (a – f) and 671 nm RS system (g – i). For each specimen, a fluorescence image captured by Odyssey/Pearl is shown. Each shown spectrum (for both systems) is an average of 3 recorded spectra. The upper two rows (measured with 909 nm RS system) present very high signal quality.

Typical laser wavelengths used in clinical Raman spectroscopy are 514 nm, 532 nm, 671 nm, 785 nm, 830 nm, 976 nm, and 1064 nm [46, 47]. Figure 6 illustrates the overlap of the fingerprint and HWN Raman spectra of the above-mentioned laser wavelengths as well as the laser wavelength used in the current study (909 nm) with the absorption band of ICG, SGM-101, and water. Raman spectra recorded by lasers with wavelengths below 900 nm would increasingly suffer from intense signal background of fluorescent agents. Although

laser excitation wavelengths of 976 nm and higher have been shown to solve the problem of strong fluorescence signal background, its HWN Raman region overlaps with the water absorption peak between 1400 nm and 1500 nm leading to significant tissue self-absorption, which is difficult to correct for. Therefore, 909 nm is the optimal wavelength which avoids the absorption band of the most used fluorescent agents, including ICG, and avoids significant tissue self-absorption of Raman signal in both fingerprint and HWN regions.

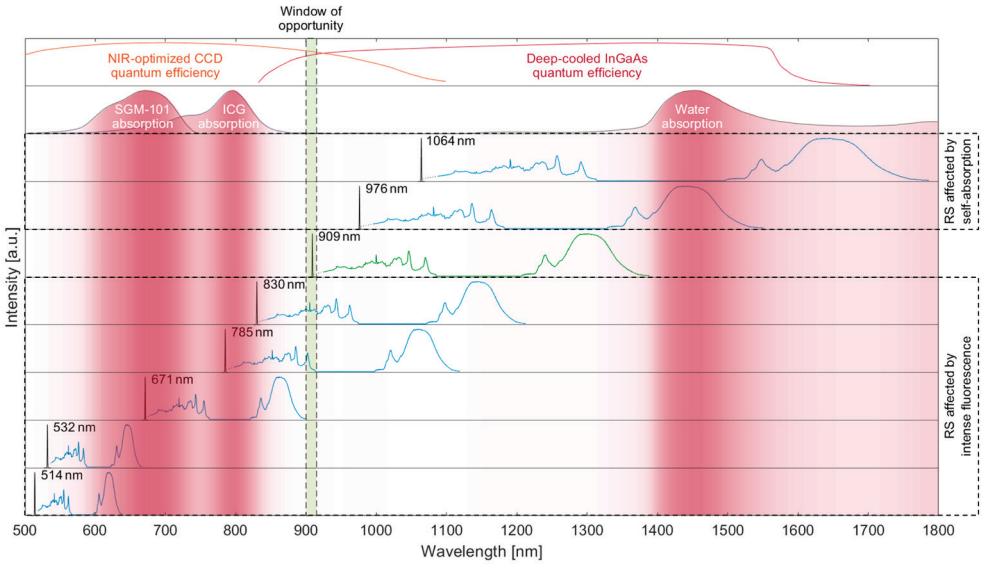

Figure 6. Overlap of Raman spectra excited with typical laser wavelengths used in clinical trials, i.e., 514 nm, 532 nm, 671 nm, 785 nm, 830 nm, 909 nm, 976 nm, and 1064 nm with absorption spectra of SGM-101, ICG, and water. A laser wavelength below ~900 nm overlaps with the absorption band of exogenous fluorescent agents (left red shaded zones) and consequently hinders Raman signal by photon shot noise originating from exogenous fluorescent agents. Excitation above ~915 nm shifts the HWN part of the Raman spectra toward higher water absorption (right red shaded zone), resulting in intense tissue self-absorption.

CONCLUSIONS

We demonstrated the first fiber-optic RS setup capable of acquiring high-quality Raman spectra from the resected tumor tissue containing exogenous NIR fluorescent agents (including ICG). High-quality Raman spectra are obtained due to high Raman signal to fluorescence signal ratio. In this setup, the Raman excitation wavelength does not overlap with the absorption band of most used exogenous fluorescent agents, nor does the Raman emission wavelength overlap with the water absorption band, therefore avoiding intense exogenous fluorescence and Raman signal absorption, respectively. In the rapidly growing field of FGS, the complementary information provided by RS can be the long-sought answer to dealing with many of the limitations as described by Keereweer et al [40]. This novel setup opens the door to clinical trials benefiting from the complementary use of FGS and RS with the goal of avoiding positive margins in cancer surgery.

REFERENCES

1. Lauwerends, L.J., et al., *The complementary value of intraoperative fluorescence imaging and Raman spectroscopy for cancer surgery: combining the incompatibles.* European Journal of Nuclear Medicine and Molecular Imaging, 2022. **49**: p. 2364–2376.
2. Brouwer de Koning, S.G., et al., *Assessment of the deep resection margin during oral cancer surgery: A systematic review.* European Journal of Surgical Oncology, 2021.
3. Balasundaram, G., et al., *Biophotonic technologies for assessment of breast tumor surgical margins—A review.* Journal of Biophotonics, 2021. **14**(1): p. e202000280.
4. Lauwerends, L.J., et al., *Current Intraoperative Imaging Techniques to Improve Surgical Resection of Laryngeal Cancer: A Systematic Review.* Cancers, 2021. **13**(8): p. 1895.
5. Heidkamp, J., et al., *Novel imaging techniques for intraoperative margin assessment in surgical oncology: A systematic review.* International Journal of Cancer, 2021. **149**(3): p. 635-645.
6. Schaafsma, B.E., et al., *The clinical use of indocyanine green as a near-infrared fluorescent contrast agent for image-guided oncologic surgery.* Journal of surgical oncology, 2011. **104**(3): p. 323-32.
7. van Dam, G.M., et al., *Intraoperative tumor-specific fluorescence imaging in ovarian cancer by folate receptor-alpha targeting: first in-human results.* Nature medicine, 2011. **17**(10): p. 1315-9.
8. Vahrmeijer, A.L., et al., *Image-guided cancer surgery using near-infrared fluorescence.* Nature reviews. Clinical oncology, 2013. **10**(9): p. 507-18.
9. Handgraaf, H.J.M., et al., *Real-time near-infrared fluorescence imaging using cRGD-ZW800-1 for intraoperative visualization of multiple cancer types.* Oncotarget, 2017. **8**(13): p. 21054-21066.
10. Boogerd, L.S.F., et al., *Safety and effectiveness of SGM-101, a fluorescent antibody targeting carcinoembryonic antigen, for intraoperative detection of colorectal cancer: a dose-escalation pilot study.* Lancet Gastroenterol Hepatol, 2018. **3**(3): p. 181-191.
11. Lauwerends, L.J., et al., *Real-time fluorescence imaging in intraoperative decision making for cancer surgery.* The Lancet Oncology, 2021. **22**(5): p. e186-e195.
12. Mieog, J.S.D., et al., *Fundamentals and developments in fluorescence-guided cancer surgery.* Nature Reviews Clinical Oncology, 2022. **19**(1): p. 9-22.
13. Barroso, E.M., et al., *Discrimination between oral cancer and healthy tissue based on water content determined by Raman spectroscopy.* Anal Chem, 2015. **87**(4): p. 2419-26.
14. Liao, Z., et al., *Feasibility of integrated high-wavenumber Raman imaging and fingerprint Raman spectroscopy for fast margin assessment in breast cancer surgery.* Journal of Raman Spectroscopy, 2020. **51**(10): p. 1986-1995.
15. Pence, I.J., et al., *Discrimination of liver malignancies with 1064 nm dispersive Raman spectroscopy.* Biomed Opt Express, 2015. **6**(8): p. 2724-37.
16. Thomas, G., et al., *Evaluating feasibility of an automated 3-dimensional scanner using Raman spectroscopy for intraoperative breast margin assessment.* Sci Rep, 2017. **7**(1): p. 13548.
17. Haifler, M., et al., *Discrimination of malignant and normal kidney tissue with short wave infrared dispersive Raman spectroscopy.* J Biophotonics, 2018. **11**(6): p. e201700188.
18. Wang, H., et al., *Improving skin Raman spectral quality by fluorescence photobleaching.* Photodiagnosis and Photodynamic Therapy, 2012. **9**(4): p. 299-302.
19. Puppels, G.J., et al., *Description and performance of a highly sensitive confocal Raman microspectrometer.* Journal of Raman Spectroscopy, 1991. **22**(4): p. 217-225.
20. Kagan, M.R. and R.L. McCreery, *Reduction of Fluorescence Interference in Raman*

Spectroscopy via Analyte Adsorption on Graphitic Carbon. Analytical Chemistry, 1994. **66**(23): p. 4159-4165.
21. Martins, M.A.d.S., et al., *Shifted-excitation Raman difference spectroscopy for in vitro and in vivo biological samples analysis.* Biomedical Optics Express, 2010. **1**(2): p. 617-626.
22. Cordero, E., et al., *Evaluation of Shifted Excitation Raman Difference Spectroscopy and Comparison to Computational Background Correction Methods Applied to Biochemical Raman Spectra.* Sensors, 2017. **17**(8): p. 1724.
23. Korinth, F., et al., *Assessment of shifted excitation Raman difference spectroscopy in highly fluorescent biological samples.* Analyst, 2021. **146**(22): p. 6760-6767.
24. Angel, S.M., et al., *Computer-controlled instrument for the recovery of a resonance Raman spectrum in the presence of strong luminescence.* Analytical Chemistry, 1984. **56**(14): p. 3000-3001.
25. Matousek, P., et al., *Fluorescence suppression in resonance Raman spectroscopy using a high-performance picosecond Kerr gate.* Journal of Raman Spectroscopy, 2001. **32**(12): p. 983-988.
26. Martyshkin, D.V., et al., *Effective suppression of fluorescence light in Raman measurements using ultrafast time gated charge coupled device camera.* Review of Scientific Instruments, 2004. **75**(3): p. 630-635.
27. Ksantini, N., et al., *Time-gated interferometric detection increases Raman scattering to fluorescence signal ratio in biological samples.* Journal of Biophotonics, 2022. **15**(1): p. e202100188.
28. Puppels, G.J., et al., *Carotenoids located in human lymphocyte subpopulations and natural killer cells by Raman microspectroscopy.* Cytometry, 1993. **14**(3): p. 251-256.
29. Hubbard, T.J.E., et al., *Utilization of Raman spectroscopy to identify breast cancer from the water content in surgical samples containing blue dye.* Translational Biophotonics, 2021. **3**(2): p. e202000023.
30. Horgan, C.C., et al., *Integrated photodynamic Raman theranostic system for cancer diagnosis, treatment, and post-treatment molecular monitoring.* Theranostics, 2021. **11**(4): p. 2006-2019.
31. Horgan, C., et al., *Image-guided Raman spectroscopy probe-tracking for tumor margin delineation.* Journal of Biomedical Optics, 2021. **26**(3): p. 036002.
32. Grimbergen, M.C.M., et al., *Raman spectroscopy of bladder tissue in the presence of 5-aminolevulinic acid.* Journal of Photochemistry and Photobiology B: Biology, 2009. **95**(3): p. 170-176.
33. Livermore, L.J., et al., *Raman spectroscopy to differentiate between fresh tissue samples of glioma and normal brain: a comparison with 5-ALA–induced fluorescence-guided surgery.* Journal of Neurosurgery, 2021. **135**(2): p. 469-479.
34. Santos, I.P., et al., *Implementation of a novel low-noise InGaAs detector enabling rapid near-infrared multichannel Raman spectroscopy of pigmented biological samples.* Journal of Raman Spectroscopy, 2015. **46**(7): p. 652-660.
35. Santos, I.P., et al., *Raman Spectroscopic Characterization of Melanoma and Benign Melanocytic Lesions Suspected of Melanoma Using High-Wavenumber Raman Spectroscopy.* Analytical Chemistry, 2016. **88**(15): p. 7683-7688.
36. Aaboubout, Y., et al., *Intraoperative assessment of resection margins by Raman spectroscopy to guide oral cancer surgery.* Submitted, 2022.
37. Framery, B., et al., *Toxicity and pharmacokinetic profile of SGM-101, a fluorescent anti-CEA chimeric antibody for fluorescence imaging of tumors in patients.* Toxicology Reports, 2019. **6**: p. 409-415.
38. Gutowski, M., et al., *SGM-101: An innovative near-infrared dye-antibody conjugate that targets CEA for fluorescence-guided surgery.* Surgical Oncology, 2017. **26**(2): p. 153-162.
39. Santos, I., *Improving Clinical Diagnosis of Melanocytic Skin Lesions by Raman*

Spectroscopy. 2018, Erasmus University Rotterdam.

40. van der Vorst, J.R., et al., *Near-infrared fluorescence sentinel lymph node mapping of the oral cavity in head and neck cancer patients.* Oral Oncol, 2013. **49**(1): p. 15-9.
41. Leiloglou, M., et al., *Tissue texture extraction in indocyanine green fluorescence imaging for breast-conserving surgery.* Journal of Physics D: Applied Physics, 2021. **54**(19): p. 194005.
42. Johansson, A., et al., *5-Aminolevulinic Acid-induced Protoporphyrin IX Levels in Tissue of Human Malignant Brain Tumors.* Photochemistry and Photobiology, 2010. **86**(6): p. 1373-1378.
43. Koch, M., P. Symvoulidis, and V. Ntziachristos, *Tackling standardization in fluorescence molecular imaging.* Nature Photonics, 2018. **12**(9): p. 505-515.
44. Voskuil, F.J., et al., *Fluorescence-guided imaging for resection margin evaluation in head and neck cancer patients using cetuximab-800CW: A quantitative dose-escalation study.* Theranostics, 2020. **10**(9): p. 3994-4005.
45. Caspers, P.J., et al., *In Vivo Confocal Raman Microspectroscopy of the Skin: Noninvasive Determination of Molecular Concentration Profiles.* Journal of Investigative Dermatology, 2001. **116**(3): p. 434-442.
46. Santos, I.P., et al., *Raman spectroscopy for cancer detection and cancer surgery guidance: translation to the clinics.* Analyst, 2017. **142**(17): p. 3025-3047.
47. Paraskevaidi, M., et al., *Clinical applications of infrared and Raman spectroscopy in the fields of cancer and infectious diseases.* Applied Spectroscopy Reviews, 2021. **56**(8-10): p. 804-868.


10

Chapter 10

Optimizing Tumor Resection: The Added Value of Raman Spectroscopy in Fluorescence-Guided Cancer Surgery

Lorraine J. Lauwerends, Bo E. Zweedijk, Senada Koljenović, Sjors A. Koppes, Michail Doukas, Bernd Kremer, José. A.U. Hardillo, Cornelis Verhoef, Alexander L. Vahrmeijer, Robert J. Baatenburg de Jong, Denise E. Hilling, Stijn Keereweer, Hamed Abbasi

Submitted for publication

ABSTRACT

Wide-field fluorescence imaging (FI) using near-infrared (NIR) tumor-targeted tracers such as cRGD-ZW800-1 and SGM-101 highlights resection margins in oral squamous cell carcinoma (OSCC) and rectal cancer, but cannot reliably quantify margin distance and is prone to false- positives from tracer uptake in non-malignant tissue. Depth profiling with Raman spectroscopy (RS) using a needle probe addresses these limitations via local, point-based tissue characterization. We integrated ex vivo RS depth profiling with fluorescence-guided margin assessment in 19 patients (13 OSCC, 6 rectal cancer; 344 Raman spectra). Two spectral biomarkers, OH-stretching percentage and the CH2/CH3 ratio (reflecting water content and lipid- to-protein ratio, respectively), differed significantly between malignant and healthy tissue in both cancer types ($p<0.001$), and a principal component analysis-based classifier differentiated malignant from healthy tissue with 100% accuracy. RS depth profiling quantified margin distance in millimeters, matching final histopathology, and correctly classified fluorescent non-malignant tissues (gingiva, salivary gland, lymph nodes, and fatty tissue) as normal, resolving false-positive FI signals. Combining RS's depth-resolved specificity with FI's wide-field visualization improved intraoperative margin assessment beyond either modality alone. This study demonstrates the clinical feasibility of integrating RS with FI, and holds promise for improving surgical precision and patient outcomes in cancer surgery.

INTRODUCTION

Solid cancers pose significant challenges in precision surgery, where achieving adequate resection margins is critical for improving patient outcomes. Inadequate margins remain a common issue across various solid tumors, adversely affecting survival rates, requiring additional treatment and therefore necessitating advancements in intraoperative assessment techniques. For instance, oral squamous cell carcinoma (OSCC) frequently presents with inadequate margins in >50% of cases, highlighting the pressing need for more precise surgical tools [1,2]. Our previous research demonstrated that near-infrared (NIR) fluorescence imaging (FI) with cRGD-ZW800-1, a tumor- targeting agent binding to integrin, could effectively identify tumor tissues and inadequate margins, even those overlooked during routine intraoperative assessments by surgeon and pathologist [3].

Similarly, locally advanced and recurrent rectal cancer exemplifies the intraoperative difficulties faced by surgeons. Challenges in distinguishing malignant from benign tissue are particularly pronounced after neoadjuvant therapy, where reduced tumor visibility can lead to either unnecessary resection of healthy tissue or incomplete removal of malignancies. The use of NIR FI with SGM-101, a tumor-targeting agent binding to carcinoembryonic antigen (CEA), has shown promise in addressing these challenges. (Pre-)clinical studies have demonstrated SGM-101's ability to delineate tumors, detect millimeter-sized nodules, and improve surgical outcomes by identifying primary, recurrent, and metastatic lesions, resulting in altered treatment plans and more precise resections [4-7].

Integrating NIR FI with tumor-specific fluorescent agents into surgical practice offers significant potential to improve the precision of tumor resections, thereby enhancing patient survival and quality of life. However, FI has two key limitations that this study addresses. First, FI provides no direct information about tumor depth, since fluorescence intensity (measured in the arbitrary unit of camera counts) is influenced by tissue optical properties and does not reliably indicate how far a tumor lies from the resection surface. Second, it is prone to false positives, since FI can be confounded by fluorescence arising from non-malignant tissues located near or within the resection margin, whose signal can spatially overlap with tumor-derived fluorescence and cannot be reliably resolved by wide-field FI alone. The extent and cause of this overlap depend on the tumor-specific tracer and cancer type: in OSCC, cRGD-ZW800-1 uptake in the gingiva (junctional epithelium), salivary gland tissue, and lymph nodes can produce ambiguous fluorescence [3], while in rectal cancer, CEA-positive histiocytes within lymph nodes or fluorescence associated with fibrotic or chronically inflamed tissue can similarly yield ambiguous SGM-101 fluorescence [6]. Raman spectroscopy (RS) addresses these limitations through label-free, depth-specific tissue characterization based on molecular vibrations [8]. Our recently developed short-wave infrared (SWIR) RS system maintains this capacity even in fluorescent agent presence and, using a needle probe, assesses tissue at specific depths [8-10]. Because RS characterizes tis-

sue by its intrinsic molecular composition rather than tracer uptake, the Raman needle probe can both localize the true depth of the tumor and discriminate malignant from healthy tissue at fluorescent sites, resolving ambiguities that FI alone cannot address. The integration of RS into the FI framework could, therefore, represent a significant advancement in oncological surgery, offering a more nuanced and comprehensive approach to margin assessment.

This study evaluates the clinical impact of integrating RS with FI to improve the precision of margin assessment during OSCC and rectal cancer surgeries. First, by incorporating the Raman needle probe for depth profiling, we measure the exact distance from cut surface to any residual tumor to address the depth/adequacy limitation of FI. Second, we examine RS's capacity to discern fluorescence in non-malignant tissues such as the gingiva, salivary glands, and lymph nodes – areas where FI alone may present ambiguities – to mitigate false positives. In other words, we aim to combine the sensitivity of FI with the specificity of RS, while delivering these data rapidly enough to inform real-time surgical decisions. This study aims to establish the clinical feasibility of this integrated approach, facilitating further validation of its potential to enhance margin identification and, ultimately, contribute to improved oncological outcomes among multiple cancer types.

METHODS

Ethical approval

This clinical study was performed on oral tissue resected from patients included in the Guided By Light clinical trial registered in the European Clinical Trials Database (*EudraCT 2019-003416-30*) and ClinicalTrials.gov (*NCT04191460*), as well as rectal tissue resected from patients included in the SGM-LARRC trial registered in the European Clinical Trials Database (*EudraCT 2019-001748-23*) and ClinicalTrials.gov (*NCT04642924*). The study was approved by the local Ethics Review Committee (*METC Erasmus MC: MEC-2019-0794*), and conducted in full compliance with the principles of the Declaration of Helsinki of 1975, and the laws and regulations of the Netherlands. Written informed consent was obtained from patients.

Patients

Patients (male and female, 18 years or older) diagnosed with oral cavity squamous cell carcinoma (OSCC) at the Erasmus Medical Center (Rotterdam, The Netherlands) received 0.01–0.05 mg/kg of NIR fluorescent tracer (cRGD-ZW800-1, a zwitterionic, integrin-targeted fluorescent agent [15, 16] approximately 18 hours before surgery. Eligible OSCC patients underwent surgical removal of the tumors based on the specimen-driven intraoperative assessment of resection margin (IOARM) procedure, which is uniquely standard-of-care to the Erasmus Medical Center [17].

Eligible patients (male and female, 18 years or older) diagnosed with (recurrent) rectal cancer at the Erasmus Medical Center (Rotterdam, The Netherlands) received 10 mg of NIR fluorescent tracer (SGM-101, a fluorescent antibody targeting carcinoembryonic antigen (CEA)) about 4 days before surgery and underwent surgical removal of the tumors.

Fluorescence imaging

The procedure for open-field *in vivo* and closed-field *ex vivo* FI of the oral tissue is described elsewhere in detail [3]. In short, the tumor area was imaged *in vivo* before and after resection (imaging the wound bed for possible residual tumor). After removing the OSCC tumor, the resected specimen was imaged from different angles using a close-field FI system, as pictured in Figure 1 (*Pearl Trilogy, by LI-COR Biosciences*). The regions of highest fluorescence on the deep margin were marked in the software of the imaging system (i.e., the sentinel margin approach [14, 18]). Subsequently, the surgeon and pathologist (initially blinded to the fluorescence signal) performed the IOARM for OSCC patients. If required, the tissue was inked on the resection surface before cutting the specimen during IOARM. After IOARM, specimens were selected for RS. Specimens fully covered with ink were excluded from Raman spectroscopy (RS) analysis, while partially inked (for the purposes of this study) specimens were included. Following final histopathological processing, tissue slides were scanned using a flatbed FI system (Odyssey M, LI-COR Biosciences Inc., Nebraska, USA). The procedure for open-field *in vivo* FI of rectal tissue mirrored that used for oral tissue. However, closed-field *ex vivo* FI for fresh rectal tissue was often omitted, as the resected specimens were typically larger than the field-of-view of the closed-field imager (Pearl Trilogy, LI-COR Biosciences).

Raman spectroscopy

The RS instrument used in this study was a combination of a NIR-II/SWIR Raman spectrometer previously developed in-house specifically for tandem use with fluorescence-guided surgery (FGS) [9] and a Raman needle probe (by RiverD International B.V. the Netherlands) described in detail elsewhere [8]. In short, a BaySpec spectrometer (BaySpec Inc., USA) equipped with a volume phase holographic (VPH) grating and a 100 μm entrance slit, and an InGaAs detector (Cougar-640, Xenics, Belgium) was used. The Raman spectrometer utilized an excitation at 909 nm (laser: Model MDL-III-915L, CNI, China) and recorded the high wavenumber region (2714–3918 cm–1; OH, CH2, and CH3 stretching bands); and the Raman needle probe consisted of an optical fiber with a conical tip (Figure S1 (supplementary data)) mounted on a motorized translation stage used to drive the needle probe into the tissue under investigation. The laser power at the sample was around 100 mW. This excitation wavelength (909 nm) was selected to avoid fluorophore excitation (peak ~800 nm) and to minimize tissue absorption while maintaining adequate Raman signal intensity. Targeting the high-wavenumber region captures diagnostically relevant CH and OH vibrations and reduces interference from residual fluorescence background. The needle probe was also equipped with a vacuum system to apply negative pressure, preventing tissue deforma-

tion during the needle insertion. The integration time was fixed at 10 s per spectrum for all local surface measurements and depth-resolved measurements in both the OSCC and rectal cancer cohorts. Areas marked during the *ex vivo* closed-field FI or IOARM were measured with the Raman instrument in two modes:

- Local measurement, with the goal of differentiating areas with true positive fluorescence signal (originating from the tumor) and areas with false positive fluorescence signal (e.g., originating from non-tumor gingiva tissue with high integrin expression).
- Depth profiling measurement, with the goal of measuring the resection margin. The definition of a tumor-negative (adequate/clear) surgical margin varies depending on the tumor type [16]. In colorectal cancer, an adequate margin is defined as the absence of tumor cells within 1 mm of the cut surface [17]. For OSCC, a margin greater than 5 mm is considered adequate, 1 to 5 mm is classified as close, and less than 1 mm is deemed positive [18]. For measurements in depth, the Raman needle probe was held perpendicular to the surface, driven inside the tissue, and every 0.5 or 1 mm, a new spectrum was recorded until the depth of ~10 mm (Figure 1). As each spectrum was acquired locally at the needle tip, the ~10 mm depth range reflects mechanical translation of the probe rather than optical penetration.

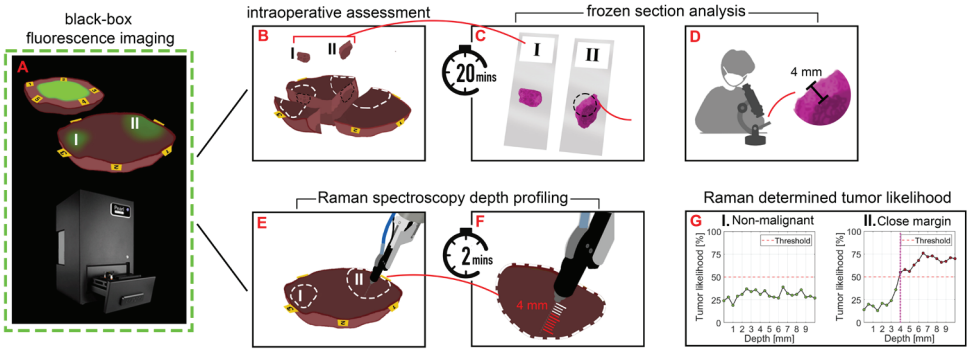

Figure 1. Study protocol. The upper row shows the standard sentinel margin approach, and the bottom row shows the alternative performed in this study. As part of our clinical study for fluorescence imaging in head and neck cancer, closed-field fluorescence imaging of the specimen from different angles was performed, marking the areas of highest fluorescence in the software (A). Then, routine intraoperative assessment of the resection margins was performed by the (blinded) pathologist and surgeon (B). Subsequently, the areas of highest fluorescence were disclosed, potentially leading to frozen section analysis of these areas (C,D). This process takes ca. 20–40 minutes. With Raman spectroscopy depth profiling (E,F), the Raman needle probe is used to perform local or depth profiling (pictured in F, with the Raman needle fully (~10 mm) inserted into the tissue) measurements in the areas of highest fluorescence (A-I and A-II). This process takes an additional ca. 2 minutes, with the resulting Raman measurements (G) informing directly on tumor presence and/or margin width, which are finally correlated with H&E histopathology (D) and fluorescence images. *H&E: Hematoxylin and Eosin.*

The Raman instrument was calibrated daily. Raman measurements were performed immediately after IOARM in a room with ceiling lighting comprised of LED lamps without NIR/SWIR emissions. Therefore, measurements were performed with room light on without any interference with the collection of Raman spectra. After Raman measurement, the location of a measurement was marked by inserting a pin inside the tissue on the measurement location. The pin location served as the reference point for histopathological annotation afterwards. The tissue, together with the marking pin, was put in the formalin for fixation overnight (or over the weekend, depending on the day of surgery). After fixation, tissue was cut into bread loaves, and a superficial straight incision was made on the marking pin position for the histological annotation. This incision provided a continuous structural landmark that is more robust to shrinkage-related displacement than a pin mark alone. In one case, the marking pin was removed before cutting the tissue into bread loaves, and therefore, no incision line was created afterwards. In this case, the relevant margin described in the pathology report was used to label the RS data points, for the rest, the following procedure was used to label the RS data points. Tissue slides were stained with Hematoxylin and Eosin (H&E) and were digitally scanned with a virtual microscope (*Nanozoomer 2.0 HT, Hamamatsu Photonics, Shizuoka, Japan*) and later were digitally (*using NDP.view2 Viewing software by Hamamatsu Photonics, Shizuoka, Japan*) annotated by experienced pathologists. Finally, the RS trajectory was correlated with H&E histopathology (Figure 1) and the fluorescent signal. If the RS trajectory was not visible on the H&E slide directly cut from the top side of the paraffin block, deeper sections were cut and stained with H&E to locate the RS trajectory.

Statistical analysis

Raw measured data were preprocessed and analyzed using an in-house developed MATLAB (*version 2022b, Mathworks, Natick, MA, USA*) code. Recorded raw spectra were first calibrated for intensity and wavenumber. After calibration, the background signal of the system was subtracted from each calibrated spectrum. Any remaining fluorescence background signal was fitted with a 3rd-order polynomial to separate Raman from residual fluorescence. Later, each spectrum was normalized on the CH band, and the following two parameters were calculated for each spectrum: CH_2/CH_3 ratio (intensity of 2852–2884 cm^{-1} divided by that of 2910–2966 cm^{-1}), and OH (3350–3550 cm^{-1}) percentage, expressed in grams of water per 100 grams of wet tissue, calculated using of a method developed by Caspers et al. [22] and described in detail in previous studies [23-25]. The former is indicative of the lipid-to-protein ratio, and the latter indicates the water concentration. Later, each Raman spectrum was labelled "normal" or "tumor" based on the final histopathology. Following labelling of all spectra, the median and mean (± standard deviation) of both CH_2/CH_3 ratio and OH percentage for each group (normal/tumor, oral/rectal/combined) were calculated, and a statistical test (Mann-Whitney U test) was employed to calculate the p-value and figure out if there was a significant difference between the CH_2/CH_3 ratio and OH percentage of the normal and tumor group.

Additionally, principal component analysis (PCA) was performed to reduce the dimensionality of the data while preserving as much variance as possible in the dataset. PCA transforms correlated variables into a smaller number of uncorrelated variables, known as principal components (PCs), which capture the dominant patterns in the data. The PCs required to explain 95% of the data's variability were kept for further analysis. Data were projected into this lower-dimensional PC space.

To distinguish between tumor and normal tissue, a threshold referred to as *tumor likelihood* was defined based on the first principal component (PC1). This threshold was determined to have an equal distance between the mean of the normal and tumor data points projected into PC1. For visualization, PC1 scores were linearly rescaled to a tumor likelihood percentage covering the range of observed PC1 scores. The lower limit (0%) was defined as the minimum PC1 score minus one unit, while the upper limit (100%) was positioned symmetrically around the classification threshold, ensuring that the threshold corresponded to 50%. Data points with tumor likelihood below 50% were classified as normal, and those above 50% were classified as tumor.

Later, the whole PCA procedure and tumor likelihood threshold determination were performed separately on the oral and rectal datasets. The tumor likelihood threshold trained on the oral dataset was used for validation in the rectal dataset and vice versa. The data partitioning was performed at the cancer-type level, with no overlap between training and validation datasets. Sensitivity and specificity of the validation dataset were calculated for the developed classification method.

RESULTS

Resection specimens from 19 patients (n = 13 for OSCC; n = 6 for rectal cancer) were included in this study, with multiple measurement locations per patient (n = 23 for OSCC; n = 11 for rectal cancer). Most RS measurements were performed in depth profiling mode, creating trajectories within the tissue (n = 15 for OSCC; n = 10 for rectal cancer). In some cases, local measurements were performed, resulting in pointwise local data (n = 8 for OSCC; n = 1 for rectal cancer). In total, 344 Raman spectra (n = 216 for OSCC; n =128 for rectal cancer) were recorded, of which 86 spectra (n = 74 for OSCC; n = 12 for rectal cancer) were labeled as tumor and 258 spectra (n = 142 for OSCC; n =116 for rectal cancer) were labeled as normal, based on final histopathology. Of the 344 Raman spectra acquired, 299 were obtained through depth-resolved measurements and 45 through local surface measurements. Patient and study characteristics are summarized in Table 1.

Table 1. Study characteristics

		Clinical information		Raman spectroscopy			
Tracer and cancer type	**#**	**Tumor site (gender)**	**T-stage**	**Measurement # and trajectory**	**Margin width with Raman**	**Margin based on histo-pathology[§]**	**Fluorescent false-positive differentiation**
cRGD-ZW800-1 for oral cancer	1	Lateral tongue (f)	pT3	1 local	N/A[¶]	N/A[¶]	
	2	Posterior tongue (m)	pT3	2 depth profiling	0–1 mm 1–2 mm	0.8 mm 1.9 mm	
	3	Lateral tongue (m)	pT2	1 depth profiling	8–9 mm	8.1 mm	
	4	Retromolar trigone (m)	pT4	2 depth profiling	10^{+} mm 1–2 mm	10^{+} mm 1.6 mm	
	5	Lateral tongue (m)	pT1	1 depth profiling	9^{+} mm	9^{+} mm	Salivary gland
	6	Lateral tongue (m)	pT4	3 depth profiling	7–8 mm 10^{+} mm 1–2 mm	7.3 mm 10^{+} mm 1.4 mm	
	7	Floor of mouth (m)	pT3	2 depth profiling	6–7 mm 10^{+} mm	6.2 mm 10^{+} mm	
	8	Alveolar process (f)	pT1	1 depth profiling	9^{+} mm	9^{+} mm	Lymph node
	9	Buccal mucosa, mandibula (m)	pT2	1 depth profiling	10^{+} mm	10^{+} mm	
	10	Alveolar process (m)	pT4a	6 local	N/A[¶]	N/A[¶]	Gingiva
	11	Lateral tongue (m)	pT2	1 depth profiling	5.5–6 mm	5.6 mm	
	12	Lateral tongue (m)	pT3	1 depth profiling	4–4.5 mm	4.3 mm	
	13	Lateral tongue (f)	pT1	1 local	N/A[¶]	N/A[¶]	
				23 total			
SGM-101 for rectal cancer	14	Rectum (f)	ypT3	2 depth profiling	8–9 mm 10^{+} mm	8.4 mm 10^{+} mm	
	15	Rectum (f)	N/A[*]	1 local	N/A[¶]	N/A[¶]	

Table 1. Study characteristics (*continued*)

	Clinical information		Raman spectroscopy			
16	Rectum (f)	ypT3	3 depth profiling	9⁺ mm 4–5 mm 3–4 mm	9⁺ mm 4.3 mm 3.1 mm	
17	Rectum (m)	ypT1-2	1 depth profiling	9⁺ mm	9⁺ mm	
18	Rectum (f)	N/A*	2 depth profiling	10⁺ mm 10⁺ mm	10⁺ mm 10⁺ mm	
19	Rectum (m)	ypT2	2 depth profiling	10⁺ mm 10⁺ mm	10⁺ mm 10⁺ mm	Fat tissue
			11 total			

* recurrent rectal cancer

¶ margin was not measured in local measurements

§ margin at the location where the Raman needle was inserted

⁺ no deeper measurement was performed

Raman Spectroscopy for Differentiating Tumor and Normal Tissue in the Presence of a Fluorescent Agent

Intensity-normalized Raman spectra (Figure 2A–C) revealed key differences between tumor and normal tissues. Tumor tissues exhibited significantly higher intensity in the OH-stretching region (3350–3550 cm^{-1}), reflecting increased water concentration, compared to normal tissues. Conversely, the CH_2/CH_3 ratio was lower in tumor spectra, indicating a reduced lipid-to-protein content. These findings were consistent across both oral and rectal cancer tissues. To evaluate whether OH% and CH_2/CH_3 ratios exhibit consistent discriminatory power across distinct cancers, oral and rectal datasets were also analyzed in combination. This combined analysis aimed to assess the robustness and generalizability of RS parameters independent of tumor type, supporting its potential as a broadly applicable tool. The OH-stretching percentage (OH%) and CH_2/CH_3 ratios were quantitatively assessed (Table 2), and the results are visually summarized in histograms (Figure 2D–I). Tumor tissues consistently showed statistically significant higher OH% values and lower CH_2/CH_3 ratios compared to normal tissues, highlighting distinct biochemical differences (Table 2).

Table 2. Summary of OH% and CH_2/CH_3 Ratios in Tumor and Normal Tissues

	Oral tissue	Rectal tissue	Combined tissues
OH% (mean ± SD)	74.52% ± 5.07% (tumor) 62.93% ± 15.64% (normal)	69.61% ± 4.23% (tumor) 47.66% ± 16.51% (normal)	73.83% ± 5.23% (tumor) 56.06% ± 17.72% (normal)
CH_2/CH_3 ratio (mean ± SD)	0.31 ± 0.03 (tumor) 0.40 ± 0.13 (normal)	0.30 ± 0.07 (tumor) 0.45 ± 0.15 (normal)	0.31 ± 0.04 (tumor) 0.42 ± 0.14 (normal)

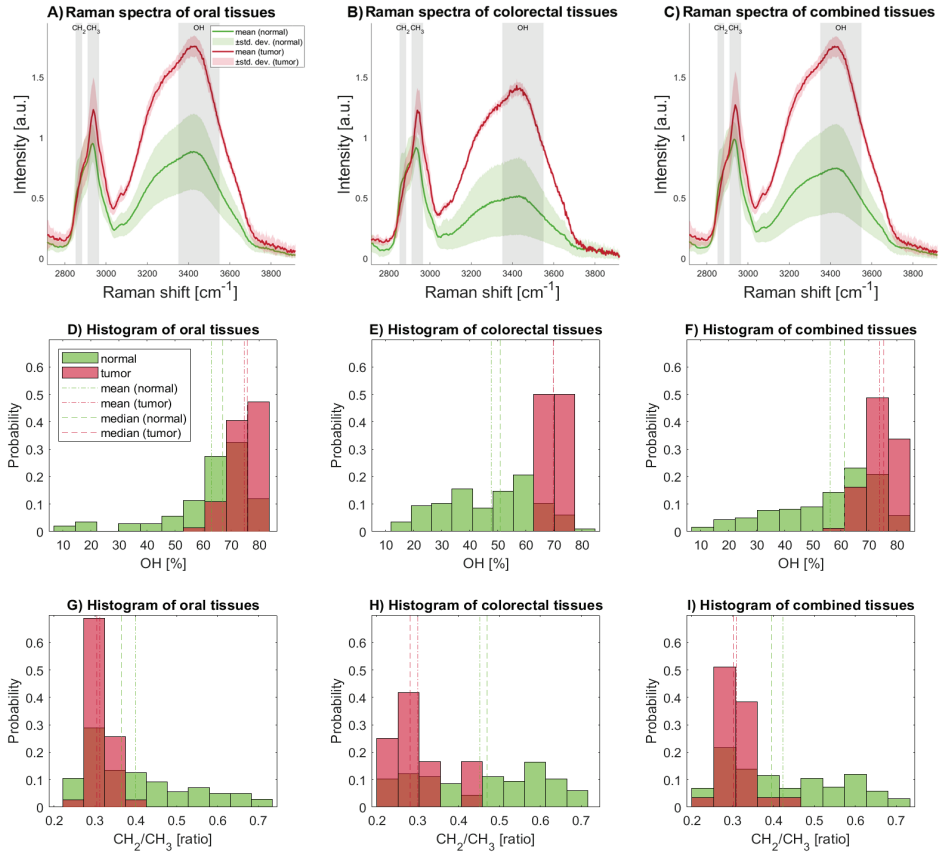

Figure 2. Raman spectra of tumor and normal tissue. (A–C): Intensity-normalized Raman spectra for (A) oral cancer tissue, (B) rectal cancer tissue, and (C) combined spectra of both tissue types. Tumor spectra (red) exhibit higher intensity in the OH-stretching region (3350–3550 cm^{-1}) compared to normal tissue (green), reflecting a higher water concentration in tumor tissues. Additionally, the CH_2/CH_3 ratio is lower in tumor spectra, indicating a reduced lipid-to-protein content in tumor tissues. (D–F): Histograms of percentage intensity in the OH-stretching region for tumor (red) versus normal tissues (green) in (D) oral cancer, (E) rectal cancer, and (F) combined oral and rectal cancer samples. (G–I): Histograms of CH_2/CH_3 ratios for tumor versus normal tissues in (G) oral cancer, (H) rectal cancer, and (I) combined oral and rectal cancer samples.

All calculated p-values (OH% and CH_2/CH_3 ratio) in all datasets (oral, rectal, and combined) were smaller than 0.001, showing a significant difference between the OH% and CH_2/CH_3 ratio of tumor and normal tissues.

PCA was employed to reduce the dimensionality of the Raman spectral data while retaining most of the variance. Figure S2 (supplementary data) shows the cumulative variance explained by PCA of oral, rectal, and combined datasets. In all datasets, the first two PCs accounted for over 96% of the data variance. Only, the first two PCs were kept for further analysis. The loadings of the first two principal components (PC1 and PC2), are shown in Figure 3 (left panel). PC1, accounting for 92.83% of the variance, primarily represented contributions from the water band and also included lipid and protein signals. PC2, explaining an additional 3.98%, was dominated by lipid and protein bands. The projection of the data onto the first two PCs (Figure 3, right panel) demonstrated a clear separation between tumor and normal tissues. Normal tissues formed distinct clusters (green), separate from tumor tissues (red), indicating that Raman spectroscopy could differentiate tumor from normal tissue with 100% accuracy.

To explore the transferability of the identified spectral features between cancer types, reciprocal cross-cancer classification was performed. This analysis was motivated by the consistent tumor- associated changes in OH% and CH_2/CH_3 ratios observed in both datasets. The entire training process (PCA and determination of the tumor likelihood threshold in PC space) was performed separately for the oral dataset. The rectal data points were then projected onto this trained PCA space, and the trained threshold was applied for classification (validation). Conversely, the entire training process (PCA and threshold determination) was repeated using the rectal cancer dataset, and the resulting model was applied to classify the oral cancer spectra. Figure S3 (supplementary data) shows the projection of data points onto PC space for both training and validation datasets.

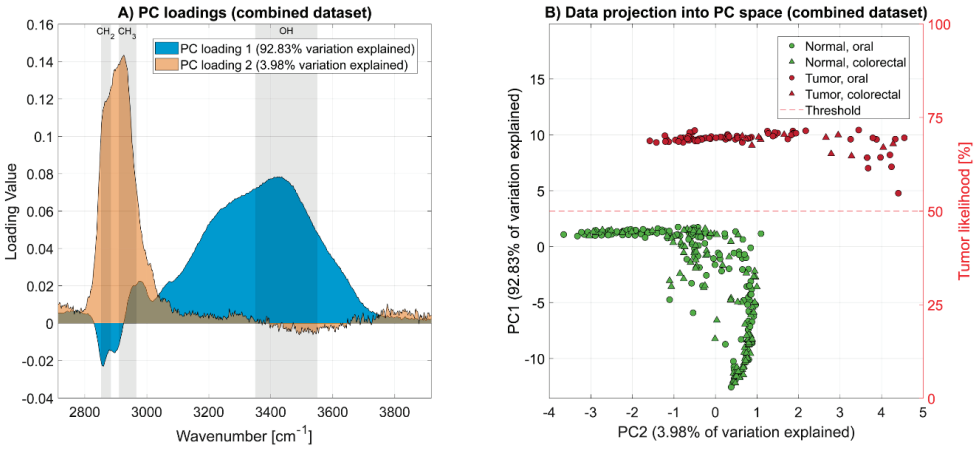

Figure 3. Principal Component Analysis of Combined (Oral and Rectal Tissues) Raman Spectroscopy Data. *Left panel:* Loadings of the principal components (PCs) required to explain 95% of the data variance. The y-axis represents the loading value, and the x-axis corresponds to the Raman wavenumber (cm^{-1}). The first PC (PC1; blue) explains 92.83% of the data variance, primarily accounting for the water band and some contributions from the lipid and protein bands. The second PC (PC2; orange) explains an additional 3.98% of the variance, predominantly capturing the lipid and protein bands. Together, PC1 and PC2 account for more than 95% of the total variance in the dataset. *Right panel:* Projection of Raman spectroscopy data onto the first two PCs. The x-axis represents PC2, and the y-axis represents PC1. A clear separation between the normal (green) and tumor (red) clusters suggests that Raman spectroscopy achieves 100% accuracy in differentiating tumor from normal tissue.

Raman spectroscopy margin assessment

RS performed at depth profiling mode was used to evaluate whether the resection margin was adequate (5 mm for OSCC and 1 mm for rectal cancer).

Figure 4 illustrates the integration of FI and RS in a representative oral cancer specimen (patient #12; Table 1) with an inadequate close (i.e., between 1–5 mm) surgical margin. FI revealed a visible signal at the deep margin, where Raman depth measurements identified inadequate margins. Histopathological analysis confirmed the margin status, corroborating the findings from RS. Individual Raman spectra are shown in Figure S4 and S5 (supplementary data).

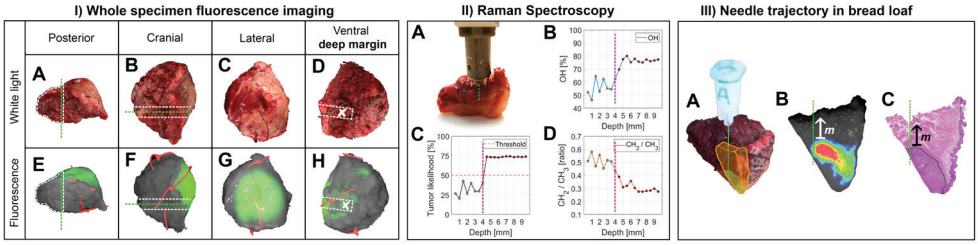

Figure 4. Fluorescence imaging and Raman Spectroscopy in a representative oral cancer specimen with a close surgical margin. *Ex vivo* fluorescence imaging of the resected specimen was performed in a closed-field system (IA–IH). The specimen was imaged from various angles, including the deep margin (images ID and IH), where a fluorescence signal is visible. In ID and IH, an 'x' marks the location where Raman depth measurements were conducted. Dotted green lines indicate the trajectories of the Raman needle, and white dotted lines outline the "bread loaf" section that was subsequently cut for histopathological processing. IIA shows Raman spectroscopy being performed on the oral cancer specimen, with the Raman needle probe held perpendicular to the deep margin surface and inserted into the tissue. Spectra were recorded every 0.5 mm as the needle advanced to a depth of 9.5 mm. IIB and IID display a sharp increase in water content, and a sharp decrease in CH_2/CH_3 ratio, respectively, as the needle entered tumor tissue, clearly demonstrating margin inadequacy at the marked depth. IIC shows the tumor likelihood based on the recorded spectra, revealing a margin width of 4 mm. III shows histopathological confirmation of the margin status. The needle trajectory was preserved inside the specimen using a needle (IIIA) before it was processed into bread loaves. The orange-shaded area represents the bread loaf containing the Raman measurements, which underwent further fluorescence imaging (IIIB) and correlation with H&E histopathology (IIIC). Consistent with the Raman spectroscopy findings (IIB-D), standard histopathology revealed an inadequate margin at the marked location. (IE-H) were obtained with the Pearl Trilogy, IIIC was digitally scanned with a virtual microscope (Nanozoomer 2.0 HT, Hamamatsu Photonics, Shizuoka, Japan). *H&E: Hematoxylin and Eosin.*

Figure 5 illustrates RS depth profiling in a freshly resected rectal cancer specimen containing SGM-101 FL tracer (patient #16; Table 1) with an adequate surgical margin. Depth measurements identified the margin, showing sharp increases in water content and sharp degrees in the CH_2/CH_3 ratio as the needle entered tumor tissue. Histopathological analysis confirmed the adequacy of the margin.

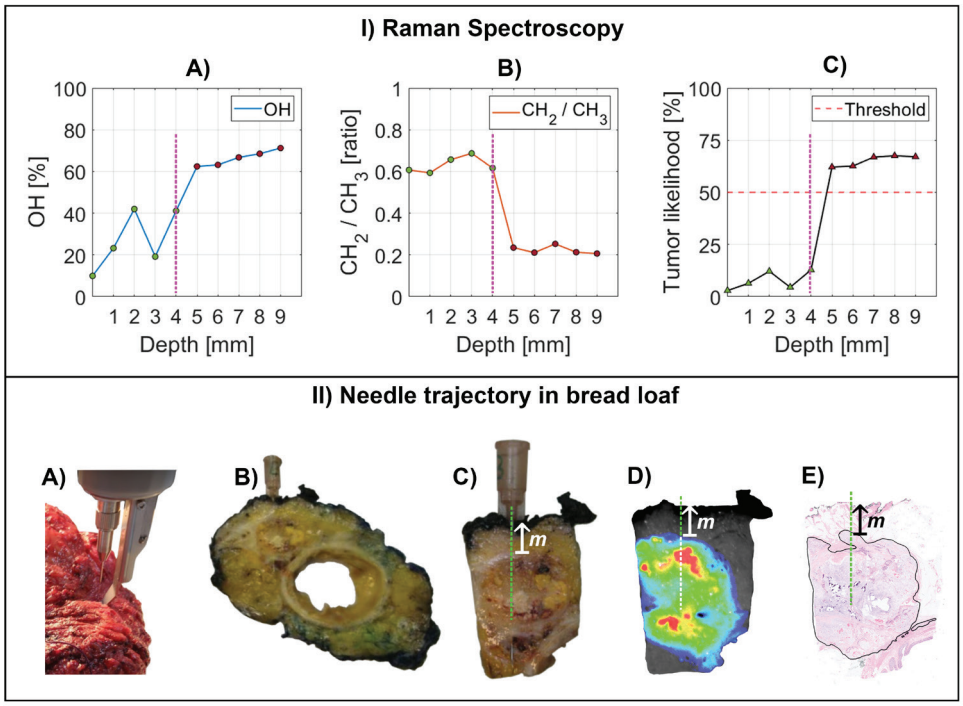

Figure 5. Raman Spectroscopy in a rectal cancer specimen with adequate surgical margin. Spectra were recorded every 1 mm as the needle advanced to a depth of 9 mm. IA and IB display a sharp increase in water content, and a sharp decrease in CH_2/CH_3 ratio, respectively, as the needle entered tumor tissue, clearly demonstrating margin at the marked depth. IC shows the tumor likelihood based on the recorded spectra, revealing an adequate margin width of 4 mm. II shows histopathological confirmation of the margin status. IIA shows Raman spectroscopy being performed on the tumor in the whole rectum specimen, with the Raman needle probe held perpendicular to the surface and inserted into the tissue. The needle trajectory was preserved inside the specimen using a needle before it was processed into bread loaves (IIB) and cut into blocks for cassette placement and paraffination. The block containing the Raman measurements (IIC) underwent further fluorescence imaging (IID) and correlation with H&E histopathology (IIE). Consistent with the Raman spectra findings (I), standard histopathology revealed an adequate margin at the marked location. (IID) was obtained with the Pearl Trilogy, (IIE) was digitally scanned with a virtual microscope (Nanozoomer 2.0 HT, Hamamatsu Photonics, Shizuoka, Japan). *H&E: Hematoxylin and Eosin.*

Characterization of non-malignant fluorescence

RS measurement, was performed on four specimens (n = 3 for OSCC; n = 1 for rectal cancer) with the goal of differentiating areas with true positive fluorescence signal (originating from the tumor) and areas with false positive fluorescence signal (e.g., originating from non-tumor gingiva tissue with high integrin expression). OSCC samples include a pair of fluorescent-positive tumor-negative lymph nodes, gingiva, and salivary gland. Local RS measurement was also performed on a rectal fat sample with residual tracer left in the tissue. Figure 6 shows the local RS measurement results.

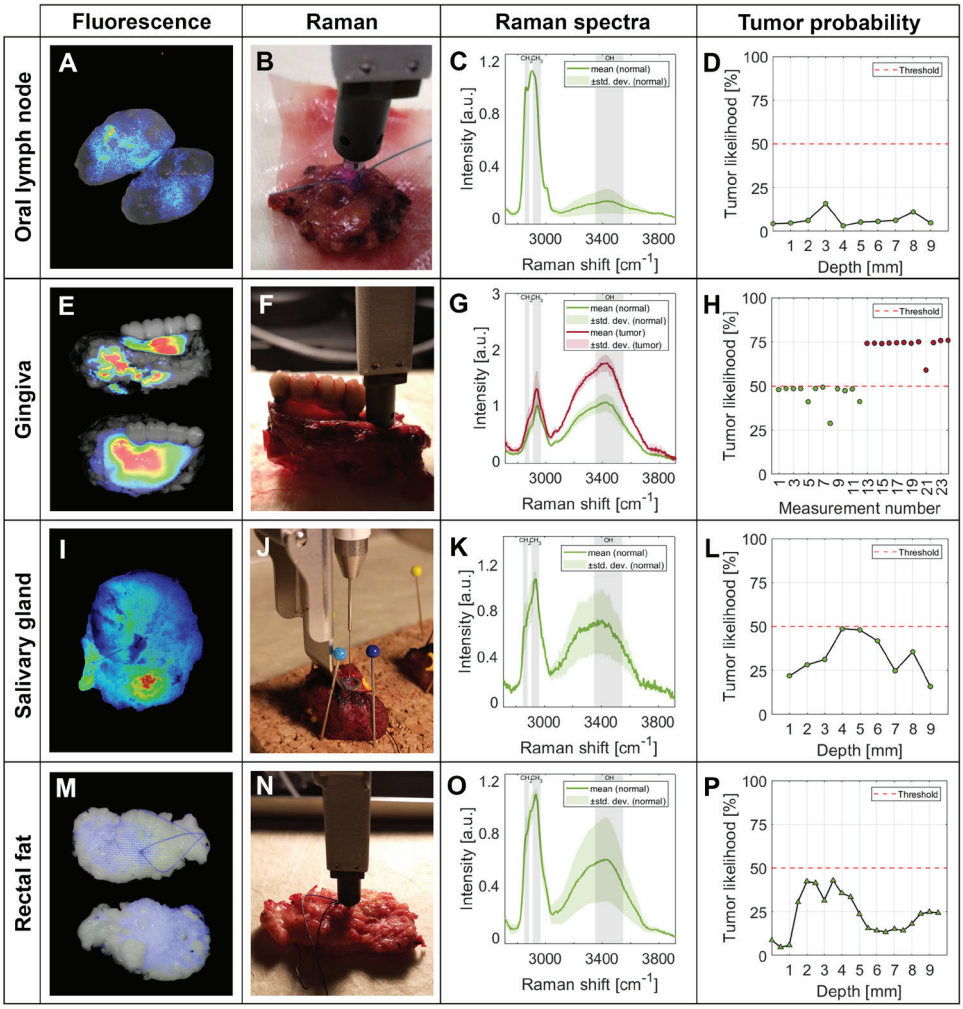

Figure 6. Closed-field fluorescence images in non-malignant tissues and corresponding Raman spectra. Intraoperative fluorescence was observed in various healthy tissues, including benign lymph nodes in oral cancer (A–D), the junctional epithelium of the gingiva (E–H), salivary gland (I–L), and a sample with residual of the tracer in fatty rectal tissue (M–P), corresponding to patients #8, #10, #5, and #19 in Table 1, respectively. Raman spectroscopy classified all these measurement locations as normal, thereby correctly identifying these fluorescent false-positives.

DISCUSSION

FI has recently emerged as a valuable tool for tumor localization and (ex vivo) margin assessment during cancer surgeries. Conventional intraoperative margin assessment relies on visual inspection and palpation by the surgeon and pathologist, as well as frozen section analysis of selected areas when needed. FI improves on this by providing real-time, wide-field visualization of suspicious regions not reliably identified by inspection and palpation alone [3], while RS, as detailed below, adds specificity and quantitative depth resolution that neither traditional methods nor FI can offer alone [10]. Beyond its advantages, a key limitation of FI lies in its inability to provide direct information about tumor depth. Fluorescence photons traveling to and from a subsurface fluorophore are attenuated by tissue absorption and scattering, both of which vary by tissue type and increase with depth [11]. Because measured fluorescence intensity—expressed in arbitrary camera counts—reflects the combined effect of fluorophore concentration, depth, and these variable tissue optical properties, it cannot be accurately correlated with the actual depth of the tumor. Conversely, RS, when used independently, is also prone to false negatives due to sampling error. To address this issue, we integrated RS depth profiling with FI, providing a more reliable method for ex vivo margin assessment on the resected specimen.

Another limitation of FI is the potential for false positives, particularly when healthy tissues surrounding the tumor also take up the fluorescent tracer. The extent of tracer uptake in healthy tissue varies with the molecular target and tracer, as demonstrated in this study with cRGD- ZW800-1 targeting integrins and SGM-101 targeting CEA. For cRGD-ZW800-1, we previously showed that fluorescent gingiva and salivary gland tissue express αvβ6 integrin, at the junctional epithelium and ductal cells respectively, independent of malignancy [3], while fluorescent bone marrow showed no αvβ6 expression, indicating non-specific rather than targeted uptake. Fluorescence observed in benign lymph nodes was similarly non-specific but transient: it consistently resolved after pathological processing, likely reflecting residual tracer released from transected lymphatic vessels during specimen handling (Zweedijk et al, manuscript in preparation). Conversely, in rectal cancer, false-positive SGM-101 fluorescence has been reported in fatty tissue with fibrosis and inflammation but without malignancy. Weak CEA expression in epithelial tissue within such regions may account for SGM-101 binding and fluorescence. For fluorescent lesions without detectable CEA expression, autofluorescence at the approximately 700-nm imaging wavelength has been proposed as an alternative explanation [6]. Consistent with our previous findings, RS correctly classified all four of these non-malignant fluorescent tissue types observed in this study (Figure 5) as normal, extending those observations to direct diagnostic performance at the point of measurement. Here, RS complements FI by accurately characterizing tissue at fluorescent spots, discriminating malignant from non-malignant tissue regardless of the underlying cause of fluorescence. In this workflow, FI localizes the most suspicious regions, while RS verifies tissue type and margin adequacy with depth resolution.

Despite these advantages, our study has important limitations. The relatively small sample (n=19 patients, 344 spectra) limits generalizability. The limited cohort size may affect the robustness of the classification model by insufficiently capturing biological and spectral variability within each cancer type. While 100% accuracy was achieved in this controlled setting, larger prospective studies are needed to confirm these findings during real-time intraoperative decision-making. In the present dataset, PC1 alone provided complete separation between malignant and normal tissues. However, classification accuracy may decrease in larger, more heterogeneous cohorts. Future studies could therefore investigate the additional discriminatory value of PC2 and other PCs to improve classification performance when PC1 alone is insufficient. Although cross-cancer classification suggests potential transferability of the identified spectral features, differences in tissue composition and unequal cohort sizes may influence classification performance. Larger, balanced cohorts are required to establish the generalizability of these findings.

RS measurements were also acquired on fresh tissue, whereas histopathological correlation was performed on formalin-fixed, paraffin-embedded sections, a process that can introduce tissue shrinkage. However, prior validation of this needle-probe methodology revealed that the mean difference between RS-predicted and histopathology-confirmed margin length was -0.17 mm [8], suggesting this effect is small relative to the clinically relevant margin thresholds used in this study. In addition, RS measurements were primarily acquired at FI-positive or otherwise suspicious locations, which maximizes clinical relevance but introduces selection bias and prevents evaluation of RS performance in non-fluorescent tumor areas, such that this design cannot address whether RS recovers tumors missed by FI. Nonetheless, in the same OSCC trial cohort, cRGD-ZW800-1 achieved 100% patient-level sensitivity and detected all 23 inadequate margins, versus 70% by conventional assessment [3], while SGM-101 at the dose used here showed 96% sensitivity for lesion detection in colorectal cancer [6]. Given the already high sensitivity of FI, the value of RS in this workflow lies primarily in improving specificity and providing depth-resolved margin information at fluorescent sites, rather than in reducing FI's false negative rate.

Our findings indicate that RS, particularly with a SWIR setup and Raman needle probe, can achieve excellent sensitivity and specificity in distinguishing tumor from non-malignant tissue, translating into more precise margin evaluation than wide-field FI alone. The biomarkers identified, OH% and the CH_2/CH_3 ratio, could serve as promising indicators that may extend beyond OSCC and rectal cancer, though this requires validation in larger cohorts and additional tumor types before broader applicability can be established.

Previously, we identified an optimal excitation wavelength interval (900–915 nm) for RS in the presence of fluorescent agents, which avoids both the excitation of fluorescent dyes and the self- absorption of the Raman signal by the tissue [9]. Our identified optimum excitation wavelength avoids both autofluorescence and fluorescence originating from exogenous NIR

tracers. This study extends that technical finding to the clinical setting: using an excitation wavelength around 900 nm, combined with detection in SWIR, we achieved higher sensitivity and specificity than earlier Raman needle depth profiling studies conducted with 785 nm excitation [8], a wavelength at which fluorophore excitation and tissue autofluorescence are harder to avoid. Our improvement likely reflects reduced fluorescence interference and more faithful band-intensity measurement, as SWIR detection avoids post-processing errors caused by mathematically separating intense fluorescence from Raman signals, and produces a Raman signal with a higher signal-to-noise ratio and greater dynamic range as the detector is not overwhelmed by fluorescence photons. Direct comparison with earlier 785 nm studies remains challenging, however, due to differences in tissue sites, tumor stages, sampling locations, and acquisition protocols, underscoring the need for standardized evaluation frameworks [12], converging evidence that excitation in this range is broadly advantageous for RS in the presence of fluorescence. This benefit, however, comes with a practical tradeoff: detecting signals in the SWIR range does require longer integration times (5– 10 seconds per location) and more expensive detectors than conventional 785 nm systems.

In a recent review, we highlighted the limitations of FGS [10], including false positives and the inability to detect resection margins independently, and outlined the potential of RS to address them by providing complementary biochemical data [13]. Our current findings offer initial clinical corroboration of that framework. In rectal patients who underwent FGS using SGM-101 in this study, all margins were adequate; however, in oral patients who underwent FGS using cRGD- ZW800-1, a few inadequate margins were present in the primary resection, which were detected with both FI and RS. Moreover, our SWIR Raman needle system distinguished false positives from true positives during FGS and differentiated tumor from normal tissue with 100% sensitivity and 100% specificity, although tested in a small number of patients.

Using the Raman needle probe, we demonstrated the feasibility of measuring resection margins at user-selected locations, which may offer an alternative to fresh frozen sectioning in the sentinel margin approach [14]. Unlike frozen sectioning, which is limited to only a few sites on a specimen and typically requires 20–40 minutes per margin, Raman needle depth profiling can be performed in multiple locations. In our study, integrating RS into FGS added only 2–3 minutes per assessed margin, thereby reducing sampling errors relative to frozen sectioning with minimal disruptions to operative timing. In practice, the number of RS measurements per specimen must still be balanced against procedural time. Targeted sampling of FI-identified sentinel margins or the most suspicious regions, rather than all fluorescent spots, is therefore likely to be the most practical strategy and should be optimized in future implementation studies. We investigated this approach in two distinct cancer types, OSCC and rectal cancer, where the OH% and CH2/CH3 ratio biomarkers showed consistent discriminatory patterns, suggesting they may extend to other solid tumors as broadly applicable indicators. While implementation requires training in the use of the

Raman needle probe and spectral interpretation, the learning curve is modest and can be addressed through standardized protocols. Although initial equipment costs may be a barrier, these could be offset by improved margin accuracy, fewer reoperations, and better long-term outcomes.

Future studies should aim to validate the integration of RS with FGS in larger, multicenter cohorts and across a broader range of cancer types, and prospectively evaluate long-term clinical outcomes, including recurrence and reoperation rates. Evaluating the utility of RS biomarkers, such as OH% and the CH_2/CH_3 ratio, as universal indicators for solid tumors could further expand its applicability. Additionally, optimizing RS hardware to reduce integration times and improving accessibility in clinical settings would enhance its practicality. Formal cost-effectiveness and implementation studies will be essential for widespread adoption and for establishing RS as a standard complementary tool to FGS in precision oncologic surgery. If broadly implemented, this integrative approach could set new standards for intraoperative tumor resection, improving surgical outcomes and patient care in oncology.

In conclusion, this study demonstrates the clinical utility of integrating ex vivo RS with intraoperative FGS for enhanced tissue characterization and margin assessment in cancer surgery. By combining the wide-field visualization of FGS with the depth-profiling and biochemical specificity of RS, this approach addresses critical limitations of FGS, such as false positives and its limited ability to accurately determine margin adequacy in close or indeterminate margins.

REFERENCES

1 Smits, R. W. et al. *Resection margins in oral cancer surgery: Room for improvement.* Head Neck, 2016. **38 Suppl 1**, E2197-2203.

2 Orosco, R. K. et al. *Positive Surgical Margins in the 10 Most Common Solid Cancers.* Sci Rep, 2018. **8**, 5686.

3 Zweedijk, B. E. et al. *Near-infrared fluorescence imaging-guided surgery using cRGD-ZW800 to improve surgical resection margins in oral cancer: a phase I/II feasibility trial.* Nature Communications, 2026.

4 Gutowski, M. et al. *SGM-101: An innovative near-infrared dye-antibody conjugate that targets CEA for fluorescence-guided surgery.* Surgical Oncology, 2017. **26**, 153-162.

5 Boogerd, L. S. F. et al. *Safety and effectiveness of SGM-101, a fluorescent antibody targeting carcinoembryonic antigen, for intraoperative detection of colorectal cancer: a dose-escalation pilot study.* The Lancet Gastroenterology & Hepatology, 2018. **3**, 181-191.

6 de Valk, K. S. et al. *Dose-Finding Study of a CEA-Targeting Agent, SGM-101, for Intraoperative Fluorescence Imaging of Colorectal Cancer.* Annals of Surgical Oncology, 2021. **28**, 1832-1844.

7 Framery, B. et al. *Toxicity and pharmacokinetic profile of SGM-101, a fluorescent anti-CEA chimeric antibody for fluorescence imaging of tumors in patients.* Toxicology Reports, 2019. **6**, 409-415.

8 Aaboubout, Y. et al. *Intraoperative assessment of resection margins by Raman spectroscopy to guide oral cancer surgery.* Analyst, 2023. **148**, 4116-4126.

9 Abbasi, H. et al. *Development of a near-infrared Raman spectroscopy setup compatible with fluorescence-guided surgery.* Analyst, 2023. **148**, 2676-2682.

10 Lauwerends, L. J. et al. *The complementary value of intraoperative fluorescence imaging and Raman spectroscopy for cancer surgery: combining the incompatibles.* Eur J Nucl Med Mol Imaging, 2022. **49**, 2364-2376.

11 Keereweer, S. et al. *Optical image-guided cancer surgery: challenges and limitations.* Clin Cancer Res, 2013. **19**, 3745-3754.

12 Arús, B. A. et al. *Macroscopic label-free biomedical imaging with shortwave infrared Raman scattering.* bioRxiv, 2024. 2024.2006.2010.597863.

13 Krafft, C. & Popp, J. *Opportunities of optical and spectral technologies in intraoperative histopathology.* Optica, 2023. **10**, 214-231.

14 van Keulen, S. et al. *The Sentinel Margin: Intraoperative Ex Vivo Specimen Mapping Using Relative Fluorescence Intensity.* Clin Cancer Res, 2019. **25**, 4656-4662.

15 *Choi, H. S.* et al. *Synthesis and in vivo fate of zwitterionic near-infrared fluorophores.* Angew Chem Int Ed Engl, 2011. **50**, 6258-6263.

16 de Valk, K. S. et al. *First-in-Human Assessment of cRGD-ZW800-1, a Zwitterionic, Integrin-Targeted, Near-Infrared Fluorescent Peptide in Colon Carcinoma.* Clin Cancer Res, 2020. **26**, 3990-3998.

17 Aaboubout, Y. et al. *Specimen-driven intraoperative assessment of resection margins should be standard of care for oral cancer patients.* Oral Dis, 2021. **27**, 111-116.

18 Krishnan, G. et al. *Fluorescent Molecular Imaging Can Improve Intraoperative Sentinel Margin Detection in Oral Squamous Cell Carcinoma.* J Nucl Med, 2022. **63**, 1162-1168.

19 Voskuil, F. J. et al. *Intraoperative imaging in pathology-assisted surgery.* Nature Biomedical Engineering, 2022. **6**, 503-514.

20 Loughrey, M. B., Quirke, P., Shepherd, N. A. & Williamson, L. *Standards and datasets for reporting cancers Dataset for histopathological reporting of colorectal cancer September 2018.* Royal College of pathologists, 2018.

21 Hunter, K., Da Forno, P., Hall, G., Jones, A. & Thomas, G. *Standards and datasets for reporting cancers.* Dataset for the histopathological reporting of carcinomas

of the oral cavity. The Royal College of Pathologists, 2023.

22 Caspers, P. J., Bruining, H. A., Puppels, G. J., Lucassen, G. W. & Carter, E. A. *In Vivo Confocal Raman Microspectroscopy of the Skin: Noninvasive Determination of Molecular Concentration Profiles.* Journal of Investigative Dermatology, 2001. **116**, 434-442.

23 Barroso, E. M. et al. *Discrimination between Oral Cancer and Healthy Tissue Based on Water Content Determined by Raman Spectroscopy.* Analytical Chemistry, 2015. **87**, 2419-2426.

24 Barroso, E. M. et al. *Water Concentration Analysis by Raman Spectroscopy to Determine the Location of the Tumor Border in Oral Cancer Surgery.* Cancer Research, 2016. **76**, 5945-5953.

25 Barroso, E. M. et al. *Raman spectroscopy for assessment of bone resection margins in mandibulectomy for oral cavity squamous cell carcinoma.* European Journal of Cancer, 2018. **92**, 77-87.

SUPPLEMENTARY MATERIALS

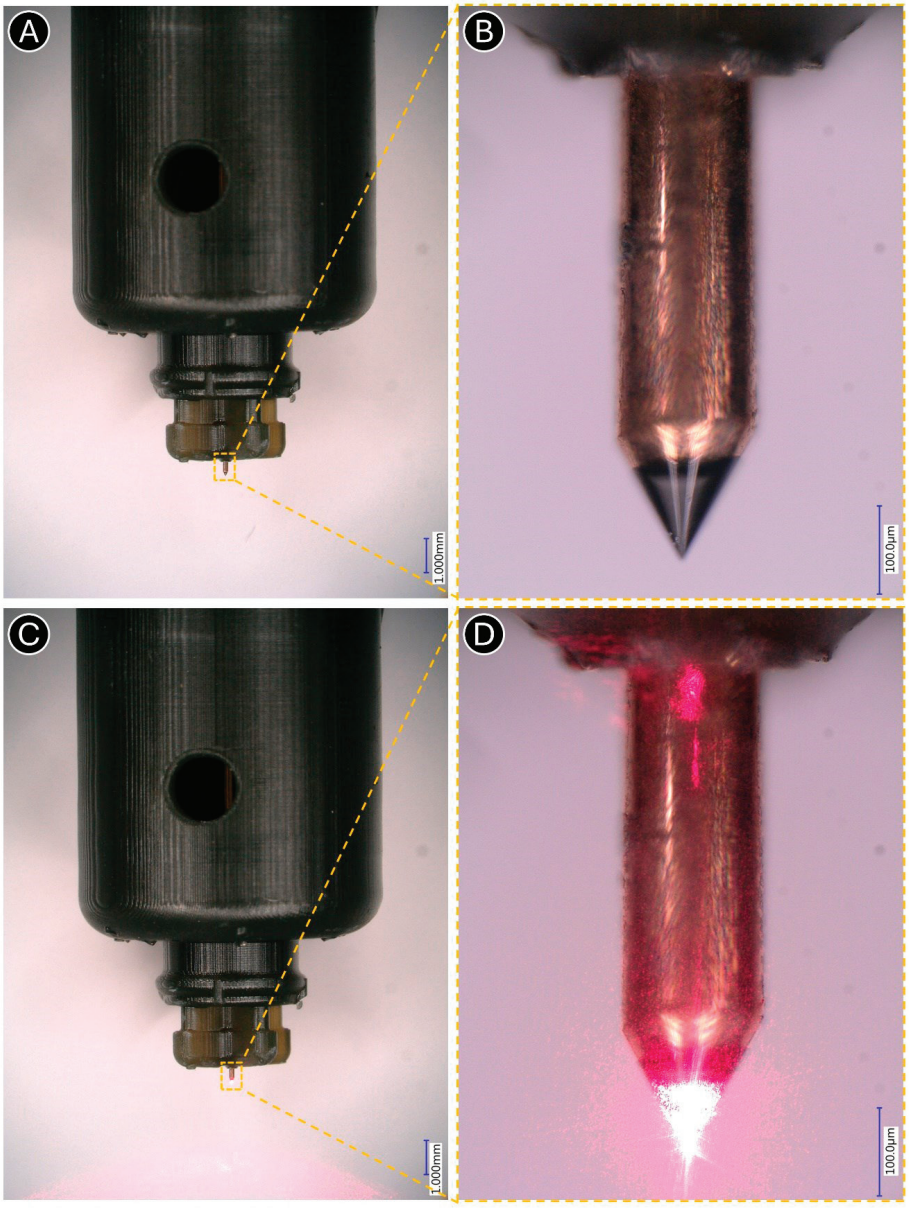

Supplementary Figure S1. Raman needle probe with a conical tip. (A) Raman needle with the laser light off. (B) Zoomed-in view of the Raman needle tip with the laser light off. (C) Raman needle with the laser light on. (D) Zoomed-in view of the Raman needle tip with the laser light on. The scale bars in (A) and (C) represent 1000 µm, and in (B) and (D) represent 100 µm. All images were captured using the Keyence VHX-6000 Digital Microscope. For visualization purposes, a visible 650 nm laser (DELIPOP 30 mW Visual Fault Locator Fiber Optic Cable Tester) was coupled to the Raman needle during image acquisition, instead of the actual invisible NIR laser light used in the study.

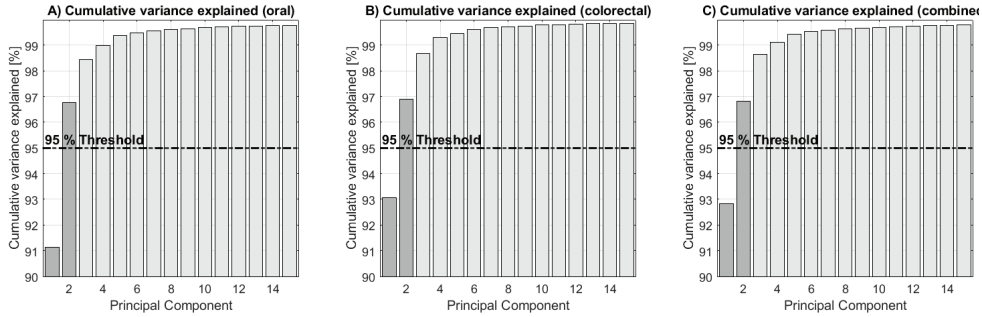

Supplementary Figure S2. Cumulative variance explained by principal components analysis (PCA)Cumulative variance explained by principal components analysis (PCA) of (A) oral, (B) rectal, and (C) combined datasets. In all datasets, two principal components (PCs) accounted for 95% of the data variance, with the first component alone explaining over 91% of the variance.

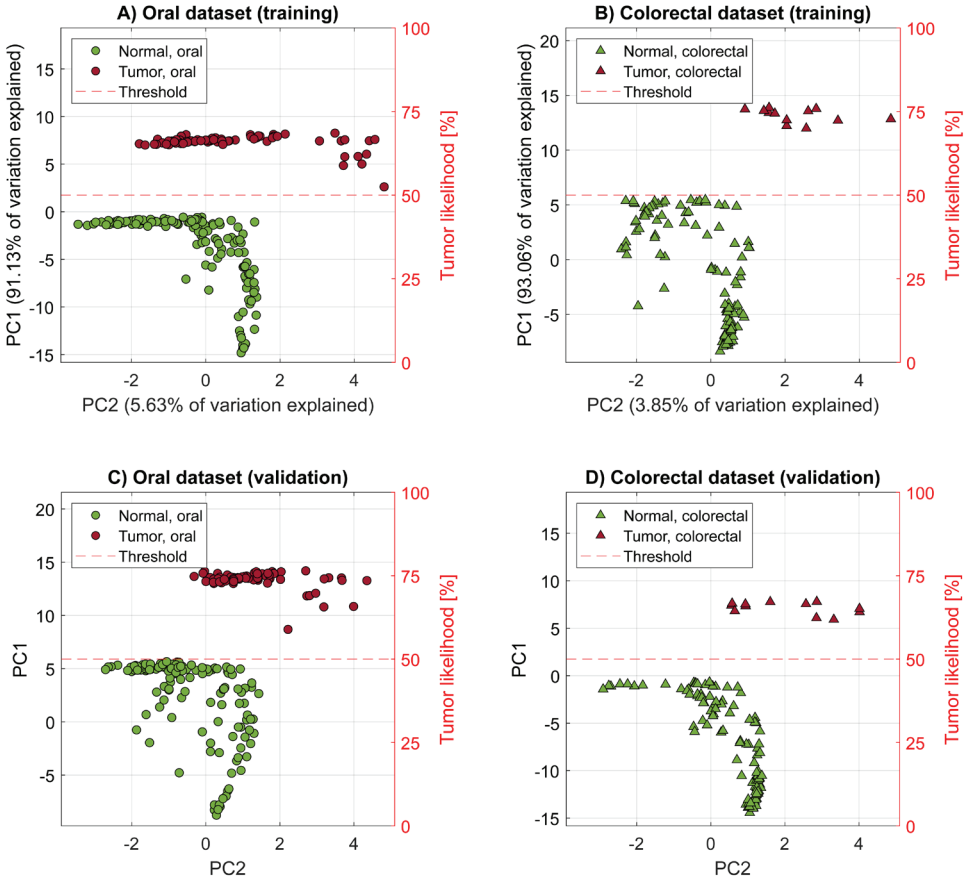

Supplementary Figure S3. Projection of Raman spectroscopy data onto the first two principal components (PCs). The x-axis represents PC2, and the left y-axis represents PC1. The second y-axis (in red, shown on the right side of each panel) represents tumor likelihood, with a threshold of 50%. The threshold position in PC space was defined during training as the midpoint between the mean of normal data points and the mean of tumor data points. This threshold in each PC space was subsequently used for classifying tumor versus normal tissue during validation. Panels (A) and (B) show the projection of data points onto the PC space developed during training for oral and rectal datasets, respectively. Panel (C) shows rectal data points projected onto the PC space trained using oral data points, while panel (D) shows oral data points projected onto the PC space trained using rectal data points. The clear separation between normal (green) and tumor (red) clusters confirms that Raman spectroscopy achieved 100% sensitivity and specificity in distinguishing tumor from normal tissue.

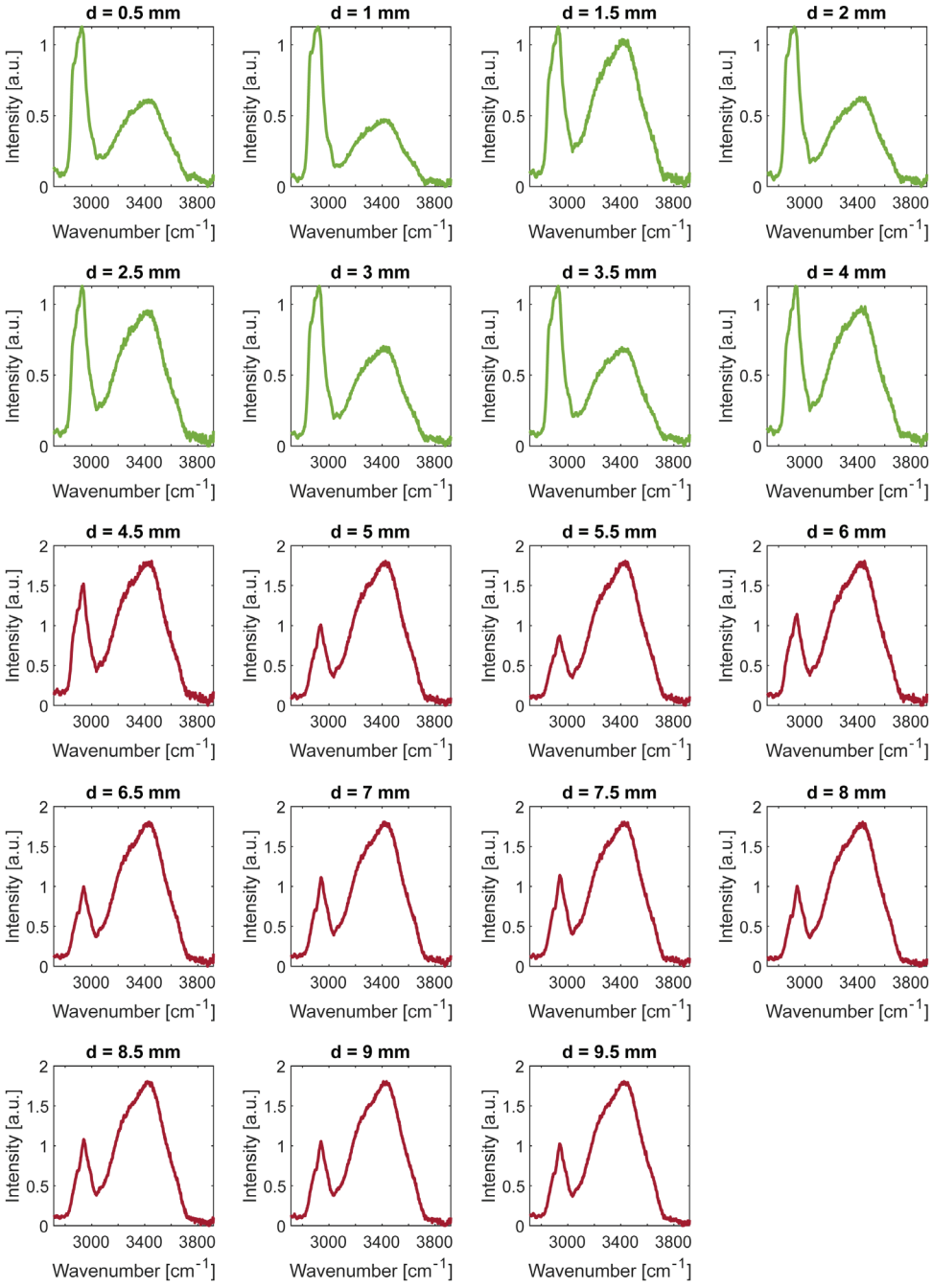

Supplementary Figure S4. Individual Raman spectra measured at different depths on a resected OSCC specimen (Fig. 4) with a close margin (see Table 1; patient #12). The header of each panel indicates the depth at which the Raman needle was positioned during spectrum collection. Normal spectra are shown in green, while tumor spectra (4.5 mm and beyond) are shown in red. As the needle probes deeper toward the tumor, the OH% increases, and the CH_2/CH_3 ratio decreases.

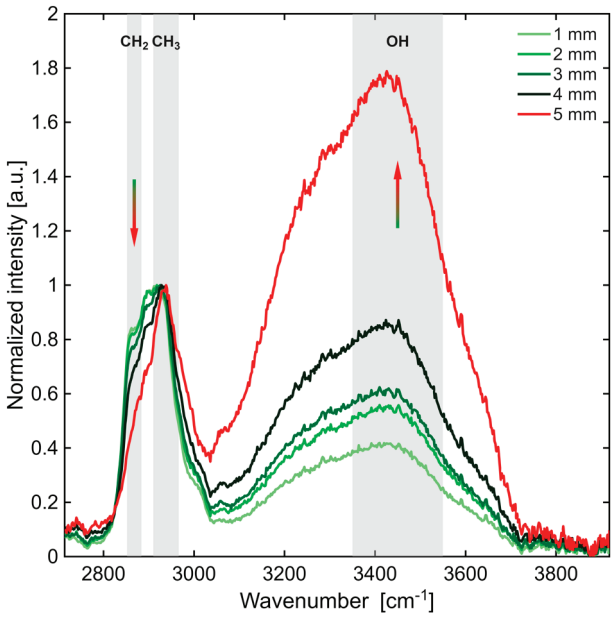

Supplementary Figure S5. Overlaid Raman spectra measured at different depths on a resected OSCC specimen (Fig. 4) with a close margin of 4.3 mm at the measurement location (see Table 1; patient #12). Representative spectra acquired at 1, 2, 3, 4, and 5 mm are overlaid to visualize the spectral transition from normal to tumor tissue across the resection margin. Each spectrum was independently normalized to the maximum intensity of the CH_3 band (2910–2966 cm^{-1}). Normal spectra are shown in green, while the tumor spectrum (5 mm) is shown in red. Gray-shaded regions indicate the CH_2, CH_3, and OH bands. As the needle probes deeper toward the tumor, the OH intensity increases and the CH_2/CH_3 ratio decreases, as indicated by the arrows, illustrating the progressive biochemical changes associated with the transition from normal to malignant tissue.

Part V

Summary and General Discussion

11



Chapter 11

Summary

The main objective of surgery is to accurately distinguish between malignant and normal tissues, thereby ensuring the removal of solid tumors with clear margins, as well as safeguarding the integrity of surrounding healthy tissues. Traditional reliance on visual inspection and manual palpation during surgery is limited by the often subtle distinctions between healthy and malignant tissues.

NIR fluorescence imaging, an emerging optical technique in intraoperative visualization, promises to enhance surgeon and pathologists' ability to differentiate between malignant and normal tissues. By facilitating more precise resection of solid tumors, fluorescence imaging has the potential to significantly improve patient outcomes. Nevertheless, the integration of fluorescence imaging into clinical practice is still in its early stages. The aim of this thesis was to investigate the integration of optical imaging into surgical practice – particularly for HNC - to enhance the intraoperative precision of tumor delineation. It considers this advancement within the broader context of improving surgical outcomes and patient prognoses through enhanced intraoperative guidance.

Part I: Reviewing Intraoperative Imaging Technologies

Part I examines the range and applications of fluorescence imaging, offering a comprehensive review of existing intraoperative imaging technologies utilized in various cancers. *Chapter 2* systematically reviews the current intraoperative imaging modalities for surgical resection of laryngeal cancer, identifying limitations in deep margin assessment and suggesting future directions for optical imaging applications. *Chapter 3,* also a systematic review, discusses the application of FGS in colorectal cancer, outlining its clinical benefits and potential to improve surgical precision and patient outcomes.

Part II: Conceptual Foundations of Fluorescence Imaging in Cancer Surgery

Part II establishes the theoretical underpinnings and practical applications of fluorescence imaging. *Chapter 4* explores the significant role of (real-time) fluorescence imaging in intraoperative decision-making in cancer surgery, highlighting the method's potential to alter (post-)surgical strategies. It emphasizes the necessity for refined study designs and reporting standards to accurately assess the clinical benefits of fluorescence imaging. Recommendations on how to report changes in intraoperative decision-making that result from fluorescence imaging are thus presented, with the aim to accelerate the widespread clinical implementation of fluorescence imaging. *Chapter 5* continues with our response to a correspondence letter ("*a pathologist's perspective*"), containing arguments in favor of the core message of *Chapter 4*: the effect of fluorescence imaging on intraoperative decision-making as the ultimate measure of FGS's clinical benefit.

Part III: Advances in Fluorescence Imaging for Head and Neck Cancer

Part III presents novel research on the (clinical) application of fluorescence imaging in HNC. *Chapter 6* investigates potential targets for NIR fluorescence imaging in this area through an immunohistochemical study performed on OSCC, LSCC, and PTC, with the aim to contribute to the development of targeted imaging agents. As the focus was on potential rapid translation towards clinical applications, this study evaluated marker expression of six targets with (pre-)clinically available NIR fluorescence tracers that are currently being investigated in various cancers: CEA, EpCAM, integrin αvβ6, VEGF-α, EGFR and c-MET. The most notable result from this study was that integrin αvβ6, in particular, was found to offer a strong contrast for tumor margin delineation in OSCC and LSCC.

Subsequently, *Chapter 7* demonstrates the safety, feasibility and effectiveness of cRGD-ZW800-1 – an integrin-targeted (including integrin αvβ6) fluorescent agent consisting of a cyclic pentapeptide (cRGD) conjugated to an 800 nm fluorophore ZW800-1 – in improving the rate of adequate surgical resection margins in OSCC. In this clinical trial, fluorescence imaging with cRGD-ZW800-1 successfully visualized all clinically relevant inadequate resection margins, including nine inadequate margins (three positive and six close) that were initially overlooked during routine intraoperative assessment by the surgeon and a pathologist. In five out of 16 patients (16%), these fluorescence imaging findings directly impacted intraoperative decision-making and led to additional resections; in three of these patients, adjuvant radiotherapy could be prevented. Fluorescence imaging achieved a sensitivity of 100% at patient level, compared with 70% for standard IOA. Moreover, the unique approach of this study not only yielded qualitative imaging data, but also substantiated its reliability through quantitative spectroscopy. By leveraging the insights gained from temporal *in vivo* quantification of the fluorescent agent with *MDSFR/SFF* spectroscopy, this approach also successfully informed the decision-making process concerning dose-finding and timing, demonstrating that cRGD-ZW800-1 can be administered as early as 2 hours before surgery, thereby enabling significant logistical advantages through same-day administration. The study further demonstrated the significant clinical value of intraoperative fluorescence imaging in OSCC surgery, with fluorescence imaging reliably identifying all inadequate margins and directly influencing surgical management. The integration of fluorescence imaging with cRGD-ZW800-1 in this study demonstrates significant oncological impact, underscoring the potential of this technology in enhancing surgical precision and patient outcomes.

Part IV: Integrating Fluorescence Imaging with Raman Spectroscopy

Part IV proposes to overcome the limitations of fluorescence imaging by integrating it with RS. *Chapter 8* reviews the complementary value of combining fluorescence imaging with RS to achieve clear surgical margins, addressing the technical challenges and presenting strategies for integrating these technologies in clinical practice. *Chapter 9* presents the development of a NIR RS setup designed to be compatible with FGS. This setup circumvents the spectral overlap between fluorescence and Raman emissions, enabling the concurrent use

of both imaging modalities to enhance tumor specificity and surgical precision. *Chapter 10* extends the previous work on the successful use of fluorescence imaging for margin delineation in OSCC surgeries by examining the clinical benefits of using *ex vivo* RS alongside fluorescence imaging for intraoperative assessment of OSCC and rectal cancer specimen. While NIR fluorescence imaging effectively identifies the closest margins, frozen section analysis remains necessary to confirm margin status. RS, through depth profiling with a Raman needle probe, may present a suitable complement (or alternative) by offering local measurements at known depths, enabling a clear determination of margin adequacy. Furthermore, RS's ability to differentiate fluorescence in non-malignant tissues like the gingiva and salivary glands may reduce the performance of unnecessary frozen sections, and (if performed *in vivo*) facilitate more precise, conservative resections. This study emphasizes the clinical value of merging RS with fluorescence imaging, highlighting its potential to improve the accuracy of intraoperative decisions across a wide array of cancers, marking a significant step forward in the field of cancer surgery.

Part V: Summary, General discussion and future perspectives

All results are summarized here (*Chapter 11*), as well as in the Dutch Summary in the **Appendix**. *Chapter 12* contains the general discussion and future perspectives.

In this thesis, we propose that the intraoperative integration of fluorescence imaging signifies a monumental step forward in the field of surgical oncology. By significantly enhancing both surgeon and pathologist's ability to accurately distinguish between malignant and healthy tissues, fluorescence imaging promises to not only improve surgical outcomes, but also reduce the likelihood of disease recurrence and positively impact patient prognoses. This thesis presents a comprehensive overview of the current state of optical imaging techniques, their practical applications in HNC surgery, and the potential future developments that could further revolutionize the field of surgical oncology.


12

Chapter 12

General discussion

The most alluring promise of fluorescence imaging might be its real-time aspect; allowing surgeons to adjust their surgical strategy during the operation itself. Indeed, FGS implies *in vivo* Guidance by Light, where the surgeon delineates an adequate yet conservative rim of dim tissue surrounding the well-demarcated, brightly lit tumor. However, fluorescence imaging in the surgical theatre is associated with many variables that are difficult to quantify, as well as challenges in creating standardized protocols: lighting conditions [1], imaging distance, the availability and expertise of personnel are just a few examples of influences that are difficult to control and/or cumbersome during surgery [2]. Crucially, while oncologic surgeries aimed at debulking or identifying occult lesions may strongly benefit from fluorescent wound bed inspection, margin status for tumors requiring wide local excision can only be limitedly assessed in this manner [2]. Fluorescence imaging of the wound bed has no utility for close margins, which are a far more likely surgical outcome than the occasional positive margin [3-5]. Indeed, as outlined in the AJCC Cancer Staging Manual for oral cancer, margin status is recommended to be determined from the specimen.

EX VIVO FLUORESCENCE IMAGING

The appeal of real-time fluorescence imaging should thus not overshadow the strong utility of *ex vivo* fluorescence imaging, performed on the resected specimen while the wound bed is still accessible for further resection. Closed-field fluorescence imaging of specimen offers margin assessment of all surfaces under consistent and controlled circumstances, and is particularly useful to investigate the deep margin where the majority of inadequate margins occurs [6]. Indeed, the changes in intraoperative decision making prompted by fluorescence imaging in OSCC presented in Chapter 7 all resulted from *ex vivo* fluorescence imaging: frozen section analysis of areas of highest fluorescence resulted in extra resections (and eventually, clear margins) in five cases. Naturally, this approach is not perfect: besides encompassing a full extra step after resection, requiring extra time and logistical finetuning, it especially hinges on robust and elaborate intraoperative assessment procedures, where surgeon and pathologists jointly inspect the specimen macroscopically. Also, measures to accurately relocate (findings on) the specimen to the wound bed should be in place (e.g. the parallel tagging procedure [7], should the surgeon need to take an extra resection based on IOA outcome[8]. Further, care should be taken for fluorescence imaging to not disrupt or be impacted by routine pathological protocols. In research settings, it is also important to maintain pathologist blinding of the results of fluorescence imaging.

However, thorough logistical planning and new findings offer solutions: for example, although routine specimen inking performed with blue and black dyes significantly interfere with fluorescence as well as Raman signals, yellow, red and orange dyes were recently found to retain high fluorescence intensity when used with IRDye800CW [9]. Such minor adaptations to the standard of care are warranted when they may contribute to improved margin assessment, ultimately leading to better patient outcomes. These protocols should be standardized and incorporated into clinical guidelines to ensure uniform application and effectiveness across different institutions.

Nevertheless, for tumors requiring clear surgical margins, specimen-driven fluorescence imaging offers consistent findings as long as the 'sentinel margin approach' is employed [10, 11], effectively helping surgeon and pathologist to identify areas on the specimen that may require additional microscopic analysis. Its utility to compensate for the considerable limitations of frozen section analysis [12, 13], the current gold standard for margin status assessment, is remarkable in itself. As we have demonstrated for OSCC surgery, black-box fluorescence imaging on its own may offer significant clinical benefits, while avoiding costly wide-field fluorescence imaging devices as well as interference in the operating room. Furthermore, based on our findings, we presume that lower dose levels are sufficient for closed-field fluorescence imaging, as the imaging conditions are optimized and constant.

Moreover, black-box fluorescence imaging may extend beyond identifying sentinel margins by performing additional fluorescence imaging of their perpendicular cross-sections. At Erasmus MC, during routine IOA, suspicious areas prompt the pathologist to make one or more (complete or partial) perpendicular incisions to the tissue surface. This enables macroscopic, and if necessary, microscopic measurement (via frozen section analysis) of the deep margin. Given the stark fluorescent contrast (TBRs > 5) observed between OSCC and adjacent muscle tissue on black-box fluorescence images of formalin-fixed bread loaves (Figure 1A), black-box fluorescence imaging of these cross-sections immediately after IOA, alongside frozen section analysis, could be highly insightful. Comparing *ex vivo* fluorescence-measured resection margins with frozen section analysis would validate *ex vivo* fluorescence imaging for rapid, accurate margin assessment. Thus, incorporating this additional step into future FGS study designs, depending on logistical feasibility, would be worthwhile.

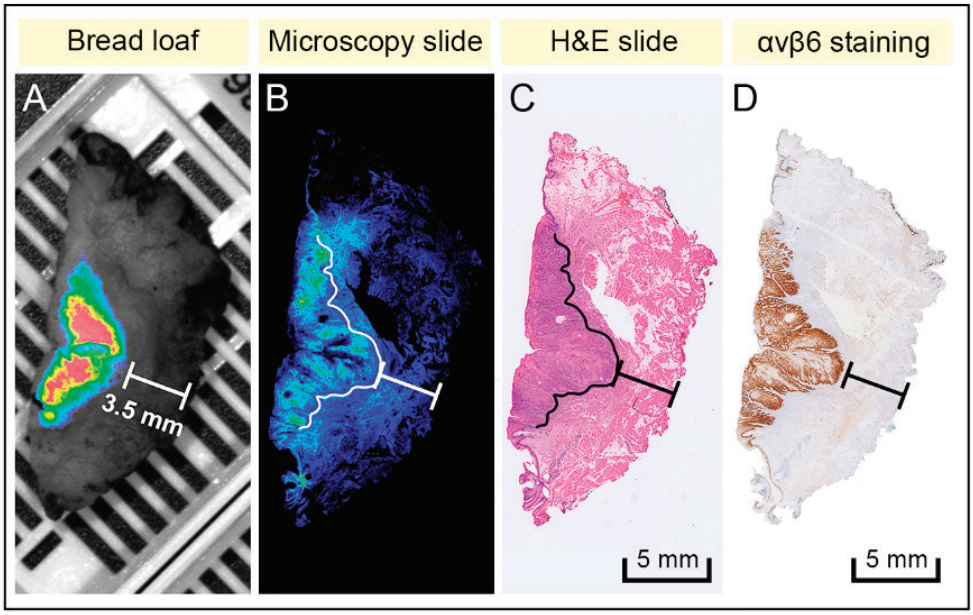

Figure 1: Postoperative fluorescence imaging using cRGD-ZW800-1 of oral cancer specimen from a patient with a close surgical margin (3.5 mm). Fluorescence in formalin-fixed bread loaf (A) and microscopy slides (B) are correlated with H&E histopathology (C) and αvβ6 immunohistochemistry (D). (A) was obtained with the Pearl Trilogy, B was obtained with the Odyssey CLx Imaging System, (C&D) were digitally scanned with a virtual microscope (Nanozoomer 2.0 HT, Hamamatsu Photonics, Shizuoka, Japan), and the scale bar was determined using NDP.view2 Viewing software (Hamamatsu Photonics, Shizuoka, Japan). H&E: Hematoxylin and Eosin.

FLUORESCENT AGENTS: SMALLER MOLECULES ARE BETTER

A hypothetical, "minimally disruptive", more readily implementable *ex vivo* fluorescence imaging protocol would involve topical administration of the fluorescent agent on the specimen, just before closed-field fluorescence imaging (and routine IOA). Besides avoiding disruptions to the current surgical workflow and doing away with toxicity risks and patient logistics associated with prior systemic administration, topically applied fluorescent agents are cost-effective: a lower dose can be used as there is no systemic volume of distribution, and the agent is not metabolized or excreted. As a result of these procedural, safety, and financial benefits, this approach would face far fewer hurdles towards approval to perform clinical trials, and subsequent clinical implementation. Although not a new concept (besides systemic administration, 5-ALA applied topically for the detection of glioblastoma and bladder cancer (among others) has been widely studied [14-16], only few affinity- (e.g. PARPi-FL [17] and cMBP-ICG [18]) or activity-based (e.g. gGlu-HMRG [19, 20]) fluorescent agents have been investigated for topical use thus far. Newly designed activatable imaging agents for topical administration are currently under investigation [21]. However, significant obstacles

remain, mainly centering around penetration depth, time constraints and specimen handling. A fluorescent signal emitting solely from malignancy extending to the surface of the whole specimen has no utility for close margin identification, but longer waiting times (to facilitate deeper penetration) or cutting or bread-loaving *prior* to topical administration (to facilitate cross-sectional, deep margin imaging) do not fit into the surgical workflow. However, this approach is still it its infancy, and time will tell which practical solutions or superior imaging agents will arise.

Furthermore, *ex vivo* topical administration would not be suitable for fluorescence imaging of occult malignancies (e.g. second primaries, occult metastases). In such applications, *in vivo* topical administration could be a feasible alternative, as has been shown with, for example, the use of gGlu-HMRG for detecting small peritoneal metastases [20], demonstrating the possibility to detect lesions during surgery without the need for systemic exposure.

Nevertheless, the vast majority of fluorescent agents currently under investigation require systemic administration prior to surgery [22]. While significant advancements in tumor-targeting strategies have been achieved in the past years, regulatory issues (among other factors) have resulted in relatively few clinically translated tracers. Monoclonal antibodies (mAbs) were among the earliest conjugates for targeted NIR fluorescent agents, largely because therapeutic mAbs could be repurposed for fluorescence imaging [23]. Although widely studied and well-established for fluorescence imaging of various cancers including OSCC [11, 24, 25], antibody-based fluorescent agents have some important practical and logistical pitfalls. They require early administration up to days in advance, and their compromised ability to provide clear contrast warranted pre-dosing with the unlabeled antibody [11, 25-28]. Smaller molecule based agents are thus emerging as preferred alternatives, due to their reduced immunogenicity and favorable pharmacodynamics: rapid tissue penetration and clearance from the body [29]. In particular, strong binding affinity and minimal nonspecific uptake is achieved with peptide-based agents, which are designed to contain highly selective and noncovalent peptide moieties for biomolecule recognition [30]. Furthermore, NIRF dyes with a net-neutral charge eliminate from normal tissues more rapidly, and have minimal non-targeted interactions [31]. Indeed, zwitterionic, integrin-targeted fluorescent agent cRGD-ZW800-1 was demonstrated to yield adequate *in vivo* contrast as early as 4 hours post-dose, facilitating administration on the day of surgery. Safety and efficacy of FGS with cRGD-ZW800-1 has thus far been confirmed in OSCC (Chapter 7) and colon cancer [32], is currently under investigation in pancreatic carcinomas (NCT05518071), and is set to be investigated in laryngeal cancer (NCT05752149), where integrin αvβ6 is highly overexpressed [33]. Although a singular, universal fluorescence imaging target is unlikely in the near future, cRGD has potential as a broadly applicable conjugate, warranting further immunohistochemical and subsequent clinical evaluations in other cancers. Additionally, microenvironment-sensitive probes, such as the pH-sensitive probe ONM-100, offer a pro-

mising alternative by exploiting the acidic extracellular environment of tumors, potentially offering a universal approach applicable across various cancer types [30, 34].

INTEGRATING FLUORESCENCE IMAGING WITH RAMAN SPECTROSCOPY

While fluorescence imaging using cRGD-ZW800-1 has demonstrated substantial success in identifying the location of close and positive margins in oral cancer, the need to confirm the adequacy of resection margins using frozen section analysis, remains. Furthermore, in our studies, selected examples of (unwanted) fluorescent signal from physiologically upregulated integrins were found in healthy gingiva and salivary glands. These findings open up a new realm for complementary techniques to refine intraoperative tissue characterization.

cRGD-ZW800-1 binds to a range of integrin heterodimers, including αvβ6. Although αvβ6 is a promising target, as it is highly overexpressed in most invasive epithelial cancers, its upregulation can also occur in non-cancerous tissues. This is a common challenge in oncology, where treatments such as chemotherapy have side effects because they affect both cancerous and healthy rapidly dividing cells. In the case of cRGD-ZW800-1, the (healthy) junctional epithelium of the gingiva naturally expresses levels of integrin αvβ6, thereby exhibiting a fluorescent signal.

The integration of Raman Spectroscopy (RS) with fluorescence imaging directly addresses the limitations inherent in FGS. This combined approach can help avoid superfluous frozen sections of fluorescent spots on resected specimens through precise margin width identification and tissue characterization, saving time and effort. Potentially, this approach could also be applied *in vivo* before excision to prevent overly extensive resections.

In the final chapter, we evaluate the integration of RS with fluorescence imaging, performed on fresh specimen from our clinical trial using cRGD-ZW800-1 in oral cancer and rectal cancer. This study explores the added clinical value of combining wide-field fluorescence imaging with depth-specific diagnostic precision offered by *ex vivo* RS (Chapter 10). Notably, we utilized a Raman needle probe for depth profiling [35]: by enabling specific depth assessment of the closest margins identified with fluorescence on top of precise characterization of tissue characteristics, RS offers a critical adjunct to fluorescence imaging. This combined methodology emerged in part in response to the issue of indeterminate margins identified with fluorescence imaging in OSCC, proposing a more refined approach. By incorporating fluorescence imaging to delineate resection boundaries, followed by RS for in-depth tissue examination, surgeons and pathologists are afforded a more comprehensive evaluation of the resection specimen. Moreover, by correlating Raman metrics with both fluorescence imaging and histopathological findings, the integration offers a holistic assessment of tumor margins

and tissue specifics. This would significantly contribute to the surgical decision-making process, potentially reducing unnecessary tissue resection and improving patient outcomes.

Altogether, the trend is towards minimizing dependence on subjective evaluations by utilizing supportive technologies that reduce the need—or at least the frequency—for expert human intervention. Case in point: RS depth profiling may in certain scenarios replace the expert (pathologist's) opinion on the ambiguity of fluorescent false positives, or the laborious performance of a frozen section followed by microscopic analysis. This progression towards advanced technologies is a significant development within the field.

The following chapter explores such topics that extend beyond the direct findings of this thesis. These include the pivotal role of Artificial Intelligence (AI) in reducing the cognitive load of fluorescence-based decision-making. Such advancements highlight potential directions for further research and development, aiming to enhance the accuracy, efficacy, and standardization of fluorescence imaging in surgical oncology.

FUTURE PERSPECTIVES

Artificial Intelligence in Fluorescence Imaging

Human visual (or tactile) judgment is traditionally directive for key surgical decision making. However, not unlike the anatomical site that is to be operated on, the interpretation of fluorescence signals is rarely straightforward, especially *in vivo [36, 37]*. Mathematical and computational algorithms are emerging as powerful tools to overcome these challenges, potentially improving predictive and diagnostic accuracy by extracting complex medical imaging information that may not (initially) be apparent to human observers. Research on AI within medicine is thus rapidly progressing, especially in image-dominant fields such as surgical oncology.

AI has proven instrumental in HNC care [38], particularly in the (early) diagnosis of oral cancer [39, 40]. Moreover, the utility of AI as an adjunct to optical imaging technologies such as OCT, AF, CE-NBI and Fluorescence Lifetime Imaging (FliM) has been explored for both preoperative (virtual) surgical planning as well as for intraoperative guidance, with tentatively promising results [39, 41, 42]. Similarly, AI is being explored as a "procedure companion" in endoscopy and laparoscopy, to assist in polypectomy [43] and colorectal cancer detection and classification [44], with efforts underway to validate the effectiveness of AI in analyzing ICG fluorescence perfusions signals to differentiate between benign and malignant rectal tumors [45].

The integration of AI with fluorescence imaging is anticipated to improve the accuracy and reliability of fluorescence-guided surgery [46]. Enhanced interpretation of complex

patterns and improved accuracy in image reconstruction can promote better intraoperative decision-making. Furthermore, deep learning applied to fluorescence imaging data facilitates the development of AI-based navigation systems. This integration can also be utilized to train surgeons in fluorescence-guided surgery using virtual or augmented reality platforms. Additionally, predictive analytics derived from fluorescence imaging data could improve the precision of AI-based forecasts of postoperative outcomes, including survival rates [47].

While current algorithms are constrained by the variety of fluorophores and biological targets they can analyze, ongoing advancements in software adaptability will improve integration into surgical workflows, providing clinicians with objective insights into fluorescent signals. This technological progress is key to developing next-generation fluorescent agents and imaging devices. This notwithstanding, there are significant challenges in AI deployment, including the need for large and diverse datasets for effective AI model training and ethical/regulatory concerns regarding patient safety and privacy. Additionally, despite the proliferation of AI models, clinical implementation remains scarce. Factors contributing to this gap include the stringent regulatory approvals required for clinical use, the complexity of integrating AI systems into existing clinical workflows, and the need for robust validation in real-world settings to ensure reliability and safety. Naturally, ongoing research and refinement of the integration of AI in surgical practice are imperative. Likewise, the difficulty in explaining AI decisions in medical practice persists, which is why a synergistic approach combining AI's strength with human expertise should be employed. As with all advanced technologies, AI should be used to augment (rather than replace) the surgeon's capabilities, reducing the cognitive load and variability in human performance.

Finally, an important argument for the integration of AI with fluorescence imaging lies in its utility for standardization. Robust AI models can significantly reduce inter- and intra-observer variability by standardizing the interpretation of complex fluorescence imaging data. As fluorescence imaging datasets expand and diversify, they enhance the potential for more informed, retraceable, data-driven surgical decision-making. Moreover, AI is particularly suited to automating various cumbersome FGS -related tasks, such as calculating image quality metrics (e.g., tumor-to-background ratio, contrast-to-variance ratio[48]), and synthesizing standardized reports based on interpreted fluorescence imaging data, intraoperative decisions, and pathology reports. AI could also, for example, be used to automatically detect and annotate sentinel margins in closed-field fluorescence imaging. Such automations would save valuable time and reduce the labor intensity involved, streamlining the overall surgical process and enhancing efficiency.

Next-generation Fluorescence Imaging: Spectral diversification and other refinements

In discussions found in recent literature about AI in fluorescence imaging for cancer surgery, there is a prevalence of optical imaging technologies that constitute more novel iterations

of NIR (i.e. NIR-I, which covers 700 – 900 nm) fluorescence imaging, namely Short-Wave Infrared (SWIR), Second Near-infrared Window Imaging (NIR-II), Multispectral Imaging (MSI) and Hyperspectral Imaging (HSI). Fluorescence imaging in the SWIR (1000 – 2500 nm) and NIR-II (1000 – 1700 nm) regions stand out for their deeper tissue penetration and reduced scattering, offering enhanced visibility of tumors and more precise delineation of cancerous tissues from normal tissues during surgical resections. Meanwhile, MSI and HSI provide more comprehensive spectral information, allowing for the simultaneous detection (and customization) of multiple fluorescence signals, enhancing specificity and enabling the use of varied fluorescent dyes tailored to specific cancer types or metabolic processes. Moreover, SWIR and NIR-II wavelengths may be included in both MSI and HSI systems, offering enhanced spectral data that indeed converge well with AI processing. The spectrally rich, complex data provided by HSI and MSI in these ranges are particularly suited for analysis using machine learning algorithms, automating the interpretation process to provide rapid, reliable insights during surgical procedures [49].

Recently, the first in-human results using dual aperture fluorescence ratio (dAFR) imaging for *ex vivo* close margin detection in OSCC were published [50]. This technique compares fluorescence images taken at wide and narrow numerical apertures from the same viewpoint, providing an estimate of fluorescence depth that is unaffected by tissue optical properties. The dAFR approach achieved perfect sensitivity in distinguishing close from clear margins, significantly outperforming conventional single-aperture fluorescence (sAF) imaging. A key advantage of dAFR is its automated normalization, eliminating the need for manual selection of ROIs and enhancing standardization and reproducibility. These findings suggest that dAFR imaging could significantly improve the surgical management of OSCC and other cancers, warranting further investigation.

Advanced Evaluation of Fluorescence Imaging

FGS has seen remarkable advancements in recent years, driven by innovations in molecular agents, imaging devices, and the integration of AI, all against a backdrop of evolving regulatory frameworks. As these developments continue to enhance surgical oncology, it is critical to ensure they translate into tangible clinical benefits for patients. However, the field grapples with challenges, including the need for standardization and reproducibility amid a proliferation of literature and methodologies. This diversity, while beneficial, requires consensus on scientific efforts to convert into clinical advances effectively.

The primary goal of FGS is to prolong patient survival and improve quality of life by enabling precise intraoperative decision-making. Our findings reinforce that the impact of fluorescence imaging on surgical decisions is a robust measure of clinical utility, consistent across different settings and unaffected by institutional variances. International collaboration is crucial to define and update best practices, with AI poised to play a significant role in shaping these standards. Recent phase II data indicates that fluorescence imaging in head

and neck cancer has progressed beyond proof-of-concept studies: fluorescence-guided fresh frozen sectioning enabled accurate intraoperative margin classification in 95% of patients, reduced the inadequate margin rate from 50% to 15% after additional resections, and reduced or omitted adjuvant treatment in a substantial proportion of patients, all within a clinically feasible intraoperative workflow without delaying surgery [51]. Together with the findings presented in this thesis, this suggests that the next step for the field should be a joint multicenter study using standardized protocols, harmonized reporting and clinically relevant endpoints. Such a study is imperative to determine whether fluorescence-guided margin assessment can reproducibly improve adequate margin rates, reduce treatment escalation, and ultimately provide the level of evidence required to support changes in national clinical guidelines.

In the technical/diagnostic evaluation of FGS (precluding other important comparisons such as costs, ease of use, safety etc.), the essential task is to accurately distinguish malignant from non-malignant regions. Traditional metrics like the TBR have commonly been used to assess intraoperative contrast but fall short in environments where signal variability is high. In contrast, the Contrast-to-Variability Ratio (CVR) incorporates standard deviations of fluorescence signals from both tumor and healthy tissues, providing a more comprehensive assessment of tissue variability and heterogeneity, which is critical for advanced modeling and algorithm development in fluorescence imaging [48]. This metric proves especially effective in environments characterized by complex noise statistics, such as those encountered in FLiM [52], HSI [53], and RS [54]. By integrating CVR into AI-driven analysis frameworks, we can better utilize the rich data from (next-generation) fluorescence imaging.

Adopting more comprehensive metrics such as the CVR ensures that our methodologies are suited for the increasingly complex landscape of surgical oncology. This addition would help in standardizing fluorescence imaging protocols, further enhance the objectivity of surgical decision-making, and ultimately, improve the outcomes for patients undergoing cancer surgery.

CONCLUSION

This thesis highlights the transformative potential of fluorescence imaging in surgical oncology, particularly through its impact on intraoperative decision-making. The studies presented establish that the ultimate measure of clinical benefit for fluorescence imaging lies in its ability to influence surgical strategies (*Chapters 4 and 5*). Further research demonstrates the safety, feasibility and clinical value of fluorescence imaging with integrin-targeted agent cRGD-ZW800-1, which reliably identified all clinically relevant inadequate margins and altered intraoperative decision-making in five patients, by enabling additional resections for inadequate margins initially overlooked during standard IOA, thereby improving the rate of

adequate resection margins in OSCC (*Chapter 7*). The proposition of integrating fluorescence imaging with RS introduces a novel approach to overcoming the limitations of fluorescence imaging alone (*Chapters 8 and 9*). Its clinical evaluation showcases the benefits of sentinel margin identification with fluorescence imaging, alongside precise tissue characterization and margin depth measurement with RS, thereby facilitating more accurate intraoperative decision-making (*Chapter 10*).

Taken together, these findings represent a significant advancement in our understanding and application of fluorescence imaging in surgical oncology, while emphasizing the importance of continuous innovation and collaboration in the field. Looking ahead, advancements in AI, expanded-spectrum fluorescence imaging, and improved metrics for evaluation promise to further refine the application of fluorescence imaging, paving the way for more standardized, data-driven, and effective surgical interventions. Additionally, multicenter randomized trials will be essential to confirm the effect of fluorescence imaging on long-term oncological outcomes and to support broader implementation in standard surgical care. In closing, this thesis demonstrates how fluorescence imaging can enhance intraoperative decision-making, ultimately aiming to improve patient outcomes in surgical oncology.

REFERENCES

1. Chiti, L.E., et al., *Impact of Surgical Lights on the Performance of Fluorescence-Guided Surgery Systems: A Pilot Study.* Animals (Basel), 2023. **13**(14).
2. Lauwerends, L.J., et al., *Real-time fluorescence imaging in intraoperative decision making for cancer surgery.* Lancet Oncol, 2021. **22**(5): p. e186-e195.
3. Smits, R.W., et al., *Resection margins in oral cancer surgery: Room for improvement.* Head Neck, 2016. **38 Suppl 1**: p. E2197-203.
4. Solomon, J., et al., *The impact of close surgical margins on recurrence in oral squamous cell carcinoma.* J Otolaryngol Head Neck Surg, 2021. **50**(1): p. 9.
5. Szewczyk, M., et al., *A Matter of Margins in Oral Cancer-How Close Is Enough?* Cancers (Basel), 2024. **16**(8).
6. Brouwer de Koning, S.G., et al., *Assessment of the deep resection margin during oral cancer surgery: A systematic review.* Eur J Surg Oncol, 2021. **47**(9): p. 2220-2232.
7. van Lanschot, C.G.F., et al., *Relocation of inadequate resection margins in the wound bed during oral cavity oncological surgery: A feasibility study.* Head Neck, 2019. **41**(7): p. 2159-2166.
8. Noorlag, R., R. de Bree, and M.J.H. Witjes, *Image-guided surgery in oral cancer: toward improved margin control.* Curr Opin Oncol, 2022. **34**(3): p. 170-176.
9. Kondo, T., et al., *Identification of Optimal Tissue-Marking Dye Color for Pathological Evaluation in Fluorescence Imaging Using IRDye800CW.* Mol Imaging Biol, 2024. **26**(1): p. 162-172.
10. van Keulen, S., et al., *The Sentinel Margin: Intraoperative Ex Vivo Specimen Mapping Using Relative Fluorescence Intensity.* Clin Cancer Res, 2019. **25**(15): p. 4656-4662.
11. Krishnan, G., et al., *Fluorescent Molecular Imaging Can Improve Intraoperative Sentinel Margin Detection in Oral Squamous Cell Carcinoma.* J Nucl Med, 2022. **63**(8): p. 1162-1168.
12. St John, E.R., et al., *Diagnostic Accuracy of Intraoperative Techniques for Margin Assessment in Breast Cancer Surgery: A Meta-analysis.* Ann Surg, 2017. **265**(2): p. 300-310.
13. Cendan, J.C., D. Coco, and E.M. Copeland, 3rd, *Accuracy of intraoperative frozen-section analysis of breast cancer lumpectomy-bed margins.* J Am Coll Surg, 2005. **201**(2): p. 194-8.
14. Vahrmeijer, A.L., et al., *Image-guided cancer surgery using near-infrared fluorescence.* Nat Rev Clin Oncol, 2013. **10**(9): p. 507-18.
15. Harada, Y., et al., *5-Aminolevulinic Acid-Induced Protoporphyrin IX Fluorescence Imaging for Tumor Detection: Recent Advances and Challenges.* Int J Mol Sci, 2022. **23**(12).
16. Howley, R., S. Chandratre, and B. Chen, *5-Aminolevulinic Acid as a Theranostic Agent for Tumor Fluorescence Imaging and Photodynamic Therapy.* Bioengineering (Basel), 2023. **10**(4).
17. Demetrio de Souza Franca, P., et al., *A phase I study of a PARP1-targeted topical fluorophore for the detection of oral cancer.* Eur J Nucl Med Mol Imaging, 2021. **48**(11): p. 3618-3630.
18. Wang, J., et al., *A c-MET-Targeted Topical Fluorescent Probe cMBP-ICG Improves Oral Squamous Cell Carcinoma Detection in Humans.* Ann Surg Oncol, 2023. **30**(1): p. 641-651.
19. Urano, Y., et al., *Rapid cancer detection by topically spraying a gamma-glutamyltranspeptidase-activated fluorescent probe.* Sci Transl Med, 2011. **3**(110): p. 110ra119.
20. Nakamura, Y., et al., *Dynamic fluorescent imaging with the activatable probe, gamma-glutamyl hydroxymethyl rhodamine green in the detection of peritoneal cancer metastases: Overcoming the problem of dilution when using a sprayable optical probe.* Oncotarget, 2016. **7**(32): p. 51124-51137.

21. Li, X., et al., *Development of pH-activatable fluorescent probes for rapid visualization of metastatic tumours and fluorescence-guided surgery via topical spraying.* Chem Commun (Camb), 2021. **57**(81): p. 10636-10639.
22. Sutton, P.A., et al., *Fluorescence-guided surgery: comprehensive review.* BJS Open, 2023. **7**(3).
23. Hernandez Vargas, S., et al., *Receptor-Targeted Fluorescence-Guided Surgery With Low Molecular Weight Agents.* Front Oncol, 2021. **11**: p. 674083.
24. Debie, P. and S. Hernot, *Emerging Fluorescent Molecular Tracers to Guide Intra-Operative Surgical Decision-Making.* Front Pharmacol, 2019. **10**: p. 510.
25. de Wit, J.G., et al., *EGFR-targeted fluorescence molecular imaging for intraoperative margin assessment in oral cancer patients: a phase II trial.* Nat Commun, 2023. **14**(1): p. 4952.
26. Moore, L.S., et al., *Effects of an Unlabeled Loading Dose on Tumor-Specific Uptake of a Fluorescently Labeled Antibody for Optical Surgical Navigation.* Mol Imaging Biol, 2017. **19**(4): p. 610-616.
27. Voskuil, F.J., et al., *Fluorescence-guided imaging for resection margin evaluation in head and neck cancer patients using cetuximab-800CW: A quantitative dose-escalation study.* Theranostics, 2020. **10**(9): p. 3994-4005.
28. Nishio, N., et al., *Optimal Dosing Strategy for Fluorescence-Guided Surgery with Panitumumab-IRDye800CW in Head and Neck Cancer.* Mol Imaging Biol, 2020. **22**(1): p. 156-164.
29. van Dam, M.A., et al., *Consensus conference statement on fluorescence-guided surgery (FGS) ESSO course on fluorescence-guided surgery.* Eur J Surg Oncol, 2024. **50**(2): p. 107317.
30. Seah, D., Z. Cheng, and M. Vendrell, *Fluorescent Probes for Imaging in Humans: Where Are We Now?* ACS Nano, 2023. **17**(20): p. 19478-19490.
31. Choi, H.S., et al., *Synthesis and in vivo fate of zwitterionic near-infrared fluorophores.* Angew Chem Int Ed Engl, 2011. **50**(28): p. 6258-63.
32. de Valk, K.S., et al., *First-in-Human Assessment of cRGD-ZW800-1, a Zwitterionic, Integrin-Targeted, Near-Infrared Fluorescent Peptide in Colon Carcinoma.* Clin Cancer Res, 2020. **26**(15): p. 3990-3998.
33. Lauwerends, L.J., et al., *Tumour Marker Expression in Head and Neck Malignancies to Identify Potential Targets for Intraoperative Molecular Near-Infrared Imaging.* Mol Diagn Ther, 2024. **28**(6): p. 811-820.
34. Voskuil, F.J., et al., *Exploiting metabolic acidosis in solid cancers using a tumor-agnostic pH-activatable nanoprobe for fluorescence-guided surgery.* Nat Commun, 2020. **11**(1): p. 3257.
35. Aaboubout, Y., et al., *Intraoperative assessment of resection margins by Raman spectroscopy to guide oral cancer surgery.* Analyst, 2023. **148**(17): p. 4116-4126.
36. Keereweer, S., et al., *Optical image-guided cancer surgery: challenges and limitations.* Clin Cancer Res, 2013. **19**(14): p. 3745-54.
37. Lauwerends, L.J., et al., *The complementary value of intraoperative fluorescence imaging and Raman spectroscopy for cancer surgery: combining the incompatibles.* Eur J Nucl Med Mol Imaging, 2022. **49**(7): p. 2364-2376.
38. van Dijk, L.V. and C.D. Fuller, *Artificial Intelligence and Radiomics in Head and Neck Cancer Care: Opportunities, Mechanics, and Challenges.* Am Soc Clin Oncol Educ Book, 2021. **41**: p. 1-11.
39. Ramezani, K. and M. Tofangchiha, *Oral Cancer Screening by Artificial Intelligence-Oriented Interpretation of Optical Coherence Tomography Images.* Radiol Res Pract, 2022. **2022**: p. 1614838.
40. Ilhan, B., et al., *Improving Oral Cancer Outcomes with Imaging and Artificial Intelligence.* J Dent Res, 2020. **99**(3): p. 241-248.

41. Marsden, M., et al., *Intraoperative Margin Assessment in Oral and Oropharyngeal Cancer Using Label-Free Fluorescence Lifetime Imaging and Machine Learning.* IEEE Trans Biomed Eng, 2021. **68**(3): p. 857-868.
42. Esmaeili, N., et al., *Deep Convolution Neural Network for Laryngeal Cancer Classification on Contact Endoscopy-Narrow Band Imaging.* Sensors (Basel), 2021. **21**(23).
43. El Zoghbi, M., et al., *Artificial Intelligence-Assisted Optical Diagnosis: A Comprehensive Review of Its Role in Leave-In-Situ and Resect-and-Discard Strategies in Colonoscopy.* Clin Transl Gastroenterol, 2023. **14**(10): p. e00640.
44. Hardy, N.P., et al., *Intraprocedural Artificial Intelligence for Colorectal Cancer Detection and Characterisation in Endoscopy and Laparoscopy.* Surg Innov, 2021. **28**(6): p. 768-775.
45. Moynihan, A., et al., *CLASSICA: Validating artificial intelligence in classifying cancer in real time during surgery.* Colorectal Dis, 2023. **25**(12): p. 2392-2402.
46. Chiu, S.F., C.M. Hung, and C.C. Chiu, *A commentary on 'Approved and investigational fluorescent optical imaging agents for disease detection in surgery'.* Int J Surg, 2024. **110**(1): p. 611-612.
47. Kinoshita, M., et al., *Deep Learning Model Based on Contrast-Enhanced Computed Tomography Imaging to Predict Postoperative Early Recurrence after the Curative Resection of a Solitary Hepatocellular Carcinoma.* Cancers (Basel), 2023. **15**(7).
48. Tichauer, K.M., et al., *Task-based evaluation of fluorescent-guided cancer surgery as a means of identifying optimal imaging agent properties in the context of variability in tumor- and healthy-tissue physiology.* Proc SPIE Int Soc Opt Eng, 2020. **11222**.
49. Waterhouse, D.J., et al., *Enhancing intraoperative tumor delineation with multispectral short-wave infrared fluorescence imaging and machine learning.* J Biomed Opt, 2023. **28**(9): p. 094804.
50. Rounds, C.C., et al., *Improved intraoperative identification of close margins in oral squamous cell carcinoma resections using a dual aperture fluorescence ratio approach: first in-human results.* J Biomed Opt, 2024. **29**(1): p. 016003.
51. Nijboer, T.S., et al., *Intraoperative fluorescence-guided fresh frozen sectioning for margin control in head and neck cancer: phase 2 clinical trial.* Nat Commun, 2026.
52. Pal, R., et al., *Fluorescence Lifetime-Based Tumor Contrast Enhancement Using an EGFR Antibody-Labeled Near-Infrared Fluorophore.* Clin Cancer Res, 2019. **25**(22): p. 6653-6661.
53. Kim, A., et al., *Quantification of in vivo fluorescence decoupled from the effects of tissue optical properties using fiber-optic spectroscopy measurements.* J Biomed Opt, 2010. **15**(6): p. 067006.
54. Lemoine, E., et al., *Feature engineering applied to intraoperative in vivo Raman spectroscopy sheds light on molecular processes in brain cancer: a retrospective study of 65 patients.* Analyst, 2019. **144**(22): p. 6517-6532.


A

Appendix

NEDERLANDSE SAMENVATTING

Het hoofddoel van oncologische chirurgie is het verwijderen van solide tumoren met adequate marges en het behouden van de integriteit van omliggende gezonde weefsels. Hiervoor is het noodzakelijk om nauwkeurig onderscheid te maken tussen de tumor en omgevende weefsels. Traditionele afhankelijkheid van visuele inspectie en palpatie tijdens de operatie wordt beperkt door de vaak subtiele verschillen tussen gezonde en maligne weefsels.

Nabij-infrarood (NIR) fluorescentiebeeldvorming, een opkomende optische techniek in intraoperatieve visualisatie, belooft het vermogen van chirurgen en pathologen te verbeteren om onderscheid te maken tussen kwaadaardige en normale weefsels. Door het vergemakkelijken van nauwkeurigere resectie van solide tumoren, heeft fluorescentie-geleide chirurgie (FGC) potentie om de uitkomsten voor patiënten aanzienlijk te verbeteren. Desalniettemin bevindt de integratie van fluorescentiebeeldvorming in de klinische praktijk zich nog in een vroeg stadium. Het doel van dit proefschrift was om de integratie van optische beeldvorming in de chirurgische praktijk te onderzoeken – met name voor hoofd-hals kanker – om de intraoperatieve precisie van tumorafbakening te verbeteren. Dit wordt beschouwd binnen de bredere context van het verbeteren van chirurgische resultaten en patiëntenprognoses door verbeterde intraoperatieve begeleiding.

Deel I: Overzicht van Intraoperatieve Beeldvormingstechnologieën

Deel I onderzoekt het scala aan toepassingen van fluorescentiebeeldvorming en biedt een uitgebreid overzicht van bestaande intraoperatieve beeldvormingstechnologieën die worden gebruikt bij verschillende soorten kanker. *Hoofdstuk 2* geeft een systematisch overzicht van de huidige intraoperatieve beeldvormingstechnologieën voor chirurgische resectie van larynxkanker, identificeert beperkingen bij de beoordeling van diepe marges en suggereert toekomstige richtingen voor optische beeldvormingstoepassingen. *Hoofdstuk 3*, ook een systematische review, bespreekt de toepassing van FGC bij colorectale kanker, waarbij de klinische voordelen en het potentieel voor verbeterde chirurgische precisie en patiëntresultaten worden uiteengezet.

Deel II: Conceptuele Grondslagen van Fluorescentie Beeldvorming in Kankerchirurgie

Deel II legt de theoretische basis en praktische toepassingen van fluorescentiebeeldvorming vast. *Hoofdstuk 4* verkent de belangrijke rol van (*real-time*) fluorescentiebeeldvorming bij intraoperatieve besluitvorming in kankerchirurgie en benadrukt het potentieel van de methode om (post-)chirurgische strategieën te wijzigen. Het benadrukt de noodzaak van verfijnde onderzoeksopzetten en rapportagestandaarden om de klinische voordelen van FGC nauwkeurig te beoordelen. Aanbevelingen over hoe veranderingen in intraoperatieve besluitvorming door fluorescentiebeeldvorming te rapporteren, worden gepresenteerd met als doel de brede klinische implementatie van FGC te versnellen. *Hoofdstuk 5* vervolgt met onze reactie op een

correspondentiebrief ("*het perspectief van een patholoog*"), waarin argumenten worden aangevoerd ten gunste van de kernboodschap van *Hoofdstuk 4*: het effect van fluorescentiebeeldvorming op intraoperatieve besluitvorming als ultieme maatstaf voor het klinische voordeel van FGC.

Deel III: Vooruitgang in Fluorescentie Beeldvorming voor Hoofd- en Halskanker

Deel III presenteert nieuw onderzoek naar de (klinische) toepassing van FGC bij hoofd-hals kanker. *Hoofdstuk 6* onderzoekt potentiële doelwitten voor NIR fluorescentie op dit gebied door middel van een immunohistochemische studie uitgevoerd op mondholteplaveiselcelcarcinoom, larynxplaveiselcarcinoom en papillair schildkliercarcinoom, met als doel bij te dragen aan de ontwikkeling van tumor-specifieke fluorescente stoffen. Aangezien de focus lag op potentiële snelle vertaling naar klinische toepassingen, evalueerde deze studie de markerexpressie van zes doelwitten met (pre-)klinisch beschikbare NIR fluorescente stoffen die momenteel worden onderzocht bij verschillende kankers: CEA, EpCAM, integrine αvβ6, VEGF-α, EGFR en c-MET. Het meest opvallende resultaat van deze studie was dat met name integrine αvβ6 een sterk contrast bood voor tumormarge afbakening in mondholte- en larynxplaveiselcelcarcinoom.

Vervolgens demonstreert *Hoofdstuk 7* de veiligheid, haalbaarheid en effectiviteit van cRGD-ZW800-1 – een integrine-specifieke (waaronder integrine αvβ6) fluorescente stof bestaande uit een cyclisch pentapeptide (cRGD) gekoppeld aan een 800 nm fluorofoor ZW800-1 – bij het verbeteren van het aandeel adequate chirurgische resectiemarges in mondholtekanker. In deze klinische studie visualiseerde fluorescentiebeeldvorming met cRGD-ZW800-1 succesvol alle inadequate resectiemarges, inclusief negen inadequate marges (drie positieve en zes krappe) die aanvankelijk over het hoofd werden gezien tijdens routinematige intraoperatieve beoordeling door de chirurg en patholoog. Bij vijf van de 31 patiënten (16%) beinvloedden deze fluorescentiebevindingen direct de intraoperatieve besluitvorming en leidden zij tot aanvullende resecties; bij drie van deze patiënten kon adjuvante radiotherapie worden voorkomen. Fluorescentiebeeldvorming liet op patiëntniveau een sensitiviteit van 100% zien, tegenover 70% voor de standaard intraoperatieve beoordeling, Bovendien leverde de unieke benadering van deze studie niet alleen kwalitatieve beeldgegevens op, maar onderbouwde ook de betrouwbaarheid ervan door kwantitatieve spectroscopie. Door gebruik te maken van de inzichten verkregen uit temporele *in vivo* kwantificering van de fluorescente tracer met *MDSFR/SFF* spectroscopie, informeerde deze benadering ook succesvol het besluitvormingsproces met betrekking tot dosering en timing. De studie demonstreerde de aanzienlijke klinische waarde van intraoperatieve fluorescentiebeeldvorming bij mondholtekanker chirurgie, waarbij fluorescentiebeeldvorming alle klinisch relevante inadequate marges betrouwbaar detecteerde en direct invloed had op het chirurgisch handelen. De integratie van fluorescentiebeeldvorming met cRGD-ZW800-1 in deze studie toont aanzienlijke oncologische impact, wat het potentieel van deze technologie onderstreept in het verbeteren van chirurgische precisie en patiëntuitkomsten.

Deel IV: Integratie van Fluorescentiebeeldvorming met Raman Spectroscopie

Deel IV stelt voor om de beperkingen van fluorescentiebeeldvorming te overwinnen door het te integreren met Raman Spectroscopie (RS). *Hoofdstuk 8* bespreekt de complementaire waarde van het combineren van FGC met RS om duidelijke chirurgische marges te bereiken, waarbij technische uitdagingen worden aangepakt en strategieën worden gepresenteerd voor de integratie van deze technologieën in de klinische praktijk. *Hoofdstuk 9* presenteert de ontwikkeling van een NIR RS-opstelling die compatibel is met FGC. Deze opstelling omzeilt de spectrale overlap tussen fluorescentie en Raman-emissies, waardoor het gelijktijdig gebruik van beide beeldvorming modaliteiten mogelijk wordt om tumorspecificiteit en chirurgische precisie te verbeteren. *Hoofdstuk 10* breidt het eerdere werk uit over het succesvolle gebruik van fluorescentiebeeldvorming voor margeafbakening bij mondholtekankeroperaties door de klinische voordelen te onderzoeken van het gebruik van *ex vivo* RS naast fluorescentiebeeldvorming voor intraoperatieve beoordeling van mondholte- en rectumkanker exemplaren. Terwijl NIR fluorescentie effectief de dichtstbijzijnde marges identificeert, blijft vriescoupe analyse noodzakelijk om de margestatus te bevestigen. RS, door middel van diepteprofilering met een Raman-naaldprobe, kan een geschikte aanvulling (of alternatief) zijn door lokale metingen op bekende diepten aan te bieden, waardoor een duidelijke bepaling van marge-adequaatheid mogelijk is. Bovendien kan het vermogen van RS om fluorescentie in niet-kwaadaardige weefsels zoals de gingiva en speekselklieren te onderscheiden, het aantal onnodige vriescoupes verminderen en (indien *in vivo* uitgevoerd) meer nauwkeurige, conservatieve resecties vergemakkelijken. Deze studie benadrukt de klinische waarde van het samenvoegen van RS met fluorescentiebeeldvorming en benadrukt het potentieel om de nauwkeurigheid van intraoperatieve beslissingen te verbeteren bij een breed scala aan kankers, wat een significante vooruitgang markeert in het veld van kankerchirurgie.

Deel V: Samenvatting, Discussie en Toekomstperspectieven

Alle resultaten worden samengevat in *Hoofdstuk 11*. *Hoofdstuk 12* bevat de algemene discussie, toekomstperspectieven en conclusie.

In dit proefschrift stellen we dat de intraoperatieve integratie van fluorescentiebeeldvorming een monumentale stap voorwaarts betekent in het veld van de chirurgische oncologie. Door zowel de chirurg als de patholoog aanzienlijk te verbeteren in hun vermogen om nauwkeurig onderscheid te maken tussen maligne en gezonde weefsels, belooft fluorescentiebeeldvorming niet alleen de chirurgische resultaten te verbeteren, maar ook de kans op ziekteherhaling te verkleinen en de prognoses van patiënten positief te beïnvloeden. Dit proefschrift biedt een uitgebreid overzicht van de huidige stand van optische beeldvormingstechnieken, hun praktische toepassingen in hoofd-hals chirurgie en de potentiële toekomstige ontwikkelingen die het veld van de chirurgische oncologie verder zouden kunnen revolutioneren.

LIST OF ABBREVIATIONS

5-ALA	5-aminolevulinic acid
AF	Autofluorescence
BSA	Bovine serum albumin
CE	Contact endoscopy
CEA	Carcinoembryonic antigen
CLRM	Colorectal liver metastases
c-MET	C-mesenchymal-epithelial transition factor
CRC	Colorectal cancer
EGFR	Epidermal growth factor receptor
EMA	European Medicines Agent
EpCAM	Epithelial cell adhesion molecule
EPR	Enhanced permeability and retention
FDA	United States Food and Drug Administration
FGS	Fluorescence-guided surgery
FI	Fluorescence imaging
H&E	Hematoxylin & eosin
HIPEC	Hyperthermic intraperitoneal chemotherapy
HNC	Head and neck cancers
HWVN/HWN	High wavenumber
ICG	Indocyanine green
IHC	Immunohistochemistry
InGaAs	Indium Gallium Arsenide
IOA	Intraoperative assessment
LSCC	Laryngeal squamous cell carcinoma
MB	Methylene blue
MDSFR/SFF	Multi-diameter single-fiber reflectance and single-fiber fluorescence
NBI	Narrow-band imaging
NIR	Near-infrared
OCT	Optical coherence tomography
OSCC	Oral squamous cell carcinoma
PPiX	Protoporphyrin IX
PTC	Papillary thyroid carcinoma
RS	Raman spectroscopy
SBR	Signal-to-background ratio
SLN	Sentinel lymph node
SWIR	Short-wave infrared

TBR	Tumour-to-background ratio
TLM	Transoral CO2 laser microsurgery
VEGF-α	Vascular endothelial growth factor α

LIST OF PUBLICATIONS

1. Real-time fluorescence imaging in intraoperative decision making for cancer surgery
Lauwerends LJ, van Driel PBAA, Baatenburg de Jong RJ, Hardillo JAU, Koljenovic S, Puppels GJ, Mezzanotte L, Löwik CWGM, Rosenthal EL, Vahrmeijer AL, Keereweer S
Lancet Oncol. 2021 May;22(5):e186-e195. doi: 10.1016/S1470-2045(20)30600-8. Epub 2021 Mar 23.

2. Real-time fluorescence imaging for cancer surgery: a pathologist's perspective - Authors' reply
Lauwerends LJ, van Driel PBAA, Koljenovic S, Vahrmeijer AL, Keereweer S
Lancet Oncol. 2021 Jul;22(7):e283. doi: 10.1016/S1470-2045(21)00335-1.

3. Current Intraoperative Imaging Techniques to Improve Surgical Resection of Laryngeal Cancer: A Systematic Review
Lauwerends LJ, Galema HA, Hardillo JAU, Sewnaik A, Monserez D, van Driel PBAA, Verhoef C, Baatenburg de Jong RJ, Hilling DE, Keereweer S.
Cancers (Basel). 2021 Apr 15;13(8):1895. doi: 10.3390/cancers13081895.

4. Fluorescence-guided surgery in colorectal cancer; a review on clinical results and future perspectives
Galema HA, Meijer RPJ, Lauwerends LJ, Verhoef C, Burggraaf J, Vahrmeijer AL, Hutteman M, Keereweer S, Hilling DE
European Journal of Surgical Oncology. 2022 Apr;48(4):810-821. doi: 10.1016/j.ejso.2021.10.005.

5. Fluorescence-guided sentinel lymph node detection in colorectal cancer
Meijer RPJ, Galema HA, Lauwerends LJ, Verhoef C, Burggraaf J, Keereweer S, Hutteman M, Vahrmeijer AL, Hilling DE
The Lymphatic System in Colorectal Cancer. Basic Concepts, Pathology, Imaging and Treatment Perspectives. 2022, Pages 245-255

6. The complementary value of intraoperative fluorescence imaging and Raman spectroscopy for cancer surgery: combining the incompatibles
Lauwerends LJ & Abbasi H*, Bakker Schut TC, van Driel PBAA, Hardillo JAU, Santos IP, Barroso EM, Koljenović S, Vahrmeijer AL, Baatenburg de Jong RJ, Puppels GJ, Keereweer S*
Eur J Nucl Med Mol Imaging. 2022 Jun;49(7):2364-2376. doi: 10.1007/s00259-022-05705-z. Epub 2022 Feb 1.

7. Development of a near-infrared Raman spectroscopy setup compatible with fluorescence-guided surgery
Abbasi H, Lauwerends LJ, Bakker Schut TC, Santos IP, Caspers PJ, Hardillo JAU, Koljenović S, Vahrmeijer AL, Baatenburg de Jong RJ, Keereweer S, Puppels GJ
Analyst. 2023 Jun 12;148(12):2676-2682. doi: 10.1039/d3an00077j.

8. Effects of neoadjuvant therapy on tumour target expression of oesophageal cancer tissue for NIR fluorescence imaging
Galema HA, Neijenhuis LKA, Lauwerends LJ, Dekker-Ensink NG, Verhoef C, Vahrmeijer AL, Bhairosingh S, Kuppen PJK, Rogalla S, Burggraaf J, Lagarde SM, Wijnhoven BPL, Hutteman M, Doukas M, Keereweer S, Hilling DE
Mol Imaging Biol. 2024;26(6):955-964. doi:10.1007/s11307-024-01962-6

9. Tumor marker expression in head and neck malignancies to identify potential targets for intraoperative molecular near-infrared imaging
Lauwerends LJ, Zweedijk BE, Galema HA, Neijenhuis LKA, Dekker-Ensink NG, Baatenburg de Jong RJ, Verhoef C, Shadhvi Bhairosingh, Peter J.K. Kuppen, Vahrmeijer AL, Ginhoven TM van, Koljenović S, Koppes S, Hilling DE, Keereweer S
Mol Diagn Ther. 2024;28(6):811-820. doi:10.1007/s40291-024-00742-w

10. Molecular-Targeted Fluorescence Lymph Node Imaging Could Play a Clinical Role in the Surgical Setting: A Systematic Review
Zweedijk BE, Dalmeijer SWR, Manen van L, Galema HA, Lauwerends LJ, Abbasi H, Kremer B, Verhoef C, Robinson DJ, Koppes SA, Vahrmeijer AL, van der Vorst JR, Hilling DE, Keereweer S
Cancers (Basel). 2025;17(8):1352. doi:10.3390/cancers17081352

11. Near-infrared fluorescence imaging-guided surgery using cRGD-ZW800 to improve surgical resection margins in oral cancer: a phase I/II feasibility trial
Lauwerends LJ, Zweedijk BE, Galema HA, Robinson DJ, Bruijn HS de, Abbasi H, March TL, Valentijn ARPM, Pool M, Mast H, Jonker BP, Hardillo JAU, Monserez D, Sewnaik A, Koljenović S, Verhoef C, Baatenburg de Jong RJ, Frangioni JV, Koppes SA, Hilling DE, Vahrmeijer AL, Keereweer S
Nat Commun (2026). doi:10.1038/s41467-026-73554-7

12. Assessing intraoperative tumor-to-background ratios across different subsites of the oral cavity using an integrin-specific fluorescent tracer
Zweedijk BE, Osei-Agyeman MFAD, Lauwerends LJ, Robinson DJ, Abbasi H, de Gijsel JF, Mast H, Jonker BP, Hardillo JA, Monserez DA, Sewnaik A, Baatenburg de Jong RJ, Verhoef C, Frangioni JV, Koppes SA, Hilling DE, Vahrmeijer AL, Keereweer S
Cancers (2026). 18(12), 1910. doi:10.3390/cancers18121910

13. Optimizing Tumor Resection: The Added Value of Raman Spectroscopy in Fluorescence-Guided Cancer Surgery
Lauwerends LJ, Zweedijk BE, Koljenović S, Koppes SA, Doukas M, Kremer B, Hardillo JAU, Verhoef C, Vahrmeijer AL, Baatenburg de Jong RJ, Hilling DE, Keereweer S, Abbasi H
Submitted for publication

14. Tumor-Targeted Fluorescence-Guided Identification and Prioritization of Lymph Node Metastases in Oral Squamous Cell Carcinoma
Zweedijk BE, Gijsel JF de, Lauwerends LJ, Galema HA, Robinson DJ, Bruijn HS de, Abbasi H, March TL, Valentijn ARPM, Pool M, Mast H, Jonker BP, Hardillo JAU, Monserez D, Sewnaik A, Baatenburg de Jong RJ, Verhoef C, Frangioni JV, Koppes SA, Hilling DE, Vahrmeijer AL, Keereweer S
Submitted for publication

CONTRIBUTING AUTHORS

Hamed Abbasi
Robert J. Baatenburg de Jong
Tom C. Bakker Schut
Elisa M. Barroso
Shadhvi Bhairosingh
Henriette S. de Bruijn
Jacobus Burggraaf
Peter J. Caspers
Neeltje G. Dekker-Ensink
Pieter B.A.A. van Driel
John V. Frangioni
Hidde A. Galema
Tessa M. van Ginhoven
José A.U. Hardillo
Denise E. Hilling
Merlijn Hutteman
Brend P. Jonker
Stijn Keereweer
Senada Koljenović
Sjors Koppes
Bernd Kremer
Peter J.K. Kuppen
Clemens W.G.M. Löwik
Taryn L. March
Hetty Mast
Laura Mezzanotte
Dominiek Monserez
Lisanne K.A. Neijenhuis
Martin Pool
Gerwin J. Puppels
Dominic J. Robinson
Eben L. Rosenthal
Inês P. Santos
Aniel Sewnaik
Tom C. Bakker Schut
Alexander L. Vahrmeijer
Adrianus R.P.M. Valentijn
Cornelis Verhoef
Bo E. Zweedijk

PHD PORTFOLIO

Name PhD student:	L.J. Lauwerends
Erasmus MC department:	Otorhinolaryngology, Head and Neck Surgery
Full time PhD period:	01/04/2019 – 17/06/2024
Promotors:	Prof. R.J. Baatenburg de Jong
Co-promotors:	Dr. S. Keereweer & Dr. D.E. Hilling

COURSES	**Year**	**EC**
Erasmus MC - CPO-course: Patient Oriented Research	2019	0.30
Erasmus MC - BROK® Basic course Rules and Organisation for Clinical researchers	2019	1.50
Erasmus MC - Scientific Integrity	2020	0.30
Erasmus MC - Basic Introduction Course on SPSS	2020	1.00
Erasmus MC - CC02 Biostatistical Methods I: Basic Principles	2020	5.70
NiHES - History of Epidemiologic Ideas (ESP53)	2021	0.70
Erasmus MC - Microsoft Excel 2010: Advanced	2021	0.40
Erasmus MC - Translational Imaging Workshop by AMIE: From mouse to man	2022	1.00
NiHES - The Public Health Approach: From the Black Death to COVID-19 (ESP84)	2023	0.70

PRESENTATIONS		
Quarterly Progress Meeting Optical Image-Guided Surgery in Head and Neck Cancer	2019	1.00
Erasmus MC Cancer Institute Research Day	2019	1.00
235^{e} Algemene Vergadering KNO	2019	1.00
Focus group Fluorescence-guided Surgery, multiple	2020-2023	4.00
KNO Research Bespreking, multiple	2020-2024	3.00
Werkgroep bijeenkomst Dutch Fluorescence Guided Surgery Group	2021	1.00
Nederlandse Vereniging voor Keel-Neus-Oorheelkunde en Heelkunde van het Hoofd-Halsgebied (*NVKNO*) Jaarcongres	2023	1.00
World Molecular Imaging Congress (*WMIC*), Prague (poster presentation)	2023	0.50
Nederlandse Werkgroep Hoofd-Hals Tumoren (*NWHHT*) Symposium	2023	1.00
Erasmus MC - PhD Symposium	2024	1.00

CONFERENCE ATTENDANCE

Dutch Symposium on Fluorescence-Guided Surgery	2022	0.60
Precision Surgery Intraoperative Molecular Imaging	2022	0.30
2-daags Symposium ter gelegenheid van het afscheid van Rob Baatenburg de Jong	2023	0.60
World Molecular Imaging Congress (*WMIC*), Prague	2023	0.90
International Fluorescence Guided Surgery Congress	2023	0.60

ORGANISATION

Focus group Fluorescence-guided Surgery, bimonthly	2020-2022	3.00

OTHER

Peer reviews for journals:

- *Molecular Imaging and Biology*	0.30
- *Cancers*	0.30

Total EC	------ +
	32.7

A

ACKNOWLEDGMENTS | DANKWOORD

Dit proefschrift is het resultaat van jaren hard werken, samenwerking en groei; een periode waarop ik met trots en dankbaarheid terugkijk. Tijdens dit traject heb ik regelmatig geworsteld met het impostor syndroom, in het bijzonder wanneer ik me in een witte jas of OK pak hees, maar dat gevoel is nooit veroorzaakt door de mensen om mij heen. Integendeel.

Beste **Stijn**,
Bedankt voor de jaren van uitstekende begeleiding, waardevolle lessen, en het (h)erkennen van mijn krachten. Je weet op een bijzondere manier je promovendi uit te dagen, constructief feedback te geven, terwijl je tegelijkertijd onze successen viert met een oprechte trots. De balans die je vindt tussen scherpte, betrokkenheid en vrijheid, heb ik enorm gewaardeerd. Ik voel me vereerd deel te hebben mogen uitmaken van jouw onderzoeksgroep.

Beste **Denise**,
Bekwaam, warm en voor mijn gevoel altijd met iets nieuws bezig. Bedankt voor je begeleiding, adviezen en fijne gesprekken. Ik bewonder hoe je zoveel verantwoordelijkheden in balans houdt, terwijl je tegelijkertijd een toegewijd supervisor bent voor zoveel mensen en projecten. Ik ben benieuwd naar je toekomstige avonturen.

Professor Baatenburg de Jong, beste Rob,
Uw kritische blik en hoge verwachtingen hebben me regelmatig uitgedaagd om meer te presteren dan ik dacht te kunnen. Bedankt voor uw vertrouwen en uw persoonlijke betrokkenheid; ik heb veel van u geleerd.

Professor Vahrmeijer, beste Lex,
Uw wetenschappelijke bijdrage aan het fundament van dit proefschrift niet te overschatten. Ik heb u leren kennen als iemand met een scherpe wetenschappelijke blik en een indrukwekkende diepgang. Ik ben u dankbaar voor uw betrokkenheid en uw bereidheid om mee te denken.

Dear **Hamed**,
It has been a genuine pleasure working, writing and sharing an office with you. Your thoroughness, focus, and insight have taught me a great deal, and I am confident that you will continue to excel. I wish you all the best.

Beste **Hidde**,
Je hebt in korte tijd enorm veel bereikt, en je energie was direct aanstekelijk. Bedankt voor de soepele samenwerking, je daadkracht, en de fijne gesprekken. Ik heb veel van je geleerd, vooral over het reilen en zeilen van klinische studies en op de OK. Je wordt een geweldige chirurg.

Beste **Bo**,
Je maakte een indrukwekkende start toen je bij ons kwam en ik heb je leren kennen als een warm, ondernemend, georganiseerd en deskundig persoon, iemand die aan alles en iedereen denkt. Bedankt voor alles, en veel succes en plezier met je opleiding.

Daniëlle,
Ik heb maar heel eventjes met jou op de werkvloer gestaan, maar dat was voldoende om je mee te maken als een ontzettend leuk, gemotiveerd en warm mens. Bedankt voor de gezelligheid, en heel veel succes met je toekomstige projecten en vervolgstappen.

Beste **Senada**,
In het begin van mijn tijd in het EMC heb je me snel wegwijs gemaakt in de pathologie en op de afdeling. Dankzij jou begreep ik de literatuur beter en vond ik mijn weg in materie die eerst ruim boven mijn pet ging. Bedankt, ik heb veel aan je te danken bij de totstandkoming van dit proefschrift.

Beste **Sjors**,
Het was altijd een plezier om bij je langs te komen, of dat nu was voor een vraag of om coupes te scoren. Het is bijzonder hoe je altijd tijd maakt voor ons en bereid bent om te helpen, en op zo'n fijne manier. Heel erg bedankt, jouw bijdragen aan dit proefschrift zijn onmisbaar geweest.

Beste **Dom** & **Riëtte**,
De avonden en vroege ochtenden met jullie waren prettig en leerzaam. Bedankt voor het geduld en de grondigheid waarmee jullie voor mij nieuwe concepten bijbrachten, jullie inspanningen hebben de kwaliteit van mijn werk naar een hoger niveau getild.

Beste hoofd-hals chirurgen, **Hetty**, **Brend**, **José**, **Dominiek**, **Aniel**,
Ontzettend veel dank voor jullie medewerking, geduld en meedenken tijdens o.a. de Guided by Light-studie, en daarmee voor jullie waardevolle bijdragen aan dit proefschrift.

Lieve **familie** en **vrienden**,
Dank voor jullie steun, betrokkenheid en vertrouwen, het gevoel van thuiskomen bij het weerzien, hoe veel tijd er soms ook tussen glipt. Jullie zijn me dierbaar, en ik heb veel aan jullie te danken.

Lieve **Gio**,
Bedankt voor je steun, je vertrouwen, je geduld en je liefde. Wat hebben wij de afgelopen veertien jaar veel doorstaan, gelachen en getrotseerd. Ik ben trots op jou, en dankbaar voor wie je bent. Ik kijk uit naar wat ons nog te wachten staat. Ik hou van je.

Lieve **Solomon**,
Kleine dondersteen, je hebt me in je prille jaren op deze wereld meer geleerd dan wie dan ook. Dankbaar dat jij er bent, dankbaar voor de knuffels, het vele lachen, de uitdagingen, de verwondering — de lessen die me met jou mee doen groeien, waardoor ik steeds beter besef wat er echt toe doet. Ik hou van jou.

ABOUT THE AUTHOR



Lorraine Jean Lauwerends was born on August 2nd, 1988 in Rotterdam, to Lorna Valencia Pomperada and Jimmy Allan Eugène Lauwerends. She went to secondary school at the Erasmiaans Gymnasium, after which she studied Industrial Design Engineering at the Delft University of Technology in 2006. In 2011, she advanced her studies at the department of Mechanical Engineering, obtaining her master's degree in biomedical engineering in 2015. Her master's thesis work, performed at the department of Neuroscience of the Erasmus Medical Center, was a fundamental study on the orientation and anatomy of the semicircular canals of the vestibular system. This research phase cemented her interest in scientific research. Following three years as a research and technical engineer at the Dutch Ophthalmic Research Center (D.O.R.C. in Zuidland, Netherlands), where she focused on the development of ophthalmic surgical instruments, Lorraine returned to academia. In 2019, she started her PhD at the Department of Otorhinolaryngology at the Erasmus Medical Center, guided by Stijn Keereweer, Denise Hilling and Robert Jan Baatenburg de Jong. Her research centered on fluorescence-guided surgery, particularly applied to the complete excision of oral cancer, and its integration with Raman spectroscopy.

Lorraine lives in Rotterdam with her husband Giovanni, their son Solomon (2022), and their cats Maldita and Trivida. In late 2025 she started working part-time at the Ikazia Hospital, first as a Research Coordinator and currently as Secretary of the Local Research Committee. Alongside this work, she continues to develop her artistic practice.